A Quantitative Study into the Errors in Measuring an Automotive Vehicle Radiated Emissions Signature Using the CISPR 12 Method

Max Paterson

PhD

UNIVERSITY OF YORK

Electronic Engineering

January 2019

Abstract

This thesis presents a quantitative study into the errors in measuring automotive vehicle radiated emissions using the CISPR 12 method. This method is based upon a limited set of tests, when compared to that used for many other commercial electrical devices. This research, details the errors introduced in recording the maximum amplitude of the radiated electric field from the vehicle by using the simplified method.

Two key differences between the CISPR 12 setup and other radiated emissions test methods were researched, in order to quantify the errors. These were: not scanning the receive antenna in height, and not rotating the vehicle through 360^o in the azimuth plane whilst the E-field is measured. It was concluded that the current CISPR 12 method has the potential to under-estimate the maximum amplitude of the E-field by up to 30 dB.

Research was then performed to investigate alternative methods to those defined in CISPR 12. A number of approaches were considered before being subsequently discounted. The final alternative method considered was the 'Test Wire Method', which was originally designed for performing tests on large, industrial machines.

The Test Wire Method, TWM, was initially used as a 'proof of concept' that the approach could be used for testing a much smaller device than it was originally designed for. Once the method had been successfully used, and a reduction in the error compared to the CISPR 12 method confirmed, the TWM was then further developed into a novel, new measurement system, designated the MicroStrip Method. A small, near-field probe was designed which, along with the use of a calibration factor, allows for a closer approximation of the maximum amplitude of the radiated E-field to be recorded. Measurements performed on a range vehicles, resulted in a reduction in the mean error of over 10 dB, compared to using the CISPR 12 method.

Contents

List of Tables

List of Figures

Acknowledgements

I would like to thank my supervisors Dr John Dawson and Professor Andy Marvin for their support and encouragement during the development and writing of this thesis. Their help, particularly from Dr Dawson and his attention for detail and guidance were invaluable in the completion of my research.

This thesis would not have been possible without the financial support of HORIBA MIRA Ltd. I would like to thank Dr Anthony Martin, Dr Anthony Baxendale and Mr Stewart Howat of HORIBA MIRA for providing both the funding and allowing time out from my position at MIRA for my many visits to the University of York and attendance at three international conferences. Dr Alastair Ruddle, Dr Yu Xian Teo and Mr Mark Emery of HORIBA MIRA and Dr Lester Low of Bentley Motors for help with the questions I posed to them on a regular basis, their specialist knowledge have helped me to a much greater understanding in the field of EMC testing and Electromagnetic Modelling .

I would like to thanks HORIBA MIRA Ltd for the use of their EMC measurement facilities, without which this research would have proved impossible.

My gratitude is extended to Professor Davy Pissoort and Professor Johann Catrysse for their support with providing the reports and background information regarding the 'Test Wire Method' and their continued interest and encouragement in my research. Additionally, I would like to thank Mr Mart Coenen for his help regarding the 'Surface Current Sense Wire' project.

I would like to thank my wife Wendy and daughter Matilda for putting up with the late nights and early mornings of me sitting working in the office, without their love, support and encouragement this thesis would never have been written.

A final thanks goes to Mrs Sheila Yeomans for her hospitality on my many visits to York.

Declaration of Authorship

I, Max Paterson, declare that this thesis is a presentation of original work, and that I am the sole author. This work has not previously been presented for an award at this, or any other university. All sources are acknowledged as References. In addition to this thesis I have published the following papers as part of the research conducted towards part of my PhD.

1. M. Paterson, J.F. Dawson 'An Investigation into the Errors in the CISPR 12 Full Vehicle Radiated Emissions Measurements Due to Vehicle Directivity', International Symposium on Electromagnetic Compatibility (EMC Europe), Brugge, pages 310 - 315, September 2013.

2. M. Paterson, J.F. Dawson 'Using the Test Wire Method as an Alternative to the CISPR 12 Full Vehicle Measurement Method', International Symposium on Electromagnetic Compatibility (EMC Europe), Wroclaw, pages 649 - 654, September 2016.

3. M. Paterson, J.F. Dawson 'An Investigation into Alternatives to the CISPR 12 Full Vehicle Measurement Method', International Symposium on Electromagnetic Compatibility (EMC Europe), Amsterdam, pages 885 - 889, August 2018.

Signed: _____

Date: _____

Chapter 1

Introduction

1.1 Overview

Radiated emissions can be defined as:

> An unintentional release of Electromagnetic, EM, energy from any piece of electronic equipment

All electronic devices have the ability to propagate electromagnetic fields; whether it be intentional as in the case a radio transmitter, or un-intentional from a domestic audio equipment, for example.

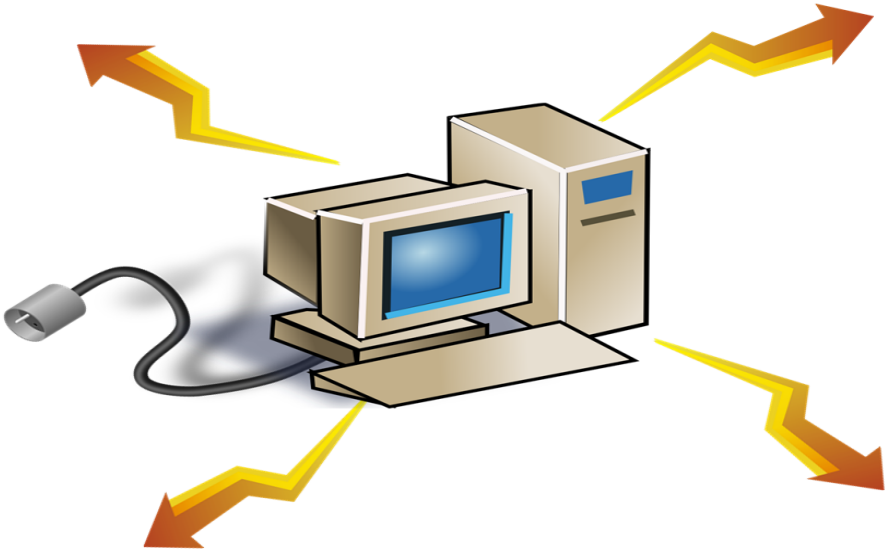

FIGURE 1.1: Emissions Radiating From Equipment Under Test

The fields radiated by the device have the potential to cause disruption to the operation of other electrical equipment in the vicinity. With this in mind, the ability to both measure and control the emissions is essential. Control of the level of the emissions can be achieved by many means, starting with the original design of the device, through to additional filters and shields that can be added to the device after it has been built. By using good EMC practices in the design process, many emissions problems can be dealt with before the design reaches the prototype stage. This is by far the most cost-effective approach. There is an increasing scale of cost to addressing emissions problems once the design has gone into production. The position all manufacturers aim to avoid is product recall in order to 'fix' a problem.

As well as being able to control the emissions radiated from a device, a method of measuring the amplitude of the emissions, and confirming that they are below a level that can be considered acceptable is necessary. The level of radiated emissions of the device allowed is strictly defined through International Standards. Some of these Standards are described in more detail in later chapters of this thesis. Compliance with these standards is used to give a level of confidence that the device will not cause potential interference with other electrical equipment.

1.2 Research Motivation and Scope

This thesis presents a quantitative study into the errors in measuring an automotive vehicle radiated emissions signature using the CISPR 12 [1] method. All electrical devices can be considered as a transmitter of Radio Frequency, RF, energy, whether it be intentional or unintentional as is the case with a motor vehicle. This energy will propagate away from the device with unknown directions and amplitudes. This, it is known [2], [3], means that an electrically large item will have a complex emissions radiation pattern and if the maximum amplitude of the energy is to be recorded a full, spherical scan around the device would be required. This is both complex, in terms of the equipment required, and also very costly due to the time required to perform the tests. As a typical vehicle , car, van bus lorry etc., can be considered as electrically large over the frequency range of 30 MHz to 1000 MHz, specified in CISPR 12, a complex radiated emissions pattern can be expected.

The CISPR 12 method involves performing radiated emissions measurements from two positions around the vehicle; broadside to the passenger and driver side. Almost all other commercial radiated emissions test standards specify that as a minimum a full 360^o azimuth scan of the EUT should be employed, along with receive antenna height scanning being specified in many cases to further maximise the measured emissions. Within the automotive industry, a minimal programme of testing used for radiated emissions has been employed, mainly due to financial constraints, as full azimuth and receive antenna scanning would dramatically increase both the cost and time taken to perform the test. However, should this approach to testing be used; for instance to determine the tallest person in a given population, the idea of measuring only two people and extrapolating the data to imply significance would be wholly inaccurate. Ergo, the process of CISPR 12 measurements, it can be argued, fails to fully and significantly determine the maximum field amplitude, rather follows the given analogy and simply measures the EM equivalent of 'two people'.

It is acknowledged that an electrically large radiator will have a radiation pattern that is not omni directional at all frequencies [3]. For a typical vehicle: a car, van or bus for example, this will be the case over the full frequency range of 30 MHz to 1 GHz, as specified in CISPR 12. It follows, therefore, that following the Standards requirements, and performing measurements at just two azimuth angles, will drastically reduce the likelihood of recording the maximum emissions signature of the vehicle in that particular test environment [1].

Having worked within an automotive research organisation for many years, predominantly within the EMC department, I have developed an interest in the methods employed during automotive radiated emissions measurements. In particular why the methods employed differ from those used for almost all other product types and the impact this may have upon electronic devices in the near vicinity.

To date, little research has been published to investigate either: the effect that the limited scope of the test methods defined in CISPR 12 has on the maximum amplitude of the measured emissions, or possible alternative methods that could be employed to address this problem.

[1] It has been shown by the author that errors of up to 30 dB can be recorded using the CISPR 12 method [4]

The scope of the research presented in this thesis includes:

- Measurement and simulation of the radiated emissions from a range of devices, both electrically small and large devices using both the CISPR 12 and CISPR 22 [5] method.
- Define the upper and lower frequency of emissions from a range of commercially available vehicles
- Perform a study into possible alternative techniques to the CISPR 12 method that could potentially reduce the errors recorded in the maximum emissions amplitude
- Development of the Test Wire Method for automotive emissions measurements
- Production of the MicroStrip Method for measuring vehicle level radiated emissions

1.3 Original Contributions

This thesis presents the following original contributions to the field of automotive radiated emissions measurements:

1. The analysis of the error in the maximum amplitude of the electric field, recorded during a CISPR 12 radiated emissions test, as a consequence of performing measurements at a limited number of azimuth angles around the vehicle, and using a single receive antenna height. This analysis enabled the following:
    - Consequences of not using EUT azimuth scanning during a CISPR 12 measurement, error introduction for both electrically small and large EUTs was determined and additionally quantified. Full details of this can be found in Section 4.3 of this thesis, the results are summarised in Section 4.5.
    - Consequences of not using antenna height scanning during a CISPR 12 measurement, error introduction for both electrically small and large EUTs was determined and additionally quantified. Full details of this can be found in Section 4.2 of this thesis, the results are summarised in Section 4.5.

2. A novel, new method for measuring the radiated emissions from a vehicle, that reduces the errors in the maximum amplitude of the electric field recorded by over 10 dB, compared with those recorded during a CISPR 12 full vehicle radiated emissions test. The background and development of the MicroStrip method is detailed in Section 7.1, measurement results from the validation of the MicroStrip Method are detailed in Section 7.2 of this thesis.

1.4 Outline of the Thesis

An overview of radiated emissions testing methods are described in Chapter 2. The chapter begins a brief history of radiated emissions measurements, describing how the early emissions tests and Standards were developed. A typical facility, an Open Area Test Site (OATS), for performing radiated emissions measurements is then detailed. The test procedure used to perform radiated emissions measurements on a vehicle is then contrasted with a method used to perform the measurements on an item of Information Technology, IT, equipment. The two methods have a number of fundamental differences in how the test are performed and as a consequence, the likelihood of each the tests recording the maximum amplitude of the emissions radiated by the equipment under test.

Chapter 3 contains an overview of Electromagnetic (EM) Modelling for automotive applications. The chapter gives a brief introduction to the subject of EM modelling, detailing some of the parameters needed to build a model of the device to be simulated. The mesh size used to build the model is described and guidelines for the minimum mesh element size is introduced. Details of how the results can be validated once the simulations have been run is discussed. The final Section of the chapter illustrates the EM model of the Vehicle Body Shell (VBS) that was simulated in the later chapters of this thesis.

Chapter 4 describes the experimental work carried out to investigate the affect that receive antenna height scanning and EUT azimuth scanning during a radiated emissions tests has upon the likelihood of recording the maximum amplitude of E-field. The affect of the two parameters is used to quantify the errors introduced during a vehicle level radiated emissions tests by using a simplified test methodology. The chapter also describes analysis of the radiated emissions measured from a range of different vehicle types. From this analysis, the frequency range utilised in the measurements performed in the research described in this thesis, were determined.

In Chapter 5 a range of alternative test methods to the procedure currently used to measure radiated emissions from automotive vehicles is described. The chapter highlights the advantages and disadvantages of the alternate methods and concludes with the a suggested alternative, to be further investigated, to the current vehicle level test. F

Chapter 6 describes the investigation into the 'Test Wire' Method (TWM), suggested as a possible alternative in Chapter 5. The TWM is used as a basis for measurements performed on a sub-scale model, as a means of proof of concept, to determine if the Error Bias could be reduced. Based upon the results obtained, it was concluded that the TWM was a viable alternative to the current vehicle level test, although it still exhibited a number of disadvantages.

Chapter 7 describes further development of the TWM, resulting in an improved design, designated as the 'MicroStrip Method' (MSM). The MSM recorded an improved Error Bias, compared to the TWM and also addressed the disadvantages that were found with using the TWM. The EB recorded using the MSM was quantified, and compared to the EB recorded using the current vehicle level test methods.

Chapter 8 closes the thesis with details of the conclusions that were drawn from the previous chapters of the thesis. A discussion of the key achievements of the research presented and future work to further develop the MicroStrip Method is proposed.

Chapter 2

Overview of Automotive Radiated Emissions Testing

2.1 Introduction

In this Chapter an introduction to radiated emissions measurements is presented. Starting with a brief history of radiated emissions measurements from the early days, around the time of Marconi's telegraph transmissions, through to the current requirements of the EMC Directive [6]. A time-line of how the current test Standards and Directives became European and worldwide law is described. The second part of the chapter describes an Open Area Test Site, OATS, the typical test site used for performing vehicle level radiated emissions measurements. Finally an overview of a range of commercial radiated emissions standards is then detailed, contrasting how the methods used for automotive measurements detailed in CISPR 25 [7] and CISPR 12 [1] differ from those used for almost all other types of product.

2.1.1 A Brief History of Radiated Emissions Measurements

Radiated emissions can be described as an electromagnetic field emitted from any source, whether it be intentional or non-intentional. One of the earliest man made intentional transmission sources was produced in the late 1900's by Marconi when he made the first transatlantic transmissions. It could be argued that this transmission 'sparked' the need

for corrective action to be taken to address interference caused with early radio receivers. Radio equipment at this time was very crude by today's standards; and were prone to problems with interference.

In 1892, the German Parliament issued the first law that dealt with electromagnetic interference, known as the 'Law of Telegraph in the German Empire' [8]. This law also gave details regarding the procedures that should be followed when cases of interference were encountered.

The United States, US, Navy started to implement radio telegraphy onto its ships in 1899. They encountered what is possibly the first case of radio frequency interference. At the time all radios transmitted on the same frequency. The Navy found that when multiple transmitters were used simultaneously, reception of the signal was corrupted. The problem became known as Radio Frequency Interference, RFI. As technology has advanced, the sources of emissions and the proliferation of devices that could be prone to being affected has increased massively. By the 1930's electric motors, the electrification of the railway network and a multitude of other electrical devices were beginning to cause widespread problems with interference with the broadcast radios of the day. [9].

This increase in development of electrical devices accelerated during World War II, with the military being the main driving force. Cases of breakdown and interference noise in communication devices due to navigation equipment on board planes and other military vehicles started to become widespread. However, at this time a simple change in transmission frequency was sufficient to remedy the problem due to the minimal use of the RF spectrum at that time. At the end of the war, a special subcommittee of the American Standards Association, ASA, known as the Sectional Committee C63, Radio-Electrical Coordination issued the Radio Frequency Interference, RFI, standard known as the Joint Army-Navy Specification JAN-I-225 [10]. Around this time the first conferences to discuss the issue of RFI started, the Armour Research Foundation conference on Radio Frequency Interference [11] being one of the first in 1954.

By the end of the war electronic device development had moved on significantly and the advent of the semiconductor age introduced a whole range of new interference problems. By the 1970's, the introduction of integrated circuits had helped, in part, to allow electronic designers to introduce digital signal processing techniques, which by virtue of the ever increasing digital switching speeds and reduction in device size lead to

systems that contained more and more sources of components all generating waveforms with a spectrally rich content. Electromagnetic Interference, EMI as it became known, was now a problem to a wider range of devices. As the amount of electronic devices purchased by the general public increased, the interference problems that had previously been encountered only on military platforms began to manifest themselves on radios, HI-Fi equipment and televisions in the home and workplace.

With the rise in EMI issues being reported, Europe lead the way in tackling the problem. In 1933 a meeting of the International Electrotechnical Commission, IEC, suggested the formation of the International Special Committee on Radio Interference (Comité International Spécial des Perturbations Radioélectriques), CISPR. CISPR published a document that outlined the need for measurement equipment required to determine the level of interference being caused by electronic devices. In the post-war years, CISPR held meetings that delivered a range of technical papers dealing with all aspects of measurement systems and also defined recommended emissions limits. Some European countries also started to implement their own requirements for the emissions from digital electronic devices, based upon the CISPR recommendations. In 1973 the IEC set up Technical Committee TC77 whose function was to develop the standards related to the field. The Federal Communications Commission, FCC, in the USA published regulations in 1979 that detailed the maximum level of emissions that were acceptable from electronic devices. The FCC took things one stage further, making the compliance with the limits a legal requirement rather than a recommendation.

Many European countries continued to use the recommendations of CISPR up until the launch of the EMC Directive, 89/336/EEC [12],in January 1989, as one of a series of measures introduced under Article 100a of the Treaty of Rome. The primary objective of Article 100a was to create a single European market for goods and services. The Directive set out to standardise the requirements across Member States of the European Union, it details the essential legal requirements for the protection of electronic devices from radio interference that are placed on the market within Europe. The Directive, does not, however, detail specific emissions limits, this information is provided through a range of generic and in some cases, product type specific standards. These Standards were then used by the manufacturer of the item trying to release their device onto the market as a means to be able to demonstrate compliance with the Directive. Compliance can be achieved through a range of tests or by the production of a Technical Construction

File, TCF. There is no mandatory requirement under the Directive to physically test the device, however, proving compliance by a purely documentation route is not always straightforward and testing may be the only option. The original version of the EMC Directive has subsequently been revised and re-issued, at the time of writing this thesis under the reference of 2014/30/EU [13]

While the vast majority of products must comply with EMC Directive there are a number of exceptions, these include; components and sub-assemblies that have no intrinsic function and products that are covered by other Directives. Examples of products covered by different Directives are detailed in Table 2.1.

TABLE 2.1: Devices Not Covered under the EMC Directive

Device Type	**Applicable Directive**
Medical Devices	Medical Device Directive (93/42/EEC) [14]
Marine Equipment	Marine Equipment Directive (2014/90/EU) [15]
Agricultural Tractors	Agricultural and Tractors Directive (2009/64/EC) [16]
Cars and Vans	Automotive EMC Directive (UNECE Regulation 10.05) [17]
Radio Equipment	Radio Equipment Directive (2014/53/EU) [18]

Since the early 1970's the suppression of radio interference from spark ignition engines has been covered by the Automotive Directive. The automotive industry initiated an amendment to the EMC Directive to cover the EMC requirements of motor vehicles. The first generation of the document was released in 1972 under the reference of 72/245/EEC [19] with the aim of regulating the radio interference problems found in vehicles. The scope of the directive was limited, at this time due to the minimal amount of electronics found in cars of the day. However, by the mid 1990's cars, and other automotive vehicles, were beginning to advance and more and more electronic devices were beginning to be implemented into the latest designs. In an attempt to keep pace with the automotive industry, 72/245/EEC was replaced with a new Directive, 95/54/EC [20] which extended the frequency range at which radiated emissions and radiated immunity tests were required to comply. Where 72/245/EEC only required measurements to be performed up to 300 MHz, 95/54/EC required emissions tests to be performed up to 1 GHz. In the late 1990's a project was setup by the EU Commission, which set out to examine revisions to the then current EMC Directive 95/54/EC. The project was run by York EMC

Services and detailed changes to the Directive that had been requested by automotive manufacturers, automotive Tier 1 suppliers and EMC test houses. The result of the report was the issue of a revised Directive under the reference of 2004/104/EC [21]. One of the major differences implemented in the latest version was that it now referenced international automotive test standards for some of the test methods and setups. The latest incarnation of the Directive is known as ECE Regulation 10, revision 5 [17] being the current version. This Directive is no longer regulated regulated under the European Directives, instead it is legislated by the United Nations Economic Commission for Europe, UNECE. In order for a vehicle to be released on to the open market compliance must be shown with the requirements of the Regulation.

2.1.2 Radiated Emissions Test Methods

2.1.2.1 Open Area Test Site

Radiated emissions measurements can be performed at a number of different test sites, possibly the most common being the Open Area Test Site, OATS.

An OATS test site should be flat and free from electromagnetic reflecting objects, other buildings etc., this means that the test support building will need to be located some distance away from the test site; very often underground. As the ground around the test site will reflect RF differently depending on such factors as conductivity of the soil, surface roughness and moisture content the ground effect is regulated by the use of a metal ground plane. The minimum dimensions of this ground plane are defined in CISPR 16-1-42 [22] and shown in Figure 2.1.

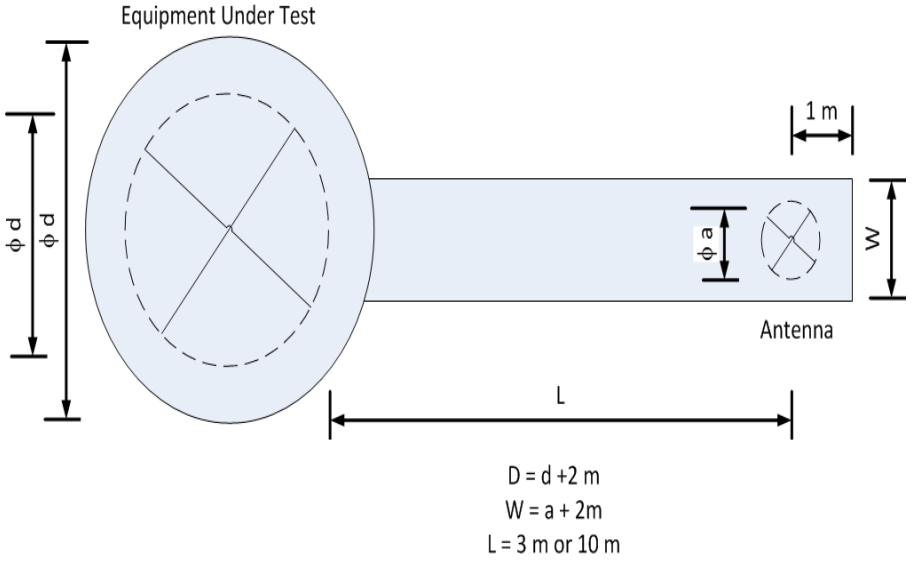

FIGURE 2.1: CISPR OATS Size Requirements. Reproduced from CISPR 16-4-2

The ground plane employed at an OATS should preferably be made of solid metal sheets that have been welded together, this is not, however, always practical. There will be a tendency for such a ground plane to hold water in wet conditions and warp in hot weather. A popular method of avoiding both of these problems is to use a metal mesh, this will allow water to drain and will resist distorting due to high temperatures. The mesh should not have any holes greater than 0.1 λ at the highest frequency of operation, typically 3 cm at 1GHz. Scattering from the edges of the ground plane is possible [23], [24], so the edges should be terminated into the soil.The ground plane should be flat to within 0.15 λ at the highest frequency of operation, typically 4.5cm at 1 GHz for a 3 m test site or 0.28 λ, 8.4 cm for a 10 m site. Figures 2.2 and 2.3 show two typical OATS layouts. The site at Eurofins Castleford shows a small enclosure for the EUT being tested while the receive antenna in not enclosed,

FIGURE 2.2: CISPR12 OATS Typical Arrangement. Located at Eurofins Castleford.

The test area is very often covered over with a non RF reflective structure,usually fibreglass or plastic, this allows for all weather testing to be performed. It has been shown that test results can be affected by this structure in wet or icy weather as the moisture can cause the enclosure walls to become reflective [25]. Care should be taken to guard against this.

FIGURE 2.3: CISPR12 OATS Typical Arrangement. Located at HORIBA MIRA, Nuneaton.

The site at HORIBA MIRA has the entire measurement area covered by a non-conductive building.

A major source of uncertainty in the OATS facility is that of the ambient RF environment. Not only will the measurement antenna be receiving the emissions from the EUT, but it will also be receiving emissions from any number of RF sources within the the local area of the test facility, from machinery in a local factory, a nearby person with a mobile phone to a passing taxi cab etc. All these ambient sources will have the tendency to swamp the wanted emissions from the EUT. Steps can be taken to minimise the affect of this problem. The site should, where possible, be chosen to take advantage of a naturally quiet RF environment, i.e not in the middle of a large industrial estate, or next to a mobile phone mast. However a naturally quiet RF site is almost an impossibility to find due to the presence of TV and radio signals, amongst others. There are guidelines defined for the minimum field strength that broadcasters are required to produce, while this is good news for anyone wanting to listen to the radio or watch the TV it makes the job of the EMC test engineer very difficult. Within the frequency ranges occupied by TV and radio the ambient signal will almost certainly be over the allowed EMC emissions limits, resulting in any emissions from the EUT being masked. An option offered by some test standards, EN55032 [26] for example, is to perform the measurements at a closer distance, with a corresponding reduction in the limit line. This attempt at a solution has two problems, firstly even at 1 m measurement distance the likelihood of the EUT emission being stronger than that of the local TV transmitter are very unlikely and, secondly reducing the measurement distance to 1 m introduces further issues, such as near field uncertainty and antenna coupling. A further problem with ambient signals is that of transient ambients. If a signal is emitted at a constant frequency, even if it is not possible to actually measure the EUT emissions at that frequency, it can at least be tagged and ignored. Transient emissions are more difficult to deal with, and must be investigated every time a measurement is performed to determine whether they are from the EUT or are an ambient signal that can be discounted. Ambients are generally dealt with by performing an initial frequency sweep with the EUT switched off in order to obtain a baseline level. A further measurement is then performed with the EUT in its operational mode and the two sweeps compared. In theory any emissions evident in the second sweep that were not present in the first one should be attributed solely to the EUT.

2.2 Overview of Current Test Procedures used for Automotive and IT Products

2.2.1 Introduction

As described in section 2.1.1 the measurement of radiated emissions involves using a test procedure determined by one, or a combination, of the following:

- product type of concern
- the market into which the item will be sold
- the customer to whom the item may be sold for fitting into another item (a car for example)

The actual test method used to measure radiated emissions varies considerably, depending on the exact product type. Automotive tests are, as previously stated in Section 2.1.1, not required to meet the limits of the EMC Directive. They are instead regulated under the Automotive Directive. The methods used to perform the emissions test detailed in the Automotive Directive, which references CISPR 12 [1], differ from the methods used to measure most other electrical items. This section will describe the methods used for performing CISPR 12 measurements and those used for a typical piece of IT equipment. The methods will be compared and contrasted to highlight the key differences.

2.2.2 Automotive Vehicles: CISPR 12

CISPR 12 [1] is the document referenced by the Automotive Directive and is intended to set out a procedure for the testing of radiated emissions from vehicles, boats and internal combustion engine driven devices. The emissions amplitude limits defined in CISPR 12 aim to provide:

> Protection for broadcast receivers in the frequency range of 30 MHz to 1000 MHz when used in the residential environment

CISPR 12 aims to ensure that the vehicle does not cause interference with receivers outside its bounds, i.e other passing vehicles domestic radio/TV receivers situated in houses etc. The test may not ensure protection to receivers located closer than 10 m from the test vehicle.

The Standard defines the radiated emissions requirements of the following:

- Vehicles propelled by an internal combustion engine, an electric motor or hybrid vehicles powered by a combination of the two.
- Boats propelled by an internal combustion engine an electric motor or hybrid vehicles powered by a combination of the two
- Devices equipped with an internal combustion engine or traction batteries

Table 2.2 details examples of each product type listed above, note that this list is by no means exhaustive and is shown to indicate the range of vehicles and devices covered by the Standard.

TABLE 2.2: Scope of Devices covered by CISPR 12

1	Vehicle	Car, Van Truck, Moped, Agricultural Machinery, Earth Moving Machinery and Tractors, Mining Equipment, Snowmobiles.
2	Boats	Any vessel to be used on the surface of the water, no longer in length than 15 m
3	Devices	Chainsaws, Irrigation Pumps, Snow Blowers, Air Compressors, Lawn Mowers

The measurements can be performed at an Outdoor Test Site, OTS, an Anechoic Lined Shielded Enclosure, ALSE, or an Open Area Test Site (OATS). The reference test site detailed in CISPR 12 is the OTS, with a clause that the tests may be performed at with an OATS or ALSE if correlation to the results obtained using an OTS can shown. The research described in this thesis is based around measurements performed at an OATS. Other test methods, such as performing the tests in a Reverberation Chamber, RC, are not allowed as a method of showing compliance with the requirements of CISPR 12. A

brief description of RCs and their use for performing radiated emissions measurements can be found in Section 5.1.4 of this thesis.

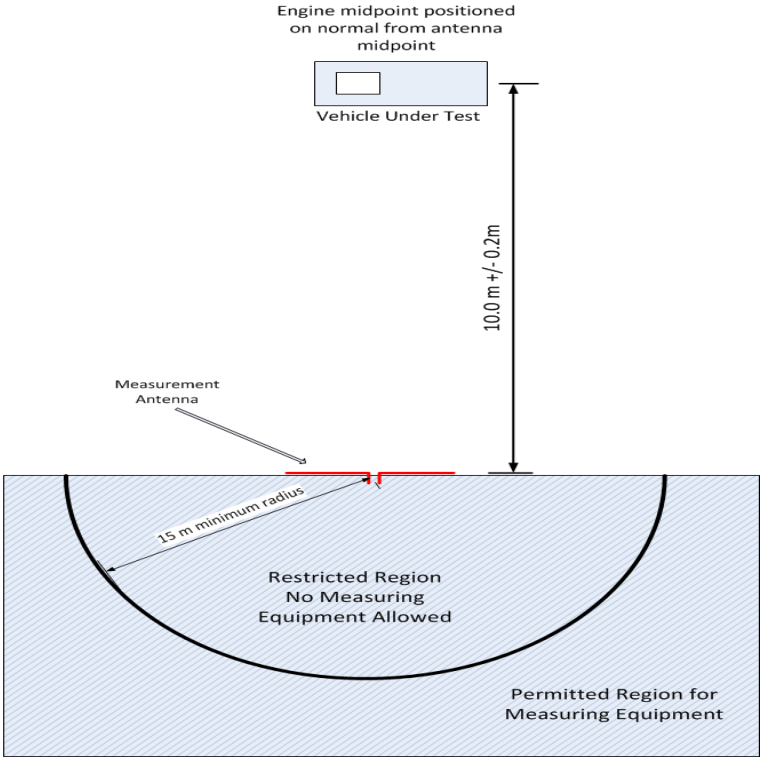

FIGURE 2.4: CISPR12 Test Layout for Vehicles. Reproduced from CISPR 12

The distance between the phase centre of the receive antenna and the closest metallic part of the vehicle, when the bore sight of the antenna is in line with the engine midpoint, is 10 m ±0.2 m. A caveat is included in the standard that a 3 m (±0.05 m) measurement distance may be used under circumstances where ambient levels preclude measurement at 10 m. If the test vehicle is longer than the area illuminated by the 3 dB beam width of the receive antenna (approximately 60 degrees for a typical log periodic antenna, which equates to a distance of 1.75 m either side of the antenna centre line at 3 m distance), multiple antenna positions must be used to fully quantify the entire emissions signature of the vehicle. If a 3 m measurement distance is used the test limits should be increased by 10 dB. The restriction is based upon the inverse distance square law [27] which states that field radiated from a point source is inversely proportional to the square of the distance from the source. The increase in limits has, however, been shown to not follow the $\frac{1}{r}$ assumption for all devices under test. Studies performed by Garn et al[28] and Hoolihan [29] have shown that when the measurement distance was reduced from 10 m to 3 m the actual measured E-field amplitude was found to vary by between 1 dB and

18 dB across the frequency range of 30 MHz to 1 GHz and not 10 dB as is implied in CISPR 12.

The receive antenna should be placed on a non conductive mast at a height of 3m ±0.05 m for a measurement distance of 10 m and a height of 1.8 m ±0.05 m for a measurement distance of 3 m. A single antenna height is used throughout the test, i.e height scanning between 1 m and 4 m is not used. This is one of the key differences between the methods described in CISPR 12 compared to those used to measure IT equipment, for example.

Measurements will be made on the left and right hand side of the vehicle with the receive antenna aligned with the centre point of the engine. For vehicles with an internal combustion engine the engine speed shall be as described in Table 2.3.

TABLE 2.3: Internal Combustion Engine Operating Speeds.

Number of Cylinders	**Engine Speed**
1	2500 rev/min
> 1	1500 rev/min

Vehicles are tested for compliance against two separate limit lines, designated 'Broadband' and 'Narrowband'. The International Electrotechnical Vocabulary, IEV,[30] defines narrowband disturbance as:

> An electromagnetic disturbance, or component thereof, which has a bandwidth less than or equal to that of a particular measuring apparatus, receiver or susceptible device.

A broadband disturbance is consequently defined as:

> An electromagnetic disturbance which has a bandwidth greater than that of a particular measuring apparatus, receiver or susceptible device

During the broadband test the vehicle is measured in 'Engine Running' mode and is configured to have all sources of electrical noise active, i.e. air conditioning at full speed, set to its coldest temperature, windscreen wipers at full speed, headlights on, engine at

the speed specified in table 2.3, CD Playing etc. The engine speed is held as detailed in Table 2.3. For vehicles that utilise an electric propulsion system, the vehicle should, additionally, be configured on a dynamometer, with the vehicle driving the wheels at a constant speed of 40 km/h, where a dynamometer is not available the vehicle should be fitted onto non-conductive axle stands. For the narrowband test the vehicle is measured in 'Key On, Engine Off' mode with the engine switched off and the ignition switched on, in the 'Run' position, as the intention of the test is to measure the emissions from sources such as oscillators and clock signals produced by devices such as the infotainment system within the vehicle.

Within CISPR 12 a flowchart is shown that should be used to ascertain which limit level should be applied to the data, this is shown in Figure 2.5.

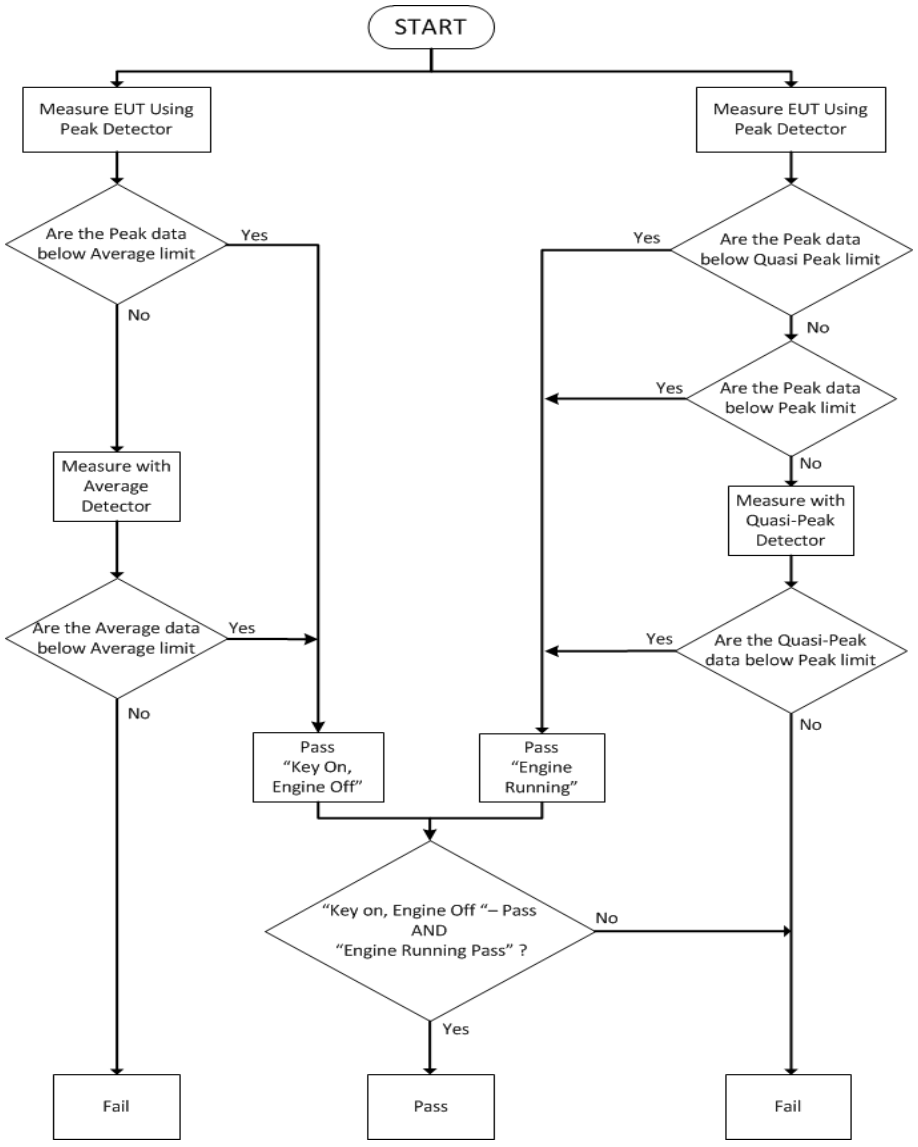

FIGURE 2.5: CISPR12 Determination of Conformance of Radiated Disturbance. Reproduced from CISPR 12

In practice the measurements are performed as two discrete tests. The broadband test is performed with the measurement receiver recording the amplitude of the emissions using a quasi peak detector. The quasi peak, peak and average detectors are described in Section 2.2.3. The narrowband test is run using a peak and average detector at the same time. In order to discriminate whether an emission is narrowband or broadband the peak and average value are compared, if there is greater than 6 dB between them the emission is deemed to be broadband in nature and not investigated as part of the narrowband test, as can be seen in figure 2.5. A brief description of the receiver detectors used during a emissions measurement are detailed below:

2.2.3 Receiver Detectors

Peak Detector

It is normal practice to perform initial measurements using the peak detector in the measurement receiver. The peak detector responds almost instantaneously to the peak value of the received signal, then discharges very rapidly. Thus if the receiver dwells on the frequency being measured, 10 ms being typical during an automotive measurement, the detector will follow the envelope of the signal and respond rapidly to any changes. The main advantage of the peak detector is the speed in which it enables measurements to be performed; with the detector very often being used for performing the initial investigations.

Average Detector

As the name implies this detector records the average amplitude of the received signal, the output is proportional to the Pulse Repetition Frequency, PRF, of the signal. The PRF is defined as the number of pulses of a repeating signal in a specific unit of time. If the detector is used to measure a continuous wave signal the amplitude recorded will be the same as if a peak detector were used. However, for pulse signals the average detector will always record a lower amplitude than the peak. If the PRF increases by a factor of 10 the average signal will increase 20 dB.

Quasi Peak Detector

The radiated emissions limits specified in CISPR 12 allow for a quasi peak detector to be used. The historic intention of CISPR type radiated emissions tests was to confirm that on-board radios would not be interfered with by other components within the vehicle. When the radiated emissions tests were first being developed the broadcast radios received signals in the long wave or medium wave bands using Amplitude Modulated, AM, signals. The quasi peak detector design was based on the output from a survey of a board of listeners. They were tasked with rating the 'annoyance factor' of signals with different PRF's on the AM radio reception as they perceived it. They concluded that high PRF signals offered the most annoying type of interference to their radio reception

experience. The quasi peak detector was designed to have a short charge time and long discharge time, thus a pulse type signal will show a lower value when measured with a quasi peak detector compared to the same signal measured with a peak detector. The output of the quasi peak detector is very dependent on the PRF of the input signal, the higher the PRF the higher the output of the detector. The limits allowable for radiated emissions, using the quasi peak detector, were then specified to guard against high PRF signals. Due to the long discharge times quasi peak measurements require a longer dwell time making the measurement very time consuming.

A comparison of the three detector types is shown in Figure 2.6.

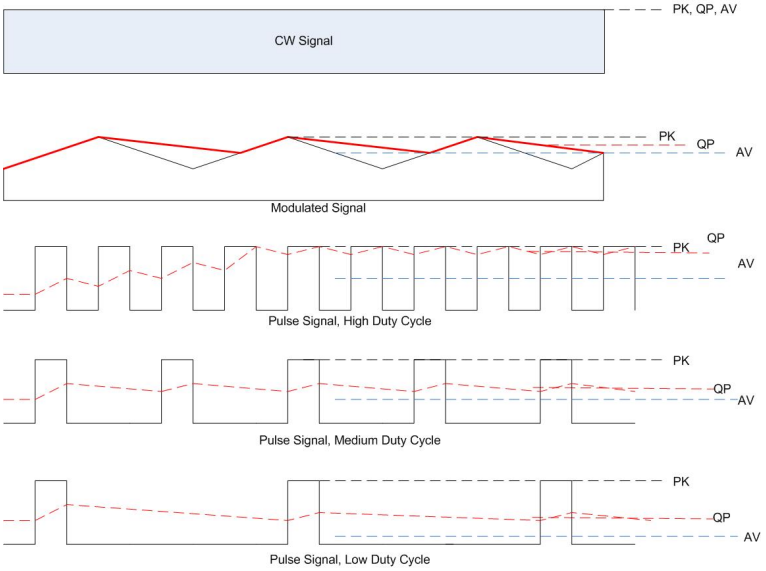

FIGURE 2.6: Detector Level Indication

2.2.3.1 Radiated Emissions Test Limits

The limits specified in radiated emissions Standards vary depending upon the frequency of interest and also the receiver detector being used to measure the amplitude of the E-field. As described in Section 2.2.3, the three main detectors used for performing radiated emissions measurements, peak, average and quasi peak, each has their own characteristics and will affect the amplitude of the signal that is recorded.

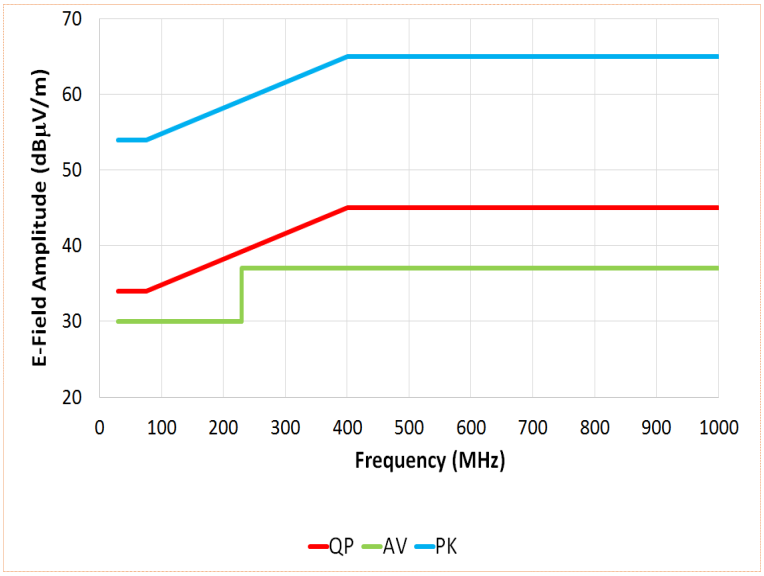

FIGURE 2.7: CISPR 12 Radiated Emissions Limits

Figure 2.7 shows the limits defined in CISPR 12 for each of the three measurement detectors. The EUT emissions measured must be below all three limit lines, for each of the detectors in order to comply with the requirements of the Standard.

2.2.4 Information Technology Equipment:CISPR 32

The first edition of CISPR 32 [31], which replaced CISPR 22 [5], was released in 2015 and has become the major international standard adopted for the measurement of radiated emissions from Information Technology Equipment, ITE. Within CISPR 32, ITE equipment is defined as any item who has a primary function of either, or a combination of the following: receiving data from external sources, processing received data, outputs data, stores data, displays data, switches or controls data or equipment that has a supply voltage rated at less than 600 V.

Many different economies have used CISPR 22 and more lately CISPR 32 as the basis for their own local standards, BS EN 55032 [26] in the UK for example. Since its initial release in 1985 CISPR 22 has been revised to the latest revision, version 6, being released in 2008 before finally being superseded by CISPR 32 in 2015. The standard describes procedures needed to measure the spurious emissions generated by ITE and states limits in the frequency range of 30 MHz to 6 GHz. Limits are applied only at certain frequency ranges within the full frequency span, measurements do not need to be performed where no limit is specified. Equipment is designated as being either Class A or Class B: Class A equipment being marketed for installation into light commercial, industrial or commercial environments, Class B devices are those marketed for use within domestic environment [26] and may include: Equipment with no fixed place of use, telecommunications equipment powered by a telecommunications network and personal computers and connected peripheral equipment.

The limits applied to Class B equipment are more stringent than those applied to for Class A products.

CISPR 32 specifies that equipment should be measured with a distance of 10 m between the EUT and the receive antenna. If measurements can not be performed at 10 m due to high ambient signal levels, for example, a 3 m measurement distance may be used. The following statement is made in Section C2.2.4 of CISPR 32 with reference to the reduced measurement distance:

> 'Where a test facility has been validated for a different measurement distance not defined in Table A2 to A7, the measurement may be performed at that

distance. In this case the limit L_2, corresponding to the selected measurement distance d_2 shall be calculated by applying the following formula:'

$$L_2 = L_1 + 20log(\frac{d_1}{d_2}) \tag{2.1}$$

where L_1 is the specified limit at the distance d_1 and L_2 is the limit at distance d_2,

For measurements performed at 3 m, the final version of CISPR 22 [32] detailed a limit increase of 20 dB should be applied. This change in limit has been reduced to 10 dB in CISPR 32 for the same measurement distances. This revised statement would suggest that the investigations performed by Garn et al, described in Section 2.2.2 should possibly be taken into account and testing at 3 m should be used with caution.

Measurements are normally performed at an OATS, ALSE or Fully Anechoic Room, FAR, with the ALSE and FAR being the more popular sites in recent years. The OATS, if used, should be flat, free of overhead cables and nearby reflecting surfaces. A ground plane shall extend by at least 1 m beyond the periphery of the EUT and receive antenna and cover the area in between the two. Measurements may be performed at an ALSE, provided it fulfils the criteria of the site attenuation test. The EUT is placed on a non conductive table, nominally 1.5 m x 1 m, this size may be increased if necessary to accommodate larger EUTs.

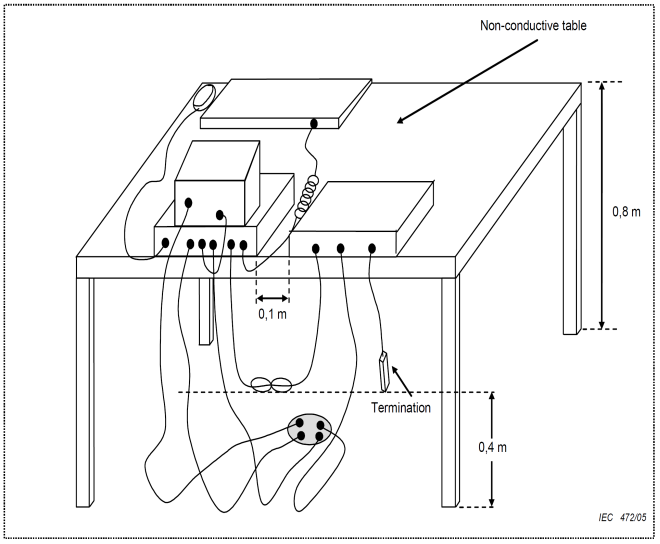

FIGURE 2.8: Typical CISPR 32 EUT Setup on Non-Conductive Table. Reproduced from CISPR 22

In contrast to the standard used for automotive components, the guidelines for the layout of the EUT within CISPR 32 are not so clearly defined. It is stated that the EUT should be positioned so that in the case of an EUT with peripheral devices there is a separation of 0.1 m between units. The rear of the EUT(s) should be flush with the support table any inter unit cables should be draped over the back of the support table. If the cable hangs closer than 0.4 m from the ground plane it should be bundled such that the centre of the bundle is at least 0.4 m above the ground plane. In order to record the maximum emissions from the EUT it should be operated in a mode and orientation of inter-connecting cables that is expected to produce this result, this 'cover all' description places the onus onto the test house to ensure that investigations are carried out to ensure that the maximum emissions are recorded. The mode, along with the rationale behind its choice should be stated in the report produced after the testing is complete.

During the measurement process the emissions are maximised by recording the emissions profile during a full 360^o rotation of the EUT. In practice this is generally achieved by performing an initial measurement sweep at a a small number of angles, typically less than 10. From these data the frequencies of maximum emissions are noted, the EUT is then rotated in order to find the angle at which the maximum level is recorded. Once this angle is found the receive antenna is scanned in height between 1 m and 4 m and once again the maximum emissions are recorded at each frequency. Using this method means that performing measurements is a very time consuming and in many cases expensive process. The likelihood that the maximum emissions amplitude from the EUT will be recorded depends in part on the azimuth resolution used during the EUT rotation and also the receive antenna height scan resolution. The finer the increment used, the higher the likelihood of recording the maximum amplitude will be. Test times will be affected by the increment size used, in both azimuth and height scan, the finer the increment, the longer the measurements will take. The above process is repeated with the receive antenna both horizontally and vertically polarised, with respect to the test facility floor.

2.2.5 Summary of Measurement Differences between the CISPR 32 and CISPR 12

As has been described in Sections 2.2.4 and 2.2.2 it can be seen that there a number of major differences between the CISPR 12 and CISPR 32 methods for recording the radiated emissions from a device under test. These differences are summarised in Table 2.4:

TABLE 2.4: Differences Between CISPR 12 and CISPR 32

Test Parameter	**CISPR 12**	**CISPR 32**
Emissions Maximised	No	Yes
Azimuth Scanning	No	Yes
Receive Antenna Height Scanning	No	Yes

Height scan and azimuth scan maximisation will be investigated further in Chapter 4 of this thesis. Through a program of simulations and measurements, the both factors are examined to determine the level of error in recording the maximum amplitude of the vehicle emissions introduced by not utilising them.

Chapter 3

EM Modelling for Automotive Applications

3.1 Introduction

Electromagnetic Compatibility measurements can be a very time consuming activity, with a typical suite of emissions or immunity measurements taking between several hours to several days to complete (depending upon the Standard being applied to measurements). With the advent of faster and more powerful computing capabilities it is though that simulating real world EMC problems, such as radiated emissions signatures, can become a reality. The use of simulation software to solve complex electromagnetic problems has been the aim of a great deal of research since the early 1960s, but up until very recent times the computing power offered by even some of the most advanced super computers has meant that the simulation of complex problems at high frequencies has not been possible. As computers have continued to increase in speed, in line with Moore's Law [33], it has been possible to increase the possibilities for EM simulation. It is not not known whether simulation will ever develop to the level whereby it can replace measurements altogether (if so, this juncture is probably still many years away). However the use of simulations during the design stages of a an electrical device development may help to reduce the amount of issues seen when the device enters the EMC validation process.

The complexity of Electromagnetic, EM, modelling techniques when applied to automotive applications is increased by a number of variables [34]. Two of the most influential of these variables are the complexity of the vehicle body shell and the wiring harness. In a modern road car the harness can be in excess of 3 km long if it were to be laid end to end, this enormous length, coupled with its very small cross sectional area make producing accurate EM models of it very difficult. This is further complicated by not only the electrical tolerances of the wiring, but also by the geometrical tolerances.

3.1.1 EM Modelling Development

When a model is originally designed the engineer is faced with a number of important decisions, possibly the first being what is the intention of the model i.e. what is the engineer hoping that the model will be able to tell them about its electromagnetic characteristics. This may range from electric and magnetic fields, currents, voltages, through to derived quantities such as scattering parameters and far field properties of antennas. The design of an EM model is always a compromise between the amount of time required to firstly produce the model, and also to run the simulations using the model and the amount of extra information contained in the results as a consequence of the more detailed model. Once the output has been decided upon, the level of detail required in the model can be deduced. The engineer is constantly facing the compromise of reducing the amount of detail contained in a model to the simplest level to produce the required results without reducing it so far that the results become meaningless. Even the most detailed models will only ever produce an approximation of the results that would be obtained through actual measurement of the item the model was based upon. It can be argued, however, that a measurement will also only record an approximation of the E-field. specific to the particular test setup used. The output of the simulation software is able to deliver information such as the X, Y or Z component of the radiated electric field, field amplitudes based upon the model being placed in a perfectly anechoic position amongst others. Obtaining the orthogonal components of the electric field in isolation may never be fully achieved by using real world measurements, an antenna receives a portion of the vertical component of the electric field when it is in the horizontal orientation and vice versa. The overall quality of the output from any simulation software will be governed by: the overall fidelity of the Computer Aided Design, CAD, data used to develop the EM model, how well the electrical properties of the different materials

used in the model were defined and the discretization methodology used when the model was meshed [35].

It should be noted that in the context of this research a standard CAD model that may be used during crash or aerodynamics investigations is not the same as an Electromagnetic model, which in turn, is not the same as an EMC model. If an 'EMC' model were to be developed, and this is the ideal goal hoped for by many vehicle manufacturers, the model would not only contain a comprehensive, detailed model of the device to be simulated; a vehicle for example, but it would also contain full electromagnetic information of all the individual modules and components within the vehicle and how they interact with one another. This ideal may be many years away, but with current advances in computing power and as EM modelling knowledge expands it may yet become a reality.

3.1.1.1 Meshing

With the advent of modern CAD and its subsequent use within the automotive design process, highly complex electronic model data of vehicles is being developed. These data are being used for a number of functions during the design flow, ranging from aerodynamics to crash worthiness simulation. The models produced contain many layers of detail, down to the smallest nut, bolt and bracket. Whilst this level of detail is needed for certain functions it is not required, nor can today's EM simulation packages deal with this amount of data.

The output of industry standard CAD packages such as Computer Aided Three Dimensional Interactive Application, CATIA, organise the vehicle parts into different categories, these categories can then, in turn, be extracted individually to form the required data to produce an EM model. When items such as the body shell are extracted from the initial CAD data a certain amount of work is still required to get the model to a usable state. For the purposes of an initial investigation, for example, the bare minimum of detail may be required to describe the body shell, features such as gaps between panels, air vent holes and plastic parts are more than likely not required. The body shell can quite easily amount to several thousand different parts. If all of this detail were to be included into the EM model the meshing requirements needed to model this fine detail would be far in excess of that needed or able to be dealt with by even the fasted modern Personal Computers, PC.

When a CAD model is imported from a package such as CATIA it will invariably have defects due to the import process, such as missing surfaces or incorrectly generated surfaces. These defects must be corrected using a CAD modelling package; in the case of this research GMESH [36] was used. The process of correcting problems in the model can be very time consuming, often taking several man days in the case of a complex model

3.1.2 EM Modelling Validation

In order to produce results that can be considered reliable, any electromagnetic model needs some method of validation. The preferred method of validation is to compare the unknown case against a known set of results [37], where no standard known reference is available validation can be achieved using a self referencing method. The self referencing method, though not as comprehensive as the known reference method, can still offer a high level of confidence if implemented correctly.

Validation methods can be split into a hierarchy of three levels: Mathematical level, Implementation Level and Model Level. The first of these three levels is useful to determine whether the actual computational technique being used is correct, Method of Moments, MoM, Boundary Element Method, BEM, Transmission Line Method TLM, Partial Element Equivalent Circuit, PEEC. The second level can then check that a particular software vendor's implementation of the chosen technique is correct and finally the third level validates the actual model being used. In order to obtain reliable results all three of these stages must be correct.

For many users the top level of the hierarchy is unnecessary. The actual techniques; the method by which the Maxwell's equations are solved, have been validated by many sources. If the user is developing a completely new technique, then this stage would become necessary in order to determine the strengths and weaknesses of the new approach.

The second level is needed to determine if the chosen software implementation of the computational technique is suitable for the actual problem in hand. One technique may offer excellent results for a particular problem; it does not follow that this method will be the best for every, or indeed any, other problem. Generally the software vendor will be able to supply a number of example problems where the results show good correlation

with calculated or measured results. By choosing an example problem that is similar to the users problem, confidence can be gained that the technique, and the vendors implementation of it are suitable for use.

The third level is by far the most frequently used. It is used to validate a particular model. This is, however, where some of the problems with model validation manifest themselves. If the top two levels of validation have been confirmed to be good, it can probably be relied upon that the output of the simulation software will be a very accurate representation of the solution to the 'question asked', whether that question was the 'correct' question is an entirely different matter. It can be very easy for the user to incorrectly specify vital parameters during the design stage of the model.

The Standard for the validation of Computational Electromagnetic, CEM, models [37] suggests that user must apply a certain amount of engineering judgement when designing and validating a CEM model to gain some confidence that the basic principles utilised in the model are technically sound. The Standard recommends that when using methods such as MoM and PEEC, the output of the simulation will be based upon the calculation of the surface currents over the whole structure, these currents are then used to determine the radiated electric fields. By viewing the currents at specific frequencies, in particular at resonant frequencies, standing wave behaviour around discontinuities in the metal surface of the structure can be observed. The currents should not vary rapidly in adjacent segments and should be approaching zero at the ends of planes and wires. A simple check on these points can immediately indicate that there is a problem with the model. Additionally it is suggested that a popular approach to the third level of validation is to perform simulations on the same model using two or more different modelling techniques. A similar result with the different technique should give the user confidence that the model correctly describes the physics of the problem.

3.1.3 Validation Techniques

3.1.3.1 Convergence Testing

Convergence testing is a popular method of validating a model [38]. Before the convergence testing can begin, a number of parameters within the model must be defined. Firstly the mesh size should be set, often a starting point of $\frac{\lambda}{10}$ is used in an attempt to satisfy the

condition that the current / fields etc. do not vary much within each individual mesh element. For models where the observed field or current varies rapidly with distance over the structure, the mesh size may need to be further decreased in order to ensure that the the $\frac{\lambda}{10}$ assumption regarding variation across an element is met. In order to validate the model, the mesh size is decreased and the results compared with the previous iterations, if the results have changed then the mesh size can be regarded as being too coarse, if no change is observed a fine enough meshing has been achieved.

As a further method of validating a model, the surface current distribution can be examined after the simulation has been run. The current flow lines should be smooth with slowly varying changes in orientation of the current vectors. If the vectors show sudden direction changes in adjacent patches this is a sign of a possible problem with the model, a common fault being the mesh being too coarsely discretised compared to the frequency at which the simulation is to be applied. This is illustrated in Figures 3.1 and 3.2, these figures were generated using CONCEPT II EM Modelling software [39]:

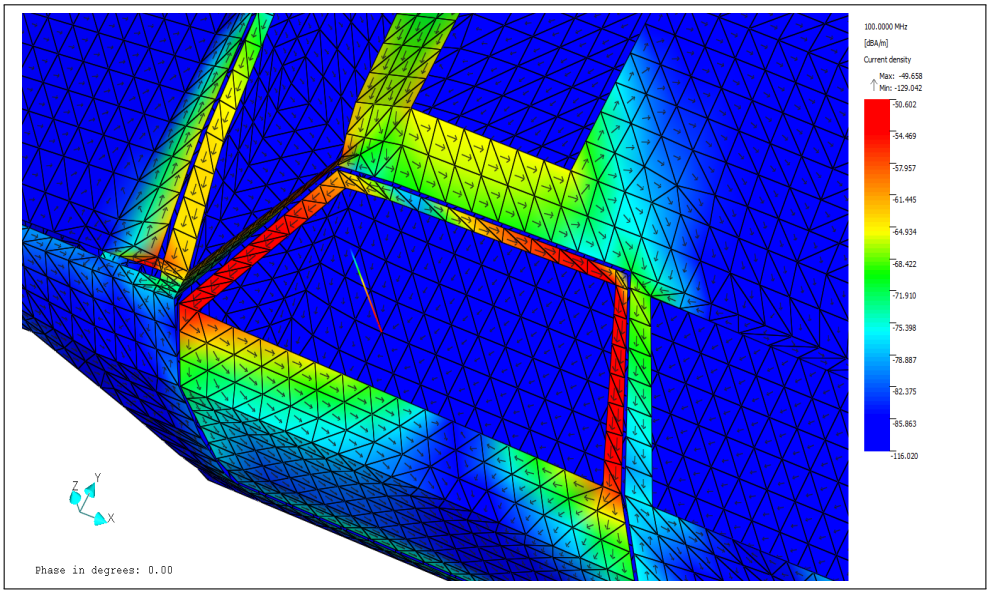

FIGURE 3.1: Correctly Discretized Mesh Surface Current Vector Distribution

As can be seen in Figure 3.1 the arrows describing the orientation of the surface current vectors can be seen to vary very little in direction from one patch to the next, forming a smooth and gentle variation.

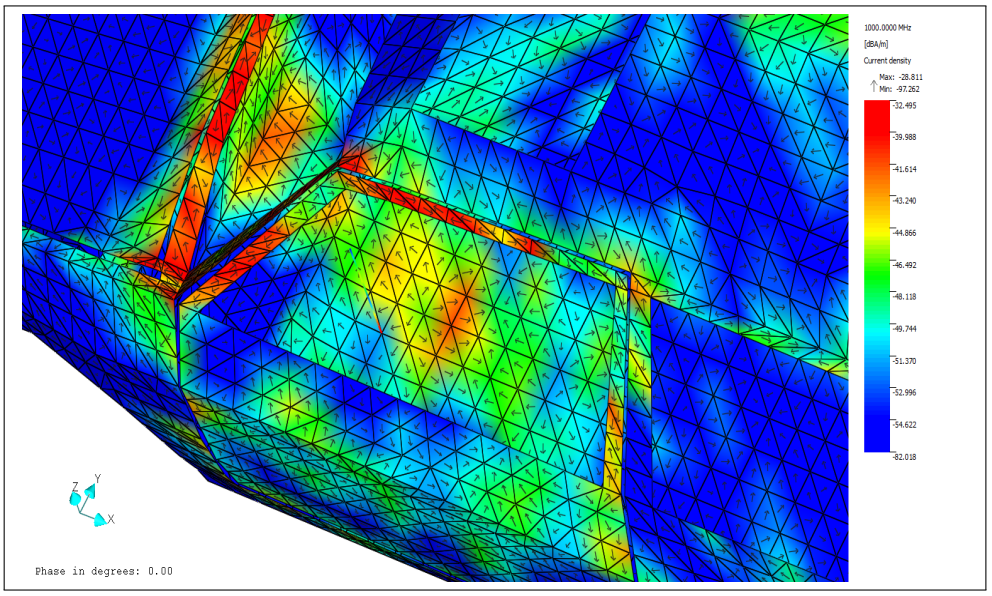

FIGURE 3.2: Under Discretized Mesh Surface Current Vector Distribution

In comparison the arrows in Figure 3.2 show an almost random direction in some places; their orientation varying dramatically from one patch to the next. These two images were produced using the same model but with the simulation run at 100 MHz and 1 GHz respectively. The only physical difference between the two simulations is at 100 MHz the model is correctly discretised, the mesh length being less than $\frac{\lambda}{10}$), whilst at 1000 MHz the model is under discretised, the mesh length being greater than $\frac{\lambda}{10}$).

3.1.4 Electromagnetic Modelling of Electrically Large Systems

Electrically large systems, such as a motor car, along with its wiring harness and on-board antenna, can be considered as a complex multi port antenna [34]. If elements of the system are changed, such as the design of the body shell, repositioning of wiring or modules or fitting of items such as heated windscreens, the 'antenna' formed by the whole system will be re-tuned resulting in a different emissions signature [40].

When modelling items such as a whole vehicle there are many things that must be taken into consideration during the process of producing the model, a selection of the questions one needs to address are: what is the model trying to show, is basic CAD data available on which to base the EM model, how will the model be validated, what level of accuracy is needed, what materials are the parts of the model made from (metal, dielectric) and what is the frequency range of interest ?

The starting point for an EM model of an item such as a car is very often a CAD model. These models are not necessarily the same. While the CAD model of a vehicle will generally show construction information to a very fine level of detail, this probably wont be required for the EM model. One of the first tasks to be under taken is to remove unwanted details in the CAD model. For the purpose of early investigations into the field levels inside the vehicle a basic body shell model may be all that is required, thus all items such as dashboard, wheels, drive train, lights etc. may be deleted. However as the design process continues some of these items could get added back in.

The outer surfaces of the vehicle body shell will determine the scattering characteristics of the vehicle under illumination from an external RF source [41], whereas the internal structure of the body shell will determine the internal resonances. In cases where the separation between the external and internal surfaces is significant both will be required in the model.

An important point to consider when producing an EM model is that all wires are connected at a node in the mesh of the model, i.e. not in the middle of a patch. This is shown graphically in Figures 3.3 and 3.4. In the example shown in 3.3 it can be seen that the vertical wire is joined to the body of the model in the middle of a patch.

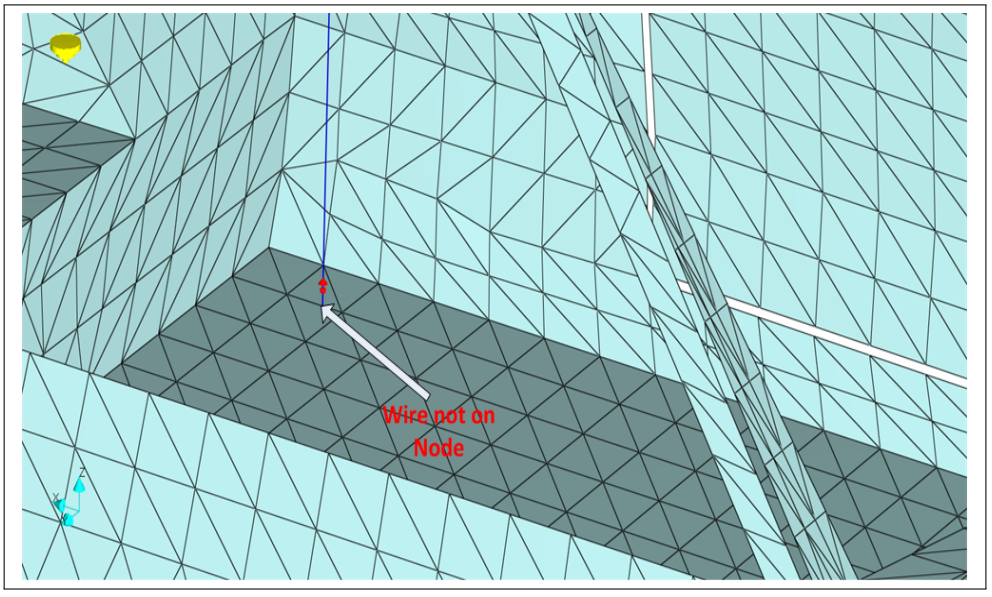

FIGURE 3.3: Example of Wire Not Connected to Node in Mesh

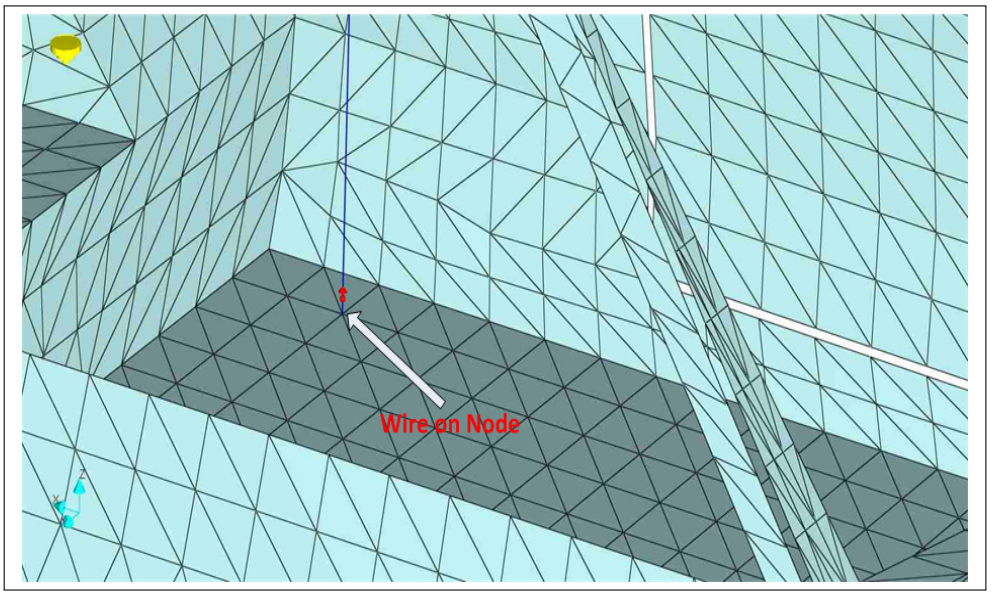

FIGURE 3.4: Example of Wire Connected to Node in Mesh

The vehicle wiring harness forms a very important part of the model. There are a number of possibilities when it comes to modelling the harness within the vehicle; initially the simplest method is to integrate the harness using a 'thin wire' representation. To fulfil the requirements of a thin wire, the length of the wire, L, must fulfil $L >> a$ and $a << \lambda$, where a is the wire radius, L is its length and λ is the wavelength of interest. Hence it can be seen that wires should be much longer than they are thick.

A method that is becoming increasingly more common, and that overcomes some of the inherent problems of the 'integrated harness' method, is to model the harness as a transmission line. In a vehicle the harness is generally routed very close to the metal chassis, thus enabling separated methods to be employed. This method involves the combination of CEM simulation of the vehicle without the harness present, with many network simulations of the harness. This method is only of benefit for the sections of the harness that run in places such as the foot well and along the rear body work (rear lighting harness for example). Where the harness is located further away from the body shell (engine bay and within the dashboard for example) the transmission line approximation no longer holds true and the harness needs to be modelled as part of the overall vehicle model.

3.1.4.1 Electromagnetic Vehicle Body Shell Model

The two electromagnetic Vehicle Body Shell (VBS) models used for the simulations within this thesis consisted of the main body shell, with doors, bonnet and a hatchback. The model did not have any interior, wheels, drive train, suspension etc. This simplified model then allowed for a reduction in the computational requirements for performing the simulations. The VBS model was based on a typical family hatch back, the overall size of the model is 3.9 m x 1.6 m x 1.4 m. The VBS 2 model is 3.8 x 1.8 x 1.3m. Due to most actual production vehicle CAD data being commercially sensitive it was not possible to obtain a model of a 'real' vehicle. The models actually used are generic body shell supplied with the CONCEPT II EM Modelling software used to perform the simulations. Figure 3.5 and 3.6 show further details of the models used:

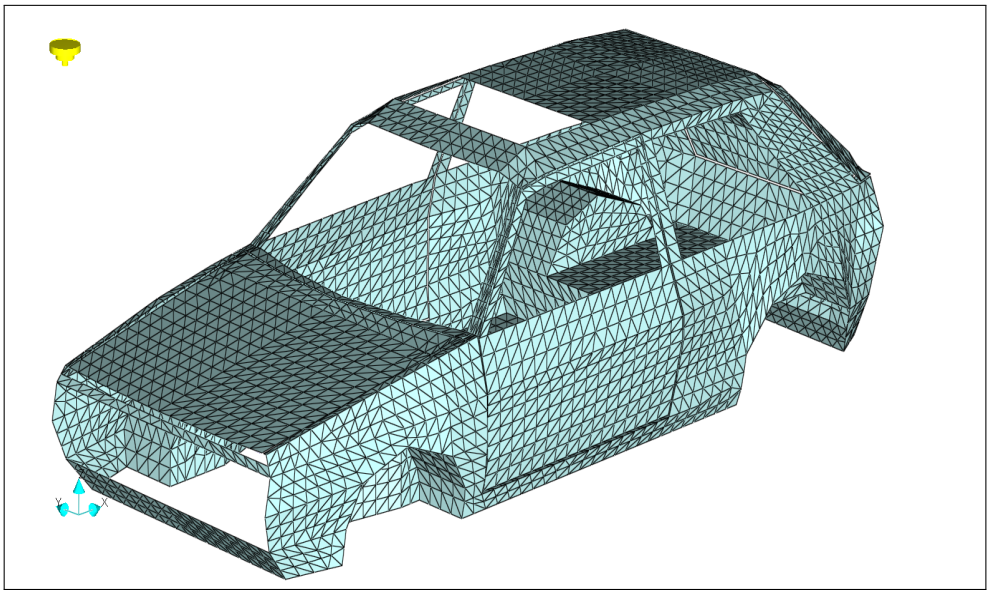

FIGURE 3.5: Vehicle Body Shell (VBS), Electromagnetic Model

Details of the VBS2 model are shown in Figure 3.6.

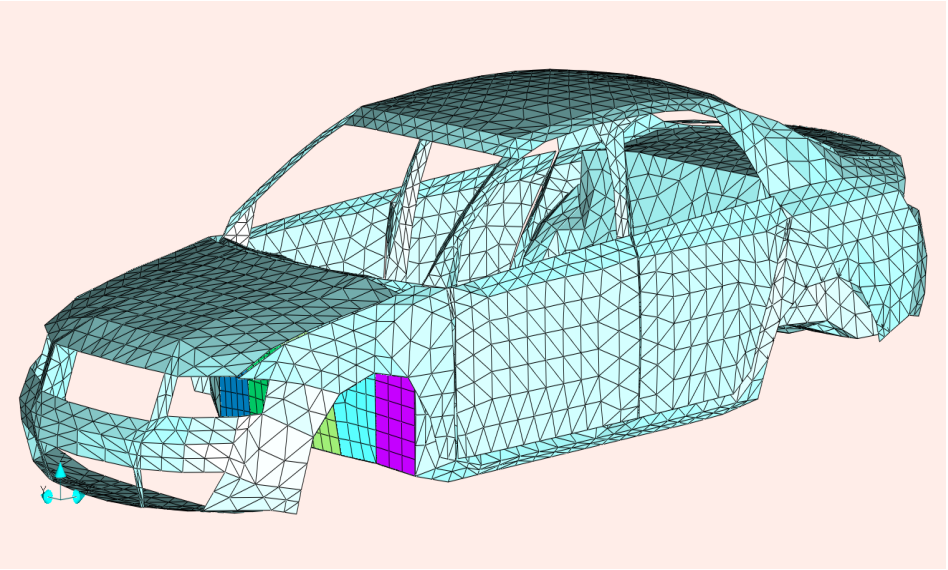

FIGURE 3.6: Vehicle Body Shell 2 (VBS2), Electromagnetic Model

Around the doors and boot / bonnet, a small gap was modelled to delineate the body from the other panels of the vehicle as detailed in Figure 3.7.

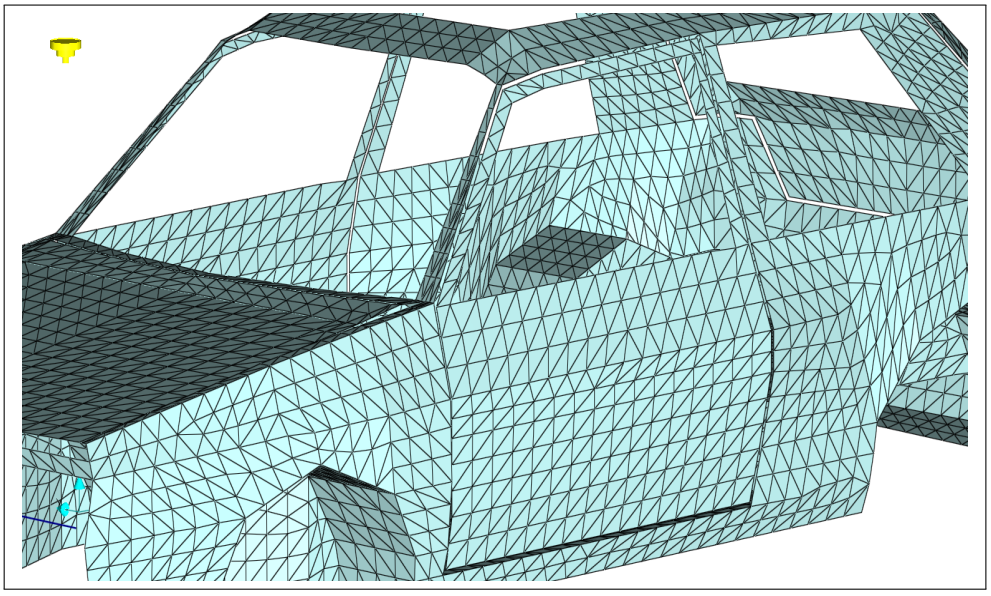

FIGURE 3.7: Vehicle Body Shell Model Detailing 'Gaps' Around Doors

Figure 3.8 shows the locations of the 'A', 'B' and 'C' pillars on a vehicle body shell. These locations will be referred to in later sections of this thesis as a means of identifying specific points on the vehicle.

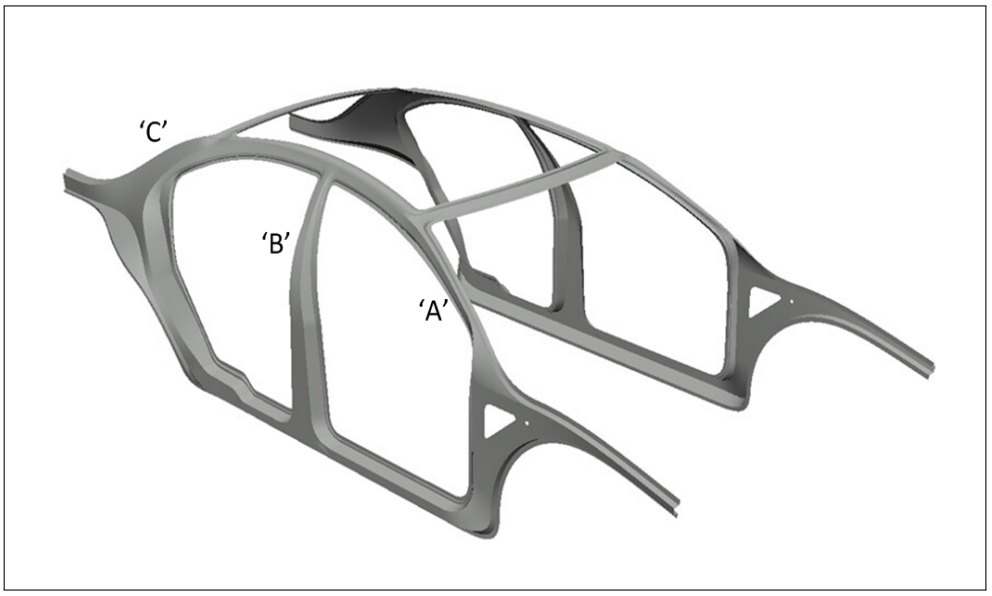

FIGURE 3.8: Location of 'A', 'B' and 'C' Pillars on Vehicle

The model of the VBS was simulated using CONCEPT II [39], over the frequency range of 50 MHz to 500 MHz for the purposes of the investigations performed during the course of this project. The model was excited using a short monopole antenna positioned at the 3 discrete positions within the body shell structure detailed in Table 4.2, two positions were within the passenger compartment and the third was in the engine bay of the car. The two monopole antennas positioned inside the passenger compartment of the model were vertically orientated, the engine bay monopole was positioned horizontally, across the width of the engine bay, as can be seen in Figures 3.9 and 3.10.

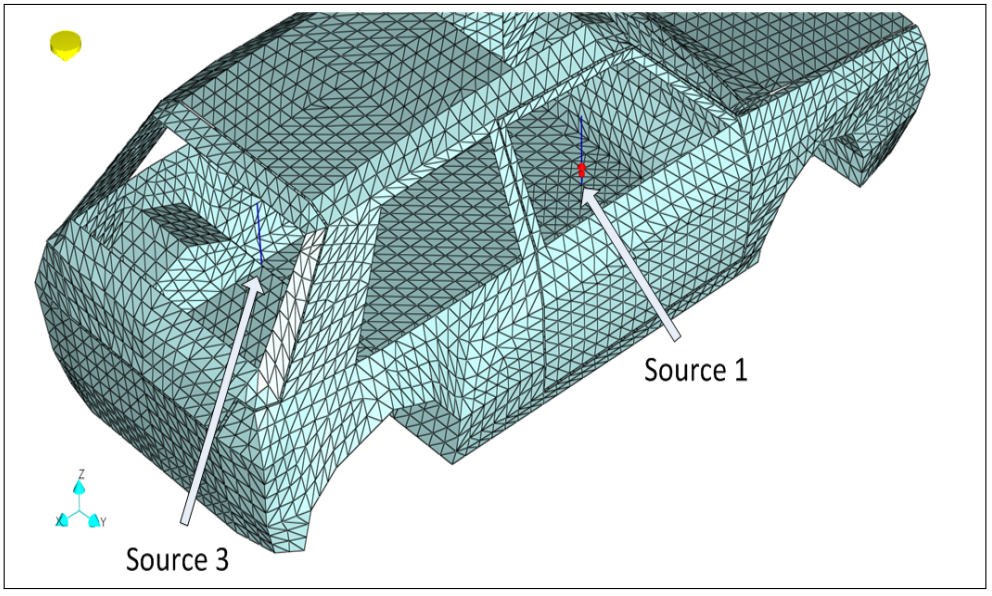

FIGURE 3.9: Location of Sources 1 and 3 Within VBS Model

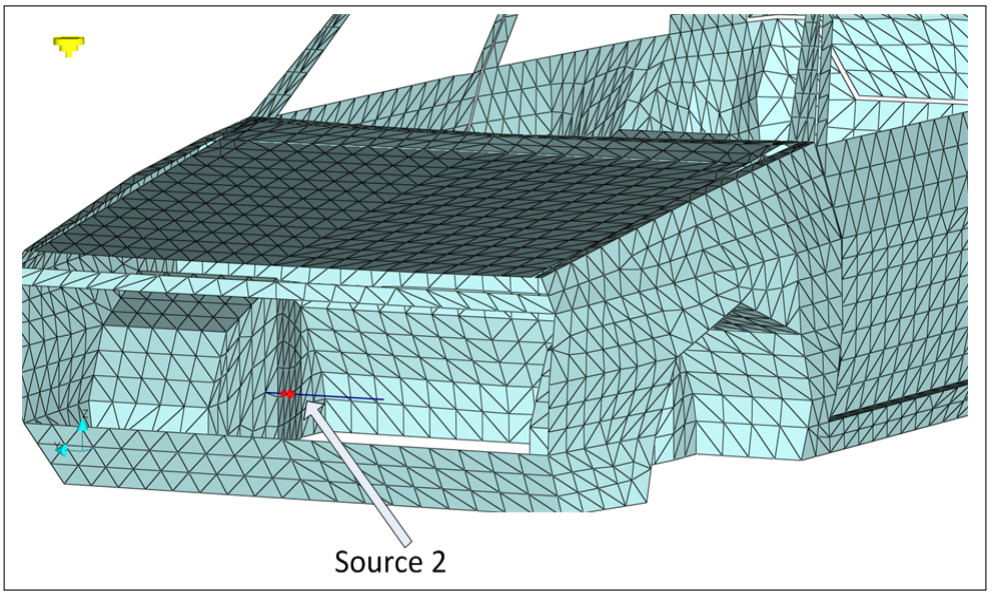

FIGURE 3.10: Location of Source 2 Within VBS Model

3.1.4.2 VBS EM Model Design

The EM models were built using a triangular mesh size of 0.06 m x 0.06 m, the dimensions were chosen in order to meet the suggested minimum mesh size of $\frac{\lambda}{10}$ at the maximum frequency of interest, 500 MHz [39]. A general mesh size that meets the criteria stated above was used for the majority of the model, however, it is known that in areas of high surface current density, or rapid spatial current change, a more refined, or smaller mesh size should be used. In order to determine the likely positions of the high level surface currents simulations were performed at 500 MHz, the highest frequency being considered for this research. Once the simulations were performed a surface map of the currents induced onto the body of the vehicle were produced. This procedure was repeated for each of the source positions to investigate whether the high current areas occurred in any common positions on the body shell. As detailed in Figure 3.11 the areas of high surface current can be seen.

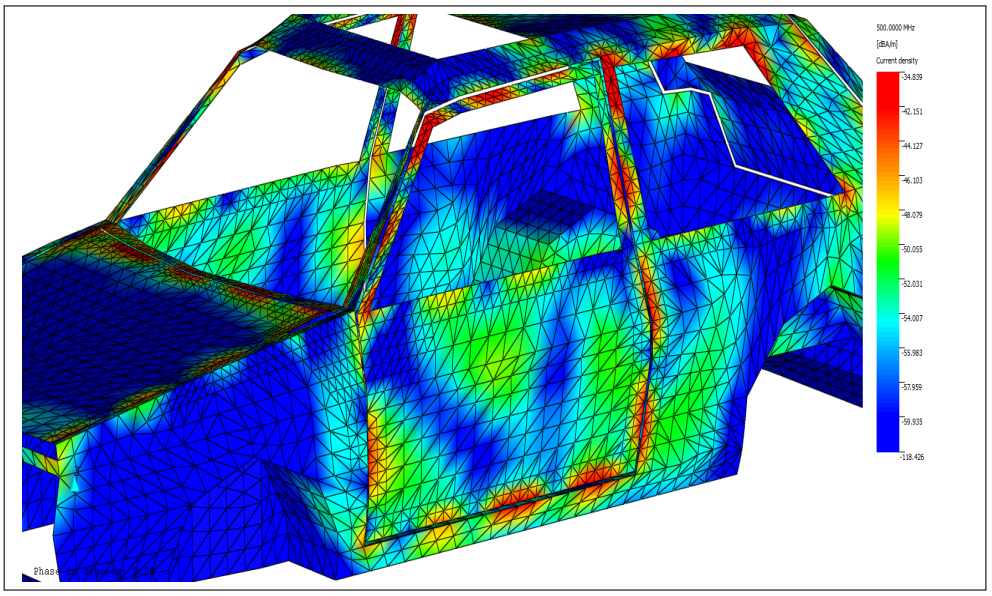

FIGURE 3.11: Surface Current Investigation

A finer mesh was used in areas that high surface current density or rapid spatial rate change of the current were evident from the surface current investigations. These areas were around the location of the monopole antennas, the door frame 'A' pillars, and gaps around the bonnet lid. The refined mesh size utilised was 0.03 m x 0.03 m, as shown in Figure 3.12. The use of localised refinement of the mesh enables these areas to be more accurately modelled without significantly affecting the overall simulation time, as would be the case if a finer mesh were used throughout the model.

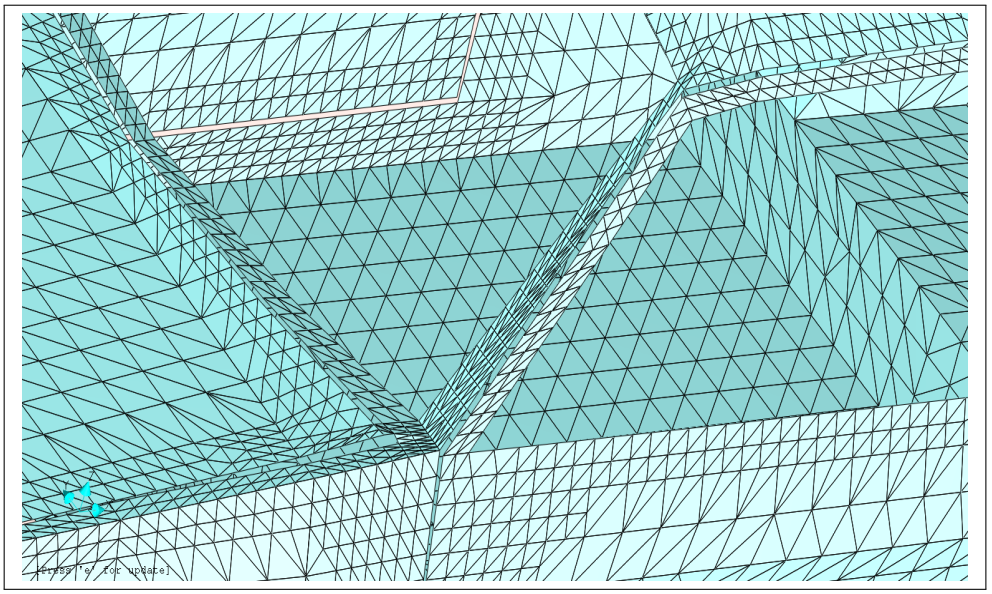

FIGURE 3.12: VBS Model with Locally Refined Mesh around 'A' Pillars and Top of Door

3.1.4.3 Chapter Summary

This Chapter has highlighted that EM modelling is becoming an increasingly more important part of the design process of electrical items. It allows the designer to investigate the EMC properties of their chosen design early in the process, very often before any items have actually been manufactured. The increase in computing power has allowed EM simulations to be run in a much more timely manner, speeding up the design process as multiple iterations can now be investigated in a much shorter period of time. In the realm of automotive EMC, it is felt that the industry is still some way off being able to simulate a 'complete' vehicle, i.e. one that comprises of all the constituent parts of the vehicle, however, this goal is getting closer with each passing year.

As an investigation tool into fundamental properties of an EM model, such as radiation patterns from sources inside the vehicle, electric fields inside the cavity of the body shell, surface currents flowing over the body shell for example, it offers many advantages over traditional measurements. Both measurements and simulations are not without their own inherent problems and both should still only be considered as producing an approximation to to the results they are aiming to produce. The comparison of measurement and simulation data is becoming an integral part of the design iteration development. However, as a method of producing EMC data with minimal financial expenditure building physical models of the device under development, EM modelling has many positive benefits to offer the design engineer.

Both EM simulations and physical measurements are used in the following chapters of this thesis, with 'proof of concept' being confirmed by simulations prior to any measurements being performed. Overall, in the majority of cases detailed through this research, a good level of agreement between the measured and simulated data was recorded.

Chapter 4

Factors Affecting Radiated Emissions Results

4.1 Introduction

This chapter presents a review of some of the fundamental concepts used in vehicle radiated emissions measurements are presented in this chapter. The main objective of this chapter is to quantify each of the parameters that affect the results of the radiated emissions test. Each of the factors will be discussed in turn. Measurement and simulated test results are presented that will quantify the effects.

The factors investigated are: receive antenna height, number of azimuth angles used, and the frequency range over which the measurements are performed. The first two items listed above have a direct influence on the amplitude of the emissions recorded and are also the parameters that differ mostly when the CISPR 12 method is compared to other radiated emissions test standards used for non-automotive applications. The frequency range was investigated to determine the typical upper cut-off frequency; where vehicle emissions have fallen to a sufficiently low threshold that they can be considered as not causing an interference issue. This upper threshold will be quantified and be used later in this study.

4.2 Receive Antenna Height Scan

4.2.1 Introduction

The main philosophy behind performing radiated emissions measurements is to give a level of confidence that an item will not interfere with other radios and other electronic devices when it is put into service. The methods employed at an OATS facility will not necessarily measure the absolute maximum emissions of the EUT, but will record a maximum level for that particular test setup in that test environment. What is meant by that is, the measurement process will only record the maximum emissions within the bounds of the parameters used, for example the rotational angular increment used, the frequency range of the measurement, height over which the receive antenna is scanned.

As described in Section 2.1.2.1 a conductive metal ground plane is employed at most OATS. The ground plane is used with an aim of improving the repeatability of the measurements, this does not represent how the emissions will impinge on other equipment in the 'real world'. If the measurements were performed without the ground plane, reflections off the ground would still occur but the reflected signal would vary over time due to variations in the moisture content and conductivity of the ground. If a conducting ground plane is used an electric field incident upon it is reflected at an angle equal to the angle of incidence, through Snell's Law: $\theta_i = \theta_r$ [9]. If the ground were non conductive, soil for example, a vertically polarised field would be reflected at all angles of incidence with a small amount being refracted through the soil as described above, except at an angle known as the Brewster angle [9]:

$$\theta = \texttt{arctan}\frac{n_2}{n_1} \tag{4.1}$$

where n_1 and n_2 are the refractive indices of the two media in question, in this case air and the soil / ground. At this angle the electric field is no longer reflected but it is fully absorbed into the ground. This angle is also dependent upon the wavelength of the electric field since the refractive index of the medium is also frequency dependent. The Brewster angle does not apply for horizontally polarised fields.

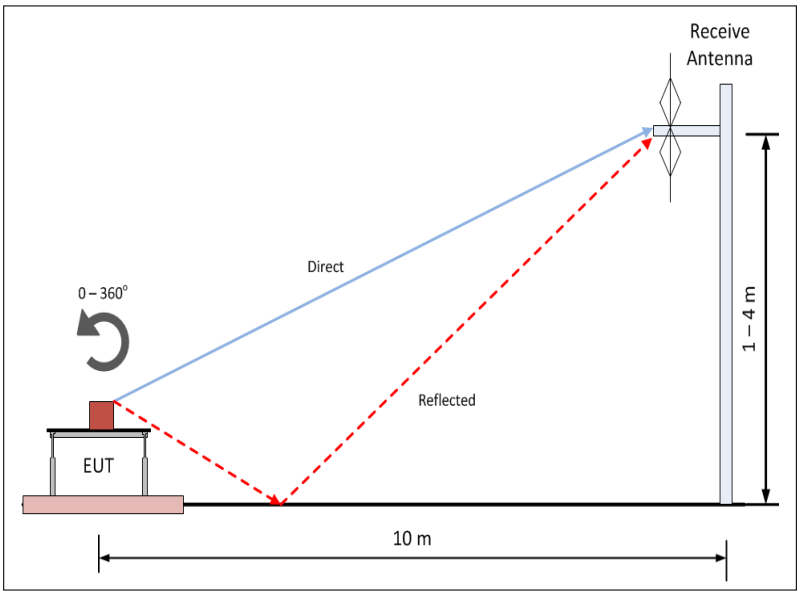

FIGURE 4.1: Basic EN55022 OATS Antenna/ EUT Setup

Due to the presence of the ground plane as shown in Figure 4.1 the measurement system in an OATS and also in a semi anechoic chamber, will actually be recording the sum of the direct and reflected emissions paths.

As detailed in Section 2.2.4 most commercial radiated emissions standards define that the amplitude of the emissions recorded should be maximised by scanning the receive antenna in height above the ground. The CISPR 12 radiated emissions test does not include height scanning of the receive antenna, instead a fixed height of 3 m for a 10 m measurement distance is used. Studies have shown [24] that by scanning the receive antenna in height to maximise the emissions, amplitude values of between 5 dB and 7 dB higher than by using a fixed 3 m receive antenna height can be recorded.

Next a summary of the theory of how scanning the receive antenna in height affects the amplitude of the emissions recorded will be explained. The theoretical calculations presented in the section are based upon the test object being an electrically small, isotropic point source. Simulated and measured test results from an electrically small dipole source are then presented to qualify the theory. The measurements were performed using both an electrically small EUT, a wide-band noise source with short monopole antenna and also using a larger, extended source; a car. The results recorded using both source EUTs will be discussed and compared to the theory.

4.2.2 Height Scan Theory

It has been shown [42] that the maximum emissions of an electrically small, isotropic source, measured at a distance of 10 m, over a conducting ground plane, do not occur at a single antenna height above the ground. In order to record the maximum level of E-field the receive antenna must be scanned in height, the height at which the maximum will be recorded varies depending on frequency. Due to the emissions being reflected by the metal ground plane the antenna will actually receive a direct signal and a reflected signal from the Equipment Under Test, EUT. These signals will add or subtract from each other, due to their phase difference caused by the differing path lengths. This would result in erroneous results if the antenna was left at a single height above the ground. To overcome this problem the antenna should be scanned in height, between 1 m and 4 m for a 10 m and 3 m test distance. At some point over this scan range a maximum emission will be found, the point at which the direct and reflected signal arrive in phase with one another and add together constructively. The maximum emissions will occur when the receive and transmit antenna are in the same plane.

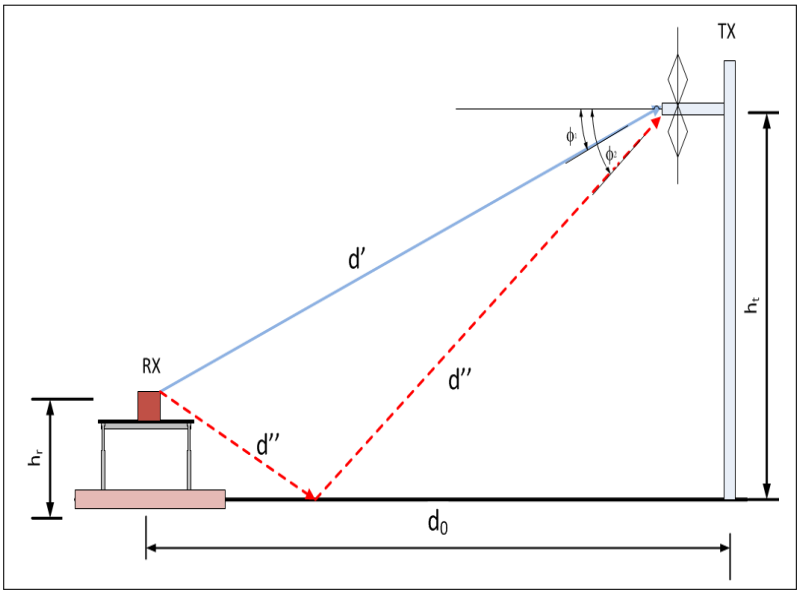

FIGURE 4.2: Basic CISPR 22 Antenna/ EUT Setup

The theory of operation of the OATS can be described using the method of images, it is based on geometric optics and considers a direct and a ground reflected emission path from the EUT to the receive antenna. The total electric field received at the antenna is

a combination of the direct signal line of sight signal, E_d and the ground reflected signal E_r.

The EUT is placed at height of 0.8 m (h_t), and the antenna is scanned in height from 1 m to 4 m (h_r).If the free space E-field is E_0 at a reference distance, d_0, from the EUT then the E-field recorded at an OATS would be the vector sum of E_d and E_r, and is given by

$$\overrightarrow{E}_{Total}(d,t) = \overrightarrow{E}_d + \overrightarrow{E}_r \tag{4.2}$$

which becomes:

$$\overrightarrow{E}_{Total}(d,t) = \frac{E_0 d_0}{d'} e^{-j\omega(t\frac{d'}{c})} + \hat{\Gamma}\frac{E_0 d_0}{d''} e^{-j\omega(t\frac{d''}{c})} \tag{4.3}$$

where ω is the radiated emission frequency (rad/s), c is the speed of light (m/s) and Γ is the reflection coefficient. and:-

$$d' = \sqrt{d_0^2 (h_t + h_r)^2} \tag{4.4}$$

$$d'' = \sqrt{d_0^2 (h_t - h_r)^2} \tag{4.5}$$

For horizontal polarisation the incident and reflected waves are parallel to the ground plane, the reflection coefficient is defined as:-

$$\hat{\Gamma_h} = \frac{\hat{E}_r}{\hat{E}_i} \tag{4.6}$$

Which becomes

$$\hat{\Gamma_h} = -1 \tag{4.7}$$

Due to the fact that the electric field of both the incident and reflected wave are both tangent to the ground plane the total electric field must be zero, from the boundary condition, thus the reflected electric field must be opposite to that of the incident wave.

For vertical polarisation the incident and reflected Electric field waves are perpendicular to the ground plane, the reflection coefficient is defined as:-

$$\hat{\Gamma_v} = \frac{\hat{E}_r}{\hat{E}_i} \tag{4.8}$$

Which becomes

$$\hat{\Gamma_h} = +1 \tag{4.9}$$

For vertical polarisation the tangential components are the z components which must be equal and opposite, in order to satisfy the boundary condition. Thus the incident and reflected electric fields must remain unchanged with respect to their propagation vectors as shown in Figure 4.3.

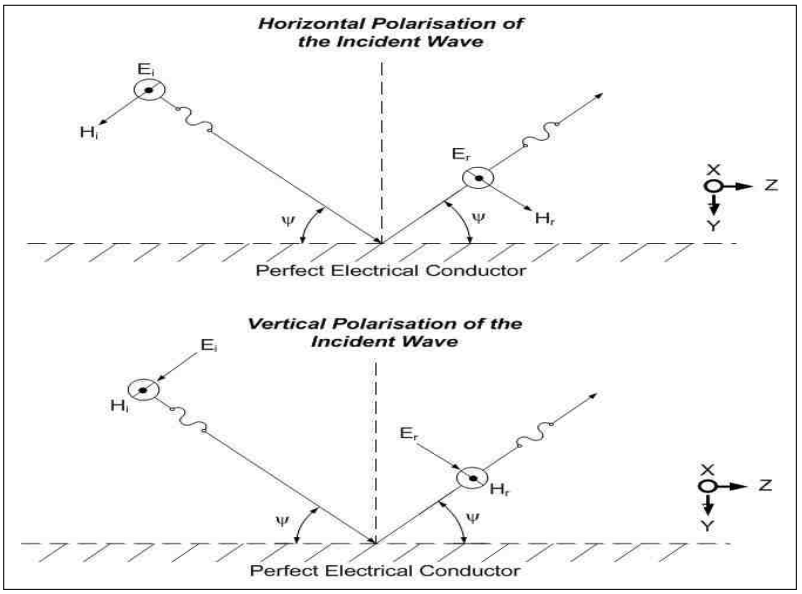

FIGURE 4.3: Uniform Plane Wave with an Oblique Incidence to a Perfect Conductor

For a perfect conductor the coefficient of reflectivity quoted in equations 4.6 and 4.8 apply regardless of the angle of incidence. Substituting these values of $\hat{\Gamma}$ into equation 4.3 allows the maximum E-field for a particular frequency to be determined for different antenna heights.

Figure 4.4 show the theoretical height at which the maximum emissions occur for frequencies between 30 MHz and 1 GHz using a height scan of between 1 m and 4 m, as calculated by Kelong and Yougang [42]. The height at which the maximum emission occurs for

frequencies below 230 MHz is detailed as 4 m. This is not exactly correct, the actual height is higher than this but is stated as 4 m due to this being the maximum height scanned in the typical radiated emissions measurement process.

Figure 4.4 shows that using a single height for the receive antenna will result in the maximum emission from the EUT not being correctly measured. These results are only true for measurements performed in the far field. They do not account for the gain of the receive antenna or the EUT. The results also demonstrate that the maximum emission from an EUT does not occur at the same height for horizontal and vertical polarisation.

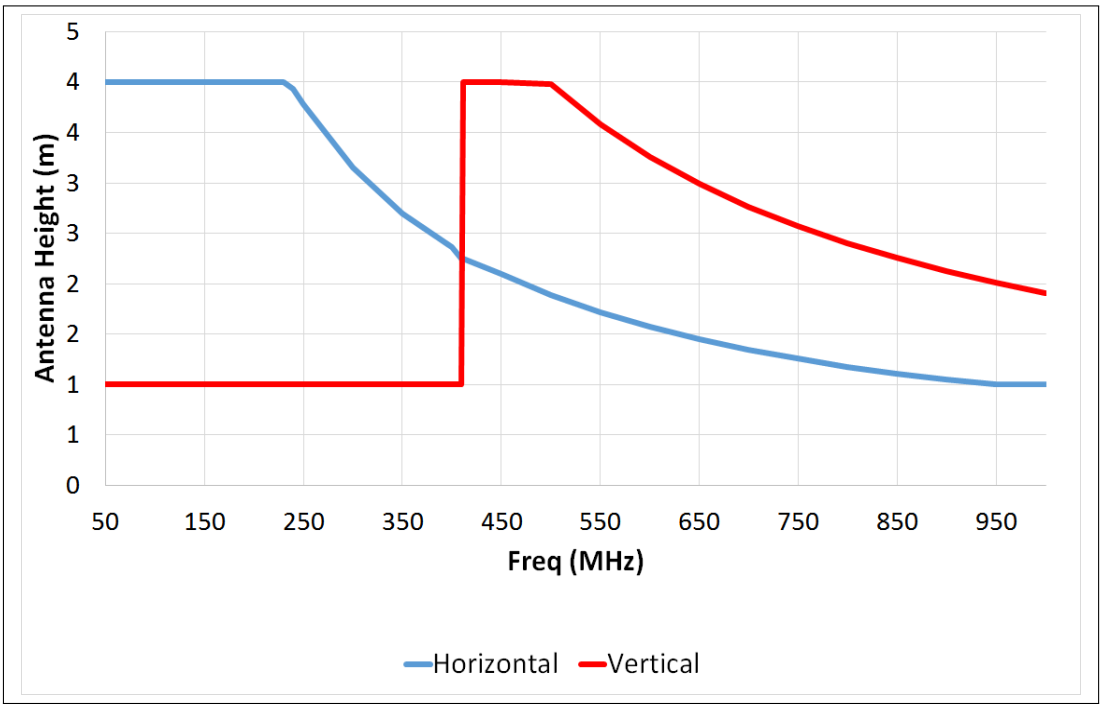

FIGURE 4.4: Height of E_{max} for OATS Measurements

The results detailed in Figure 4.4 do not account for the directivity of the receive antenna. The measured electric field is converted to a voltage by the receive antenna, which is then in turn recorded by an RF receiver. The antenna factor of the receive antenna is defined as the ratio of the incident electric field to the voltage at the antenna terminals into a 50 Ω load :-

$$A_f = \frac{E}{V} \tag{4.10}$$

The use of broadband antennas for radiated emissions measurements is now common place, enabling much faster measurements to be performed compared to using tuned dipoles, for example. The antenna factor for such antenna is only valid when the direction of the main beam of the antenna is in line with the centre line of the EUT. If the antenna is scanned in height for the purpose of maximising the emissions then the incident angle of the electric field is not always the main beam direction [43]. This change will modify Equation 4.10

$$E = V.A_f.P(\varphi) \tag{4.11}$$

where $P(\varphi)$ is the directivity of the receive antenna. As the antenna is scanned in height neither the angle of incidence or pattern remain constant making a correction factor infeasible to apply to the measured results. Substituting this modification to the received E-field into equation 4.12 gives the following:

$$\overrightarrow{E}_{Total}(d,t) \ = P(\varphi_1)\frac{E_0 d_0}{d'}e^{-j\omega(t\frac{d'}{c})} + P(\varphi_2)R\frac{E_0 d_0}{d''}e^{-j\omega(t\frac{d''}{c})} \tag{4.12}$$

In an attempt to overcome this problem a study performed by Kriz [43] suggested 'antenna tilting' or 'antenna bore sighting'. In the antenna tilting method the receive antenna is inclined down, towards the ground plane, at a constant angle for all heights of the receive antenna. This constant tilt angle can be calculated thus:

$$\varphi = \frac{arctan(\frac{h_2+h_1)}{2} + arctan(\frac{h_2-h_1}{R})}{2} \tag{4.13}$$

Using this method, as suggested by CISPR 16-1-4 [44], the tilt angle of the antenna places the main beam direction in the middle of the direct and reflected emission. However, due to the fact that the receive antenna is not at a fixed height the optimum value of tilt angle cannot be found. If an average height of 2.5 m is taken a tilt angle of $\varphi_{3m} = 38^o$ and $\varphi_{10m} = 13.9^o$ will be used.

This solution is relatively easy to implement using an existing antenna mast with just an adaptor needing to be produced to change the declination angle of the antenna.

Using this method an overall reduction in the measurement system uncertainty of 0.2 dB can be realised. It could be argued that this small reduction may not justify the outlay involved in modifying the antenna system.

The second method suggested by Kriz is antenna bore sighting. Using this method the tilt angle is increased as the antenna height is increased. The angle is calculated using the following formula:

$$\varphi = arctan(\frac{h_2 - h_1)}{R} \tag{4.14}$$

If an EUT height of 1 m is assumed using 4.14 the range of bore sight angles are:

$$0^o \leq \varphi_{3m} \leq 45^o \tag{4.15}$$

$$0^o \leq \varphi_{10m} \leq 16.7^o \tag{4.16}$$

The bore sighting method slightly improves on the tilting method; the system uncertainty is now reduced by 0.31 dB. This marginal reduction in error can still be argued as not sufficient to warrant the added complexity required in the measurement system.

4.2.3 Height Scan Investigations

4.2.3.1 Introduction

This Section of the thesis details measurements and simulations performed to investigate the effect scanning the receive antenna in height during a radiated emissions measurement has on the amplitude of the E-field recorded. Firstly an electrically small noise source was considered, with the aim of validating the theoretical height at which the maximum E-field should be recorded as described in Section 4.2. Secondly an electrically large source of noise was considered. A production vehicle was used initially as the electrically large source, however, as is highlighted later in this section, problems with exciting the vehicle with a sufficiently high amplitude noise signal lead to inconclusive results. In an attempt to improve on the quality of the results obtained with the electrically

large source, further measurements were performed with a long wire harness driven by a wide band noise source. The results obtained from both the electrically small and large devices are compared to the theoretical results highlighted in 4.2. The level of error in the maximum E-field amplitude recorded, introduced by only performing measurements at a single height, as per CISPR 12, is then quantified.

4.2.4 Measurements - Electrically Small Noise Source

In order to investigate how the theory described in the previous section compared with an electrically small source; a program of E-field measurements were conducted. The measurements were performed using a a wideband noise source positioned on a non-conductive table. The data collected were then used to compare the receive antenna height at which the maximum E-field amplitude was recorded to the theoretical value. An error value, designated as the Error Bias, EB, is introduced. The EB by not using receive antenna height scanning during measurements was then quantified. It is calculated as follows:

$$ErrorBias = \frac{E_{max}}{E_{meas}} \tag{4.17}$$

where E_{max} is the maximum amplitude of the E-field measured over the full range of measurements being performed, height scanning in the case of this section. E_{meas} is the amplitude of E-field measured at the single antenna height. The Error Bias term will be used in subsequent sections of this thesis. The term will be used to define the difference in amplitude between the 'maximised' value and the results from performing the reduced scope of testing defined in CISPR 12. This reduced scope could be the use of a single receive antenna height, two azimuth positions of the EUT or a combination of the two. Ideally E_{max} should be the result of measurements utilising a full spherical scan around the EUT, however, as has previously been noted this procedure is very time consuming and hence a range of planar scan cut measurements were performed. The scope of the planar cuts completed varied due to available lab time for each set of measurements, and is detailed in each section of this thesis when they were performed.

4.2.4.1 Measurements Setup

The theory described in the previous section was validated using a program of measurements. An electrically small noise source (Comparison Noise Emitter - York EMC CNE IV) with a 270 mm long monopole radiator was measured at the HORIBA MIRA (formerly known as 'MIRA') OATS facility. The noise source was positioned on a non-conductive table 0.8 m above the facility floor, 10 m away from the receive antenna. The radiated electric field was recorded over the frequency range of 30 MHz to 1 GHz, in 50 MHz increments, with the receive antenna being scanned in height from 1 m to 4 m above the ground in 0.2 m increments. Measurements were performed with the receive antenna in both horizontal and vertical polarisation. At each frequency measured, the receive antenna height at which the maximum E-field was recorded was noted. This height was then compared to the theoretical height at which the maximum field should be recorded. Due to high ambient signal levels recorded at the OATS test site it was not possible to record data in exactly 50 MHz increments over the frequency range previously stated, where high ambient signals were noted, the next closest frequency with a sufficiently low ambient signal level was substituted.

FIGURE 4.5: Height Scan Investigation Setup, Electrically Small Source

4.2.4.2 Measurement Results

In order to make comparisons between the theoretical and the measured data clearer, both sets of data were normalised to a maximum value of 1. As the purpose of the comparison was to determine if the maximum amplitude was measured at the same receive antenna height as predicted by the theory, absolute values were not required.

For each frequency measured, a plot of the normalised E-field recorded at each receive antenna height was produced. On the same axis of each of these plots, the theoretical normalised E-field of the measured height at which the maximum amplitude was recorded against the theoretical value, was also displayed.

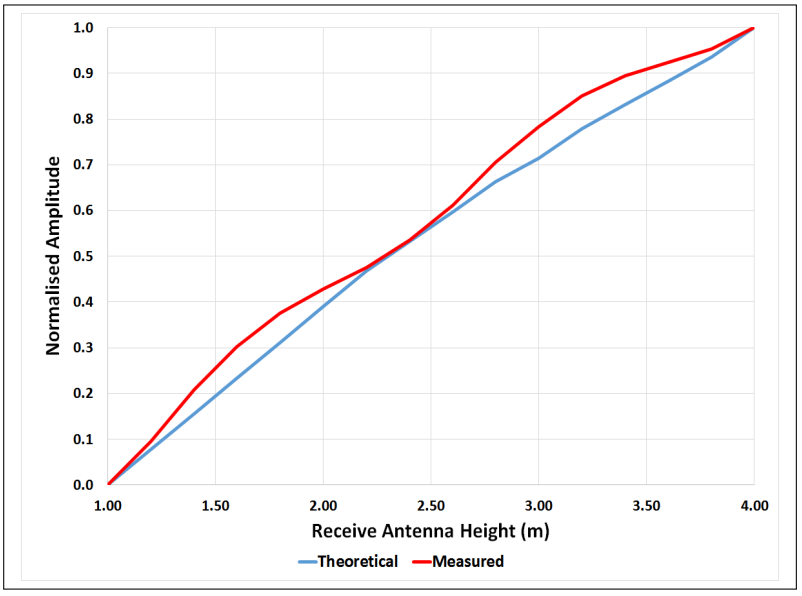

FIGURE 4.6: 100 MHz Height Scan Electrically Small Source, Horizontal Receive Antenna

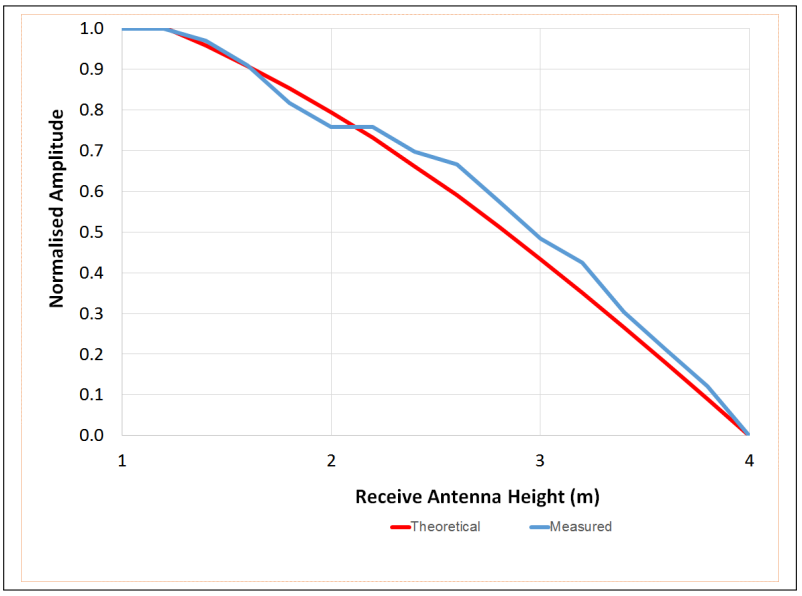

FIGURE 4.7: 100 MHz Height Scan Electrically Small Source, Vertical Receive Antenna

As detailed in Figures 4.6 and 4.7 a very good level of correlation between the theoretical and measured values, for both horizontal and vertical polarisation the maximum amplitude was recorded at the correct height. On reviewing the results it was observed that below approximately 400 MHz, using both a vertically and horizontally polarised receive antenna, the correlation between the measured results and the theory was very good, showing a Pearson Correlation factor, ρ, [45] of between 0.85 and 0.99 for horizontally polarised receive antenna and between 0.6 and 0.9 for the vertically polarised receive antenna .

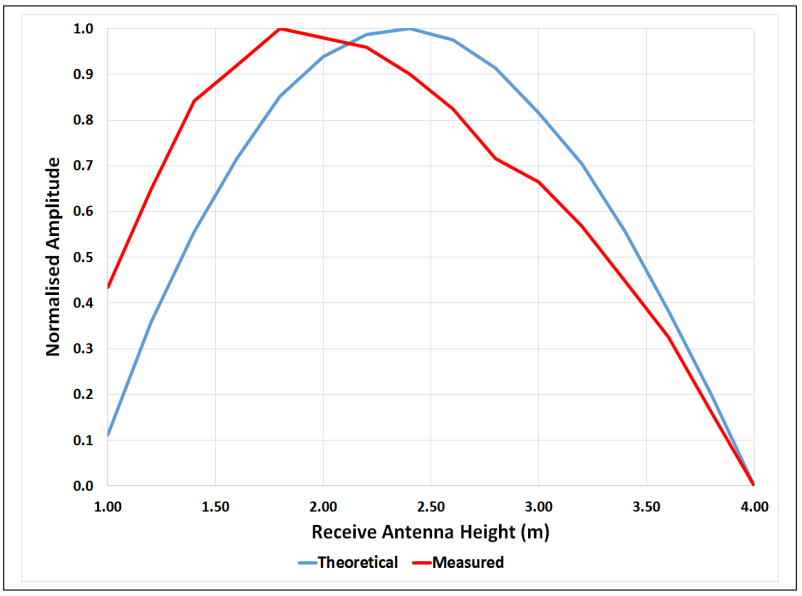

FIGURE 4.8: 400 MHz Height Scan Electrically Small Source, Horizontal Receive Antenna

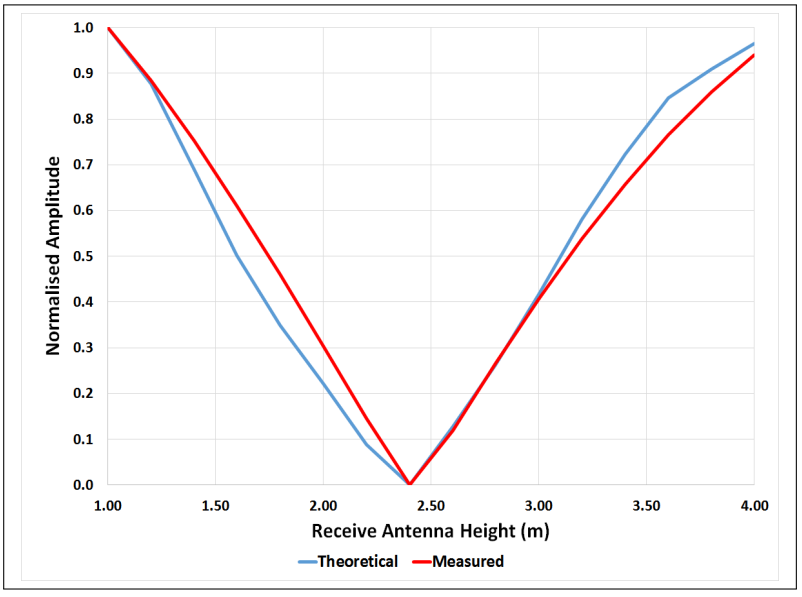

FIGURE 4.9: 400 MHz Height Scan Electrically Small Source, Vertical Receive Antenna

Above 400 MHz the overall profile of the amplitude recorded was similar between the two sets of data, however, it was observed that the height at which the maximum amplitude was recorded was approximately 0.25 m lower than the theoretical value for both horizontal and vertical polarisations. This results in a lower correlation factor of between 0.7 and 0.1, the lower value being recorded at 1 GHz for the vertical antenna polarisation. However, on a purely visual comparison, it can be seen that the overall

profile of the measured results is similar if it is 'shifted' in height by approximatively 0.25 m.

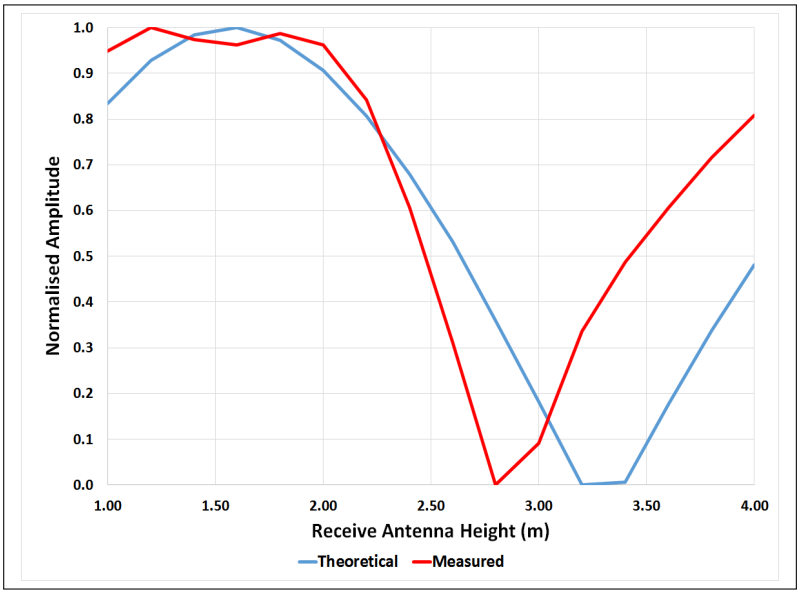

FIGURE 4.10: 600 MHz Height Scan Electrically Small Source, Horizontal Receive Antenna

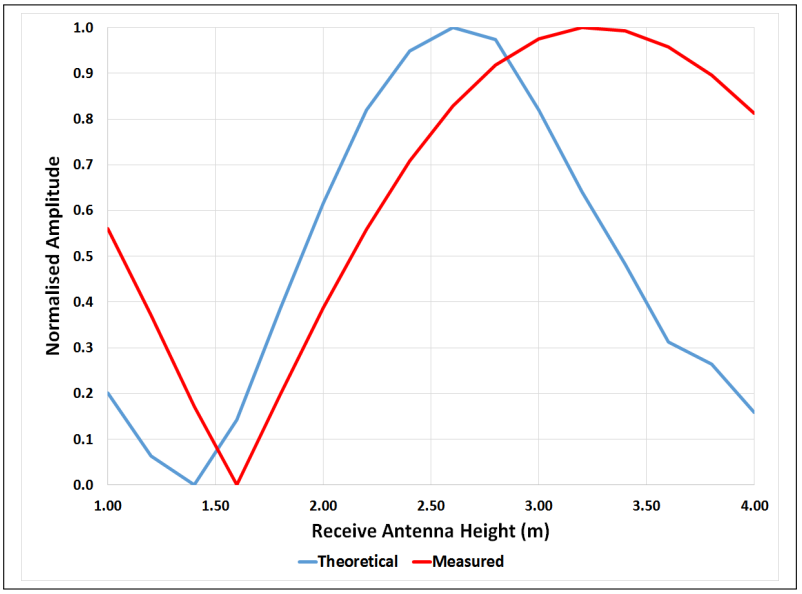

FIGURE 4.11: 600 MHz Height Scan Electrically Small Source, Vertical Receive Antenna

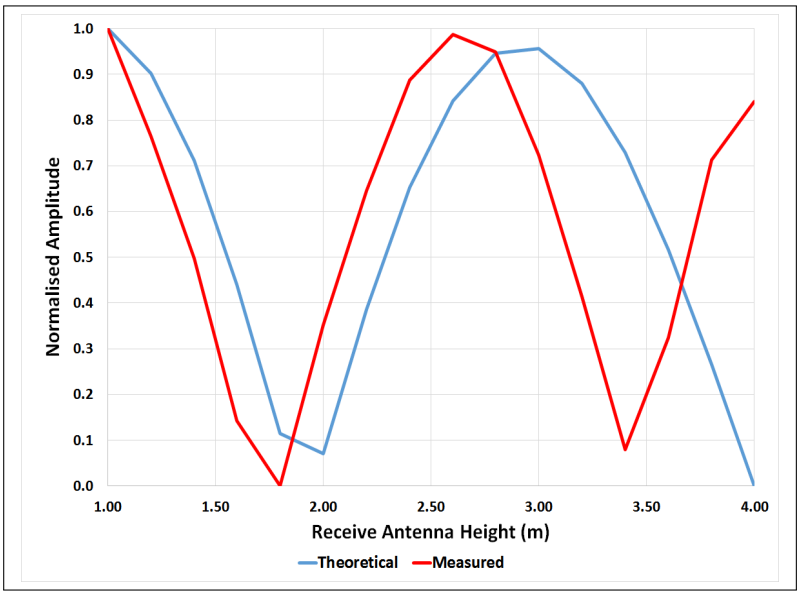

FIGURE 4.12: 1000 MHz Height Scan Electrically Small Source, Horizontal Receive Antenna

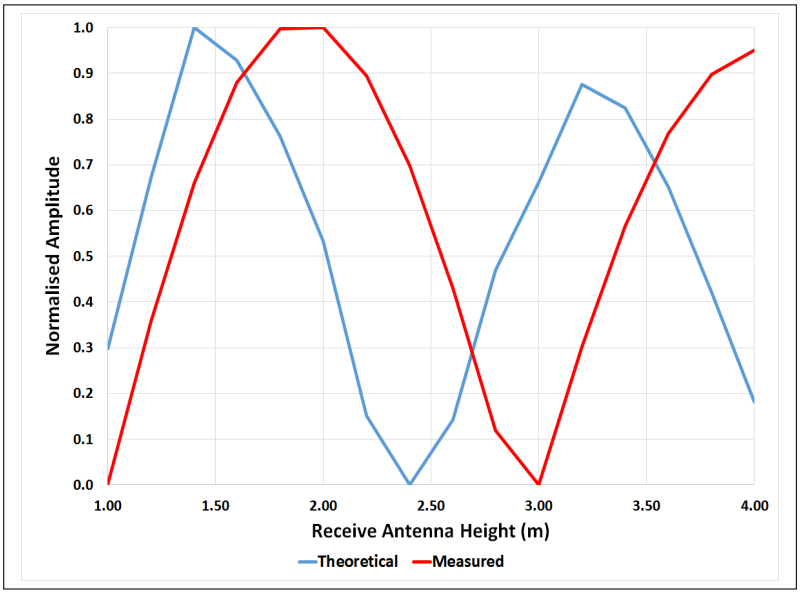

FIGURE 4.13: 1000 MHz Height Scan Electrically Small Source, Vertical Receive Antenna

The difference between the height at which the measured maximum value and the theoretical value is thought to be due to the receive antenna not being 10 m away from the electrically small source. The measurement data was compared to the theoretical height based upon a 8.75 m source to receive antenna distance. When the two data sets were then analysed a far closer correlation between them was recorded. When the measured data was compared to the theory calculated using a 10 m separation distance a

correlation factor of less than 0.1 was recorded, however if the measured data is compared to the theoretical value with an 8.75 m measurement distance a correlation factor of 0.9 was recorded. If time had allowed the measurement data set would have been repeated, checking that an accurate separation of source to receive antenna of 10 m was used and the results validated for all frequencies. Graphical data of the 8.75 m separation reworked theoretical data against the measured values is shown in Figure 4.14.

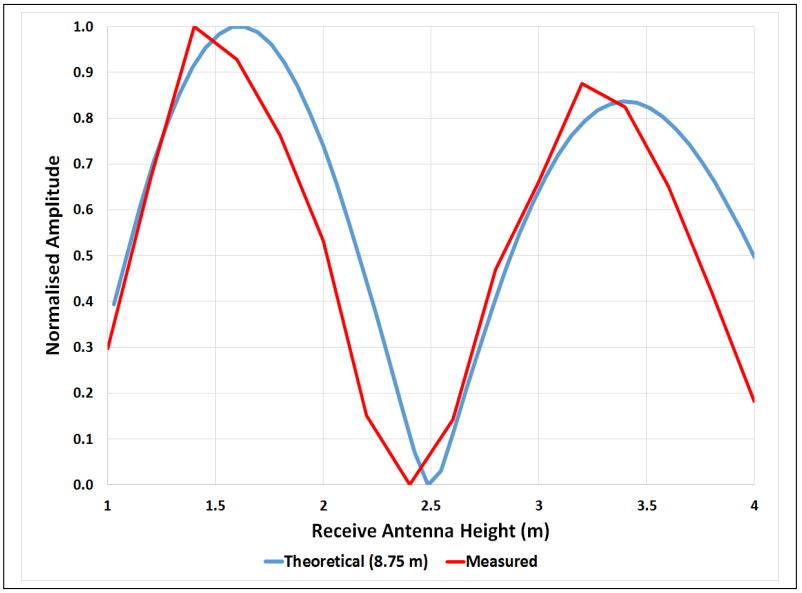

FIGURE 4.14: 1000 MHz Height Scan Electrically Small Source, Vertical Receive Antenna, 8.5 m Source to Antenna Distance

The graphs detailed in Figures 4.15 and 4.16 show a plot of the height at which the maximum E-field amplitude was recorded with respect to frequency for both the horizontal an vertical antenna polarisations. The graphs show a good level of agreement across the frequency range for both the horizontal and vertical sets of data. The horizontal data has a ρ value factor of 0.79, while the vertical data has a value of 0.97.

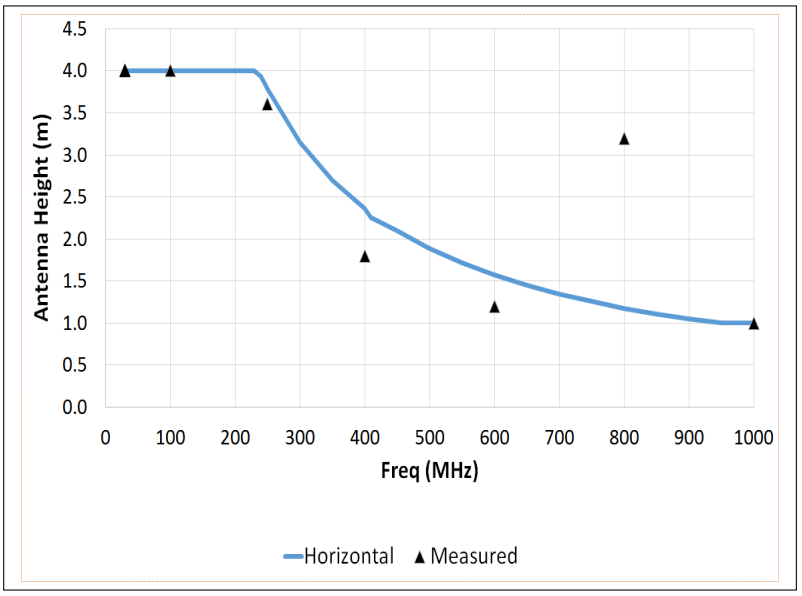

FIGURE 4.15: Antenna Height Maximum Emissions Recorded Against Frequency, Horizontal Antenna

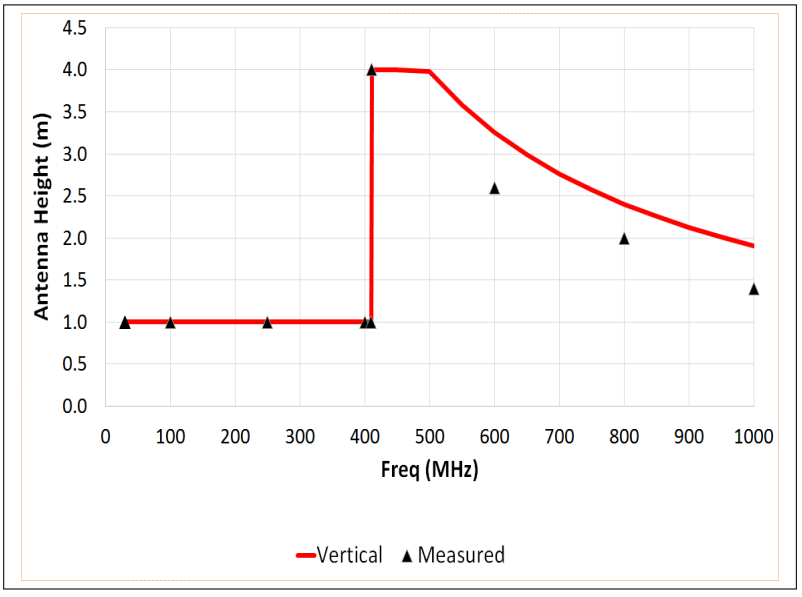

FIGURE 4.16: Antenna Height Maximum Emissions Recorded Against Frequency, Vertical Antenna

A noticeable feature of the horizontal results is the large difference between the measured and theoretical values recorded at 800 MHz. The theory states that the maximum emissions should be recorded at a height of approximately 1.2 m, the measured maximum occurred when the receive antenna was at 3.2 m above the ground. As can be seen in Figure 4.17 if emissions amplitude is plot against antenna height, it can be seen that the difference is due to an offset between the two sets of values. The measured data

follows the same overall profile as the theoretical data, but the crests of the plot occur at a height approximately 20 cm lower than predicted by the theory. This offset means that over the antenna height range measured the second crest in the plot, at 3.2 m above ground level, accounts for the maximum amplitude.

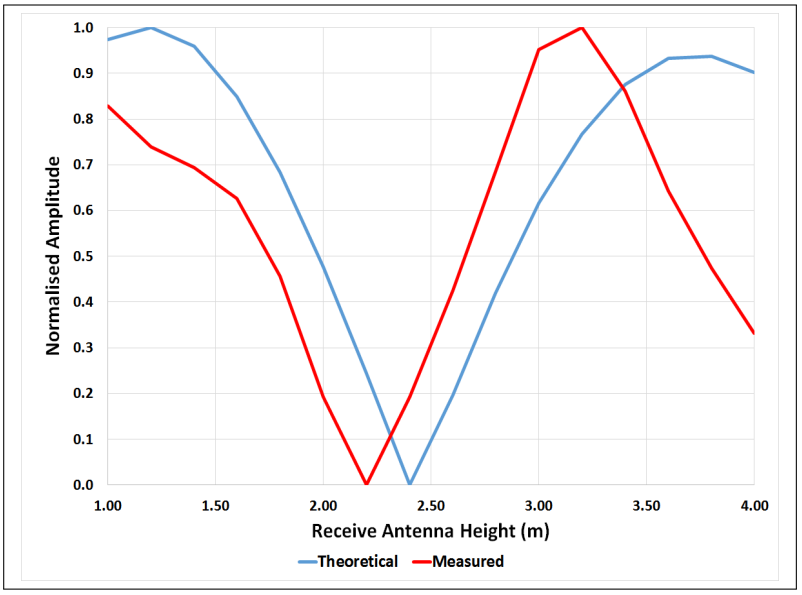

FIGURE 4.17: 800 MHz Height Scan Electrically Small Source, Horizontal Receive Antenna

From the data recorded it is possible to evaluate the amount of error in the maximum E-field amplitude introduced by only considering a single antenna height, as used during a CISPR 12 program. The maximum amplitude recorded over the 1 m - 4 m scan was compared to the value recorded at 3 m for each frequency, from this an Error Bias was calculated. This is shown graphically in Figures 4.18 and 4.19.

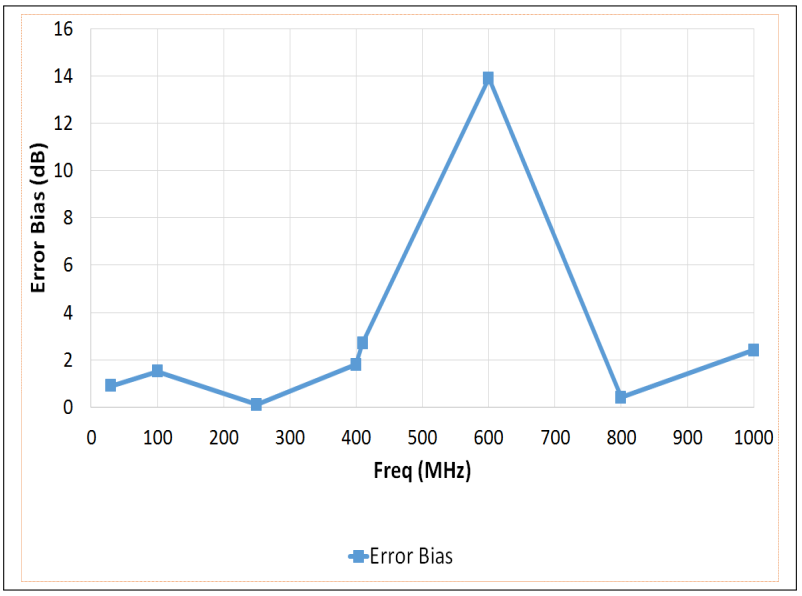

FIGURE 4.18: Error Bias due to Height Scan, Horizontal Antenna

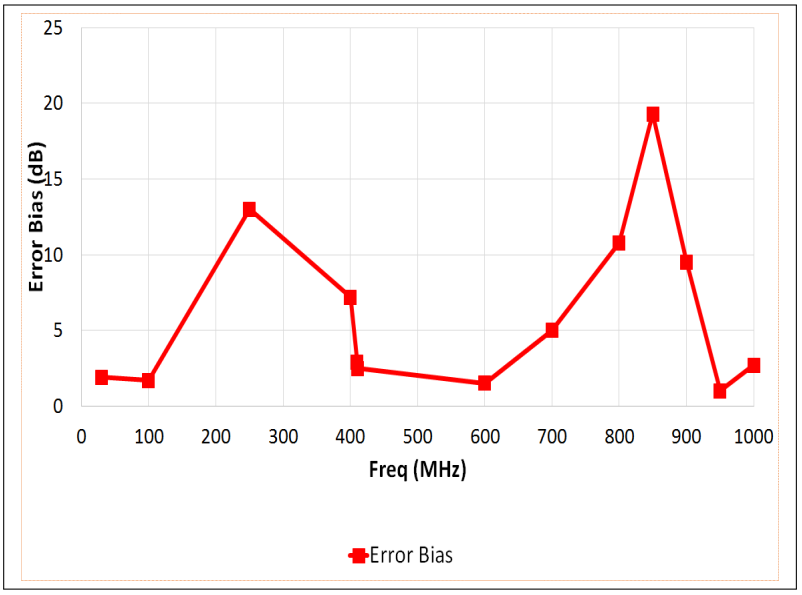

FIGURE 4.19: Error Bias due to Height Scan, Vertical Antenna

For the horizontal antenna measurements across the frequency range an EB of between 1 dB and 3 dB was seen, however at 600 MHz a value of 14 dB was recorded. For the vertical scans a maximum values of between 5 dB and 13 dB were recorded between 200 MHz and 900 MHz, with a high value of 20 dB recorded at 850 MHz. Across the whole frequency range a mean of the linear error of 4.4 dB was recorded for the horizontal data and 8.1 dB for the vertical set. These results highlight the fact that by taking data at a single antenna height there is a potential to considerably under-estimate the maximum

E-field during a radiated emissions test. The mean EB recorded was similar to those detailed by Ruddle [24].

4.2.5 Measurements - Electrically Large Noise Source

4.2.5.1 Introduction

In order to investigate how the theory described in the previous section compared with an electrically large source a program of simulations and measurements were conducted. The measurements were performed using a small town-car with a wideband noise source inside to excite the vehicle. Measurements were also performed using the noise source to excite a 2 m long harness that was positioned on a non-conductive table. Finally, EM simulations were performed using the numerical model described in Section 3.1.4.2. The data collected was then used to compare the receive antenna height at which the maximum E-field amplitude was recorded to the theoretical value. The EB introduced by not using receive antenna height scanning during measurements was then quantified. The EB recorded when measuring an electrically small EUT was then compared to that recorded for an electrically large EUT.

4.2.5.2 Measurements Setup

A small wideband noise source driving a short monopole antenna was placed inside a commercial vehicle so that the noise source excited the body shell of the vehicle. Most typical family vehicles are electrically long at frequencies above approximately 25 MHz and can not be considered as a point source.

Radiated emissions measurements were again performed at the MIRA OATS facility. The noise source was positioned on the passenger seat of the vehicle, which was positioned 10 m away from the receive antenna. The radiated electric field was recorded over the frequency range of 30 MHz to 1 GHz with the receive antenna being scanned in height from 1 m to 3.5 m above the ground in 0.2 m increments. The antenna height scan was limited to 3.5 m as the antenna mast at the test facility being used would not allow the antenna to be raised higher than 3.5 m. Measurements were performed with the receive antenna in both horizontal and vertical polarisation. At each frequency measured the

receive antenna height at which the maximum E-field was recorded was noted. This height was then compared to the theoretical height at which the maximum field should be recorded.

FIGURE 4.20: Electrically Large Source (Nissan Micra), Height Scan Measurement Setup

As noted later in this section, the results obtained by measuring the emissions with the source inside a vehicle were found to be very low in amplitude which made taking measurements difficult, as the emissions were very close to the ambient signal levels at certain frequencies. In an attempt to overcome this problem, an additional set of measurements was performed with the noise source exciting a 2.5 m long wire that was positioned on top of a non-conductive table. As the harness was not inside a largely metal box, a higher amplitude signal was recorded by the measurement system and thus was higher above the ambient signal level. An example setup photo is shown in Figures 4.21 and 4.22. For the harness measurements the receive antenna was scanned in height from 1 m to 4 m above the facility ground in 0.5 m increments. This height increment is considered as under-sampled, however, available test facility time did not allow for a finer increment to be used. In line with the vehicle measurements both horizontal and

vertical polarisation measurements were performed, this again allowed for the measured results to be compared to the theoretical height values described in Section 4.2.2.

FIGURE 4.21: Electrically Large Source, Wire Harness, Height Scan Measurement Setup

FIGURE 4.22: Electrically Large Source, Wire Harness on Non-Conductive Table

4.2.5.3 Measurement Results

The E-field data were analysed once the tests had finished. Due to limited output power of the noise source and the shielding offered by the vehicle body shell it was found that the amplitude levels recorded were considerably lower than when the noise source was measured in isolation on the non-conductive table. This had the result of making the emissions difficult to record above the ambient signal level at certain frequencies, this was particularly an issue above about 600 MHz. As the Radio Frequency, RF, spectrum is relatively well used over large frequency bands above 600 MHz, choosing frequencies to analyse where the signal was sufficiently high enough above the ambient became more difficult. This low signal to noise ratio lead to the recorded data not following a smooth increase and decrease that was evident when measuring the electrically small source described in the previous section.

A plot of the ambient E-field recorded is shown in Figures 4.23 and 4.24. The blue trace in the graphs shows the ambient signal level recorded at the time of test. Portions of the frequency range exhibit a constant amplitude ambient, FM radio (88 to 108 MHz),

DAB Radio (200 to 230 MHz) and DTV (600 to 820 MHz for example. Other ambients can be more transient in nature, due to their limited operation. The more constant transmissions can be easier to deal with, as they do not move in frequency or amplitude, distinguishing them from emissions from the equipment under test can be relatively easy. Transient ambient emissions can involve more investigation in order to be confident that they are in fact part of the 'background' RF environment and not being radiated by the EUT.

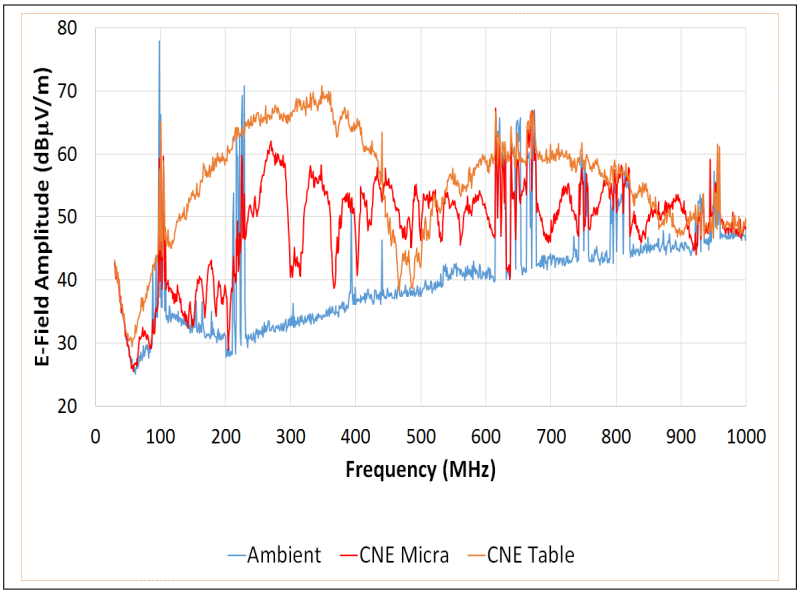

FIGURE 4.23: CNE E-Field Output Compared to Ambient Noise Floor, Horizontal Receive Antenna

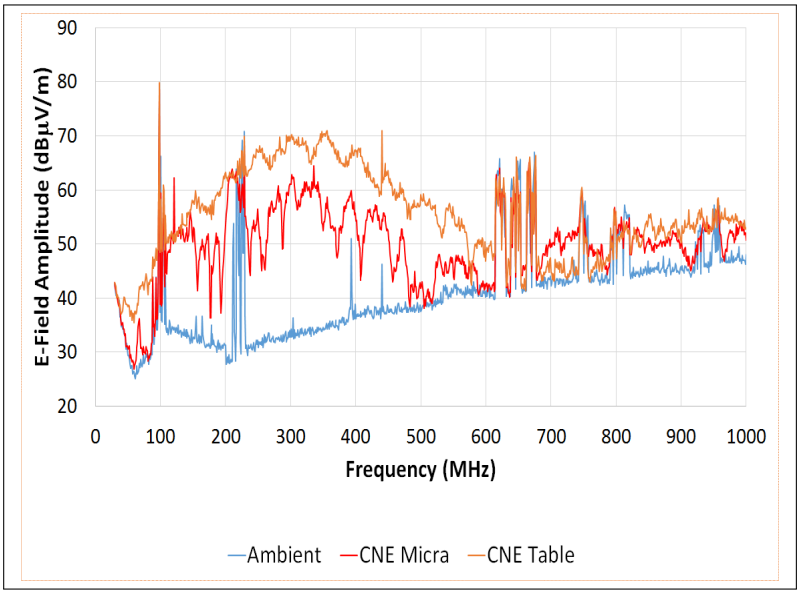

FIGURE 4.24: CNE E-Field Output Compared to Ambient Noise Floor, Vertical Receive Antenna

It can be seen that large portions of the 50 MHz to 1 GHz spectrum has large amplitude ambient signals, bands where noise source measurements were not possible are highlighted in Table 4.1. At frequencies below 600 MHz the E-field recorded when the noise source was inside the vehicle is approximately 10 dB lower than the noise source on the table. At higher frequencies the difference is lower; with the two levels being within a few dB of each other. Between 690 MHz and 760 MHz the E-field recorded when the noise source was inside the vehicle is actually higher. This is possibly due to resonances within the vehicle body shell reinforcing the signal being recorded.

TABLE 4.1: Ambient E-field Amplitude

Frequency (MHz)	**Service**
88 - 108	FM Radio
200 - 230	DAB Radio
600 - 680	DTV
730 - 770	DTV
790 - 820	DTV
930 - 960	GSM

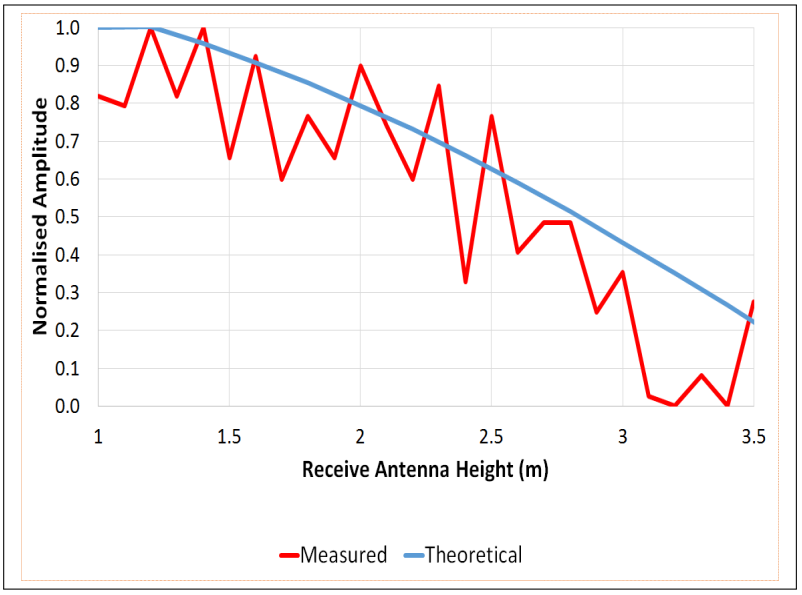

FIGURE 4.25: 100 MHz Height Scan Electrically Large Source, Vertical Receive Antenna

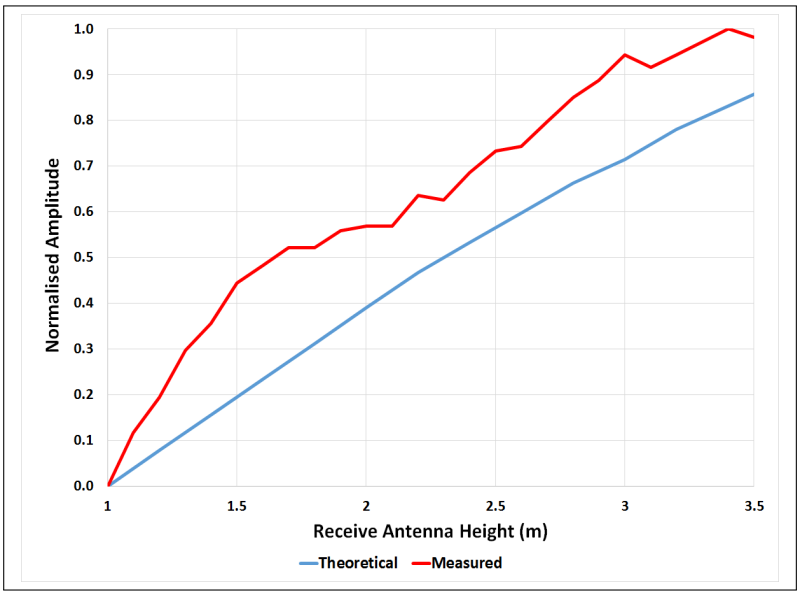

FIGURE 4.26: 100 MHz Height Scan Electrically Large Source, Horizontal Receive Antenna

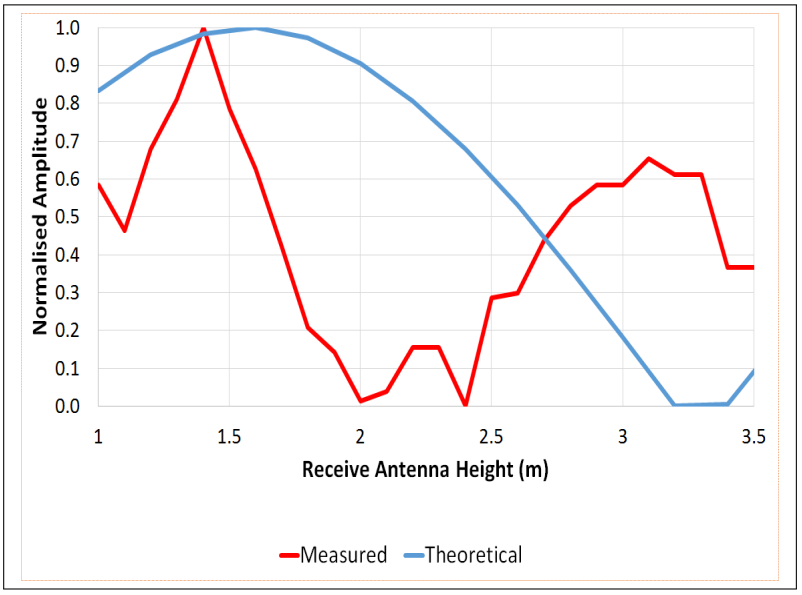

FIGURE 4.27: 600 MHz Height Scan Electrically Large Source, Horizontal Receive Antenna

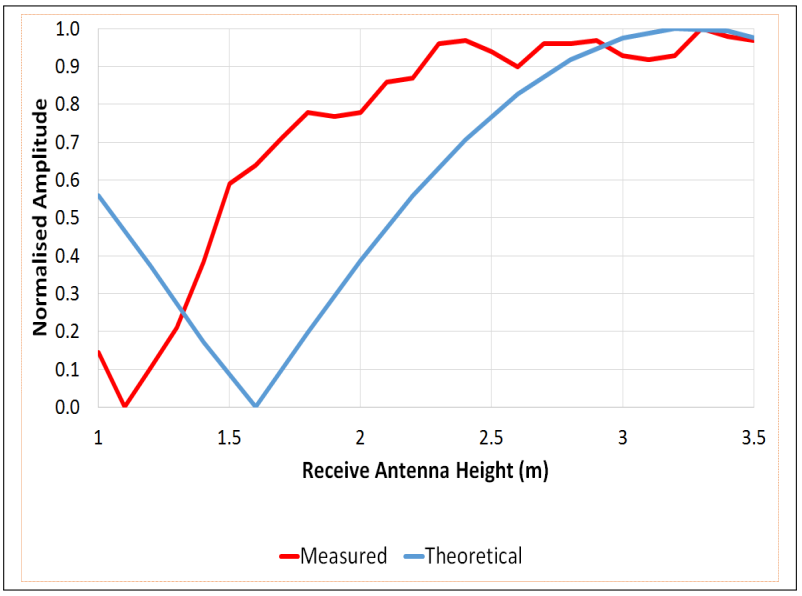

FIGURE 4.28: 600 MHz Height Scan Electrically Large Source, Vertical Receive Antenna

As can be seen from Figures 4.29 and 4.30, the height at which the maximum emissions were recorded showed larger differences around 400 MHz to 500 MHz, particularly in the vertically polarised plot. The differences were attributed to the crossover frequency, where the maximum amplitude changes from 1 m below 410 MHz to 4 m above 411 MHz. As was noted when analysing the results from the electrically small source, the actual frequency at which the changeover occurs was around 403 MHz in the measured results. This lead to a large difference to the theoretical and measured values. At the higher frequencies, above 700 MHz, the results where not so closely correlated. This was attributed to the fact that the received signal was recorded with a low signal to ambient noise level, this lead to the noise source emissions being corrupted by the ambients.

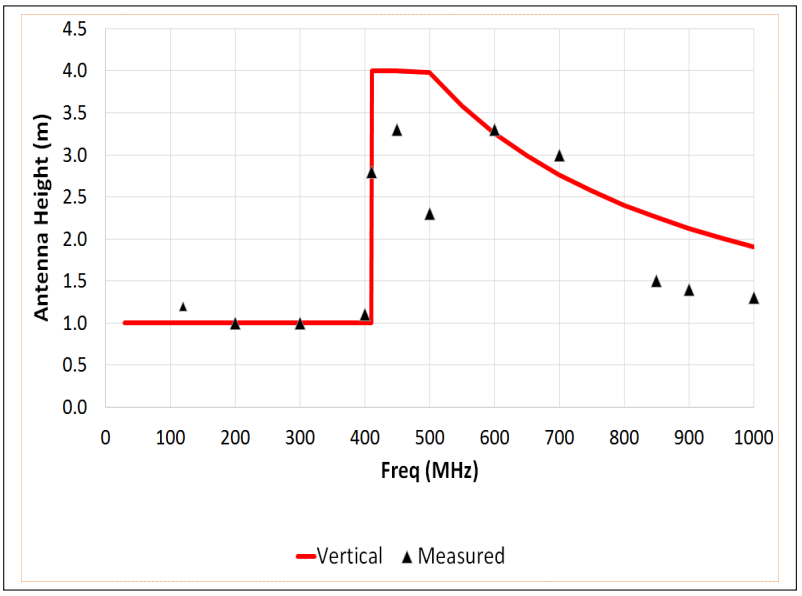

FIGURE 4.29: Antenna Height Maximum Emissions Recorded Against Frequency, Vertical Antenna

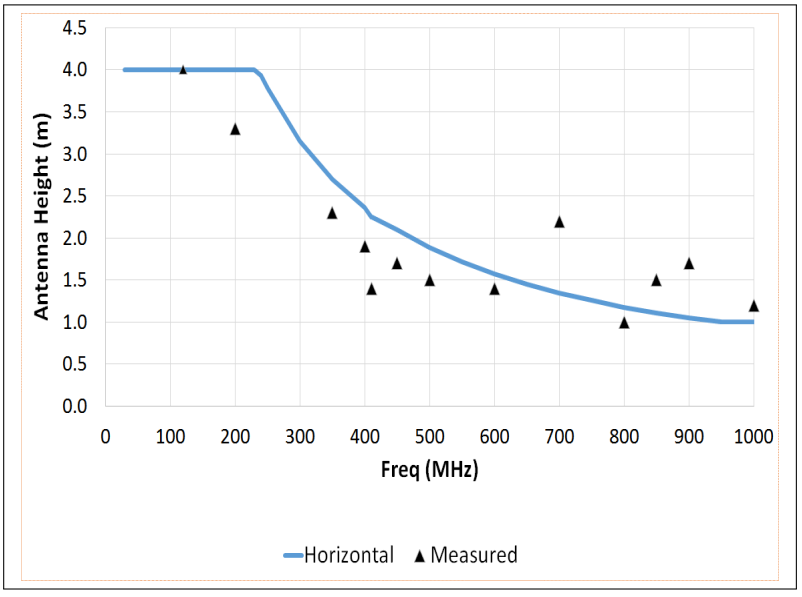

FIGURE 4.30: Antenna Height Maximum Emissions Recorded Against Frequency, Horizontal Antenna

As can be seen in Figures 4.31 to 4.34 a good level of agreement between the measurement data and the theoretical height at which the maximum emissions should be recorded was seen. As was noted when the electrically small noise source was measured a shift in height of approximately 0.25 m was recorded between the measurement and theoretical value.

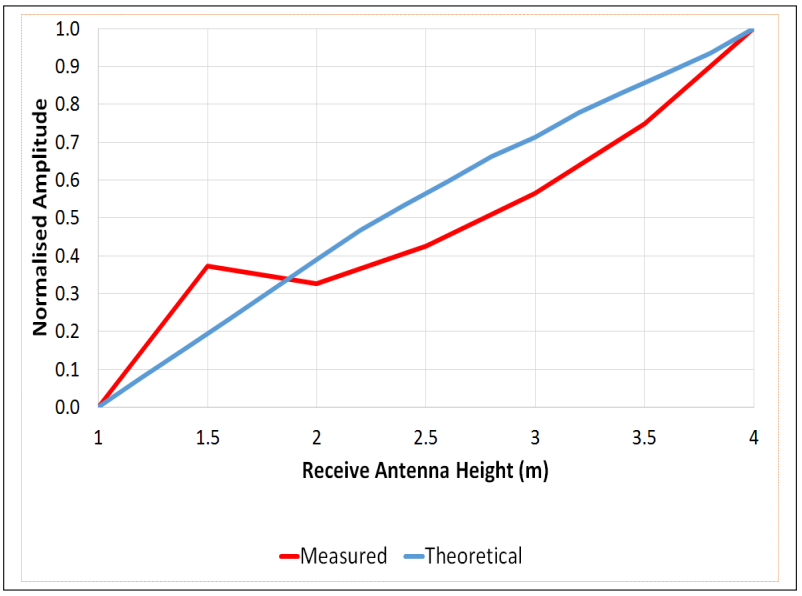

FIGURE 4.31: 100 MHz Height Scan Long Wire Source, Horizontal Receive Antenna

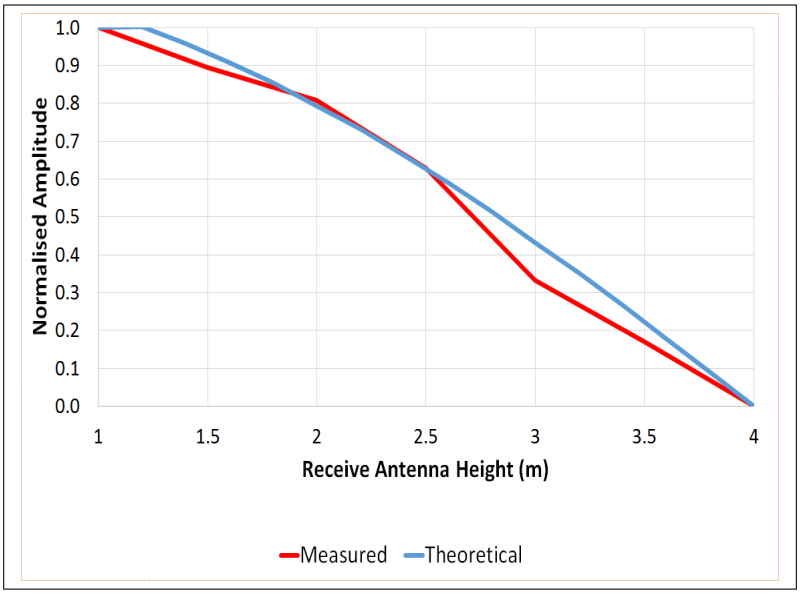

FIGURE 4.32: 100 MHz Height Scan Long Wire Source, Vertical Receive Antenna

Comparing the results to those recorded with the source inside the vehicle, a much closer fit to the theoretical values of amplitude against heigh was achieved, particularly at 600 MHz with a horizontally polarised receive antenna.

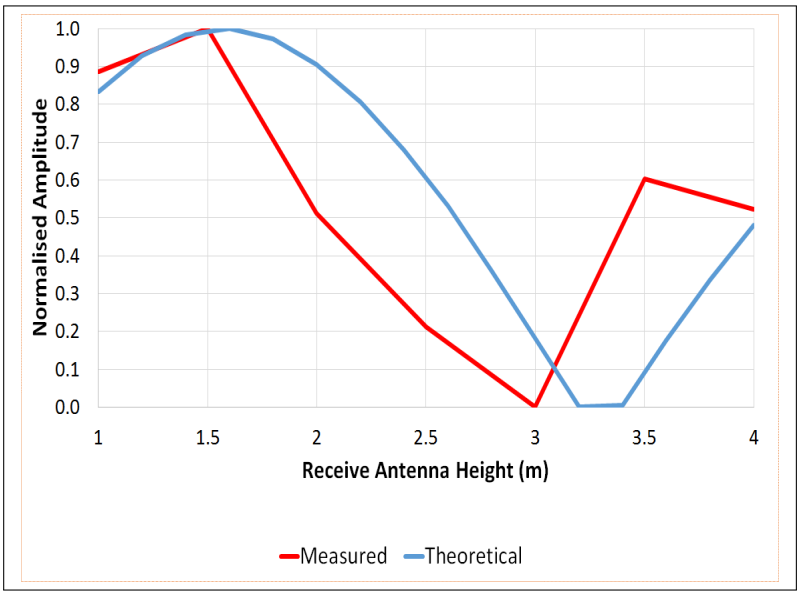

FIGURE 4.33: 600 MHz Height Scan Long Wire Source, Horizontal Receive Antenna

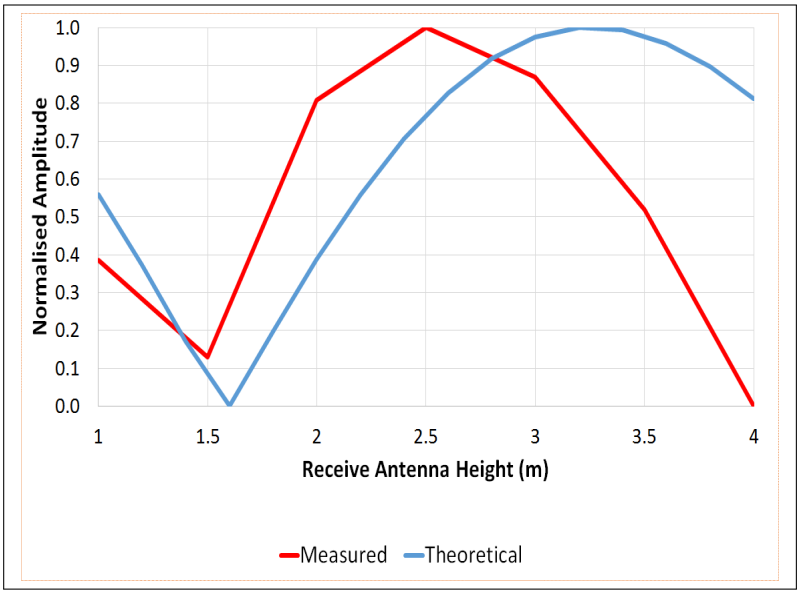

FIGURE 4.34: 600 MHz Height Scan Long Wire Source, Vertical Receive Antenna

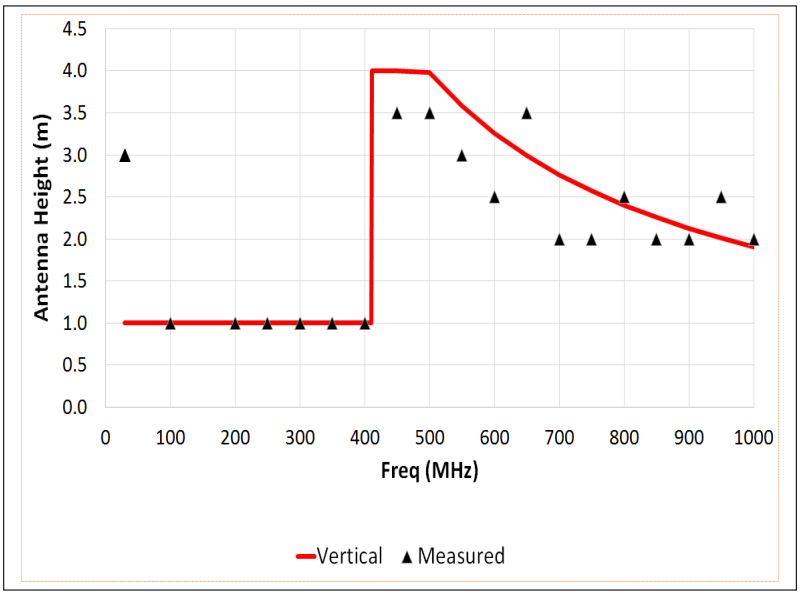

FIGURE 4.35: Antenna Height Maximum Emissions Recorded Against Frequency, Vertical Antenna

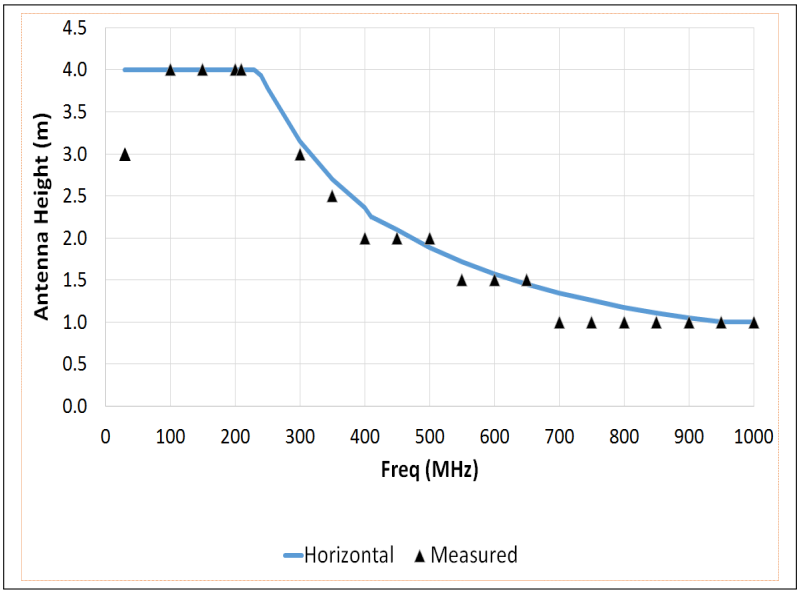

FIGURE 4.36: Antenna Height Maximum Emissions Recorded Against Frequency, Horizontal Antenna

Below 400 MHz again a good level of agreement between the calculated height at which the maximum emissions were recorded and the actual height was seen. Around the 400 MHz to 500 MHz range in particular a better correlation between the values was recorded, with the horizontal results having a correlation factor of 0.98. The results at 30 MHz are shown for information, but the level of emissions were found to have a very low amplitude that was not high enough above the ambient signals to make the results

reliable. The coarse height increment used has lead to some of the differences between the results recorded as the resolution often lead to the the next lower or higher value being recorded and hence a large difference than would have been measured with a finer increment distance. Even allowing for the errors due to the increment size a worst case correlation factor of 0.82 was recorded .

A larger discrepancy was recorded at 50 MHz in both the vertical and horizontal data sets. The horizontal data showed the maximum E-field being recorded at approximately 1 m lower than the theoretical height and for the vertical antenna measurements the maximum occurred 2 m higher than expected. This large error was attributed to the low signal levels at 50 MHz being radiated by the harness being interfered with by the ambient signals.

The Error Bias was calculated based upon the vehicle and long wire results to gain some insight into the effect of not utilising receive antenna height scan during a vehicle level test. Figures 4.37 and 4.38 show the EB against frequency for the vehicle measurements. For the source inside the vehicle, the mean of the linear error values recorded was 4 dB for the horizontal receive antenna and approximately 5.5 dB for the vertically polarised antenna, a high value of approximately 10 dB was noted for the horizontal data and 14 dB for the vertically polarised vehicle data sets.

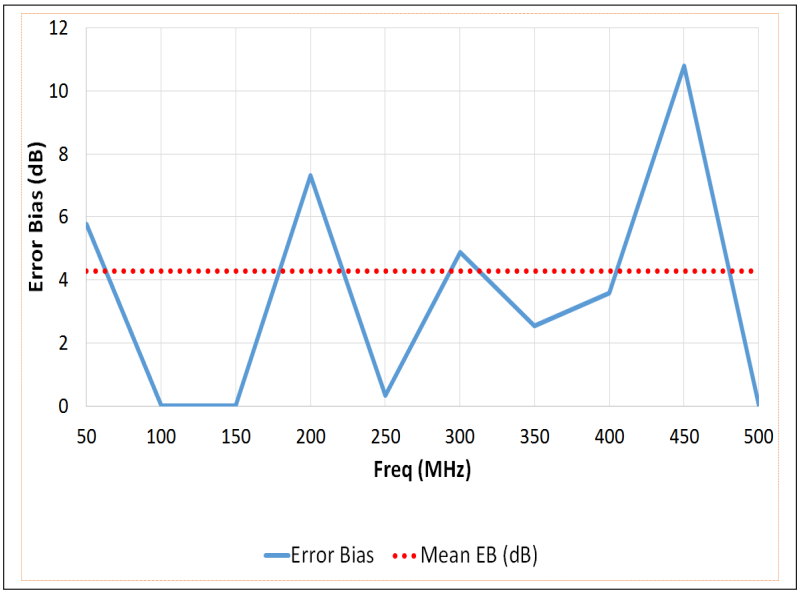

FIGURE 4.37: Error Bias Due to Height Scan Only, Electrically Large Source, Horizontal Antenna

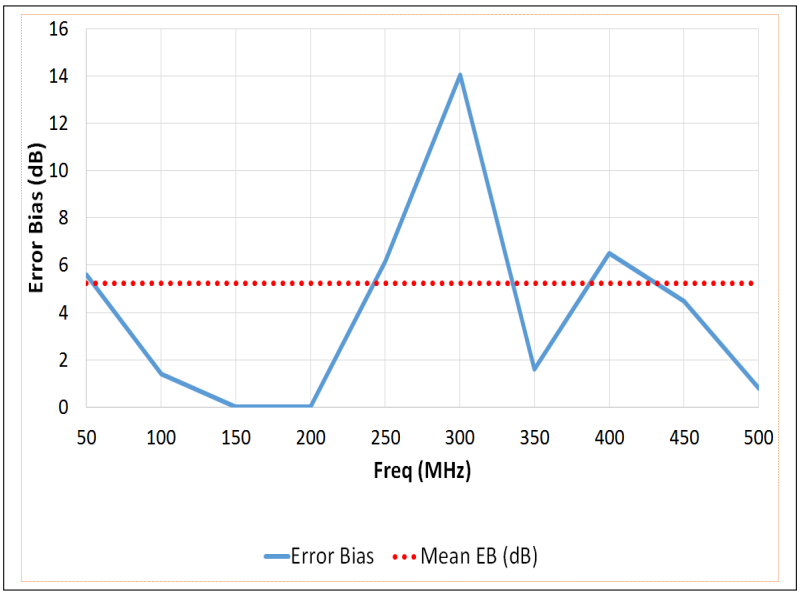

FIGURE 4.38: Error Bias Due to Heigh Scan Only, Electrically Large Source, Vertical Antenna

The long wire source resulted in high EB values of 7 dB and 16 dB for horizontal and vertical polarisation respectively.

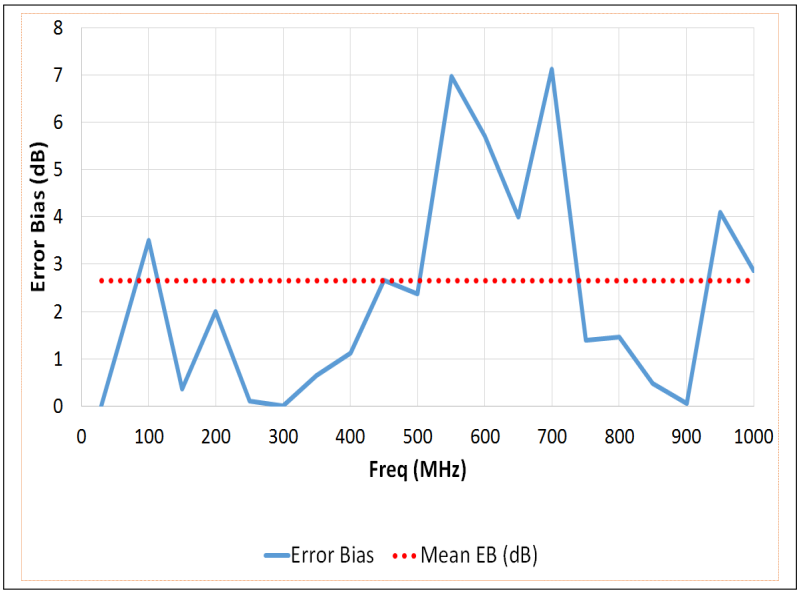

FIGURE 4.39: Error Bias Due to Height Scan Only, Long Wire, Horizontal Antenna

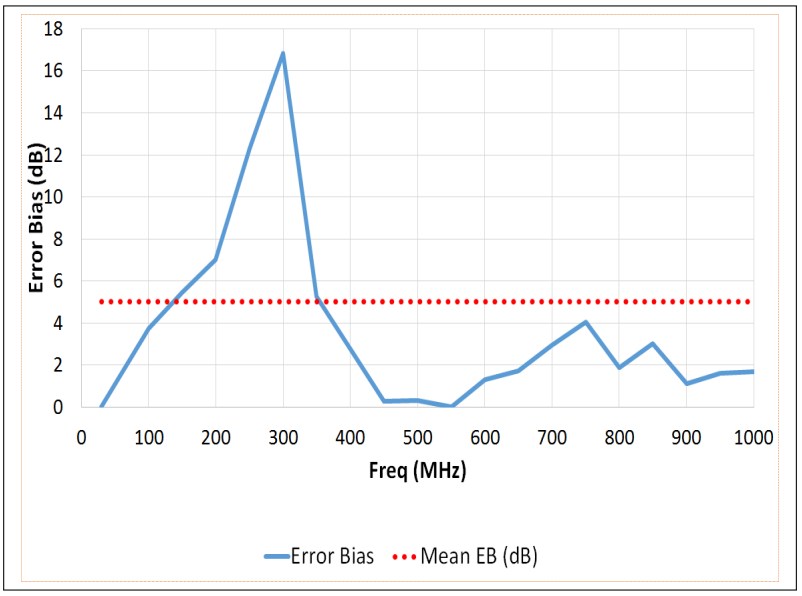

FIGURE 4.40: Error Bias Due to Height Scan Only, Long Wire, Vertical Antenna

The mean EB for both the vehicle and long wire were between 3 dB and 5 dB which is slightly higher than noted for the electrically small source. A noticeable feature of the EB graphs is that at 300 MHz for the electrically small noise source and for both electrically large noise sources an EB of approximately 10 dB higher than the mean for the vertically polarised receive antenna.

4.3 Azimuth Device Under Test Scan

4.3.1 Introduction

This Section introduces the influence the vehicle body shell can have on the directivity of the emissions radiation pattern. This can introduce errors in recording the maximum emissions when the current CISPR 12 method is utilised during a radiated emissions profile measurement program. Three main sub-sections are presented, the first offering a brief introduction to vehicle level radiated emissions measurement methods, the second section will describe work performed using a numerical model of a 'typical' vehicle body shell to asses the errors introduced during the current CISPR 12 procedure. The third section will describe radiated emissions measurements performed on a range of production vehicles that were used in an attempt to validate the EM model simulation results.

As previously described, any electronic device can be considered to be an unintentional transmitter of radio frequency energy. This energy will propagate away from the device with unknown directions and amplitudes, in order to ascertain the direction at which the maximum amplitude occurs a full spherical scan of the device with the measurement system is required. This method is both costly and time consuming. The aim of performing radiated emissions measurements of a device is to attempt to record the maximum amplitude of the emissions, however, due to the time and cost involved in performing a full spherical scan, a reduced measurement method is normally utilised.

The electrical size of an EUT has a direct relationship with the complexity of the radiated emissions pattern. As an item gets electrically larger, so the radiation pattern becomes more complex [2], [3]. An item is said to be electrically large when the expression in Equation 4.18 is satisfied [3]:

$$\frac{2\pi}{\lambda}a < 1 \tag{4.18}$$

where a is the radius of a sphere required to enclose EUT and λ is the wavelength. Thus it can be seen that a typical EUT of approximately 4 m in length will be electrically large at all frequencies covered during a typical CISPR 12 measurement program, typically 30 MHz to 1 GHz. The complex nature of the radiation pattern extends in three dimensions away from the EUT, thus a full spherical scan of the EUT, or an alternative

method such as using a reverberation chamber, would be required to record the maximum emissions.

With the advent of ever increasing clock signals in electronic equipment and the use of ever increasing use of the RF spectrum within the communications industries, there is increasingly a requirement for radiated emissions measurements to be performed at higher frequencies than in previous years. Currently many standards only require measurements to be performed up to 1 GHz, automotive CISPR 12 testing for example, but there is becoming a need for this to possibly be extended. In a research program carried out as part of the GEMCAR Project [24] it was found that emissions from a number of vehicles tested extended past the current upper test limit of 1 GHz. Broadband emissions were detected up to 3 GHz from a 'luxury' car and up to 6 GHz for a vehicle with a composite body shell. The latest version of CISPR 12 specifies an upper frequency limit of 1 GHz for emissions whilst it is being considered whether immunity measurements should be performed up to 2 GHz. The report produced by Ruddle et al. suggests that the frequency limit should be increased for both radiated emissions and radiated immunity tests.

It is assumed that the azimuth angle increment used when performing radiated emissions measurements will have an effect on the maximum amplitude of E-field recorded. It has been shown [46], that by using a coarse azimuth increment angle of approximately 20^o an error of up to 5 dB was recorded in the maximum E-field radiated by an EUT. This would suggest that the fewer measurement angles that are used, the lower the chances of recording the maximum E-field are.

It is often assumed that the face of the EUT that will radiate the maximum emissions can be identified using 'engineering judgement', the particular face with the maximum emissions will be the same at all frequencies and the angular direction of the maximum emissions is at or very close to face normal. Work carried out by Freyer and Backstrom [47] and Landgren [48] has shown these assumptions, as expected, to be incorrect. The studies conclude by quantifying various metrics by which the 'typical' measurement method employed underestimates the maximum emissions radiated by an EUT, and then stating that the Error Bias can be reduced by performing a more detailed measurement; typically by considering more measurement angles. This has been investigated as part of this thesis to ascertain the affect of using just two azimuth angles on the maximum E-field

amplitude recorded during a CISPR 12 radiated emissions measurement. As stated previously in Section 2.2.2 the methodology stated within CISPR 12 differs from many other Standards, CISPR 16-2-1 [49] and the American National Standards Institute, ANSI, 63.4 [50] for example, in a number of ways. The two parameters that have possibly the largest effect on the overall emissions signature recorded, are the orientation of the receive antenna with respect to the vehicle and the height of the receive antenna above the measurement facility ground plane. The standards noted earlier utilise a method whereby the EUT is rotated through 360^o, initially using an angular step size of no more than 15^o, in the azimuth plane in order to maximise the emissions. The use of just two azimuth angles in the automotive standard limits the possibility that the maximum emissions of the EUT will be recorded. For clarity throughout this paper the two angles, as shown in Figure 4.41, used during a CISPR 12 measurement will be referred to as 90^o and 270^o respectively.

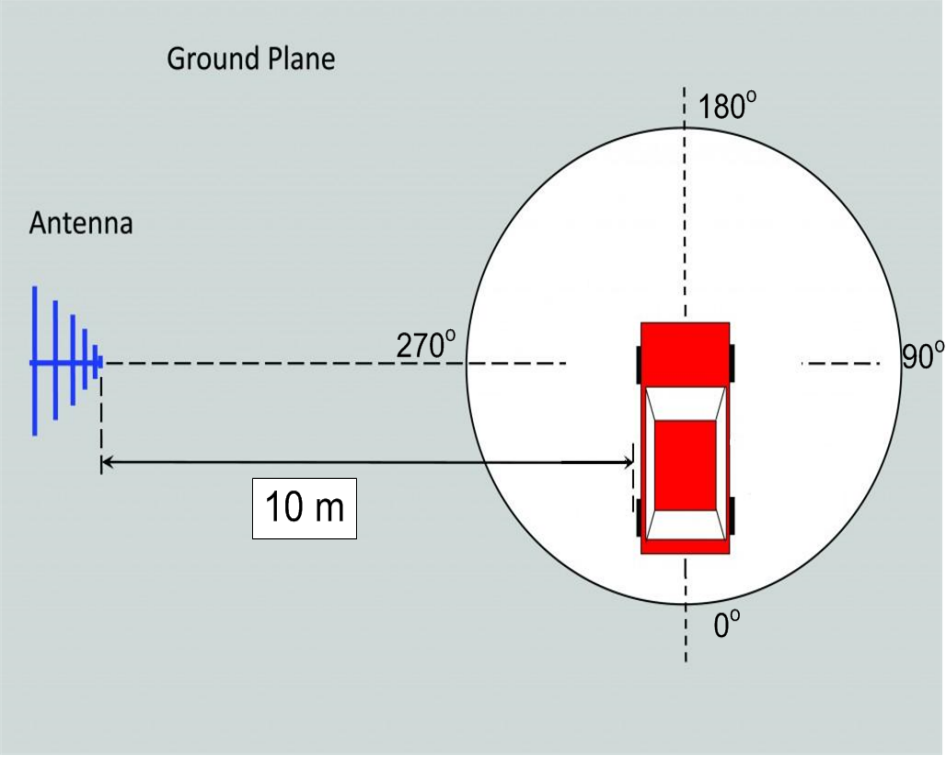

FIGURE 4.41: CISPR 12 Radiated Emissions Measurement Configuration

After reviewing the literature, it was found that some work has been carried out to investigate the external field radiated from the vehicle [24], however, specific research regarding the directivity of the emissions pattern has a little research published. The

majority of published work examines the directivity of installed antennas on the outside of the vehicle [51], [52].

Previous investigations into the vehicle emissions measurement process [24] have achieved inconclusive results. Radiated emissions measurements were performed using the antenna height and azimuth scanning approach of ANSI C63.4 [50] on a number of modern vehicles. A comb generator driving a current clamp around the wiring harness was used to excite and electric field inside the vehicle. It was found that due to drift in the frequencies of the emissions from the noise source, it was not possible determine if maximising the recorded amplitude using azimuth rotation of the vehicle actually resulted in the maximum emissions being more closely recorded. Due to the time difference between the initial scan of the frequency range to the maximisation scan, the drift meant that on many occasions the measurement receiver was no longer recording the peak of the sources emissions.

In order to quantify the error introduced by using a limited number of azimuth angles during a CISPR 12, a program of simulations and measurements were carried out. The EB was previously defined in equation 4.19, for this section it is modified as follows:

$$EB = E_{max} - E_{CISPR} \tag{4.19}$$

Where E_{max} is the maximum amplitude of the E-field recorded from the EUT as previously defined, and E_{CISPR} is the amplitude of the E-field recorded at the positions either side of the vehicle as detailed in Figure 4.41.

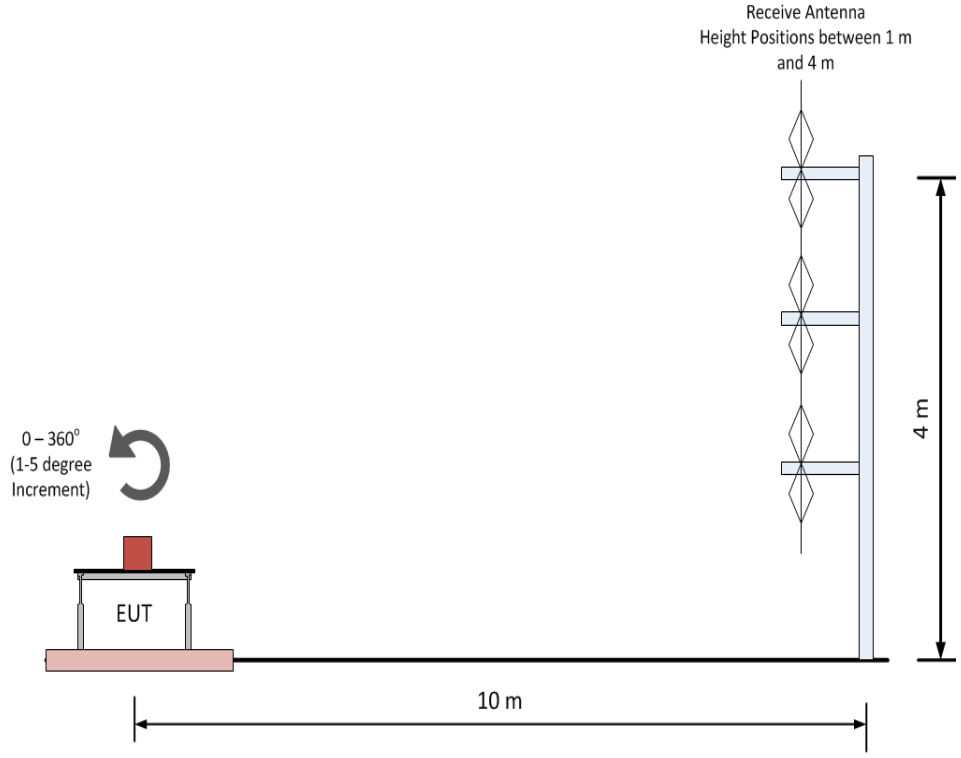

FIGURE 4.42: Error Bias Investigation Setup

The simulations were performed on a simplified body shell of a typical family hatch-back car and measurements on a range of commercially available family cars, ranging from a small town-car to a large 4x4 type vehicle. The aim of the simulations was to quantify the Error Bias introduced due to the reduced number of azimuth positions and fixed antenna height used during a CISPR 12 emissions test. The measurements were then performed on a production vehicle that had complete interior, engine and running gear, this would allow the investigation of the EB on a more complete vehicle than was possible using simulations.

4.3.2 Azimuth Scan Investigations - Vehicle Body Shell EM Simulations and Measurements

4.3.2.1 Introduction

This section details simulations and measurements performed to investigate the effect rotating the device under test during a radiated emissions measurement has on the amplitude of the E-field recorded. Firstly electromagnetic simulations were performed

on a model of simplified vehicle body shell with the aim of quantifying the amount of variation recorded in the amplitude of the E-field due to rotating the EUT through a full 360^o rotation, as described in Section 4.3. Secondly radiated emissions measurements were performed on a range of production vehicles at an open area test site, again to quantify the variations in the E-field recorded.

The results obtained from both the simulations of the VBS model and the vehicle measurements are then used to investigate the level of error in the maximum E-field amplitude recorded introduced by only performing measurements at two azimuth angles, as per CISPR 12, the error is then quantified.

Before simulations were commenced, a survey was performed of a number of typical production vehicles to ascertain the common positions of 'modules' that are likely to be sources of RF interference. Typical modules within a vehicle that are likely to be sources of broadband RF interference are: the spark ignition system, windscreen wiper motors, air conditioning blower motors and headlight steering motors. The majority of these devices can be found either in the dash area or in the engine bay, however their associated wiring could be routed over the entire length and width of the vehicle.

Chosen positions are detailed in Table 4.2. These positions were then used to locate an electrically small noise source within the simulation model. The source was modelled around the dimensions of a popular Comparison Noise Emitter (York EMC CNE IV) with a 270 mm long monopole radiator.

TABLE 4.2: Simulation Model Noise Source Positions.

Source Position No.	**Location**
Source 1	Middle of Centre Console
Source 2	Engine Bay
Source 3	Rear of Vehicle Drivers Side Rear Seat

4.3.2.2 Simulation Results

After performing the simulations on the VBS model described in Section 3.1.4.2, the E-field at points around the the model was recorded. The points were chosen to simulate an Effective Receive Antenna Height,ERAH, of 3 m above the ground level. The electric field was recorded at 360 discrete azimuth positions around the model. The radiation

pattern around the vehicle can be compared to an antenna pattern definition of 'a mathematical function or a graphical representation of the radiation properties of the antenna as a function of space co-ordinates' [53], where the word antenna is substituted for 'vehicle'. From the data recorded it is possible to produce a polar diagram of the radiation signature, in the azimuth plane, of the vehicle for each frequency. These plots make visualising the E-field structure and shape easier than a standard X-Y plot of field against azimuth angle. In order to make visualisation of subsequent comparisons of the data easier, all data was normalised to a maximum value of 0 dB.

A number of key parameters were extracted from the data sets for each frequency and source position, these were:

TABLE 4.3: E-Field References

Parameter	**Designation**
Maximum E-Field Amplitude	E_{max}
Minimum E-Field amplitude	E_{min}
E-Field Amplitude Recorded at CISPR 12 'Left Hand' Position	E_{LHS}
E-Field Amplitude Recorded at CISPR 12 'Right Hand' Position	E_{RHS}

The parameters listed in Table 4.3 allowed us to investigate the level of error introduced in recording the maximum E-field emissions radiated by the EUT if a small number of azimuth positions were considered.

For the purposes of this section data from 49 MHz to 500 MHz was considered.

Initially the EB derived from the E-field recorded in the CISPR 12 antenna positions compared to the maximum recorded from a full 360^0 rotation around the vehicle at an ERAH of 3 m was determined. The use of a single effective antenna height was so that the effect on the EB due solely to the azimuth scan and not the antenna height scan could be examined. The EB was recorded for each of the three source positions within the model. As the vehicle can be considered as electrically large at all frequencies under investigation, a complex radiation pattern could feasibly be expected.

Figures 4.45 to 4.52 give example polar plots showing the E-field recorded at a range of frequencies for the model. Data is shown at either end of the frequency range investigated and for both the ϕ and θ planes.

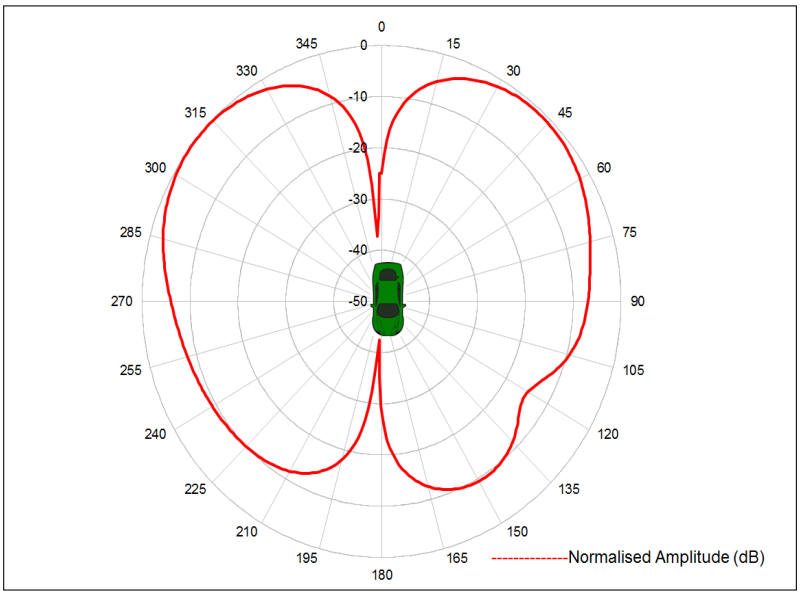

FIGURE 4.43: Polar Plot of Simulated E-field around VBS Model, 100 MHz, Source 1, Horizontal Polarisation

The pattern recorded in the horizontal plane can be seen to have an asymmetric nature, this is due to the source position not being in the plane of symmetry of the model, this has been used in order to make visualisation of the pattern easier .

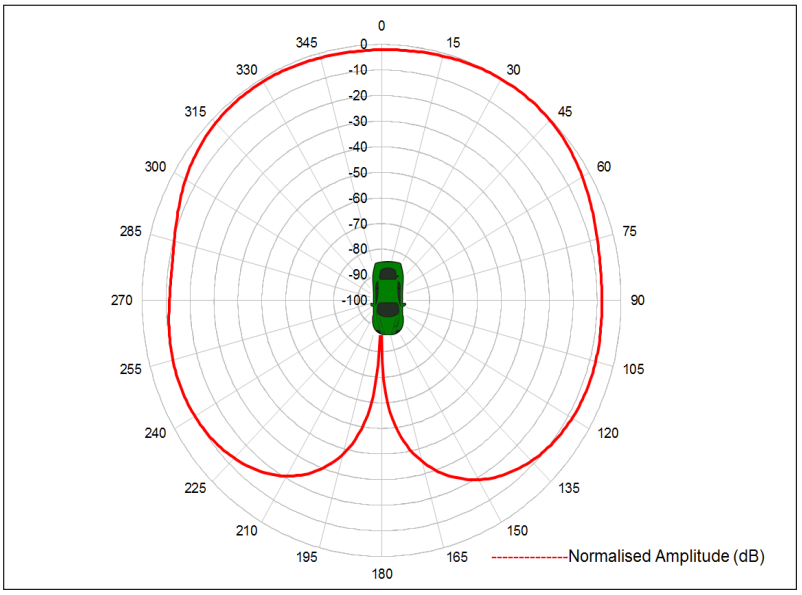

FIGURE 4.44: Polar Plot of Simulated E-field around VBS Model, 100 MHz, Source 1, Vertical Polarisation

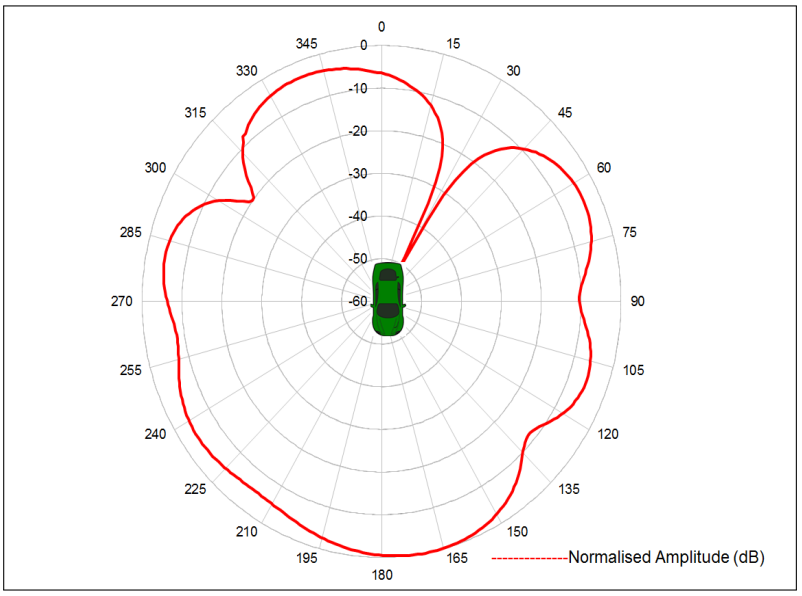

FIGURE 4.45: Polar Plot of Simulated E-field around VBS Model, 100 MHz, Source 2, Horizontal Polarisation

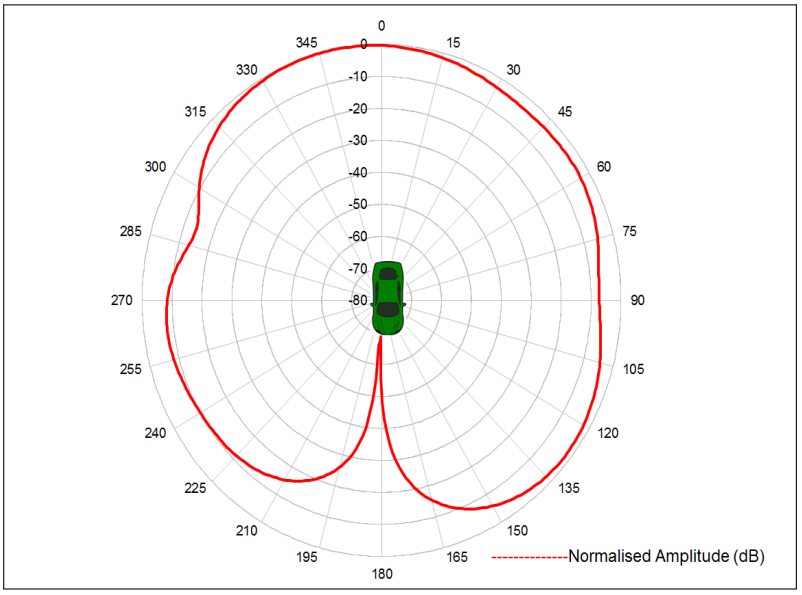

FIGURE 4.46: Polar Plot of Simulated E-field around VBS Model, 100 MHz, Source 2, Vertical Polarisation

It was noted that around 100 MHz a very deep null in the pattern was recorded around 180^o for both source position 1 and 2 in the θ plane, whilst for source position 3 the null was recorded at an angle of approximately 30^o as detailed in Figure 4.48. The overall pattern was very similar in shape between Sources 1 and 2, with the maximum emissions being recorded at approximately 0^o, for Source 3 the main lobe of the pattern was at approximately 195^o

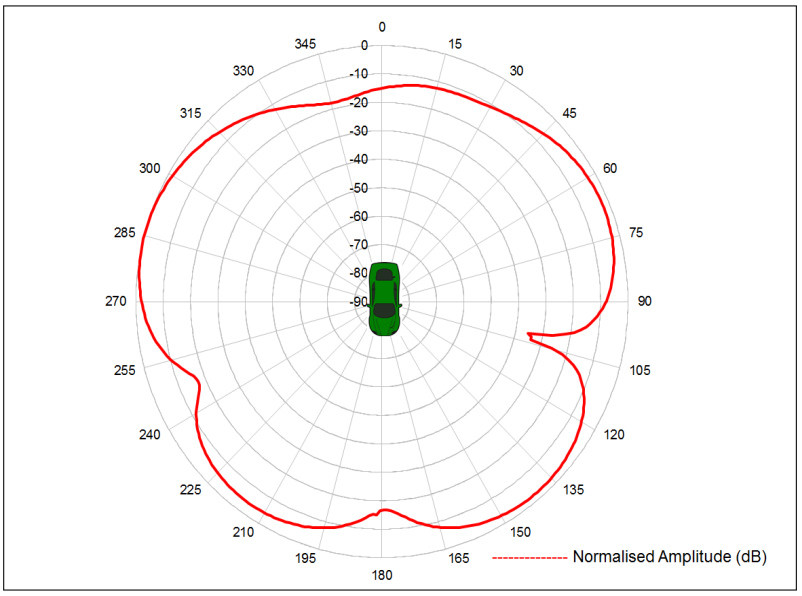

FIGURE 4.47: Polar Plot of Simulated E-field around VBS Model, 100 MHz, Source 3, Horizontal Polarisation

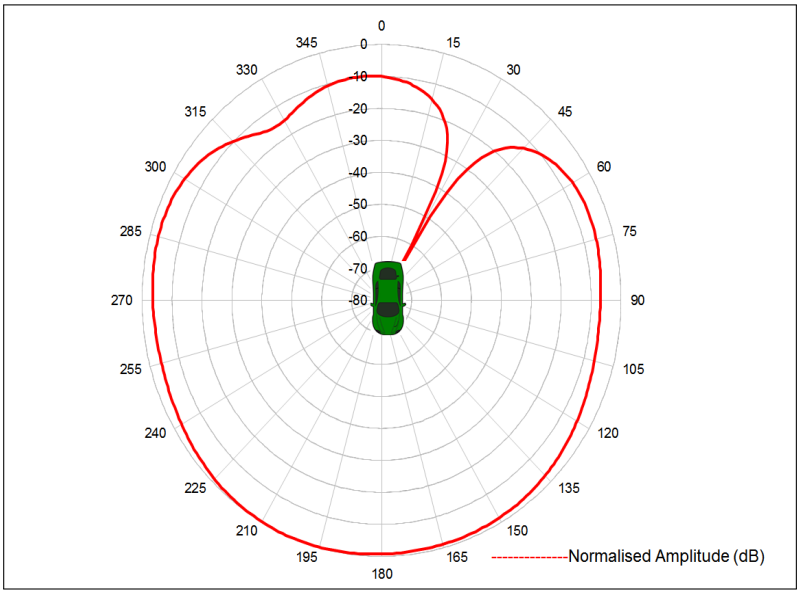

FIGURE 4.48: Polar Plot of Simulated E-field around VBS Model, 100 MHz, Source 3, Vertical Polarisation

The pattern recorded for the three sources was investigated further at 100 MHz and it was found that the position of the deep null was very frequency dependant. It can be seen in Figure 4.49 how a 1 MHz increase in frequency caused the position of the null to change from 180^o to 285^o

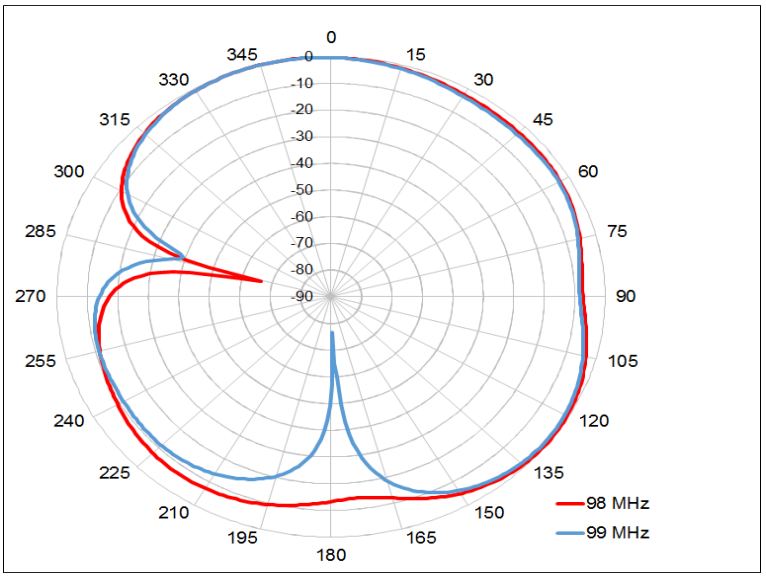

FIGURE 4.49: Polar Plot of Simulated E-field around VBS Model, 98 MHz to 99 MHz, Source 2, Vertical Polarisation

The deep null evident in the Source 3 data was also investigated. Similar to source 2, the null was found to change in position from 30^o to 270^o for an increase in frequency of just 500 kHz, this is shown graphically in Figure 4.50.

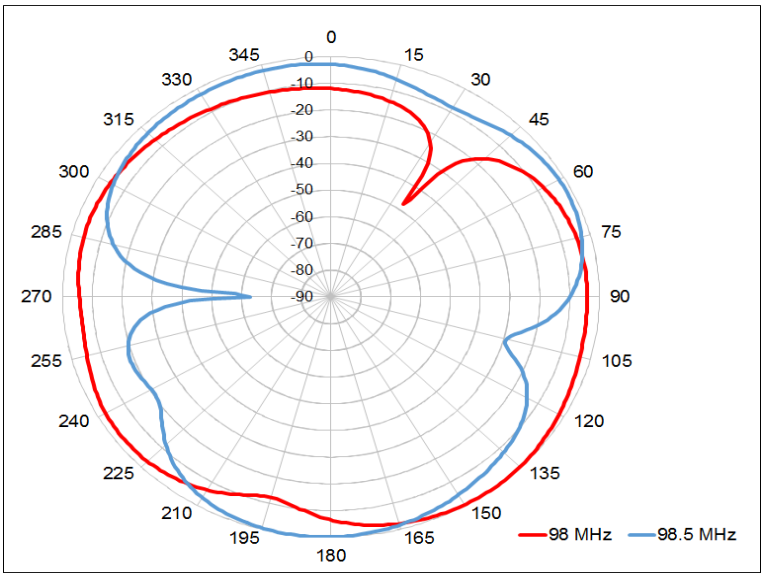

FIGURE 4.50: Polar Plot of Simulated E-field around VBS Model, 98 MHz to 98.5 MHz, Source 3, Vertical Polarisation

As expected the radiation patterns exhibit a simple lobe structure at the lower frequencies, as the frequency increased the pattern becomes correspondingly more complex. What is evident from the results is that the receive antenna positions used during a CISPR 12

measurement are highly unlikely to record the maximum amplitude of E-field and are quite often to be at the position of a substantial null in the pattern.

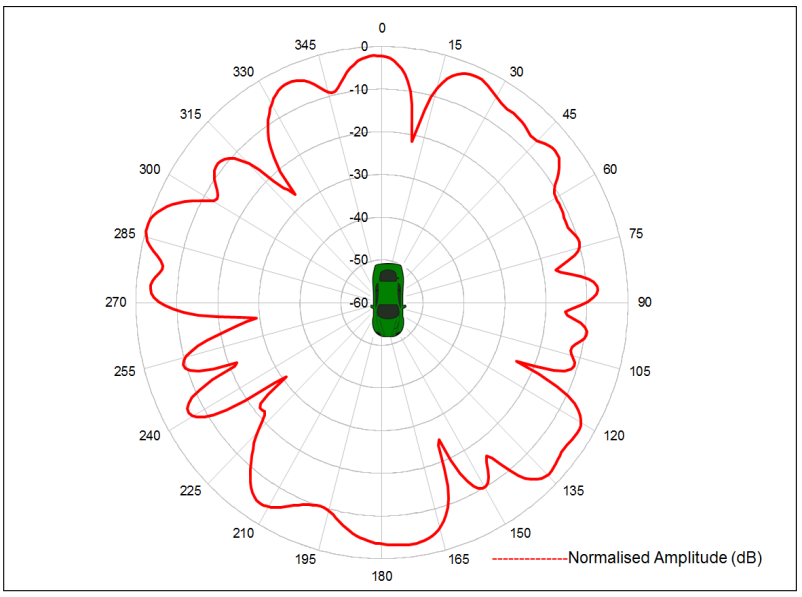

FIGURE 4.51: Polar Plot of Simulated E-field around VBS Model, 500 MHz, Source 1, Horizontal Polarisation

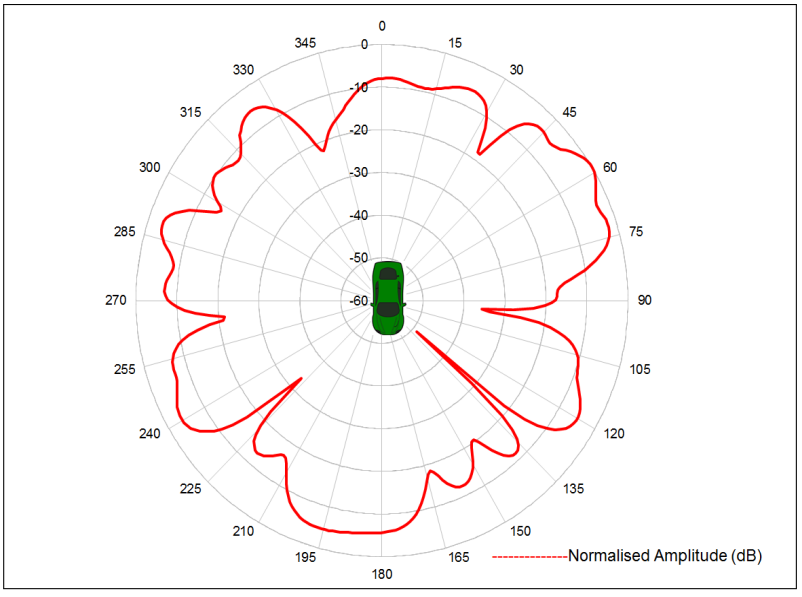

FIGURE 4.52: Polar Plot of Simulated E-field around VBS Model, 500 MHz, Source 1, Vertical Polarisation

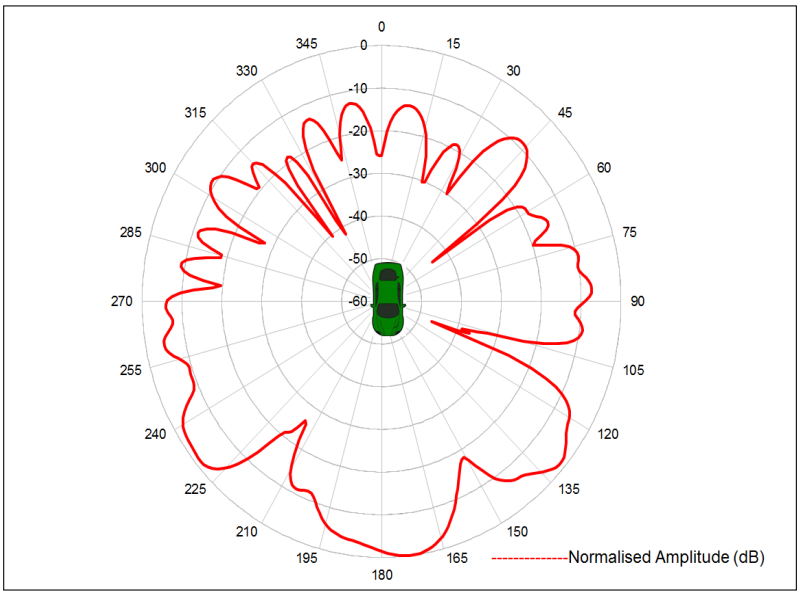

FIGURE 4.53: Polar Plot of Simulated E-field around VBS Model, 500 MHz, Source 2, Horizontal Polarisation

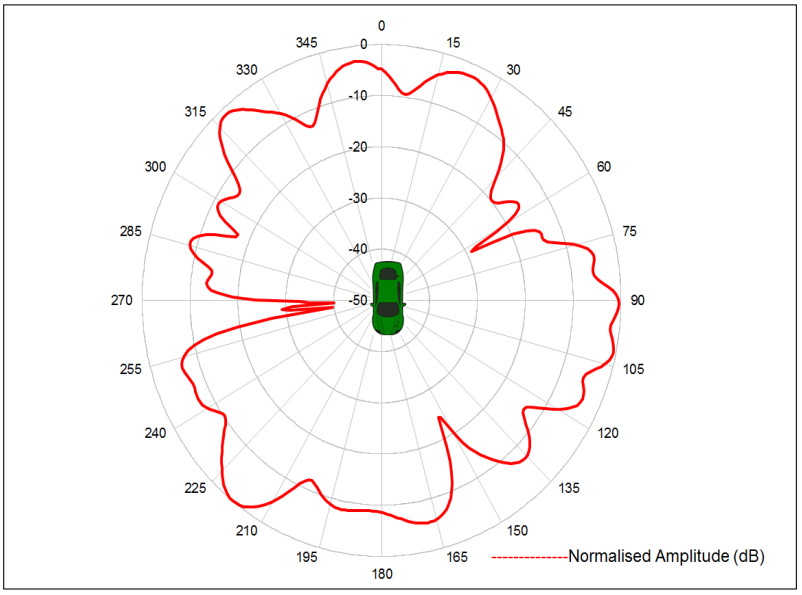

FIGURE 4.54: Polar Plot of Simulated E-field around VBS Model, 500 MHz, Source 2, Vertical Polarisation

Once the data from the simulations had been analysed, the corresponding EB in the amplitude for each source position against frequency was plot. Across the frequency span and source positions simulated the EB was found to vary in the range of from $< 1\ dB$ to a high value of over 17 dB. This is shown graphically in Figures 4.55 and 4.56.

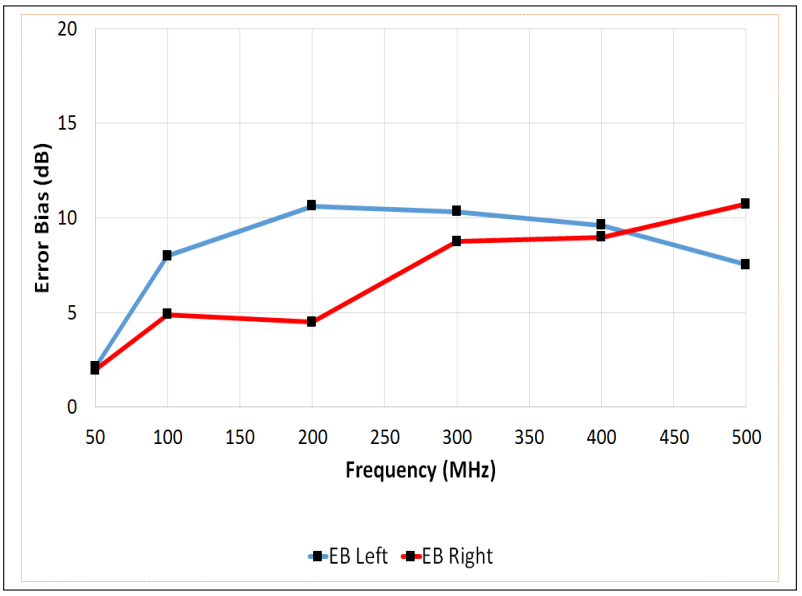

FIGURE 4.55: Worst Case Error Bias Against Frequency for All Source Positions, Horizontal Polarisation

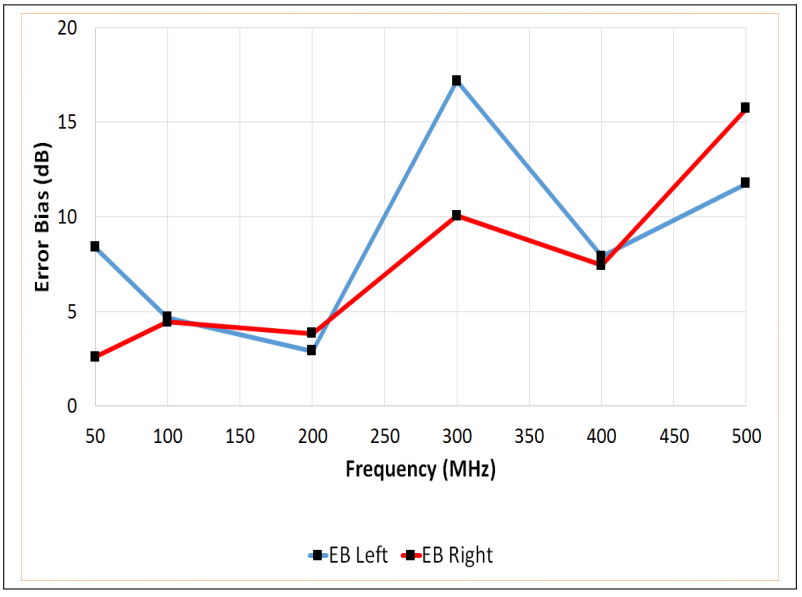

FIGURE 4.56: Worst Case Error Bias Against Frequency for All Source Positions, Vertical Polarisation

One feature that can be seen in the results recorded with the source at position 2 is a large EB at 50 MHz. This was caused by a deep null in the E-field pattern occurring at the left hand effective antenna position, detailed in Figure 4.57.

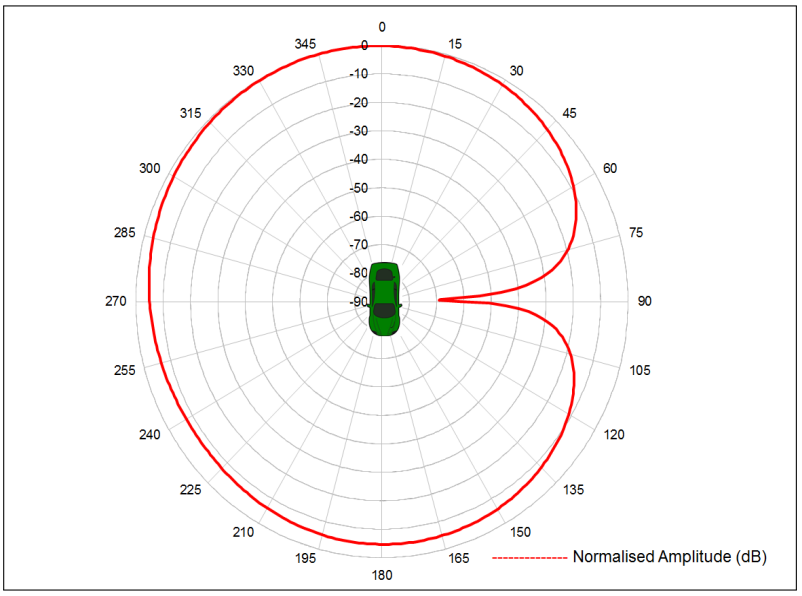

FIGURE 4.57: Polar Plot of E-field around Vehicle, 50 MHz, Source 2, Vertical Polarisation

Again this null was examined further by plotting the amplitude for small frequency increments either side of 50 MHz. Where the deep null was recorded at 50 MHz, which resulted in a large value of EB being recorded, for a 1 MHz change in frequency the null was observed to move to approximately 190^o, with a smaller null at 115^o. At 50 MHz a maximum EB of 12.7 dB was recorded, however, for a change in frequency of 1 MHz lower to 49 MHz the recorded maximum EB was 5.5 dB. When the two data sets are plot on the same graph, see Figure 4.58 the shift in position can be seen.

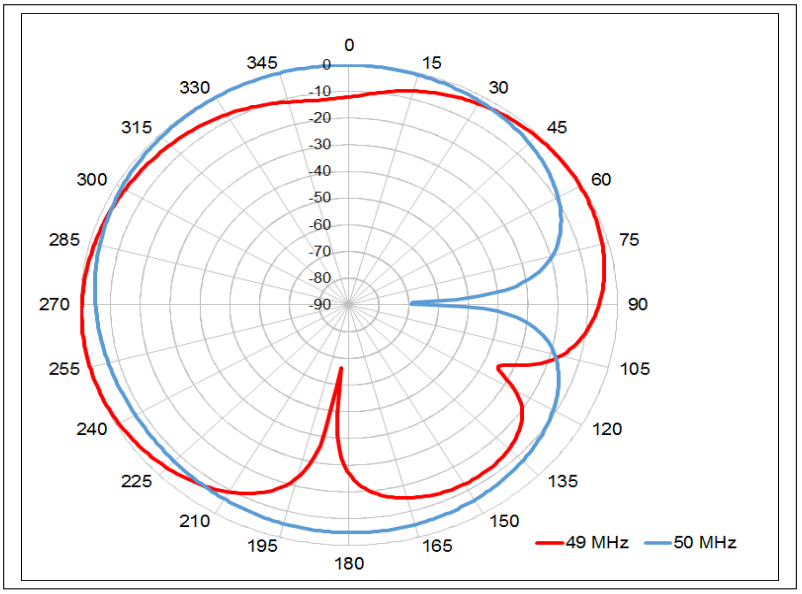

FIGURE 4.58: Polar Plot of E-field around Vehicle, 49 to 50 MHz MHz, Source 2, Vertical Polarisation

When the horizontally polarised data was examined a similar effect was recorded, again the position of a null near one of the equivalent CISPR 12 measurement points was leading to a large EB at 49 MHz, however, at 50 MHz the null had moved in position to approximately 215^o, resulting in a very low value of EB being recorded.

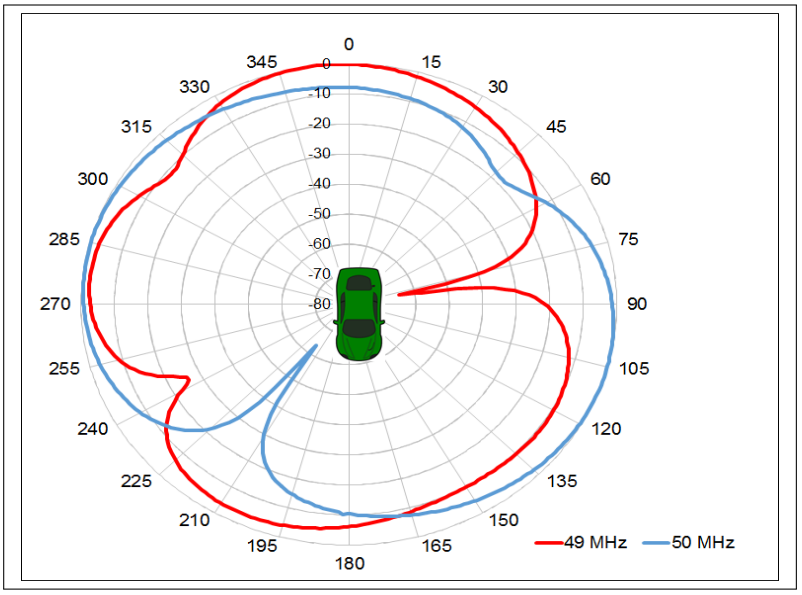

FIGURE 4.59: Polar Plot of E-field around Vehicle, 49 to 50 MHz MHz, Source 2, Horizontal Polarisation

At 300 MHz high EB values were also recorded, particularly for source positions 1 and 3, when examining the polar plots, an example is shown in Figure 4.60 it can be seen that nulls in the pattern occur very close to both the left hand and right hand CISPR 12 measurement angles.

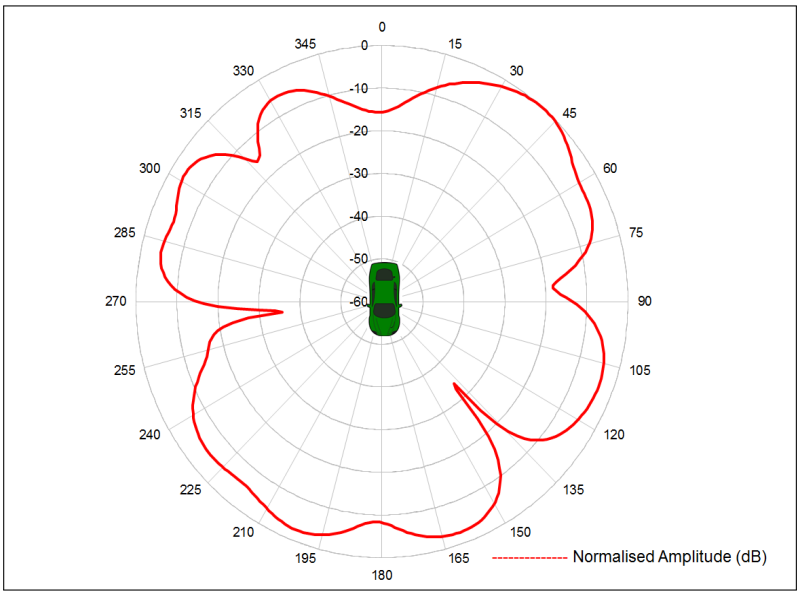

FIGURE 4.60: Polar Plot of E-field around Vehicle, 300 MHz, Source 1, Vertical Polarisation

Tables 4.5 and 4.4 show the mean of the linear EB across the three source positions. For the six frequencies considered here a mean EB of approximately 9 dB was recorded. A maximum mean error of 8.4 dB was recorded at the lowest frequency considered, this shows how, even at relatively low frequencies, a large EB can be recorded. It is commonly assumed that the radiation pattern is omni-directional at the lower frequency range, which for this particular setup is generally true, however, if a null occurs at one of the two antenna measurement angles, large amplitude errors can be introduced.

TABLE 4.4: Mean Error Bias for All Noise Source Positions (Horizontal Polarisation).

Frequency (MHz)	**Mean EB Left (dB)**	Mean EB Right (dB)
50	2.1	2.0
100	8.0	4.9
200	10.6	4.5
300	10.3	8.7
400	9.6	8.9
500	7.5	10.7

TABLE 4.5: Mean Error Bias for All Noise Source Positions (Vertical Polarisation).

Frequency (MHz)	**Mean EB Left (dB)**	Mean EB Right (dB)
50	8.4	2.6
100	4.7	4.5
200	2.9	3.8
300	17.2	10.1
400	7.9	7.5
500	11.8	15.7

4.3.3 Vehicle Measurement Azimuth Scan Investigations

To validate the simulation results obtained in Section 4.3.2 a program of measurements was performed. Radiated emissions measurements were performed on four commercially available vehicles. The vehicles were chosen to cover a range of typical sizes and styles commonly used today. They comprised of a large 4x4, a small town-car, a medium sized family hatch back and a medium sized panel van. Table 4.6 details the vehicles used:

Number	**Type**	**Make and Model**
1	Town Car	Nissan Micra
2	Family Hatchback	Ford Focus
3	4x4	Nissan X Trail
4	Panel Van	Fiat Berlingo

TABLE 4.6: Azimuth Vehicle Scan Investigations.

In contrast to the EM model documented in the preceding section, the measurements were performed on fully equipped, production vehicles. They had full interiors, engines and running gear. Where the complexity of the EM model affected the simulation time, for the physical measurements this was not a factor that needed to be considered, measurements would take the same amount of time whether a full vehicle or a stripped down body shell was used. The secondary reason for the use of production vehicles was the lack of availability of physical body shell, and vice versa - the lack of a fully equipped EM model to be used for simulation purposes. The aim of this section is not to make direct comparisons in the polar patterns between measured and simulated data, more to compare the effect of performing a full 360^o rotation of the vehicle on the amplitude of

the recorded E-field. The EM model and available vehicles were too different to allow for direct comparison of the lobe structures.

4.3.3.1 Measurements Setup

In order to have confidence that similar EB levels to those gained through performing the simulations were recorded, a wide band noise source (York CNE 3) placed inside each vehicle, in turn, was used rather than using the actual emissions generated by the vehicle electrical system. It has previously been shown [24] that using actual vehicle emissions for performing comparative measurements over an extended period, can lead to repeatability problems. The noise generator was placed on the passenger seat of each vehicle, with two additional positions being used for the large 4x4 type vehicle. The extra positions were the driver's seat and centre of the rear bench seat. Each vehicle was then placed at the centre point of the OATS facility turntable, 10 m from the measurement antenna, they were rotated through 360^o in 10^o degree increments initially, however this resulted in polar plots that were too under-sampled to enable the direction of maximum emissions to be determined. Further measurements were then performed using a 5^o increment. This data could still be possibly considered as under-sampled, however, available time did not allow for a finer angle increment. As the purpose of the data was for comparison of the directive patterns recorded, the absolute level of the emissions was not considered to be of vital importance. What was of more importance was the relative level at various different azimuth angles. One of the major issues encountered when performing measurements at an Open Area Test Site is that of ambient signals. High ambient signal levels can mean that data recorded at certain frequencies could not be considered to be entirely due to the test model. The emissions amplitude data measured while the model was active was compared to data recorded from a sweep across the band of interest with the model not radiating, any frequencies where strong ambient signals were recorded were removed from the investigations.

Each vehicle was aligned on the facility turntable with the front of vehicle facing the antenna, this angle is designated as 0^o. In contrast to the EM simulation setup used where the convention is for the model to be aligned with the rear of the vehicle facing as highlighted in Figure 4.41 the angles used to perform a CISPR 12 measurement were at 90^o and 270^o. For simplicity these angles will be referred to as Left (90^o) and Right

(270^o) from this point on. A general setup photo of the vehicle installed on the OATS turntable can be seen in Figure 4.61.

At each azimuth angle the amplitude of the radiated E-field was recorded for frequencies between 50 MHz and 500 MHz in 2.25 MHz steps. As in Section 6.2.1.4, the receive antenna was raised to 3 m above the facility ground plane. A single antenna height of 3 m above the facility ground plane was considered as only the error due to the azimuth scan was being investigated.

FIGURE 4.61: General Setup Details, Vehicle in MIRA OATS

FIGURE 4.62: Noise Source in Vehicle, Position 1

FIGURE 4.63: Noise Source in Vehicle, Position 2

FIGURE 4.64: Noise Source in Vehicle, Position 4

4.3.3.2 Vehicle Azimuth Measurement Results

The four vehicles were measured with the noise source located on the passenger seat, the drivers seat and the centre of the rear bench seat to investigate the affect on the direction of the maximum emissions due to source location. At each of the frequencies of interest a polar plot of the E-field amplitude against angle was produced. A selection of the plots are shown in Figures 4.65 to 4.70.

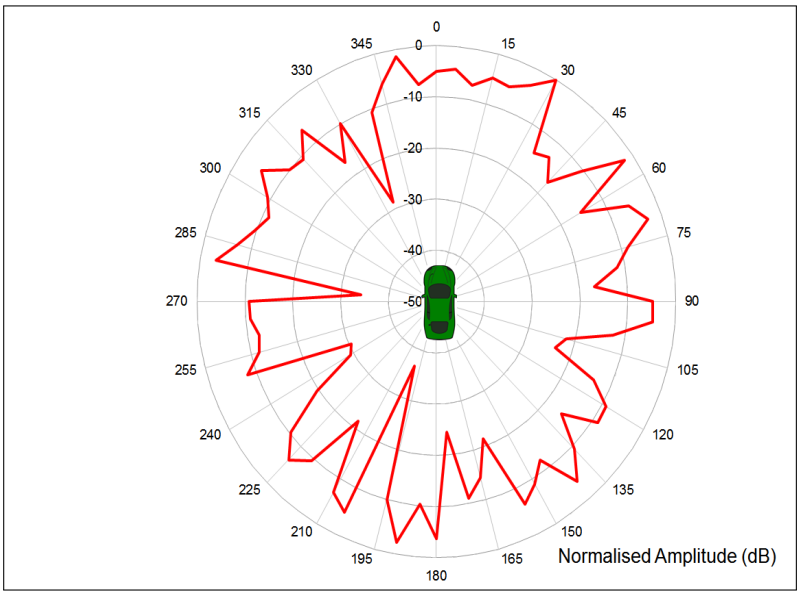

FIGURE 4.65: Undersampled Polar Plot of Measured E-Field around Vehicle 3, 50 MHz, Source 1, Horizontal

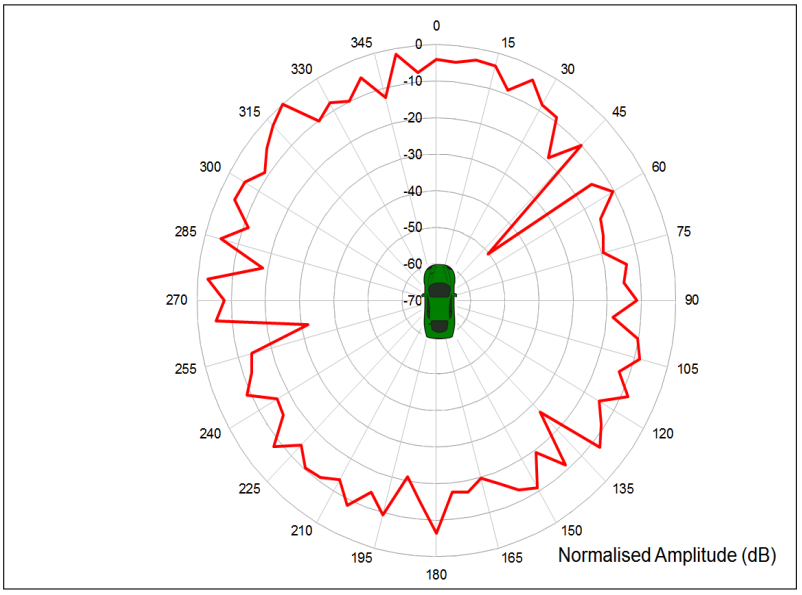

FIGURE 4.66: Undersampled Polar Plot of Measured E-Field around Vehicle 3, 50 MHz, Source 1, Vertical

One noticeable point that is evident between the measurement results and the simulations results reported on in the previous section, is the depth of the nulls in the lobe structure of the polar pattern. It has been shown [51] that EM computational simulations produce deeper and more clearly defined nulls in the polar pattern than those derived from measurements in an anechoic chamber or OATS, the actual design and construction of the chamber may contribute to the depth of the nulls. The lobe patterns obtained during

the measurements are far less clearly defined than those recorded from the simulations, this is due in part to the coarse azimuth angle used during the measurements. The receive antenna also averages the field over its aperture, whereas the simulation of a numerical model can output the field at a specific point in space.

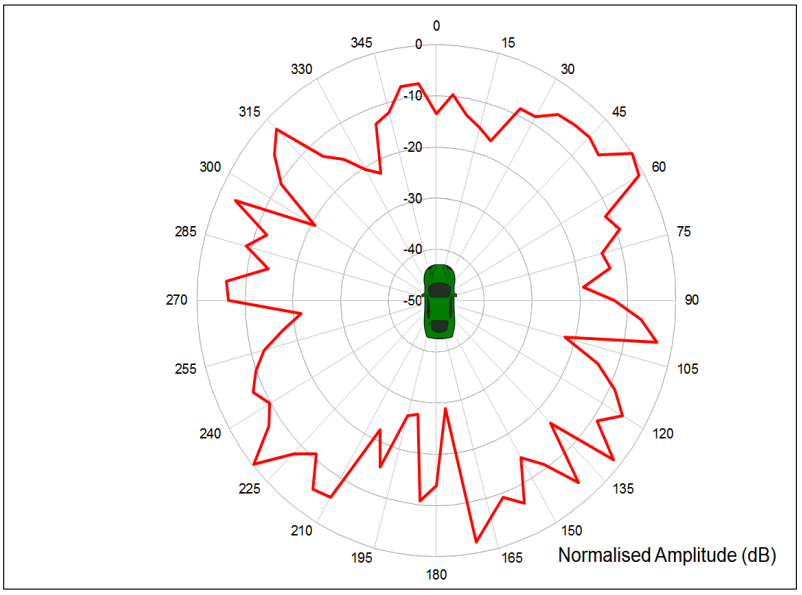

FIGURE 4.67: Undersampled Polar Plot of Measured E-Field around Vehicle 3, 50 MHz, Source 3, Horizontal

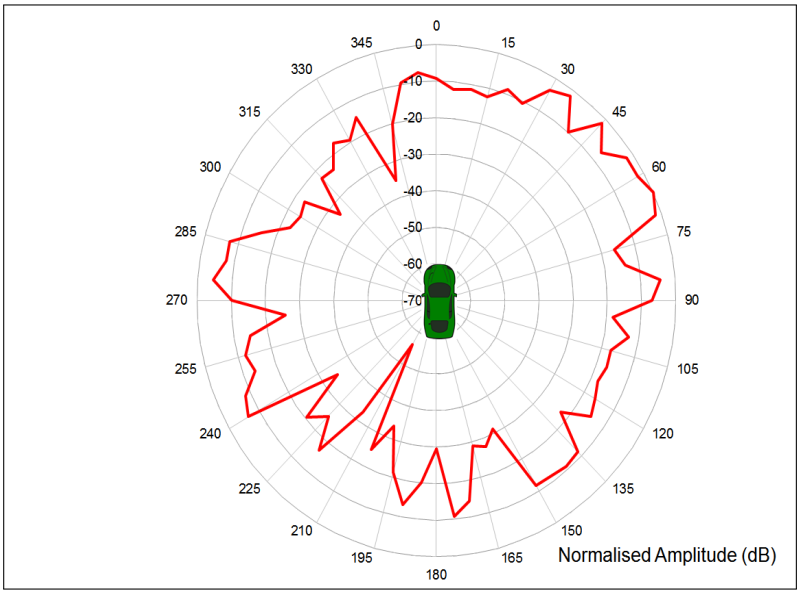

FIGURE 4.68: Undersampled Polar Plot of Measured E-Field around Vehicle 3, 50 MHz, Source 3, Vertical

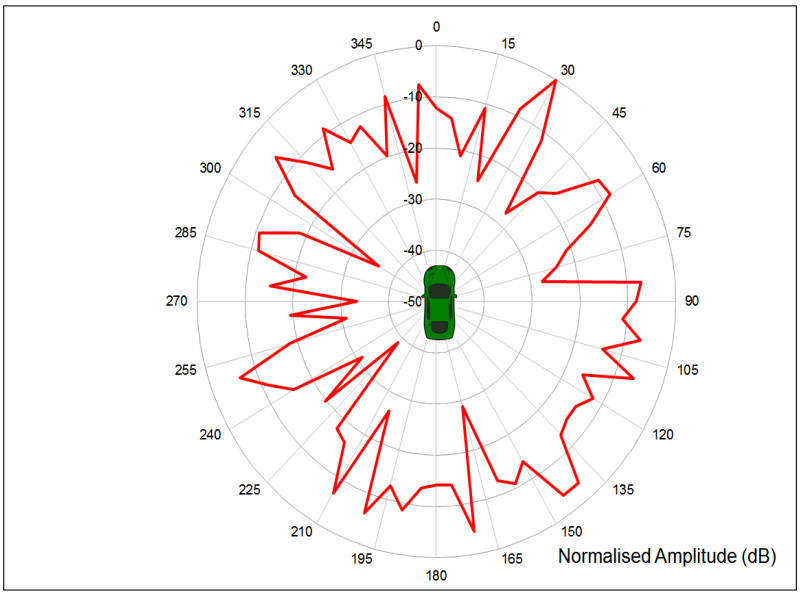

FIGURE 4.69: Undersampled Polar Plot of Measured E-Field around Vehicle 3, 500 MHz, Source 1, Horizontal

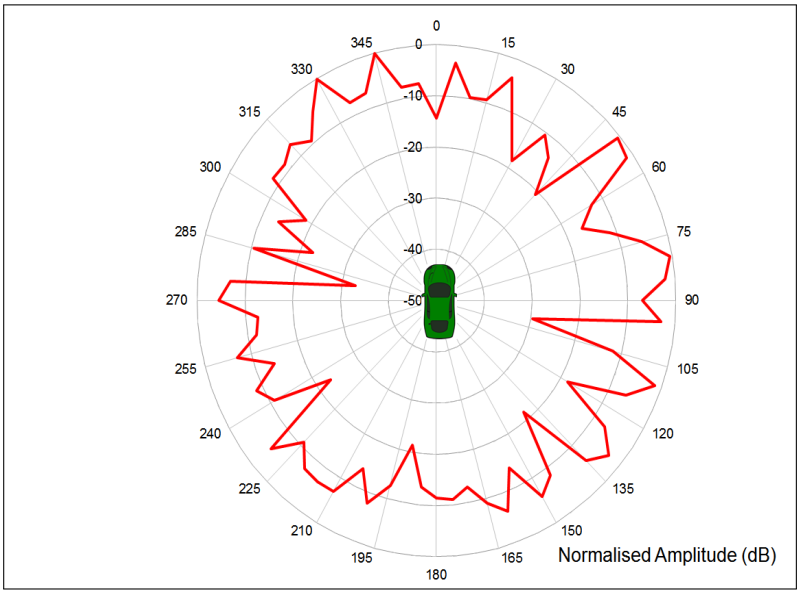

FIGURE 4.70: Undersampled Polar Plot of Measured E-Field around Vehicle 3, 500 MHz, Source 1, Vertical

The mean of the linear EB recorded for the large 4x4 type vehicle was 13.8 dB and 14.2 dB for the horizontally and vertically polarised received antenna respectively. For both polarisations a high value of approximately 25 dB was recorded between 400 MHz and 450 MHz.

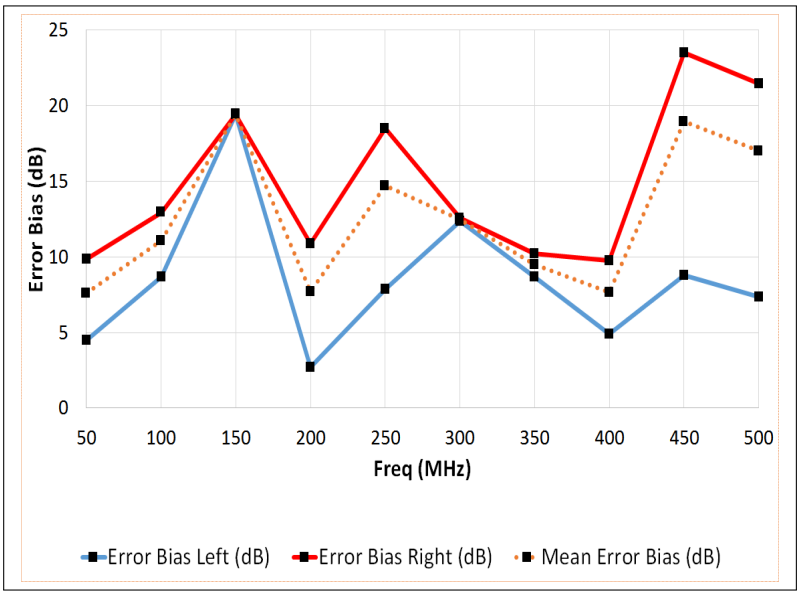

FIGURE 4.71: Nissan X Trail, Error Bias Against Frequency, Source 1, Horizontal

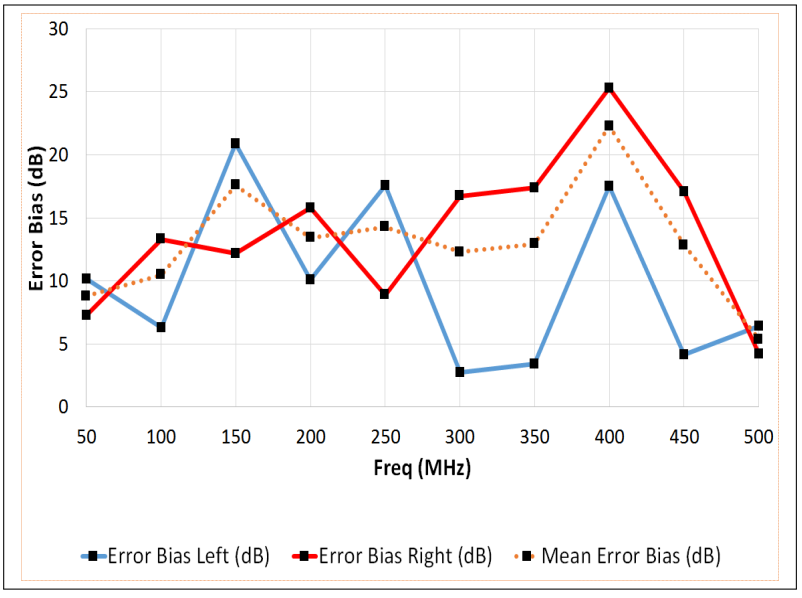

FIGURE 4.72: Nissan X Trail, Error Bias Against Frequency, Source 1, Vertical

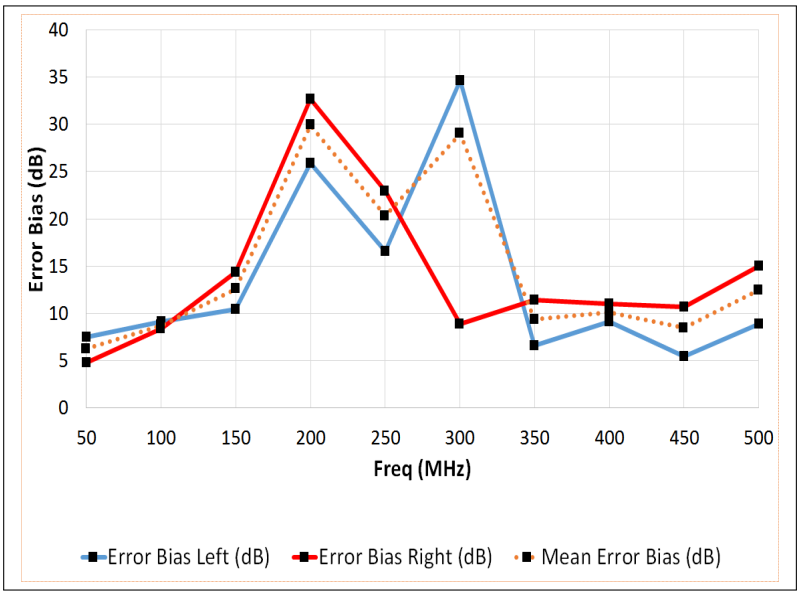

FIGURE 4.73: Nissan Micra, Error Bias Against Frequency, Source 1, Horizontal

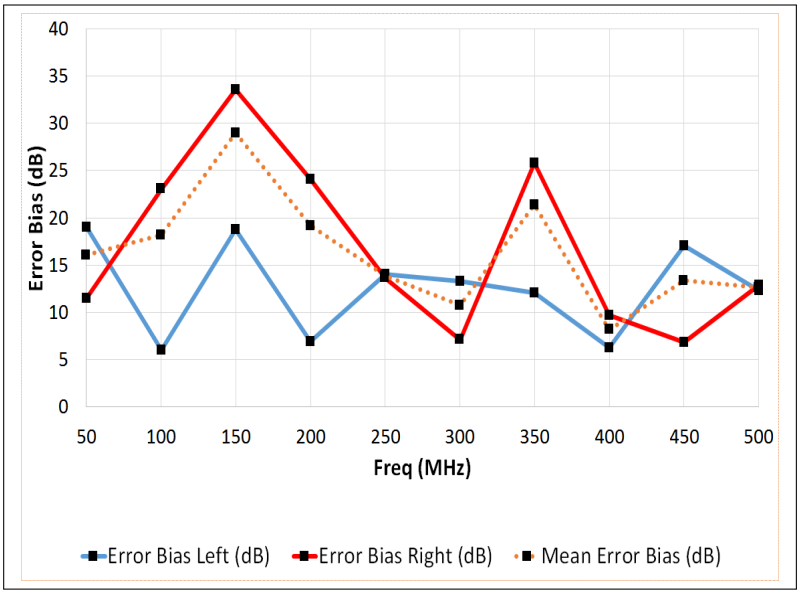

FIGURE 4.74: Nissan Micra, Error Bias Against Frequency, Source 1, Vertical

The mean of the linear EB for vertically polarised antenna using source position 1 was 18.4 dB and 19.3 dB for the horizontally polarised antenna. For the Nissan Micra the higher EB values were recorded below 300 MHz.

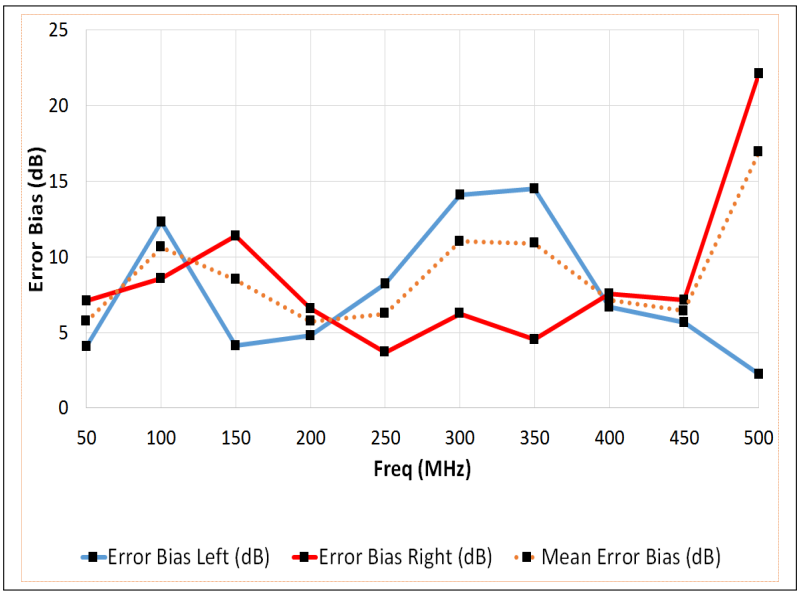

FIGURE 4.75: Fiat Van, Error Bias Against Frequency, Source 1, Horizontal

The Fiat Van recorded a horizontal EB of between 5 and 15 dB across most of the frequency range investigated with a high value of over 20 dB at 500 MHz. The vertical data had a much higher mean value of 16.8 dB, with a high value of 30 dB recorded at 100 MHz.

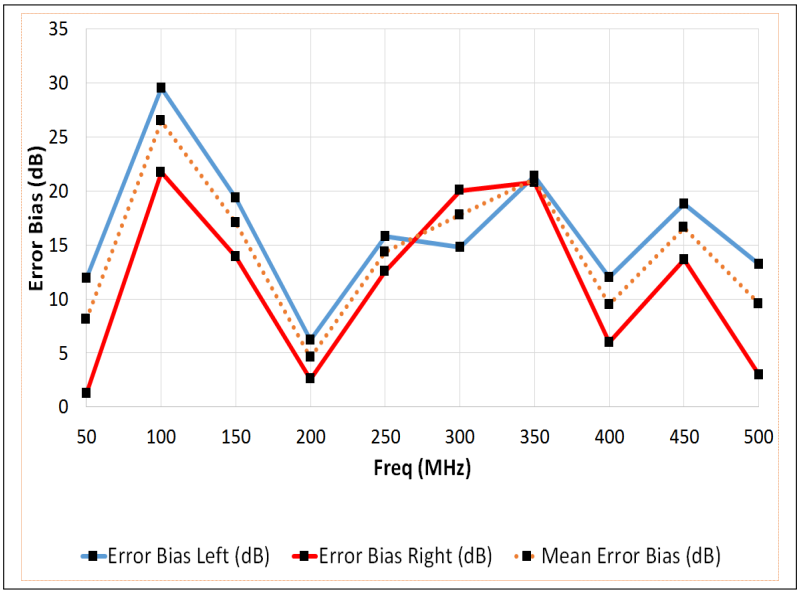

FIGURE 4.76: Fiat Van, Error Bias Against Frequency, Source 1, Vertical

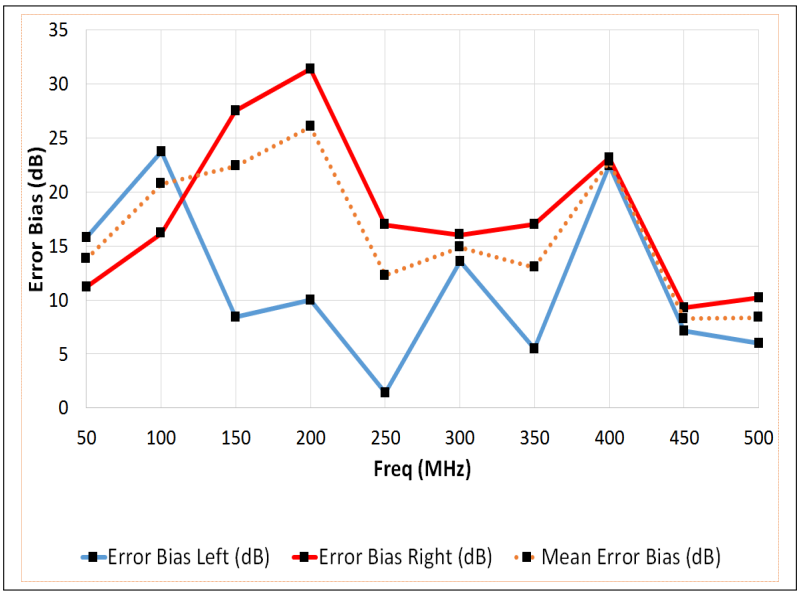

FIGURE 4.77: Ford Focus, Error Bias Against Frequency, Source 1, Horizontal

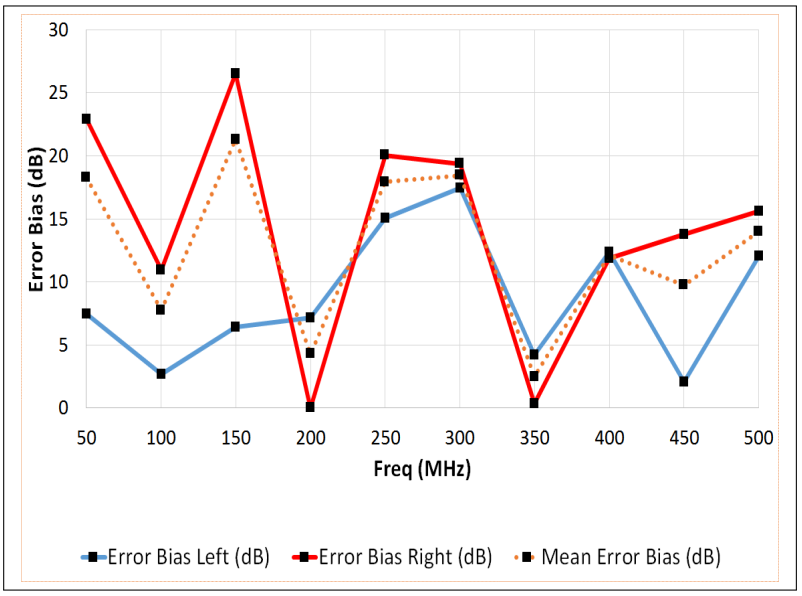

FIGURE 4.78: Ford Focus, Error Bias Against Frequency, Source 1, Vertical

The EB recorded for the Ford Focus showed a very low value at 250 MHz for the horizontal results and 200 MHz for the vertical data.

The 4x4 vehicle and the Fiat van also recorded a low value of EB at 200 MHz, however, across all frequencies and all vehicles measured a mean of the linear EB of approximately 12 dB was recorded.

This data, although possibly under-sampled, highlights the fact that by only using two azimuth angles during a CISPR 12 measurement program limits the likelihood of

recording the maximum amplitude of the emissions from the vehicle and introduces considerable errors into the results. The simulation results from the VBS model delivered a similar EB value of 11 dB.

4.4 Frequency Range

4.4.1 Introduction

In this Section the radiated emissions frequency span of a range of typical commercial passenger vehicles is investigated. The results of the investigations were used to determine the frequency range used in the research described in subsequent sections of this thesis.

CISPR 12 defines the current frequency range over which radiated emissions measurements should be performed as 30 MHz to 1 GHz [1]. Each vehicle will have a unique emissions signature over that frequency range that has to be determined, at the point before the measurements have started it is not clear at what frequency emissions will be observed. Whilst future vehicles may radiate unwanted interference at increasingly high frequencies, with the advent of devices utilising high clock speeds, Wi-Fi, drive by wire and more advanced infotainment systems, for the purpose of this research the frequency range has been limited to the upper limit of the emissions of 'typical' production vehicle.

4.4.2 Method

The emissions signature of a range of different vehicle types from: small town cars through family saloons, to a large lorry, were recorded in a semi-anechoic chamber using the frequency range defined in CISPR 12. The measurements of the individual vehicles have been made anonymous and given a designation reference to allow for them to be easily referenced within this thesis. Table 4.7 below shows the format of the references

TABLE 4.7: Vehicle Designation Examples.

Measurement Vehicle Type	**Designation Prefix**	**Number**
Small Family Vehicle	Meas-A	1
Medium Family Vehicle 1	Meas-B	2
Medium Family Vehicle 2	Meas-C	3
Large Family Vehicle	Meas-D	4
Lorry	Meas-E	5
Sports Coupe 1	Meas-F	6
Sports Coupe 2	Meas-G	7
Sports Coupe 3	Meas-H	8

For the purpose of investigating the frequency range of the radiated emissions, the vehicles were all measured in a large, 22 m by 10 m by 7 m, Semi-Anechoic Chamber, SAC, at HORIBA MIRA Ltd, using a standard CISPR 12 setup, (frequency range of 30 MHz to 1 GHz using both horizontal and vertical polarisation of the receive antenna, 10 m antenna to EUT distance, receive antenna 3 m above ground, Engine Running mode as defined in Section 2.2.2.

An example photograph is shown in Figure 4.79.

FIGURE 4.79: CISPR 12 Example Vehicle Measurement Setup

The radiated emissions from both the left hand and right hand side of the vehicles were recorded using a peak detector. To reduce the amount of data presented only the left hand side of the vehicle and vertical antenna polarisation are shown (the data recorded from the right hand side of the vehicle and using the horizontally polarised receive antenna showed a very similar span of frequencies).

As the purpose of this investigation was to obtain information regarding the frequency signature of the vehicles and not the absolute amplitude of the emissions, it was not necessary to perform full polar scan measurements.

As the measurements were performed in a SAC facility high ambient signal levels did not cause the problems highlighted in Section 4.2.5.2. An example plot of the noise floor recorded in the facility is shown in Figure 4.80.

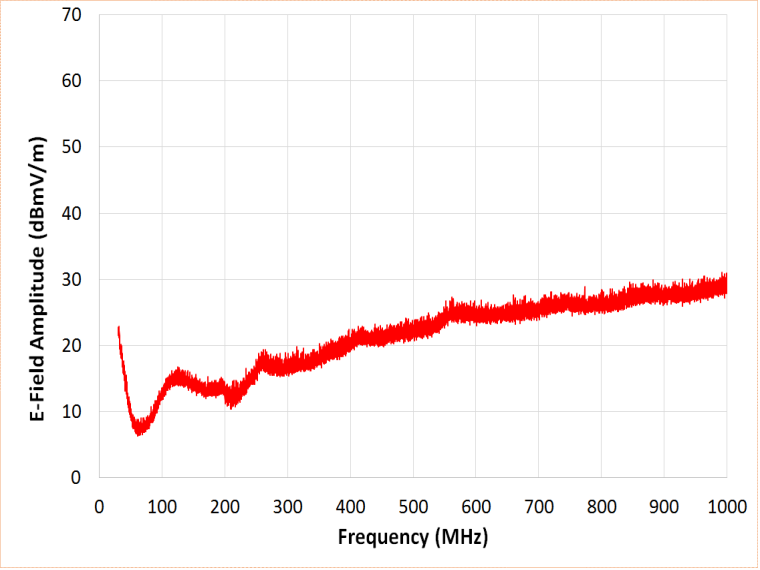

FIGURE 4.80: CISPR 12 Ambient (Measurement System Noise Floor) Level

The emissions data recorded at the time of test showed the absolute amplitude of the recorded vehicle emissions, as detailed in Figure 4.81.

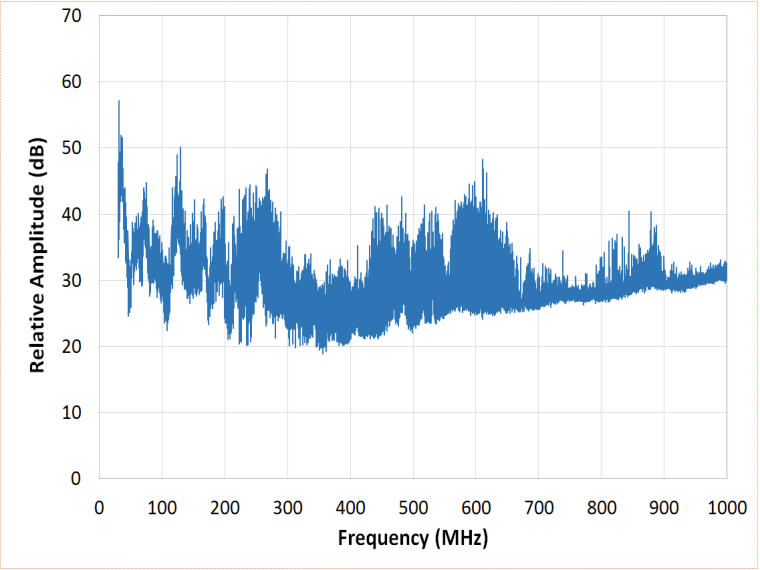

FIGURE 4.81: CISPR 12 Vehicle Emissions

Compared to Figure 4.81 a more informative data set was obtained by compensating for the ambient signal level recorded by the measurement system. For each recorded frequency the ratio of the measurement system noise floor to the measured signal from the vehicle was calculated, this gave an amplitude relative to the noise floor. This gave data that was easier to compare between different vehicle types, an example of which is shown in Figure 4.82.

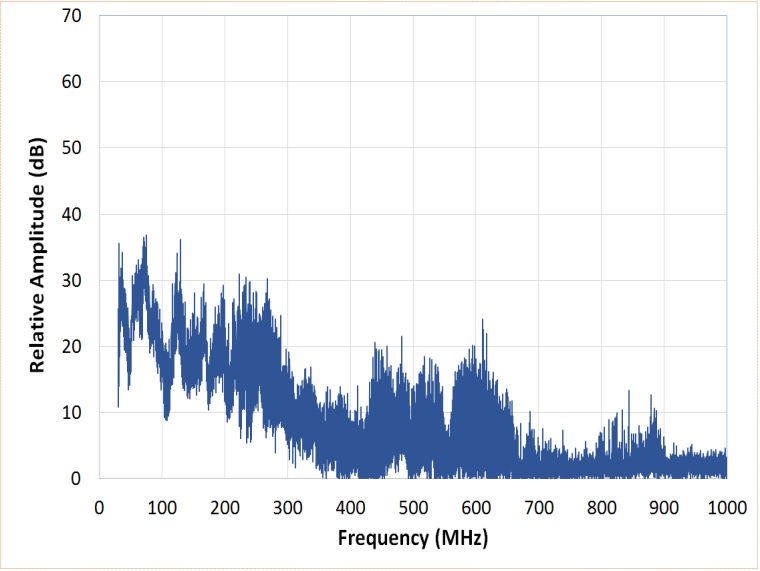

FIGURE 4.82: CISPR 12 Vehicle Emissions relative to Measurement System Noise Floor

As can be seen from Figure 4.82 above 600 MHz there are no significant emissions that can be attributed to the vehicle, between 600 MHz and 1000 MHz the figure displays mostly system noise.

The data from eight vehicles in total were measured in order to obtain a representative cross section of different vehicle types, sizes and levels of emissions.

4.4.3 Results

For each of the eight vehicles measured data was processed to give a plot of the emissions amplitude relative to the system noise floor, example plots are shown in Figures 4.83 to 4.86. These data allow for the spread and amplitude of the emissions to be analysed and provides more detail of the actual frequency range over which 'significant' emissions are actually recorded for each vehicle. Emissions were determined to be significant if they were at a level of $\geq 6dB$ above the system ambient noise floor. Anything below this was deemed to be ambient noise and not considered, 6dB was chosen as a suitable threshold based on common practice within many commercial test houses.

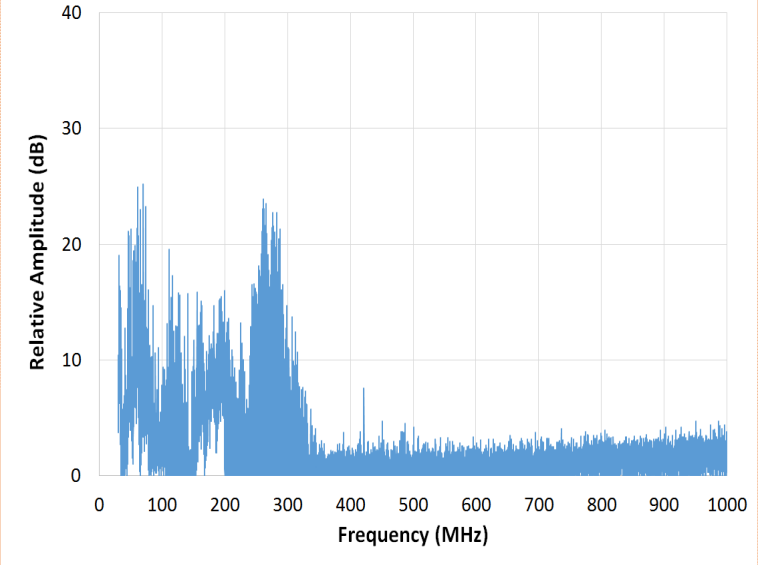

FIGURE 4.83: Vehicle Meas-A CISPR 12 Radiated Emissions Frequency Investigations

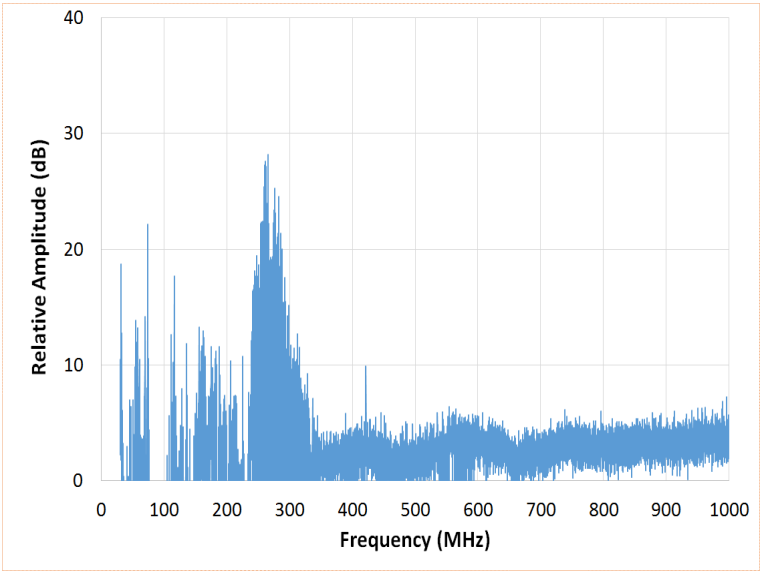

FIGURE 4.84: Vehicle Meas-B CISPR 12 Radiated Emissions Frequency Investigations

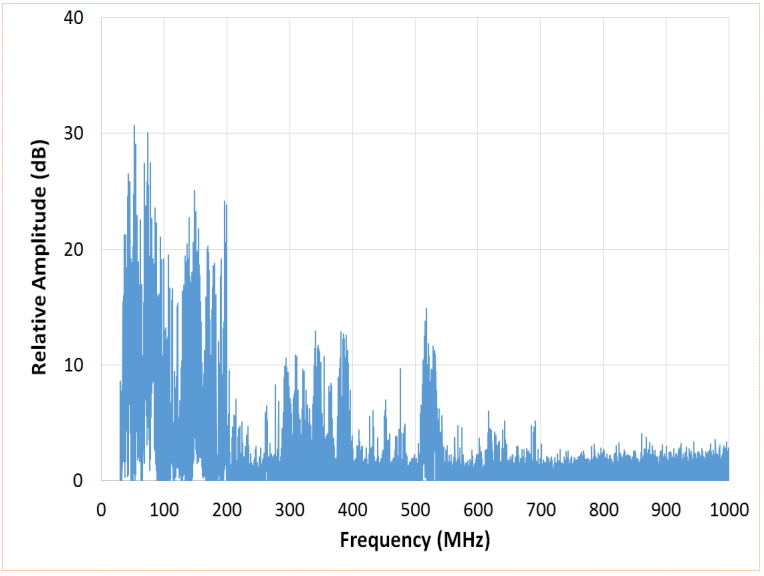

FIGURE 4.85: Vehicle Meas-D CISPR 12 Radiated Emissions Frequency Investigations

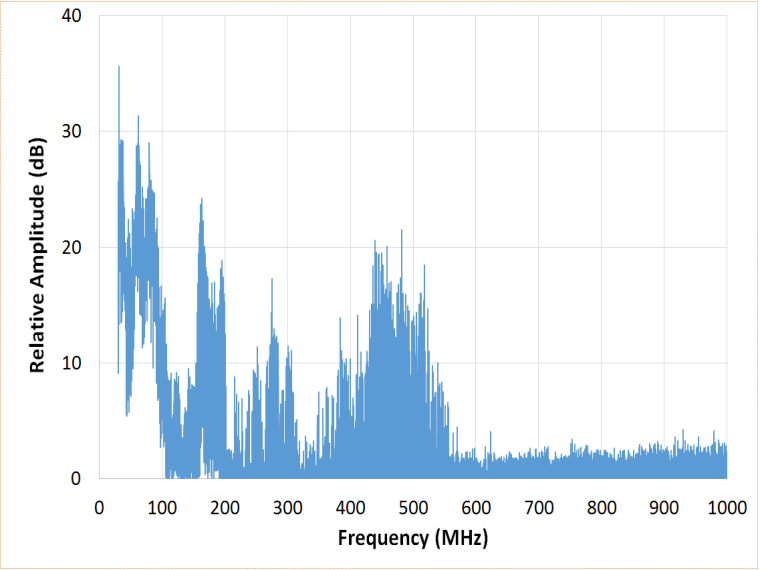

FIGURE 4.86: Vehicle Meas-F CISPR 12 Radiated Emissions Frequency Investigations

Once the emissions data from each vehicle in isolation was analysed, the maximum amplitude for each of the eight vehicles for each frequency was then collated into a single profile of amplitude against frequency, this then allowed the full range of emissions to be visualised in one simple graph, as can be seen in Figure 4.87 .

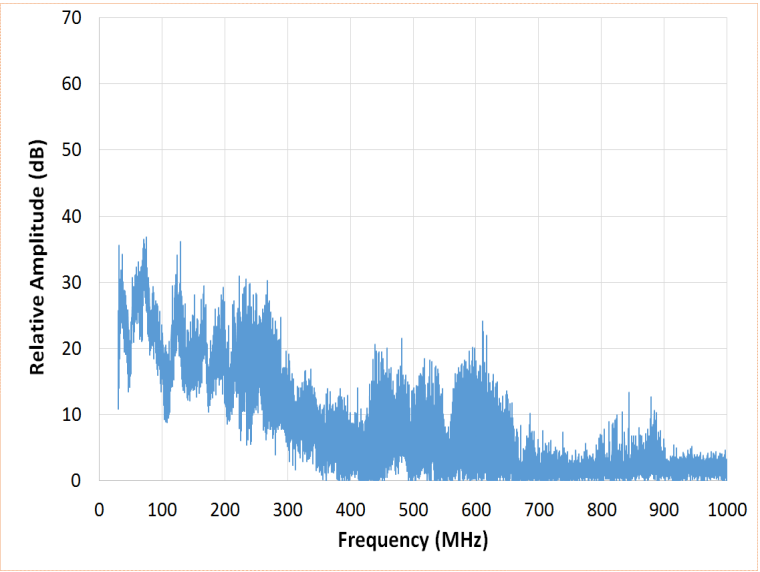

FIGURE 4.87: Worst Case Emissions Frequency Investigations

From the data presented in Figure 4.87 it was ascertained that above approximately 600 MHz the emissions amplitude across all eight vehicles had fallen below the threshold level of 6 dB above the noise floor of the system, as stated in the introduction to this Section.

For the investigations into an alternative to the CISPR 12 method for measuring vehicle radiated emissions, detailed in Chapters 6.1 and 7.1 of this thesis, an upper limit of 500 MHz was applied to the measurements and simulations performed.

4.5 Conclusions

The aims set out in this chapter were to quantify the main factors that affect the results when performing radiated emissions measurements of automotive vehicles. The two main areas highlighted were:

- Receive Antenna Height Scanning
- Azimuth Rotation of the EUT

Through a study of both the theory and performing a range of simulations and measurements, the affect of these two parameters on the chance of recording the maximum radiated emissions from the EUT was quantified.

Scanning the receive antenna in height between 1 m and 4 m above ground level was investigated in order to maximise the level of the recorded emissions. By not using height scanning during CISPR 12 vehicle measurements, the mean error recorded in the maximum E-field amplitude has been shown to be in the region of 16 dB over the 30 MHz to 1 GHz frequency range.

Not rotating the EUT through a 360^o range was found to possibly record up to 30 dB error in the maximum E-field determined. Not only is the actual rotation of the EUT important to reduce the errors recorded, but also, and possibly more importantly, the increment angle employed was found to have a considerable affect on the maximum field strength recorded. This effect was not, however, linear. That is to say, there is a trade off between the actual number of azimuth angle used to perform the measurements over and the reduction in error recorded. The CISPR 12 method only used two azimuth angles to record emissions data from.

Figure 4.88 shows a summary of the affect using the CISPR 12 method has on the Error Bias figures recorded. The red trace shows an example EB figure between 50 MHz and

500 MHz for the electrically large EUT detailed in Section 4.2.5.2, while the blue trace shows the mean EB recorded from when the three vehicles detailed in Section 4.3.3.1 as a result of only performing measurements at the E_{LHS} and E_{RHS} positions.

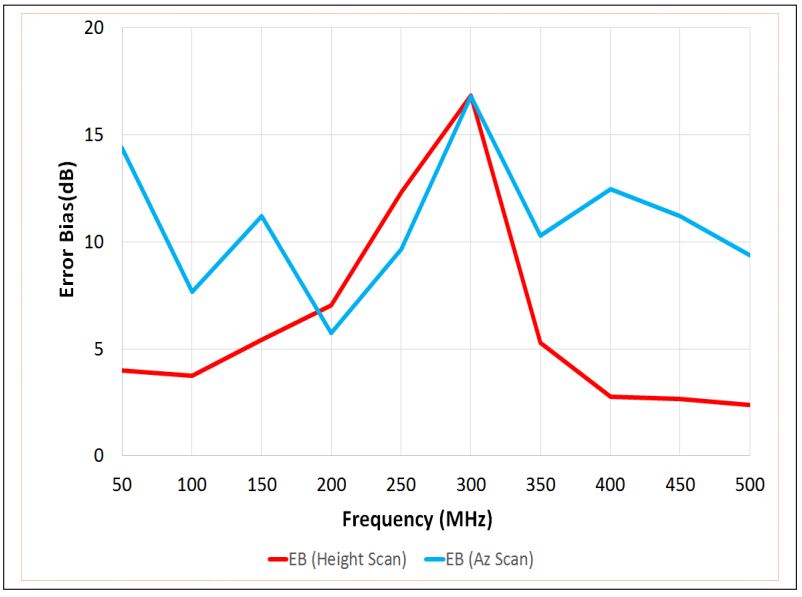

FIGURE 4.88: Summary of Error Bias Due to CISPR 12 Configuration

A third parameter was also considered, that was the frequency range over which the measurements are performed. The frequency range over which emissions that could be considered as 'significant' was determined. This frequency range was then used to define a limit in the scope of measurements and simulations performed in Chapters 6.1 and 7.1 of this thesis. It was shown that above approximately 600 MHz the emissions from a range of eight commercially available vehicles had fallen to <6 dB above the noise floor of the measurement system being used.

As a result of performing this research, evidence has been gathered to support the argument that using the current CISPR 12 procedures, in which the radiated emissions of full vehicles are measured, that the amplitude of the E field recorded will be below the level recorded if the emissions were to be maximised. The driving factor for keeping automotive radiated emissions measurements to a minimum is cost. Manufacturers of vehicles are always going to be keen to perform the minimum amount of testing necessary to conform with the relevant standards, however, it could be argued that due to the sheer number of vehicles currently on our roads and the possible threat that they pose to other electrical devices why should the automotive trade be allowed to perform such a modest amount of testing, compared to say, the domestic device market. With the advent of

ever increasing clock speeds, and more importantly clock edge rise and fall times, higher number of electronic devices within the vehicle and more electric and hybrid vehicles there should possibly be an interest in performing more testing not less.

Physical measurements are, at present, the mainstay of the methods employed to prove conformance with the required standards. There is a feeling among the EMC fraternity that in future years, the role of electromagnetic modelling will become increasingly more important. EM modelling has several distinct advantages over measurements:

- lower initial costs (no costly measurement facilities to purchase / build)
- lower maintenance costs
- all weather
- possibly quicker iterative process during development (it could be possible to either change or build a new model quicker than build a new physical vehicle

EM modelling is not without is drawbacks however. Using current computers, whether that be desktop PC's or super computers / parallel PC's, simulation of complex EM models is very computer intensive, requiring fast processors and large amounts of memory. Thus the more detail incorporated into the model, the longer the simulation will take to perform. Conformance with test standards is only via a program of measurements at present, it is unclear whether proof of conformance based on an EM model will ever be a reality and the likelihood of simulations completely replacing measurements is low. However, as more experience and knowledge is gained in performing vehicle simulations, problems should be able to be identified earlier in the design process.

Chapter 5

Alternative Test Methods

5.1 Alternative Measurement System

5.1.1 Introduction

In this section possible alternative test methods to the current CISPR 12 procedure are considered. As has been highlighted in Chapter 4 the methods currently used to perform CISPR 12 vehicle radiated emissions measurements can substantially under-estimate the amplitude of the maximum E-field measured from the vehicle under test. A number of alternative methods will be discussed and their respective benefits and disadvantages will be highlighted

The methods considered to determine if they offer a viable alternative for vehicle measurements and reduce the EB recorded using the current method are:

1. Spherical / hemi-spherical antenna scan around the vehicle under test
2. Antenna Height / Azimuth Scan (CISPR 22 Method)
3. Reverberation Chamber
4. The 'Test Wire Method'

5.1.2 Spherical Antenna Scan

In an ideal world using a full spherical, or hemi-spherical measurement scan around the vehicle under test has the potential to record the lowest possible Error Bias. This method does, however, have a number of major disadvantages. It can be argued that the reduction in EB recorded using the spherical scan does not justify the costs involved. In order to perform radiated emissions measurements using this method not only is a very expensive measurement facility required but also the time involved to fully sample the E-field at sufficiently high number of points in space means its use for testing on a commercial basis is prohibitive.

For spherical emissions measurements to be performed at a facility large enough to house a car or van would involve a very sophisticated antenna positioning system alongside the normal azimuth rotator. For each measurement position the EUT is rotated in azimuth along with the measurement antenna being scanned in an arc around the vehicle in the elevation axis. As the EUT is also being rotated in the azimuth plane, the antenna needs to be scanned from -90 to +90 degrees in the elevation plane. This method of testing is more commonly used for near field scanning of relatively small EUTs, however, in principle it would still be possible to build a system large enough to test a vehicle, but the costs and complexity would be vastly increased. The basic concept of the hemi-spherical scan is shown in Figure 5.1, the major difference between the hemi-spherical scan and a full spherical scan is the antenna would also need to be scanned from 0^o to $+90^o$ for the hemispherical scan.

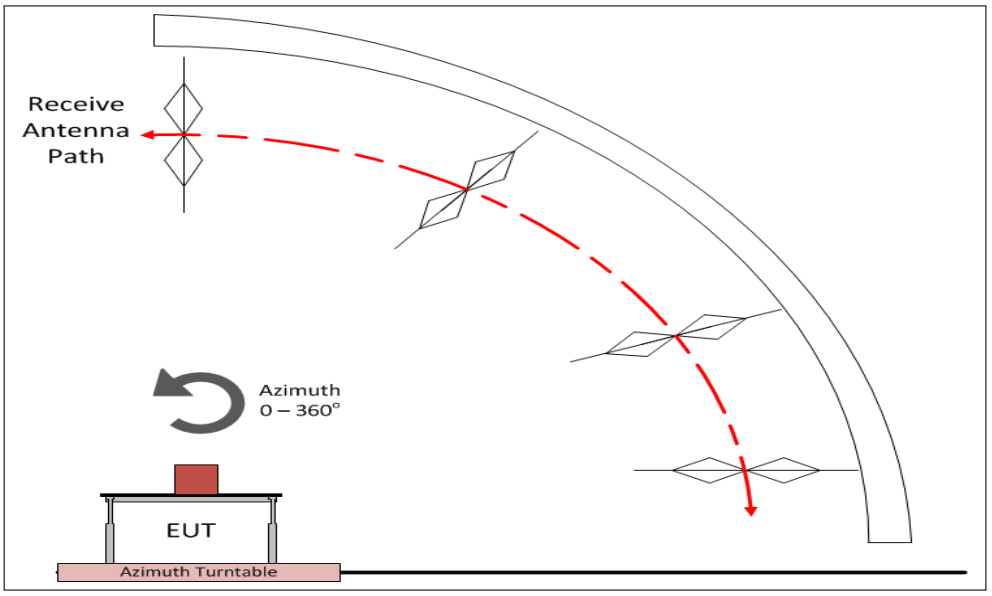

FIGURE 5.1: Hemi-Spherical General Test Setup

An alternative to performing what would traditionally be thought of as a 'spherical' scan around the EUT is to use a cylindrical scan method. This method involves taking measurements at varying antenna heights around the EUT while the EUT itself was rotated around it Z axis. Measurements would be performed with the EUT either rotated in small increment steps around either the X or Y axis or at three orthogonal orientations relative to the measurement antenna, whilst rotated around the Z axis. Again the practicalities of performing such a test with something as large as a car would be much greater than a traditional OATS type emissions measurement as rotating the vehicle to present the other two orthogonal angles to the antenna is much harder than rotating it around the azimuth axis. Studies performed by Freyer and Backstrom [47], Landgren [48] and Batterman and Garbe [46], [54], highlighted that as the increment angle used for either the receive antenna height scan, or the azimuth angle increased, the error in recording the maximum emissions also increased . These studies recorded mean errors introduced by performing azimuth scans with a coarse increment angle, 20^o in the case of [46], of approximately 5 dB compared to those recorded using an increment angle of 2.5^o. In the case of the antenna height scan studies mean errors of approximately 4 dB were observed. These error values recorded due to the use of coarse height scan increments are at a similar level to those found during measurements detailed in Section 4.2 of this thesis. The error noted as a result of performing limited azimuth scans, was lower than reported in Section 4.3. However, the azimuth increment detailed in [46] was

larger than used in this research and as such could feasibly be expected to produce lower results.

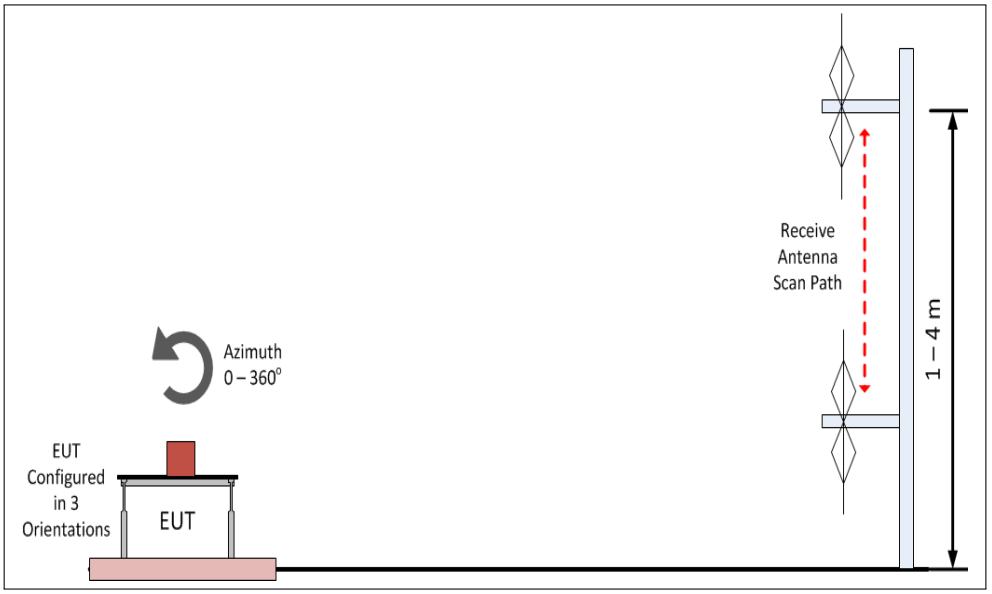

FIGURE 5.2: Cylindrical Scan General Test Setup

5.1.3 Receive Antenna / Azimuth Scan - CISPR 22 Method

The vast majority of radiated emissions test standards required the receive antenna to be scanned in height and the EUT to be rotated in azimuth in order to maximise the emissions. As detailed in Section 4 both of these factors have been shown to affect the level of error recorded when attempting to measure the maximum amplitude of the E-field radiated by the EUT.

5.1.3.1 Error as a Function of Number of Azimuth Angles Used

An obvious question raised when considering an alternative to the current CISPR 12 method could be:

> '*Why not just perform measurements at more azimuth angles?*'

While the question posed could be considered as obvious, the answer is perhaps not so pronounced. The number of angles has already been shown to directly affect the Error Bias recorded.

In order to investigate whether an optimum number of azimuth angles could be found that would offer a noticeable improvement in the Error Bias recorded without dramatically affecting the time taken to perform the tests, the data collected during the measurements performed in Section4.3 were further analysed. The EB was calculated for an increasing number of azimuth angles used. For the purpose of this investigation the additional angles were based upon the values detailed in Table 5.1. A single antenna height of 2 m was used for the purpose of this investigation, as the E-field amplitude was collected using a relatively coarse antenna height increment, there was insufficient data to offer conclusive results regarding an optimum increment step size. As the E-field amplitude was recorded using an azimuth rotation increment of 5^o, a large data set was available to extract subsets of azimuth positions to perform the comparisons.

TABLE 5.1: Increased Azimuth Angle Increment Investigation

No. Of Angles	**Angle Increment (Degrees)**
2	180
4	90
8	45
16	20
36	10
72	5

It can be seen from Figure 5.3 that the plot of number of angles used to perform the radiated emissions measurements against EB in recording the maximum E-field amplitude follows a logarithmic trend line. As the number of azimuth angles is increased from more than two angles, as is used in CISPR 12, the recorded EB falls rapidly until approximately 20 angles are used. Using greater than 20 angles, the EB improvement falls to a point where it could be argued that the improvement does not warrant the additional time and costs involved in performing the additional measurements. The EB improvement achieved by doubling the number of angles from two to four was approximately 2 dB, increasing the number of angles by a further factor of 2, 8 positions is total, reduced the EB to 6 dB, half that of the CISPR 12 EB of 12 dB. A further doubling of the number of angles to 16, reduced the EB further to just below 5 dB. The difference in EB between performing measurements at 16 positions to that when using

72 positions was only just over 2 dB, the difference in time to perform measurements at 16 angles compared to 72 would be quite considerable.

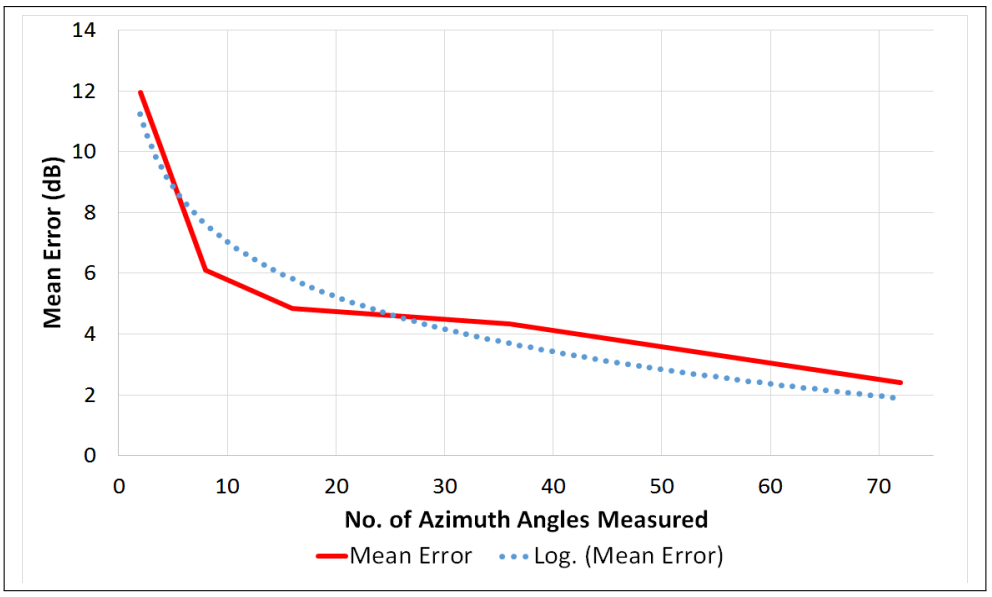

FIGURE 5.3: Error Against Number of Measured Azimuth Angles, Horizontal Polarisation

The results shown in Figure 5.3 were based upon the horizontally polarised data set. When the vertically polarised data were analysed a very similar profile to the horizontal data were recorded, the vertical data followed the profile of the logarithmic trend-line more closely than the horizontal data in fact, as shown in Figure 5.4.

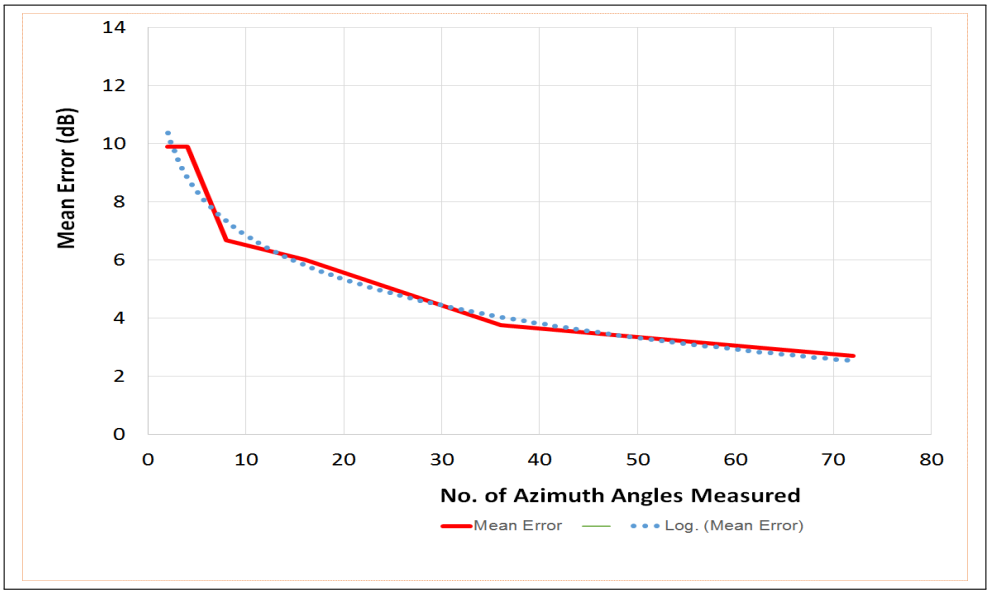

FIGURE 5.4: Error against Number of Measured Azimuth Angles, Vertical Polarisation

Table 5.2 and Figure 5.5 give an example of the increase in time that could be expected by increasing the number of azimuth angles. The timings are based upon a single frequency sweep between 30 MHz and 1 GHz taking approximately five minutes. The exact timings will depend upon the sweeping time of the measurement receiver being used and the figures are meant to be illustrative of the increase rather than offering absolute timings. These timings would only cover one antenna polarisation, the normal procedure would be to perform the tests using both a horizontally and vertically polarised receive antenna, hence the actual timings would be twice those detailed in Table 5.2.

TABLE 5.2: Test Time Increases Due to Decreased Azimuth Angle Increment

No. Of Angles	**Angle Increment (Degrees)**	**Sweep Time**
2	180	10 mins
4	90	20 mins
8	45	40 mins
16	20	80 mins
36	10	180 mins
72	5	900 mins

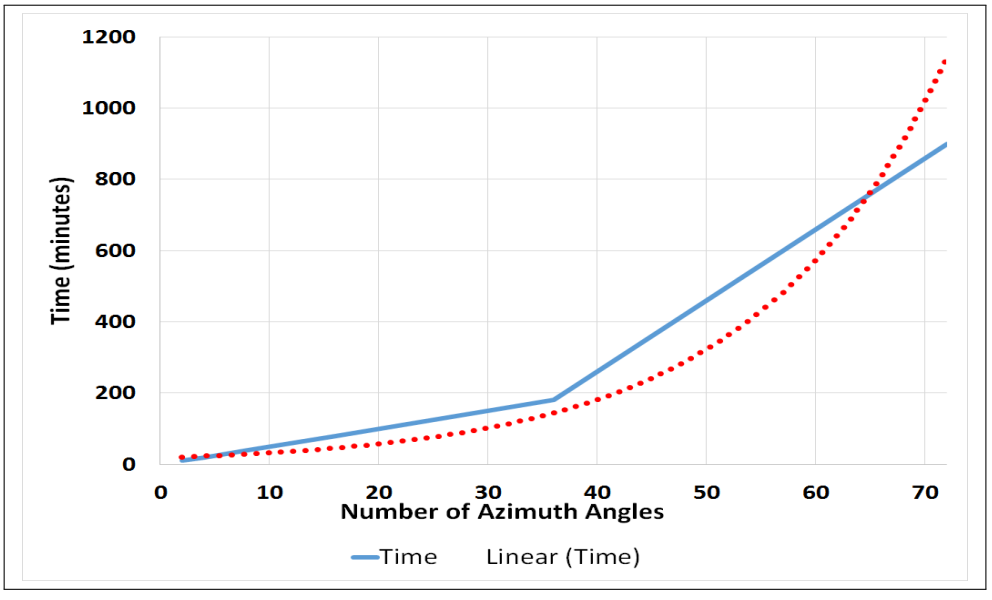

FIGURE 5.5: Time against Number of Measured Azimuth Angles

5.1.3.2 Alternate Azimuth Angles - CISPR 12 Test Parameters

As discussed throughout this thesis, CIPSR 12 radiated emissions measurements are performed at two azimuth angles around the vehicle being tested. As was shown in Chapter 4, this can lead to large EB values being recorded. However, it could be argued that if the 'optimum' two angles could be established in advance, a very low EB could be recorded, whilst still only performing measurements at two positions. The difficulty with this alternate option is how can one determine the angle without performing a full azimuth scan, utilising a fine increment angle, which by definition contradicts the aim of using just two angles. There is a possibility that the answer is that an 'optimum' angle does not exist, or certainly not a single, common angle that is valid across multiple vehicle types.

The emissions data collected by the author whilst performing the investigations detailed in Section 4.3 were used to ascertain if an alternate angle to E_{LHS} and E_{RHS} could be deduced. The emissions data recorded at five degree increments around three different vehicles were analysed, looking for common angles where the maximum amplitude of the E-field was recorded. The measurements were performed using a single antenna height of 3 m above the facility ground.

For each of the vehicles, the angle at which the maximum E-field amplitude was measured was noted for frequencies between 50 MHz and 500 MHz, in 50 MHz increments, as detailed in Figure 5.6.

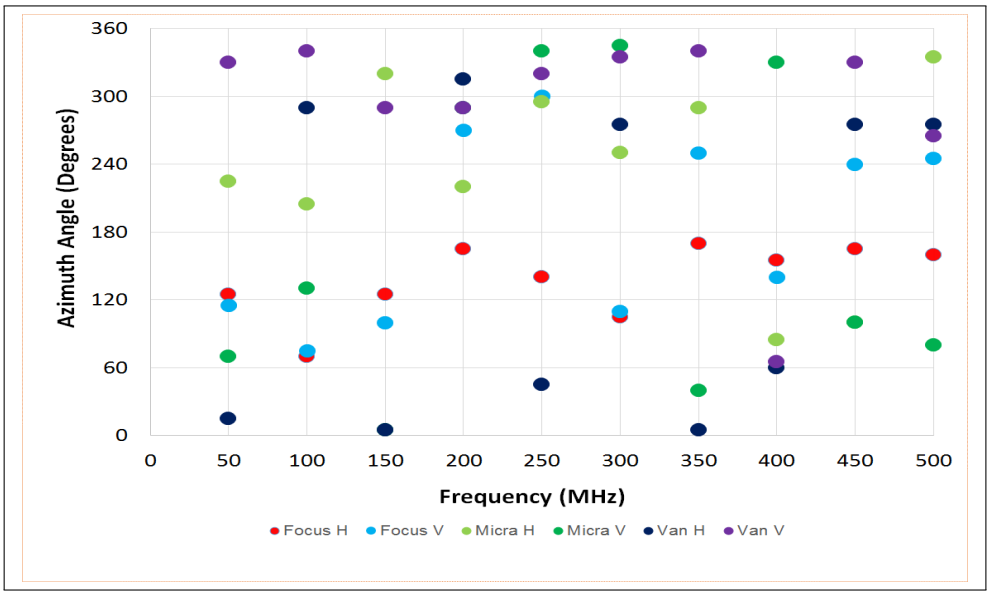

FIGURE 5.6: Azimuth Angle Maximum Amplitude of E-Field Recorded, Three Vehicles

It is evident that the direction at which the maximum was recorded not only varies with frequency, it also varies between vehicles. For each frequency examined, the maximum was recorded at a wide range of angles, there was no evidence of any common angles being highlighted. The purpose of this graph was to investigate if a particular angle or small range of angles consistently recorded the maximum amplitude. What is clear from the almost random spread of data across the graph , is that a common angle could not, as expected, be determined.

When the data from individual vehicles were analysed the range of values over which the maximum E-field was recorded can clearly be seen. Figure 5.7 shows the data for the Micra as an example, this result was typical across all the vehicle types tested.

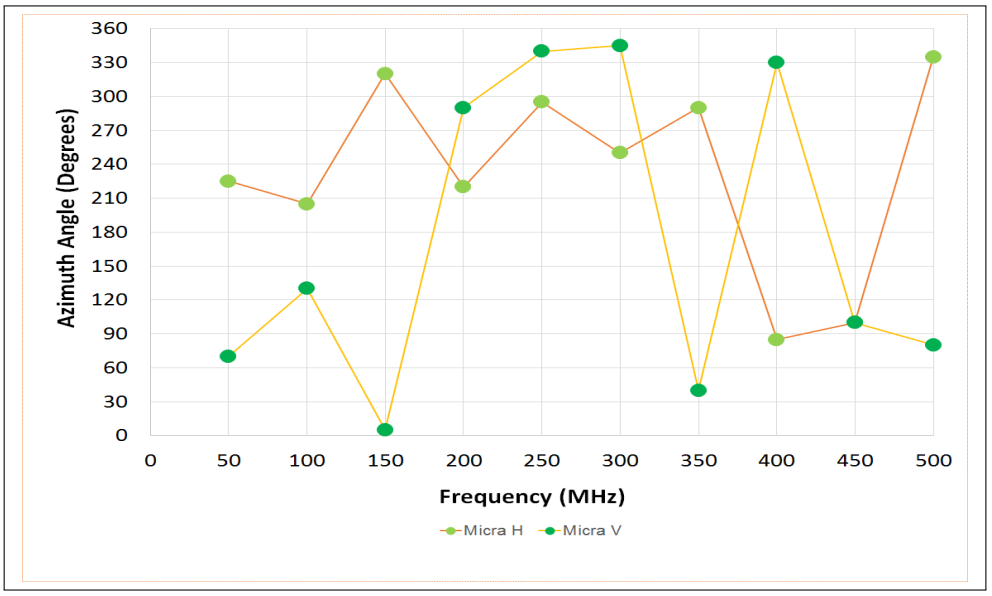

FIGURE 5.7: Azimuth Angle Maximum Amplitude of E-Field Recorded, Nissan Micra

In summary, from the small data set analysed it was concluded that alternative angles to the CISPR 12 positions were not possible to determine. The angle was seen to vary over a wide range of values as the frequency was varied and also for different vehicle types.

5.1.4 Reverberation Chamber

5.1.4.1 Introduction

As stated in Section 5.1.3.1, an obvious question regarding reducing the EB during an automotive emissions tests would be 'why not simply perform measurements from a greater number of azimuth angles and scan the receive antenna in height'. This question was answered in Section 5.1.3.1 but as was highlighted the method, whilst offering a substantial reduction in EB, the additional time and cost have ruled it as not viable from a commercial testing point of view. A second question that could be asked is:

> *'Why not perform the measurements in a Reverberation Chamber. Would this not solve the problem of not recording the maximum emissions?'*

The Reverberation chamber was investigated in an attempt to determine if it could offer an alternative to the CISPR 12 method.

5.1.4.2 Reverberation Chamber Background

The use of Reverberation Chamber, RC, for electromagnetic measurement purposes was first proposed by HA Mendes in 1968 [55]. The EMC community took some time before measurements using a reverberation chamber became accepted, but in recent years they have become a popular alternative to OATS and semi anechoic chambers.

The RC consists of a shielded enclosure in which electromagnetic measurements are performed; both radiated emissions and immunity. The inside of the enclosure is not covered with RF absorbent material; as is the case with a semi anechoic chamber, but left uncovered.

The operation of a RC is based on the resonant properties of the shielded enclosure. An RC differs from a conventional shielded enclosure by the inclusion of a large rotating non-symmetrical stirrer, or multiple stirrers in the case of some chambers. Figure 5.8 shows a typical layout of a RC.

In order to be efficient over a wide frequency range, especially at low frequencies, the paddle should be large in relation to the dimensions of the chamber. Measurements have shown [56] that the width of the stirrer is more important than the height with regard to efficiency of the paddle. The stirrer rotates during the measurement. There are two methods employed by which the stirrer is rotated, these are; continuous rotation, also known as mode stirred, and stepped rotation, also known as mode tuned.

The fact that that the chamber is a large metallic cavity, with a high Quality (Q) factor, will mean that if RF energy is introduced into the chamber, via an antenna fed by a source signal for example, and the frequency of the signal injected into the chamber matches a resonant frequency of the shielded enclosure, a 3d standing wave pattern will be created. This creates an electric field with a high amplitude. If, however, the frequency of the signal injected does not match a resonance frequency, an electric field of low amplitude is created inside the enclosure. These resonances formed within the chamber will cause it to act as a multimode resonator. The frequency of the resonant frequencies or 'modes' can be calculated using Equation 5.1:

$$f_{m,n,p} = (\frac{c_0}{2})\sqrt{(\frac{m}{a})^2 + (\frac{n}{b})^2 + (\frac{p}{c})^2} \tag{5.1}$$

where a is the length, b is the width and c is the height of the chamber, (all in metres), m, n and p are non-negative integers, only one of which may be zero and c_0 is the speed of light in a vacuum.

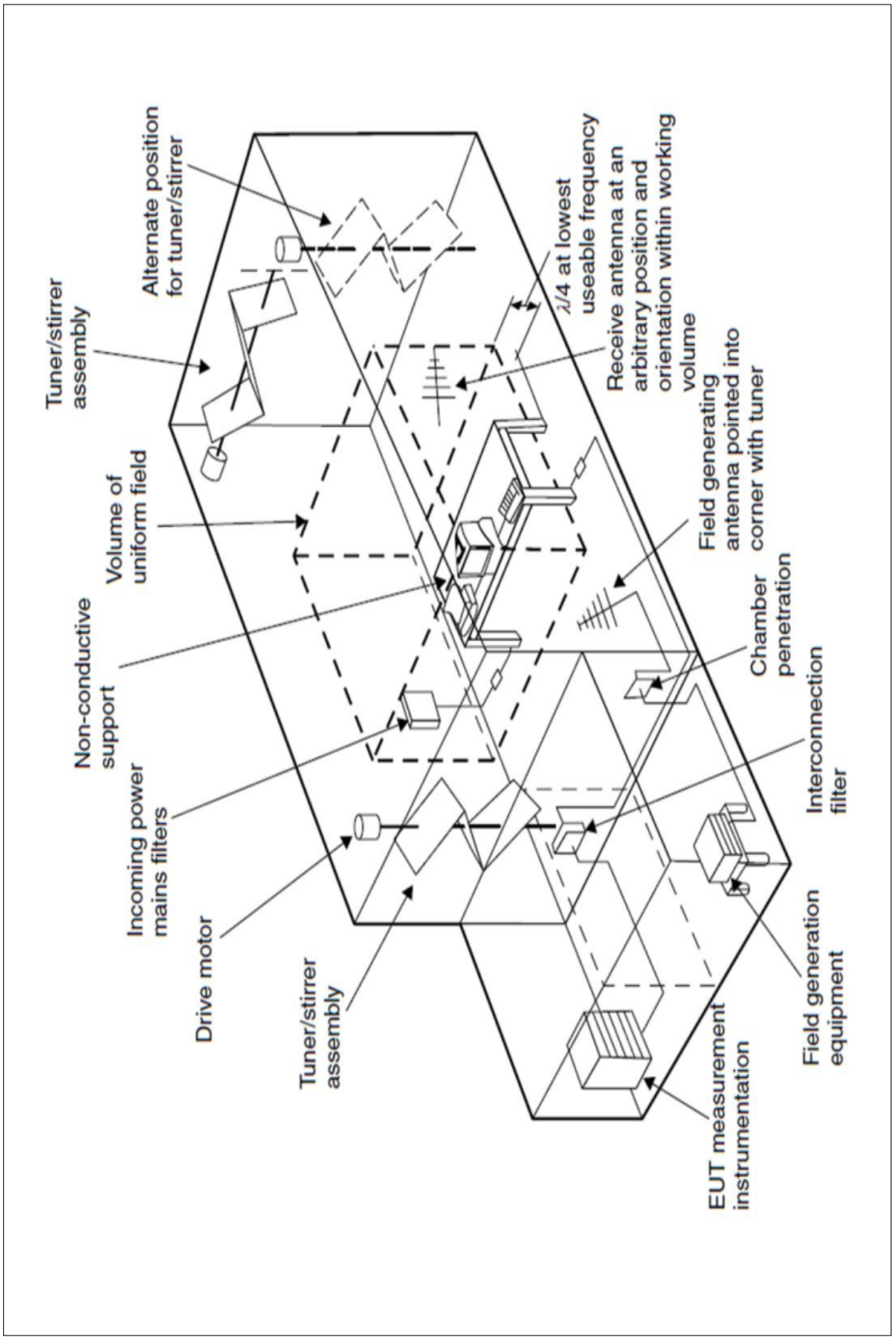

FIGURE 5.8: Reverberation Chamber Configuration. (Figure reproduced from BS EN 61000-4-21)

The 3D pattern if the resonances will cause the received field to be very strongly dependent on the position of the receive antenna within the chamber.

The fundamental axial mode of the chamber will be caused by reflections off two opposing walls of the chamber, either the end or side walls, weaker tangential resonant modes will be caused by reflections off four or more walls. The lowest, fundamental, resonant frequency of the chamber will occur when m and n are both 1 and p is zero.

The stirrer changes the field pattern inside the chamber by changing the boundary conditions. The reflected waves incident on any point in space within the chamber arrive with differing phase due to their different path lengths. Rotation of the stirrer changes these path lengths, and as a consequence the phase, for each differing position of the stirrer. This leads to the magnitude of the electric field at any point within the chamber being different from any other point and thus different for every stirrer position. A single rotation of the stirrer perturbs the electric field to give a known statistical distribution. This distribution is evident if many points in the field are measured with all objects within the chamber in the same position. The effect of the stirrer altering the resonances is that a time averaged, spatially homogeneous field distribution is achieved. At high frequencies, in the order of several hundred MHz, the stirring action is very successful at producing the required spatially homogeneous field distribution. As the frequency decreases, an increasing number of stirrer positions over a single rotation are required. The net consequence of a stirrer rotation through one revolution is that a statistically isotropic, randomly polarised uniform field is generated over a large area of the chamber volume, typically the usable volume is approximately 50 % of the total chamber volume.

Physically, the larger an RC is, the better the performance at lower frequencies. However, absolute size is not the only factor affecting the performance. The chamber walls should not be of equal lengths, i.e the height should not be the same as the width etc. Walls of the same dimension leads to resonances at the same frequencies, which does not contribute to the homogeneous field distribution [57]. The amount of other equipment inside the chamber will also have a detrimental affect on the field distribution, items such as wooden flooring, storage cupboards etc. have the effect of reducing the Quality factor of the chamber.

The RC offers some advantages over performing radiated emission at an OATS or semi-anechoic chamber. The cost of an RC compared to a SAC of a similar size, is

typically lower. The lower cost of building a reverberation chamber is realised due to the fact that expensive absorber, either ferrite tiles, pyramidal cones or a combination of the two, is not needed. This means that not only is the cost of the material not needed but also the construction of the chamber does not have to be nearly so robust. A SAC requires that the chamber walls be structurally supported using steel girders or similar to compensate for the additional weight of the absorber.

For the purpose of this research, possibly the biggest advantage of the RC is that it measures the total radiated power of the EUT, hence the EUT emissions will be accounted for from all directions without the need to rotate it either in azimuth or scan the receive antenna in the elevation plane as is the case for spherical scan tests as described in Section 5.1.2. However, the total radiated power recorded in an RC gives the average amplitude emissions from the DUT. In order to deduce the maximum amplitude, some knowledge, or presumption, of the directivity of the EUT is required. Wilson et al. [2] investigated methods of determining the level of the maximum emissions of a DUT, using measurements in an RC along with maximum directivity estimates based upon the electrical size of the EUT. They concluded that through the use of the estimated value for the directivity, good correlation between the total radiated power recorded in the RC and the maximum E-field amplitude recorded over a spherical antenna scan around the EUT could be obtained. The RC could potentially offer a low value of EB.

A study conducted by Wen [58] investigated the use of an RC for vehicle level emissions measurements, the results of the study suggest that through the use of a 'correction factor' the RC results can be calibrated to CISPR 12 results. However, based upon the conclusions drawn in Section 4.5, this would seemingly take the advantages of the RC and calibrate it to to a test method that we have shown to have an EB of up to 30 dB at certain frequencies.

The RC is, however, not without its disadvantages. In order to achieve the statistically isotropic, randomly polarised uniform field, a large chamber is required. Although this does not need to be lined with tiles or RF absorbing cones, as detailed earlier, there is still a substantial cost required to build a sufficiently large enclosure. Additionally, as the field is averaged over a complete stirrer rotation, it is statistically both isotropic and randomly polarised, this means that the measurement results are not able to convey any detail into the direction from which the emissions are radiated or their polarisation, both

of which can be resolved using a semi anechoic chamber and rotating the antenna and EUT.

5.1.4.3 Reverberation Chamber: Number of Independent Samples

The time required to perform the tests within an RC is dependent upon the number of steps used during the rotation of the paddle, the time needed by the paddle to settle after each step and the time required by the measurement system to actually record the field data at each paddle position. Historically, a typical number of paddle positions use during a test was 200 at all frequencies, however, this resulted in field uncertainties that varied with frequency due to an increased modal density. The latest version of BS EN 61000-4-21 [59], the British Standard that defines the requirements for RC testing, offers information on an optimised number of paddle steps, that decreases with increasing frequency. Figure 5.9 gives details of the suggested number of positions for a typical sized RC.

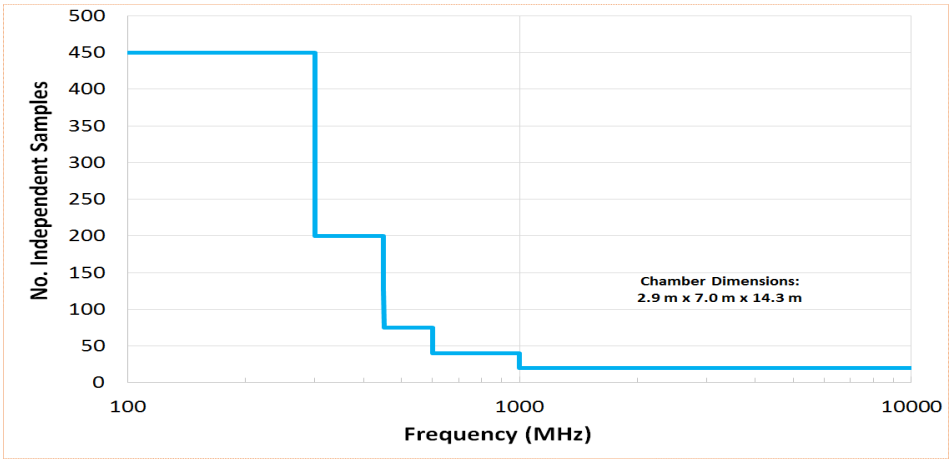

FIGURE 5.9: Reverberation Chamber Configuration. (Figure Reproduced from BS EN 61000-4-21)

In order to perform measurements over the same frequency range as covered by CISPR 12 test time will potentially be very long, particularly to cover the lower end of the frequency spectrum. Based on the suggested number of steps detailed in BS EN 61000-4-21 radiated emissions tests conducted in an RC could take up to 24 hours per EUT, based upon the timings detailed in Table 5.3:

TABLE 5.3: Estimated Reverberation Chamber Timings

Frequency Range (MHz)	**No. Of Paddle Steps**	**Time (hours)**
100 - 300	450	15
300 - 450	200	6.7
450 - 500	125	1
500 - 600	750	0.1
600 - 1000	40	0.7

These timings are based upon the measurement receiver taking approximately 5 minutes to sweep from 30 MHz to 1 GHz.

Research is continuing into the optimum number of independent stirrer positions to be used during a test [60], [61], [62]. Alternative methods to those detailed in BS EN 61000-4-21, suggested by Chen [63], highlights that through the use of the optimised number of independent samples a reduction in test time could be achieved, without the increases in the measurement uncertainty.

The reverberation chamber also possesses some disadvantages over an OATS or SAC:

- Large size required to obtain a low usable frequency;
- Many international standards still do not allow the use of reverberation chambers for compliance measurements.
- There is not a simple method allowing direct comparison of results obtained in a reverberation chamber to those produced in a SAC

5.1.5 Test Wire Method

5.1.6 Introduction

A method proposed for measuring the radiated emissions from large machines was first proposed from work carried out under a European project known as TEMCA2 carried out in 2003 [64]. The project aim was to investigate alternative methods that would allow compliance with the EMC Directive for large machines and simplify the procedure

needed to perform the measurements. The system became known as the 'Test Wire' method.

The 'Test Wire' method was the final alternative investigated as a possible substitute to the CISPR 12 approach to measuring automotive radiated emissions.

5.1.7 Test Wire Method History

Due to the physical size, weight and supply voltages used with many industrial machines, radiated emissions and immunity measurements at a typical test site, OATS, semi-anechoic chamber etc, are not possible. For large machines, there are typically three methods available to show conformance with the required EMC Directive 2014/30/EU [65] and Standards EN 50370-1 [66] and EN 50370-2 [67], they can be summarised as: perform the tests on the entire machine, perform tests on the electrical system of the machine and then perform visual type inspections to confirm the system has been correctly installed into the machine or perform measurements on individual modules of the machine in a test facility and then perform visual type inspections of the modules once they are re-installed back into the machine, this is then followed by a final test on the machine in-situ at the final location of the machine.

Of the three options highlighted above, the third procedure was investigated as part of a joint working group between CECIMO (*Comité Européen de Coopération des Industries de la Machine-Outil*, also known as the European Committee for co-operation of machine tool industries) and CENELEC (*Comité Européen de Normalisation Électrotechnique*, also known as European Committee for Electrotechnical Standardization).

In February 2003 the TEMCA2 project was started, their role was to develop a measurement method that could be used for the final 'In-Situ' test. The project which was part of the European Commission's RTD program on Competitive and Sustainable Growth (Fifth Framework Program, 1999 - 2002, project number GRD1-220-70012) with the aim of addressing the difficulties inherent with performing radiated emissions measurements on large industrial fixed machines.

The TEMCA2 project started out by issuing a questionnaire to a range of machine manufacturers with the aim of determining some understanding of their thoughts regarding the current Directives and Standards. What became evident was that the manufacturers

were dissatisfied with the cost and amount of equipment, and technical knowledge required to perform emissions tests on their large machines. It was also noted that even after the tests were performed compliance could possibly still not completely fulfil the requirements of the EMC directive. The manufacturers expectations were for a method that was low cost, quick to perform and used a simplified test method.

The two main factors concerning simplifying the test method that were highlighted were that the tests need to be performed 'in-situ', without the need for the machine to be moved to a measurement test facility and that high levels of ambient 'noise' could be dealt with. As detailed in Section 4.2.5.2 of this thesis, the ability of a measurement system to be tolerant of high levels of ambient noise would be beneficial to any alternative to the CISPR 12 method, if it allowed for tests to be performed without the need for an OATS or SAC.

5.1.7.1 Test Wire Configuration

The system developed by the TEMCA2 team became known as the 'Test Wire Method', TWM. The teams involved in the TEMCA2 project performed a range of investigations into the feasibility of the TWM as an alternative to a traditional CIPSR 22 type antenna measurement [68], [69] [64], [70]. For the development phase of the study a Generic Test Object, GTO, was used to perform a range of measurements and simulations. The GTO was designed in such a way that it would be possible to easily produce both a physical model and also a numerical model. The original concept behind the Test Wire system was based upon the work carried out by Parmantier [71] which proposed the use of a 'Test Wire' for detection of localized sources of emissions on a large EUT.

In the initial system developed by the TEMCA2 teams, the wire was stretched over the machine at a distance of approximately 10 - 50 cm. The length of the wire was chosen so that this distance could be maintained for different orientation of the wire over the machine and still preserve the same separation from the largest point. The 'Test Wire' formed a long wire antenna over the machine being tested, which would integrate the near field contributions of the E-field radiated emissions. The wire was terminated with its characteristic impedance. The ends of the wire were connected to either the metal chassis of the machine or the metal ground plane, between the machine and the ground connection was a termination resistor. The termination impedance was set to 150 Ω at

one end of the Test Wire, at the opposite end of the wire a 100 Ω termination in series with the 50 Ω nominal input impedance of the measurement receiver. Figure 5.10 shows the basic Test Wire method setup used.

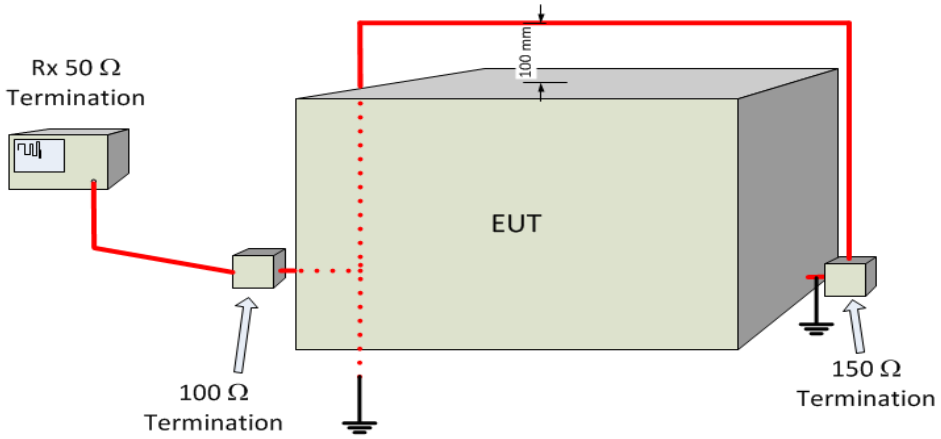

FIGURE 5.10: Basic Layout of Test Wire Method

Multiple configurations of the Test Wire were used during the investigations. The wire was positioned as shown in Figure 5.11.

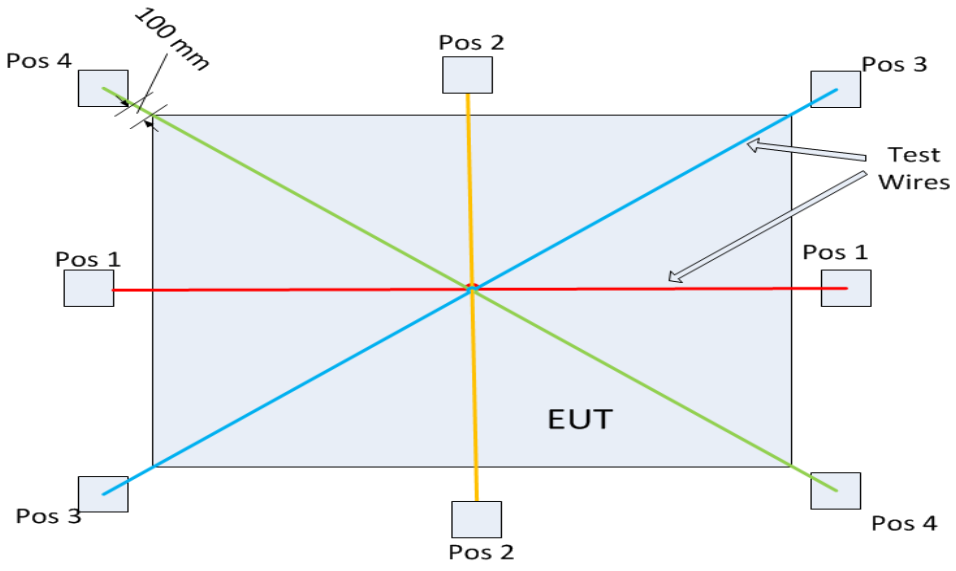

FIGURE 5.11: Test Wire Orientations Around EUT

5.1.7.2 Calibration Factor

The voltage across the termination resistor was measured for each frequency of interest in the range of 30 MHz to 1 GHz. This voltage was then converted to an equivalent field strength by means of a 'K-Factor' which is analogous to the standard antenna factor. Voltage data was collected from measurement performed with the Test Wires at each of the positions shown in Figure 5.11, with the measurement receiver located at either end of the wire, i.e. two sets of data were collected for each test wire position.

In order to calculate the K-Factor the maximum E-field needed to be recorded. A standard CISPR 22 type measurement was performed with the receive antenna positioned 10 m away from the machine. In an attempt to maximise the emissions, measurements were performed from all four sides of the machine. As the system was designed to be used for measuring very large industrial machines, rotating the EUT around the X or Y axis was not possible. The receive antenna was scanned in height between 1 m and 4 m above the ground in a further attempt to maximise the amplitude recorded.

The K-Factor is calculated as the ratio between measured maximum E-field, using standard CISPR 22 method, and the measured voltage across the termination resistor. From this a range of values for K is obtained.

The K-Factor can be calculated using the following:

$$K = 20.log\frac{E}{U} \tag{5.2}$$

Where K is measured in dB/m, E in V/m and U is measured in V.

Individual values for the K-Factor will need to be calculated for each frequency of interest, using each of the configurations detailed above, doing so will give a spread of high and low values. From the spread of values elicited, nominal value of K was determined, from a line of best fit through all the values recorded.

An important fact to note is that in order to correctly define the K-Factor, the E-field value should be the maximum, i.e. as a results of full spherical scan. The measurements performed were based upon a reduced measurement set due to the time constraints imposed performing a full spherical scan. The maximisation process used during the

antenna measurements was as rigorous as was practicable at the time, however, it would still not record the actual maximum emissions of the EUT. Due to this fact, the teams involved in the development of the Test Wire method also performed simulations on the EM model of their GTO, to enable the maximum to be derived. The use of a simulation model meant that the E-field could be recorded at a much greater number of positions around the model than was possible through measurement. This allowed for a better approximation of the maximum E-field amplitude to be recorded.

By applying the K-Factor to subsequent Test Wire measurements, an equivalent E-Field value can be recorded without the need to perform extensive antenna measurements. The TEMCA2 team deduced that the TWM showed promise for measuring the emissions from large industrial machines, and suggested further development was needed in order for the system to be further validated.

5.1.7.3 Development of the Test Wire Method

The TWM was further developed in an attempt to address some of the issues raised with its implementation. The main points raised were: the Test Wires required careful placement in order to maintain the 100 mm spacing above the EUT, the characteristic impedance was found to be difficult to control and also felt to not be truly representative or accurate in practical applications [70]. An alternative method was suggested by Coenen, Maas et al. [72] known as the 'Surface Current Sense Wire', SCSW, this method changed the way the 'Test Wire' was configured. Instead of being positioned 10-20 cm above the surface of the EUT, the Sense Wire, was configured to run on the surface of the EUT. The diameter of the wire and its insulation thickness were selected to produce a transmission line configuration with a characteristic impedance of 50 Ω. The impedance of the microstrip would then allow for a direct connection to the measurement instrument being used, reducing reflections and mismatches. Another difference between the SCSW and the Test Wire method is the length of the wire. The wires used to perform the TWM are stretched over the entire structure of the machine being tested, whereas the SCSW was limited to between 1 m and 3 m long. A later investigation into the SCSW [73] found that using a long wire produced inconsistent results. The variation to the setup they used changed the length to approximately 300 mm. The SCSW was routed in various positions over the surface of the EUT, the voltages present over the surface of the

EUT will in turn induce a voltage in the sense wire with minimal RF losses. Again the terminal voltage was measured across the frequency range of interest and the K-Factor derived from Equation 5.2. One drawback recognised with the method is that the system was still intrusive to the device being tested as it relied on a ground connection of the shield being bonded to the chassis of the EUT.

In an attempt to overcome this problem, a further development of the SCSW system was suggested by Catrysse, Vanhee et al [74]. The SCSW was replaced by a standalone microstrip that had its own ground reference plane . The 'FlexμStrip' as it was named comprised of a flexible 'sandwich' of conductive fabric strips enclosed between two layers of insulating sheet, the microstrip was completed with a further metallic strip on top of the insulating sheet, 'N' connectors were positioned at either end of the strip to allow for connection to the measurement equipment at one end, the opposite end was terminated with a 50Ω load. The advantage of the FlexμStrip over the original TWM was that as the strip was flexible, it could easily conform to the profile of the equipment under test and as it had its own ground reference plane it could be designed to have a characteristic impedance that matched the measurement system and did not rely on bond to the chassis of the EUT. The FlexμStrip was used in the same way as the original TWM, with the exception of the of the details highlighted at the beginning of this paragraph. The FlexμStrip was validated with a program of measurements where the same EUT was measured with the CISPR 22 method, the Test Wire Method and the FlexμStrip method. They concluded that although in its infancy, the FlexμStrip method showed potential as a method for both measuring the emissions of large machines in-situ and also to be used as a 'sniffer' probe for investigating localised leakage of RF emissions from different parts of the EUT.

5.1.8 Conclusions

In an attempt to find a method to perform vehicle level radiated emissions tests to be used as an alternative to the CISPR 12 procedure a number of options were considered. Whilst it could be argued that performing either a spherical, or hemi-spherical, scan of the receive antenna around the EUT or performing the measurements in a Reverberation Chamber could potentially offer a dramatic reduction in the Error Bias, both systems have some substantial disadvantages. For the spherical scan method, cost is by far the

biggest issue. Performing a complete spherical scan around the EUT would not only require a very complex measurement system but the time needed to perform the test would cause it to be prohibitive, certainly for commercial testing such is required for vehicles to show compliance with the requirements of the Automotive Directive. The spherical scan method is possibly more suited to a research type of program.

It was shown that if the number of azimuth angles used to perform emissions measurements increased, the EB reduced compared to that achieved using the CISPR 12 method. This reduction, however, was not linear. It was found that as the increment doubled from the two angles used in CISPR 12, the EB reduced following a logarithmic profile. As a consequence of the angular increment decrease, the test time increased accordingly, following a logarithmic increase. In order to gain a 6 dB decrease in the EB value recorded, an additional 6 measurement angles, eight measurements in total, were required. This change in increment accounted for a four fold increase in test time. Increasing the number of measurement points to 36 only accounted for a further decrease in EB of approximately 2 dB, however, this would increase the test time by approximately 18 times. These timings would only account for a single antenna polarisation, in reality the actual test time increases would be double the quoted figures as measurements using both a horizontally and vertically polarised antenna would be required. The use of increased azimuth angles could certainly be used as a method of decreasing the EB recorded, however, the added time required to perform the tests would potentially deem it cost prohibitive for a commercial test program.

The Reverberation chamber, also has the potential to offer a low Error Bias but still requires a fairly complex measurement facility, certainly more complex than that required to perform a CISPR type antenna test. With regards to the timing, the RC tests are potentially still long due to the multiple paddle positions required, especially at low frequencies, to ensure that a statistically isotropic and randomly polarised uniform uniform field is being generated. The total radiated field recorded during an RC test is not directly comparable to that recorded using the CISPR 12 method, but does mean that it is independent of the directivity of the EUT emissions pattern.

The final method investigated, the 'Test Wire Method' was found to offer the most potential as basis for an alternative to the current CISPR 12 method. In the subsequent chapters of this thesis, the TWM is investigated further, and work is described detailing

how the TWM concept was used as a method of recording the E-field radiated by a number of models and commercial vehicles. The resulting Error Bias is then discussed and compared to those recorded using the CISPR 12 method.

Chapter 6

Test Wire Method

6.1 Introduction

This chapter details further investigations into the 'Test Wire' method (TWM) discussed in Section 6.1 as a possible alternative methodology to the current CISPR 12 test procedure. The chapter begins by detailing how the original 'Test Wire' method was implemented on a simple representation of a vehicle body shell passenger compartment, designated 'Simple Vehicle Test Case', SVTC. A full scale EM simulation model and a $\frac{1}{3}$ scale physical model of the SVTC were designed and built. The EM model was used to investigate the impedances required to terminate the Test Wires and also to perform investigations into how the position of the Test Wire could possibly be optimised. The scaled physical model was used to perform a range of radiated emissions measurements at an OATS facility. The measurements were initially used to determine the EB in recording the maximum E-Field amplitude using the CISPR 12 method. The Test Wire Method was then implemented on the model. A K-Factor was determined using the method described in Section 5.2 and then the EB in the maximum amplitude of the emissions from the model using the TWM were compared to those recorded using the CISPR 12 method.

6.2 Original Test Wire Method Investigations

6.2.1 Simulation Model

For the initial investigations into the TWM a simplified vehicle body shell, designated Simple Vehicle Test Case, SVTC, was modelled using CONCEPT II Electromagnetic Simulation Software [39] . The model was designed to represent the size and shape of the passenger compartment of a typical family car. It was built using simple geometric shapes with the main panels forming a simple rectangular box shape, and consists of a central passenger compartment with apertures to represent windows. The apertures were left open, no attempt has been made to simulate the window glass. The simple vehicle shape was chosen not only to act as a representation of a vehicle but was also designed to enable a scale physical model to be built with relative ease. Figure 6.1 shows the overall EM SVTC model, whilst Figures 6.2 and 6.3 show dimensioned drawings of the SVTC model.

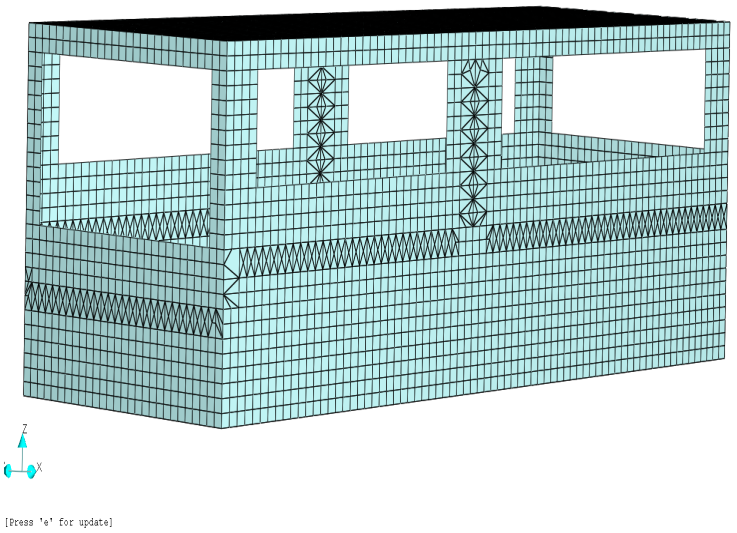

FIGURE 6.1: Simple Vehicle Test Case (SVTC) EM Simulation Model - 3D View

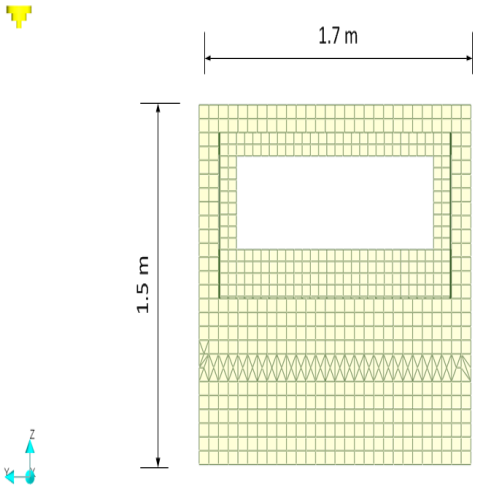

FIGURE 6.2: Simple Vehicle Test Case (SVTC) EM Simulation Model - Front View

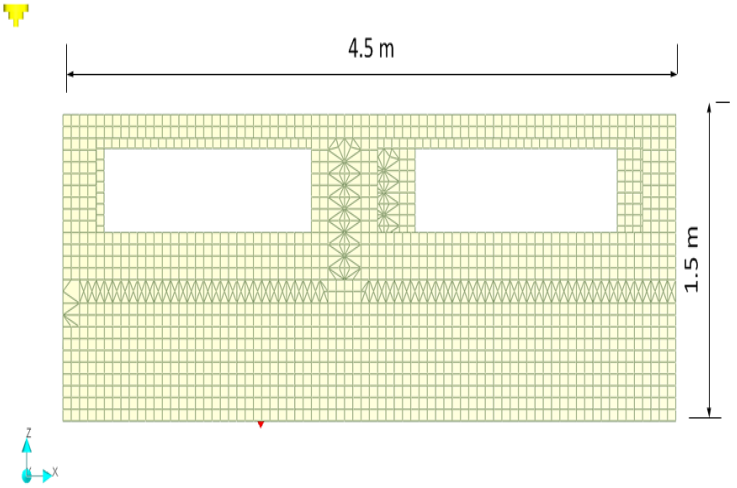

FIGURE 6.3: Simple Vehicle Test Case (SVTC) EM Simulation Model - Side View

The model was initially built using the discretisation tools within CONCEPT II . As the surfaces of the body shell did not have any curvature it was possible to construct it using the plate facility. Each side of the body shell was constructed from a basic rectangular plate. Each individual plate was then combined in CONCEPT II to form a complete surface. The VBS model used for the simulations in Sections 4.3 was not used for this part of the investigations as a physical model was also required, hence a very simple to construct model was utilised.

The model was built using a mesh size of 0.06 m x 0.06 m, the dimensions were chosen in order to meet the suggested minimum mesh size of $\frac{\lambda}{10}$ at the maximum frequency of interest, 500 MHz in this case. The upper frequency limit of the simulations was limited to 500 MHz based upon the data analysed in Section 4.4 which concluded that the majority of the radiated emissions from a range of eight different commercially available vehicles were recorded in the frequency range below 600 MHz.

In order to determine if the EM model was meshed with the optimum element size, based on the trade-off between accuracy of the results and time taken to perform the simulation, a map of the surface current was produced by the software for the upper frequency of the study being performed; 500 MHz as stated in the previous paragraph. In areas where high surface current density or rapid spatial rate change of the current were observed, a finer mesh size of 0.03 m x 0.03 m was utilised, as shown in Figure 6.5. By analysing the 'surface' map produced within CONCEPT, the high spots can easily be visualised. Figure 6.4 shows an example surface current plot at 500 MHz.

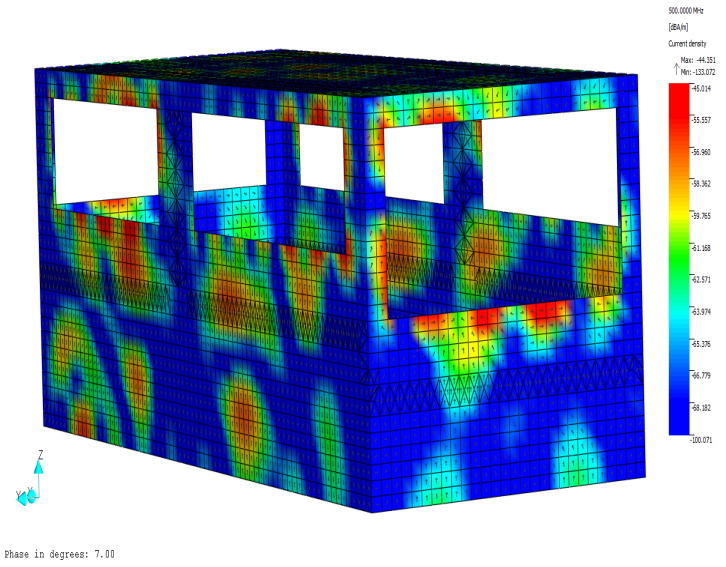

FIGURE 6.4: Simple Vehicle Test Case 'Simulation' Model', Showing Surface Currents

As can be seen in the image, high surface currents were recorded around the perimeter of the window apertures. The mesh size was decreased around all the windows and down the vertical pillars that separate the individual windows.

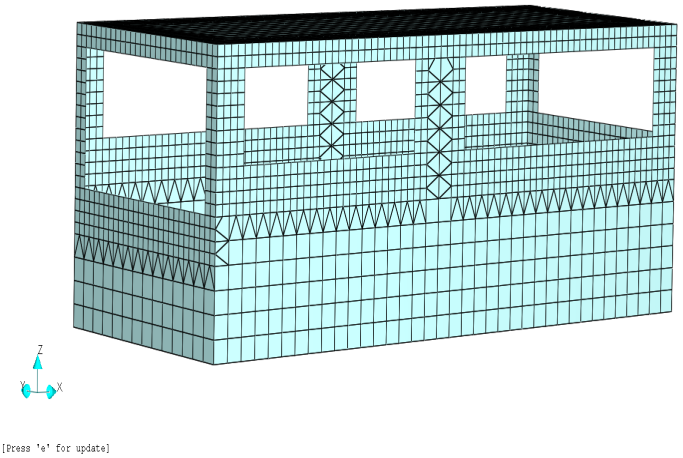

FIGURE 6.5: Simple Vehicle Test Case 'Simulation' Model', Showing Refined Mesh

The model was positioned 0.3 m above an infinite Perfect Electrical Conductor, PEC, ground plane, this height was used to represent the height the floor pan of a typical commercial vehicle above the ground.

A series of five small monopole antennas 270 mm long were positioned inside the model to excite an electric field within the enclosure. The monopoles were driven by a 1 V source, using the body of the model as a ground plane for the antenna. The position of the monopoles were chosen to offer a variety of places where electronic devices could be positioned inside a typical passenger vehicle. Details of the relative position of the monopoles are shown in Table 6.1 and Figure 6.6 :

TABLE 6.1: Relative Harness Positions and Dimensions

Description	**X Position (m)**	**Y Position (m)**
Monopole 1	-1.88514	0.607143
Monopole 2	-1.76351	-0.121429
Monopole 3	-0.485714	-0.790541
Monopole 4	0.668919	0.121429
Monopole 5	1.39865	-0.607143

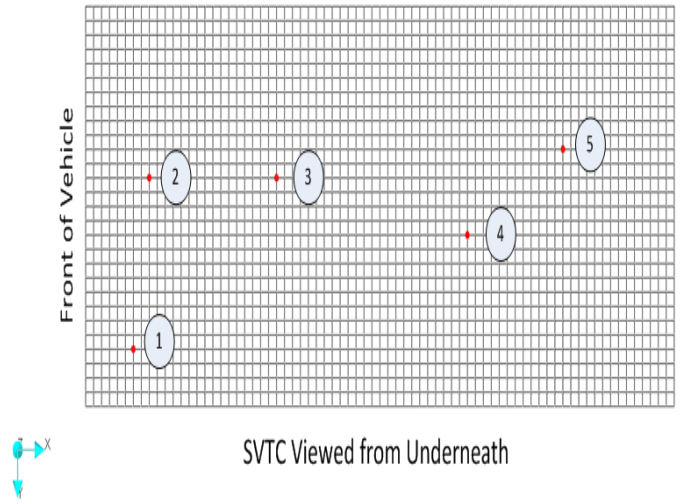

FIGURE 6.6: Floor Pan of Simple Vehicle Test Case Passenger Compartment Showing Monopole Location

Positions 1 - 3 were to replicate a source of emissions located in the dashboard area of centre console of the vehicle, points 4 and 5 represented sources either under the rear seats or in the boot of the vehicle.

6.2.1.1 SVTC Test Wire Termination Impedance Investigations

On reviewing the literature describing the initial research carried out into the Test Wire method, an impedance of 150Ω was chosen to terminate the transmission line formed by the Test Wire above the metallic ground plane formed by the SVTC body. This was assumed to be the common-mode impedance of the test wire, with a caveat that the actual routing of the wire above the test object would actually determine the impedance and as such care would need to be taken to ensure that this value was achieved [70]. As noted in the preceding section, due to the irregular shape of the machines being tested a constant impedance could not be obtained. As the spacing between the Test Wire and the SVTC model was a consistent 100 mm, an impedance that more closely matched the characteristic impedance of the line was used. Details of the simulated and measured characteristic impedance results are presented in Figures 6.8.

In order investigate the value of termination impedance that should be used, a simple EM model of a stripline, designed to replicate the Test Wire above the chassis of the EUT, was built and simulated using CONCEPT II. A 2 mm diameter, 500 mm long test

wire was modelled 100 mm above a metal ground plane. An image of the EM model can be seen in Figure 6.7

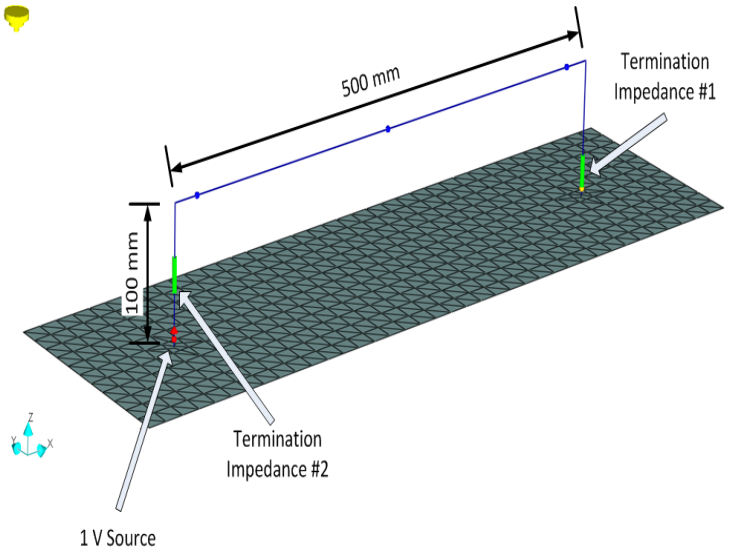

FIGURE 6.7: Stripline Above a Metallic Ground Plane EM Model

Using the formulas quoted in Equation 6.1 [75], an approximate value for the for the estimated characteristic impedance of the Test Wire was calculated:

$$Z_0 = \frac{60}{\sqrt{\varepsilon_r}} ln \left[\frac{4H}{D} \right] \tag{6.1}$$

where ε_r is the relative permittivity of the medium between the wire and the ground plane, H is the height of the wire above the ground plane and D is the diameter of the wire.

Using the parameters stated above, an impedance of approximately 319Ω was calculated. This calculated value was then used to terminate either leg of the simulation model to the ground plane of the model. The numerical model was simulated over the frequency range of 10 MHz to 1000 MHz in 1 MHz steps. At each frequency the S-parameters were calculated within the software. Using the complex values of the S_{11} parameters output, the characteristic impedance of the Test Wire was determined using the formulae 6.2 and 6.3 [76]

$$Z_{tw(real)} = Z_o \left(\frac{1 - R^2 - X^2}{(1 - R)^2 + X^2} \right) \tag{6.2}$$

$$Z_{tw(Imag)} = Z_o \left(\frac{j2X}{(1-R)^2 + X^2} \right) \tag{6.3}$$

where R is the real part and X is the imaginary part of the S_{11} values at each frequency.

A plot of the characteristic impedance of the Test Wire against frequency is shown in Figure 6.8. The calculated nominal impedance was 319Ω, up to approximately 500 MHz. A good level of correlation is recorded, with the impedance being within approximately ±4Ω . Above 500 MHz the impedance was seen to vary by approximately ±40Ω.

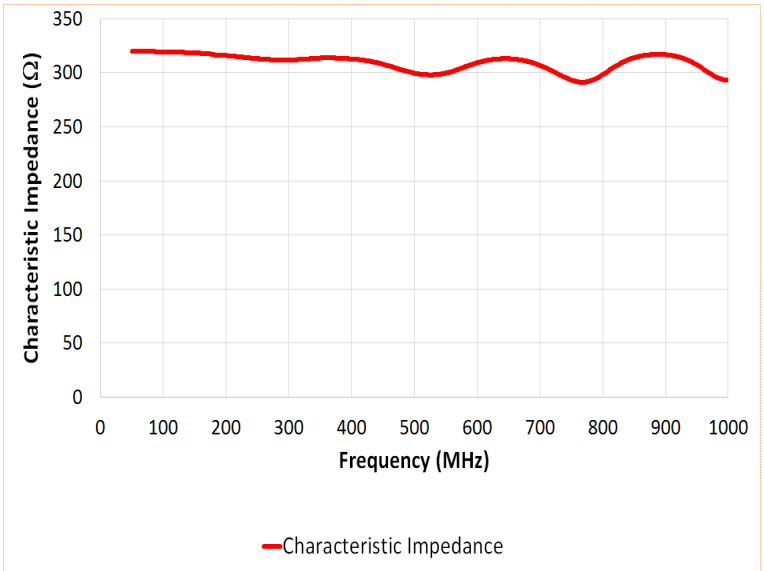

FIGURE 6.8: Characteristic Impedance Plot of Example Wire Transmission Line

6.2.1.2 Test Wire Locations

Early studies into the use of the TWM [77], [78] for performing measurements on large in-situ machines suggested that in order to not miss any local maxima in the E-field radiated by the machine being recorded, measurements at a number of Test Wire positions would be required.

The positions used for the Test Wires in this phase of the investigations were chosen purely based upon ease of construction. As will be shown in Section 7.23 more optimal test positions for the Test Wires were ascertained.

Using the methods described in Section 6.2.1.1 Test Wires were incorporated into the SVTC model and the characteristic impedance calculated. The Test Wires were located

100 mm above the surface of the SVTC model, two wires were modelled. The first ran along the centre line of the length of the model, the second wire ran along the centre line of the width of the model. Figure 6.9 shows the layout of the Test Wires on the EM model along with the positions of the termination impedances. The 319Ω impedances terminated the Test Wires to the ground plane. Figure 6.10 shows a plan view of the SVTC model with the Test Wires running along the length and width of the model.

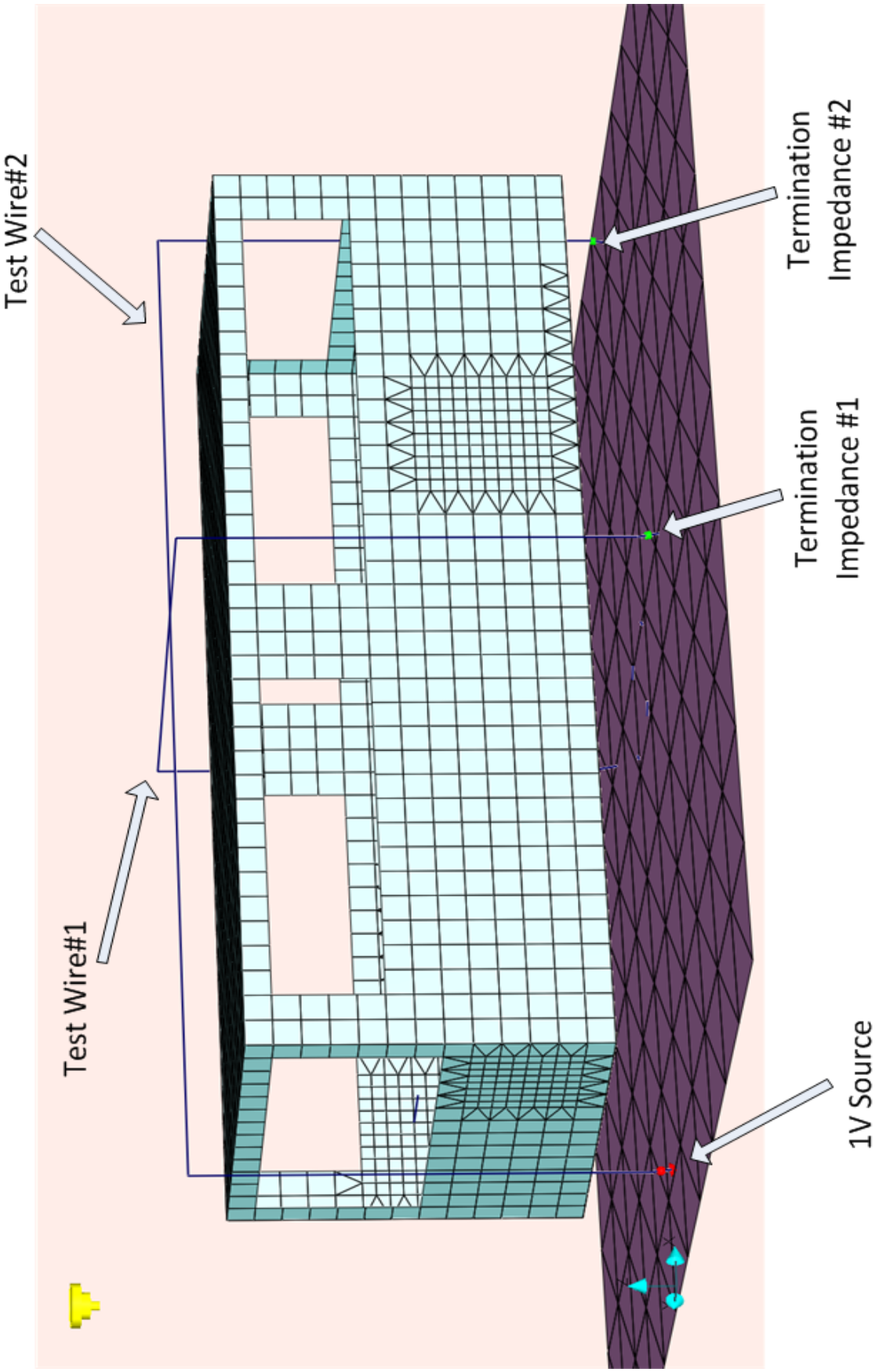

FIGURE 6.9: SVTC Model Showing Test Wire Locations

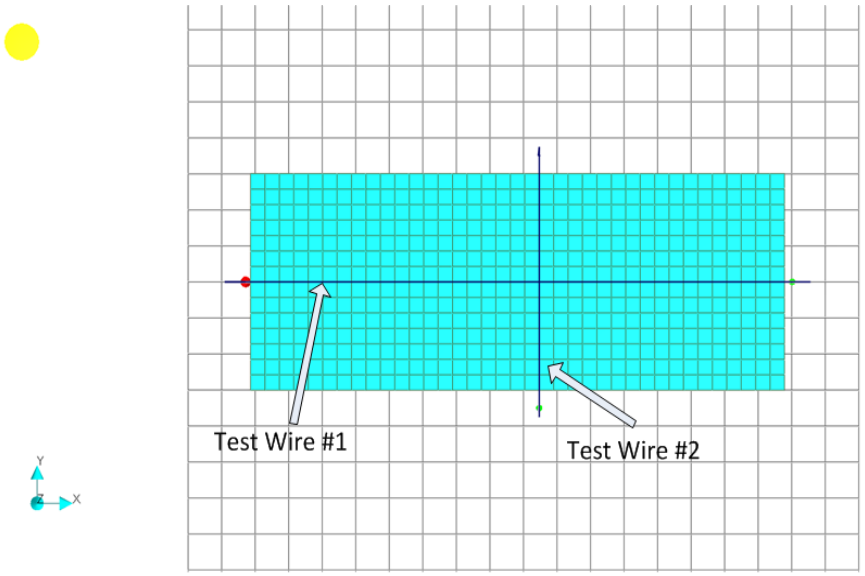

FIGURE 6.10: Plan View of SVTC Model Showing Test Wire Locations

The characteristic impedance of Test Wire #2 is shown in Figure 6.11. When compared to the impedance plot for the simple stripline it can be seen that the impedance for the Test Wire over the SVTC model is not so well matched, deviations of up to approximately 55 Ω below 800 MHz, with an impedance of 265Ω at 100 MHz. At 1 GHz a value of 222Ω was recorded. The difference between the results for the simple stripline and the SVTC Test Wire can be attributed to the incomplete ground reference plane below the Test Wire and the abrupt corners in the SVTC Test Wire causing reflections.

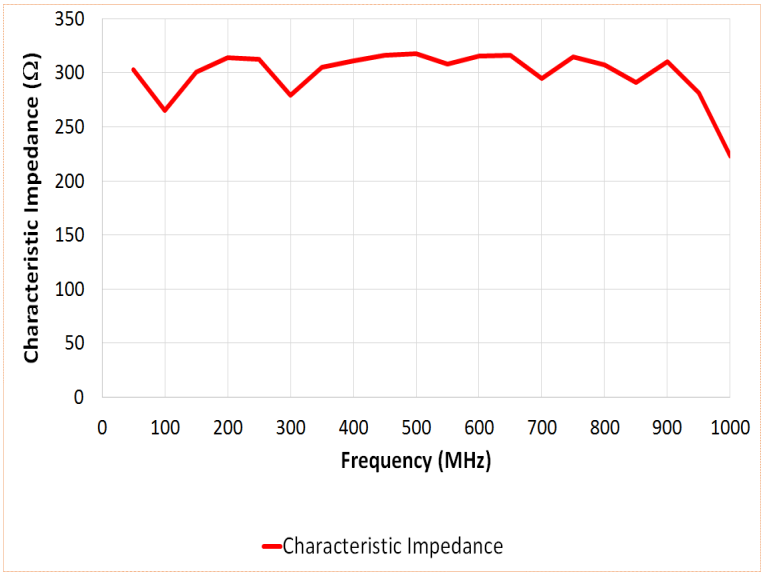

FIGURE 6.11: Test Wire 2 Impedance Plot for SVTC Model

6.2.1.3 Simple Vehicle Test Case Physical Model

In order to validate the SVTC simulations a $\frac{1}{3}$ scale model was built. The body of the physical model was constructed from 9 mm MDF sheets, the sheets were glued together using PVA glue and a minimal amount of panel pins to hold the structure together whilst the glue dried. The outer surface of the model was covered with aluminium foil, with all seams covered in conductive copper tape to ensure continuity from one piece of foil to the next. The internal base of the model was also covered in aluminium foil, which was also bonded to the outer surfaces. The overall size of the physical SVTC model was 1.5 m x 0.56 m x 0.5 m. Figures 6.12 and 6.13 show dimensioned front and side elevations of the third scale model.

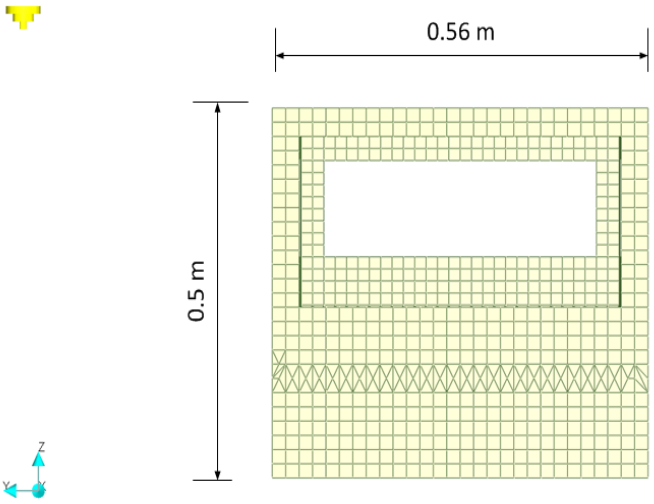

FIGURE 6.12: Third Scale SVTC Dimensioned Physical Model (Front)

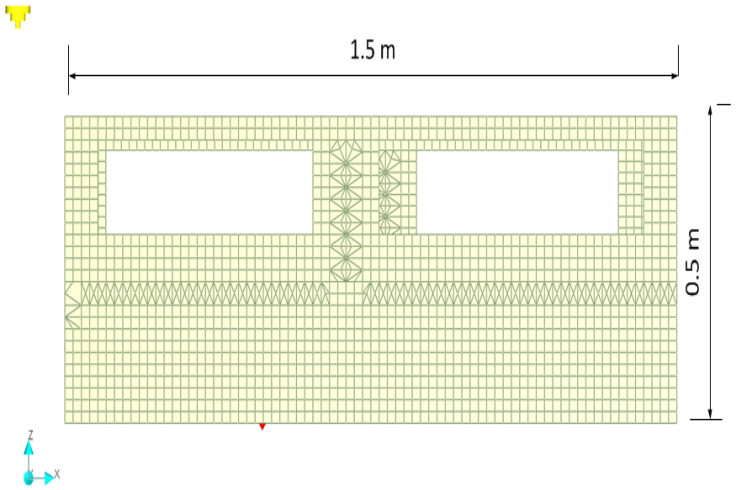

FIGURE 6.13: Third Scale SVTC Dimensioned Physical Model (Side)

Two test wires were suspended 67 mm above the surface of the model using nylon spacers which equated to $\frac{1}{3}$ the height of the full size EM model. Each end of the Test Wire was terminated to the body of the model through a resistor . The impedance used for the terminations calculated to account for the Test Wire being 67 mm above the surface and not 200 mm as suggested in the literature. Using the formula in equation 6.1 a 330Ω termination was used at one end of the Test Wire and 280Ω at the end that the measurement system would be connected to. Test Wire 1 was positioned parallel to the length of the model, along the centre line, test Wire 2 was positioned parallel to the width of the model. Details of the physical model can be seen in Figures 6.14 to 6.15.

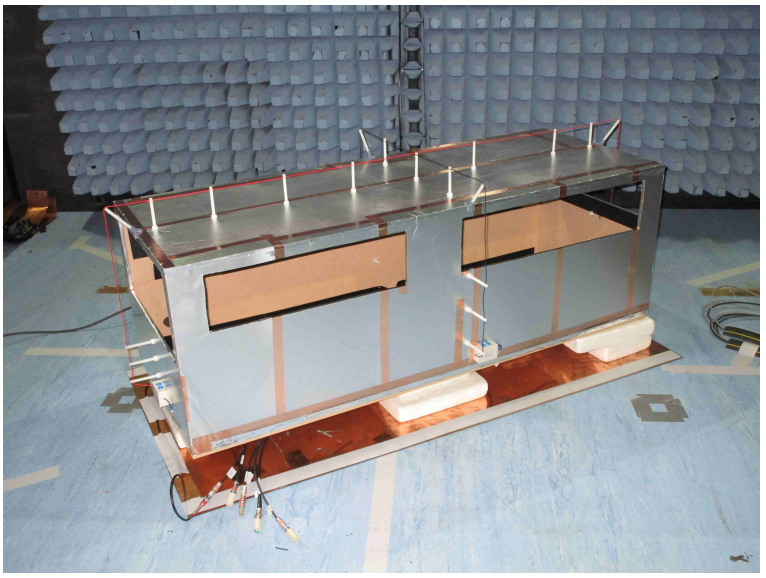

FIGURE 6.14: Third Scale Physical Model

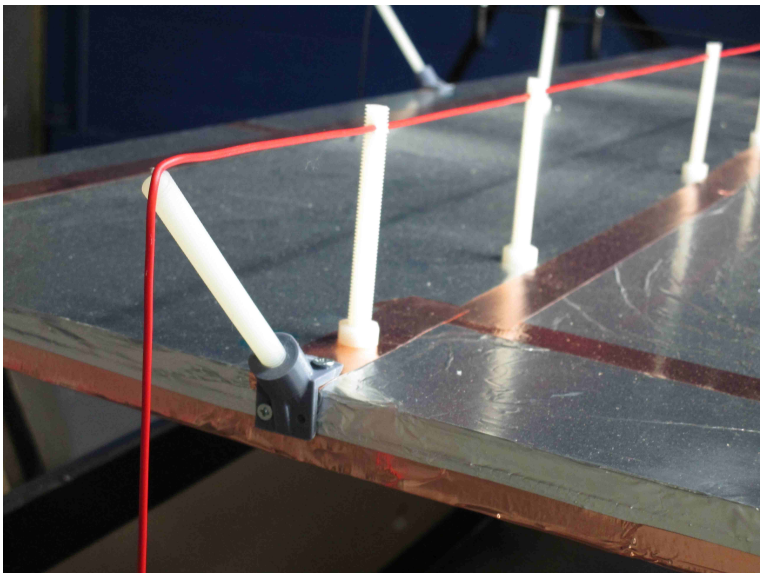

FIGURE 6.15: Close Up Detail Showing Test Wire Spacers

Figures 6.16 shows the Noise Source used inside the enclosure of the SVTC and 6.17 shows the positions of the terminations on the physical model.

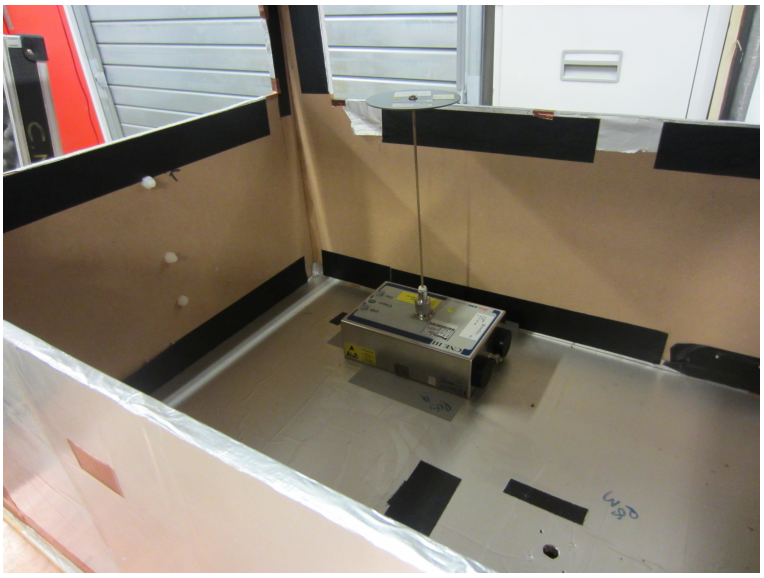

FIGURE 6.16: Noise Source Inside Model

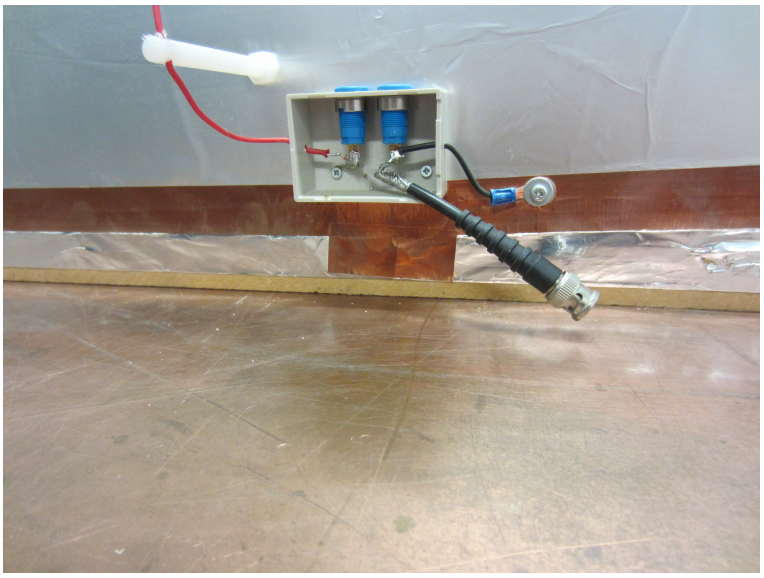

FIGURE 6.17: Test Wire Termination

The impedance of the test wire was measured before tests began, as can be seen in Figure 6.18 the measured impedance was not 330Ω at all frequencies as calculated. This was due to the wire not having a ground reference plan under its entire length, and possible reflections due to the termination connections. The impedance plot can be seen to vary with frequency, with a minimum characteristic impedance of approximately 200Ω recorded at 560 MHz.

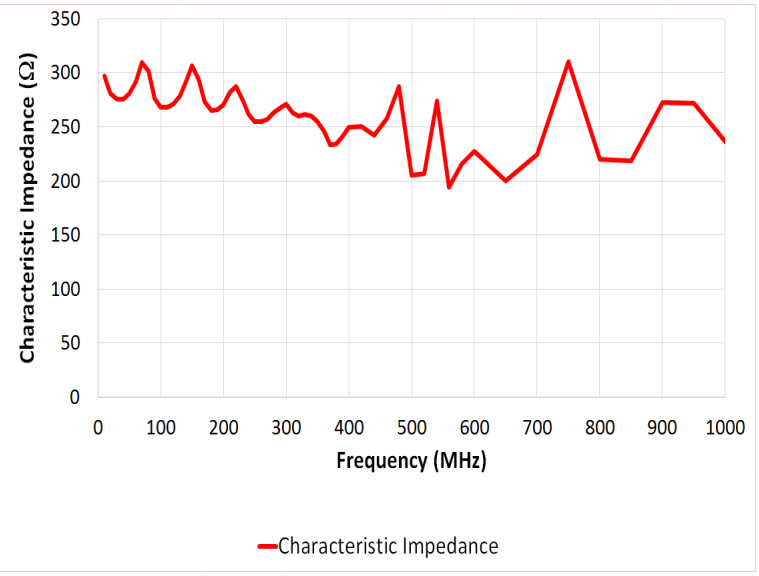

FIGURE 6.18: Measured Input Impedance of Test Wire

6.2.1.4 SVTC EM Model Simulations

Electromagnetic simulations were performed on the SVTC model with the aim of recording the amplitude of the E-field in the hemisphere surrounding the model. Simulations were performed over the frequency range of 50 MHz to 300 MHz in 50 MHz increments, the maximum frequency was limited to 300 MHz as this an approximation of the maximum scaled frequency of 334 MHz used during the $\frac{1}{3}$ scale SVTC measurements. The E-field was recorded with the noise source at each of the five positions within body shell of the SVTC.

After performing the simulations on the SVTC model described in Section 6.2.1, the E-field around the the model was recorded at Effective Receive Antenna Heights, ERAH, of between 1 m and 4 m above the ground level. The maximum E-field over a hemi-spherical scan around the model was also recorded. The electric field was recorded at 360 discrete azimuth positions around the model. Figure 6.19 shows the E-Field probe positions used in the simulations.

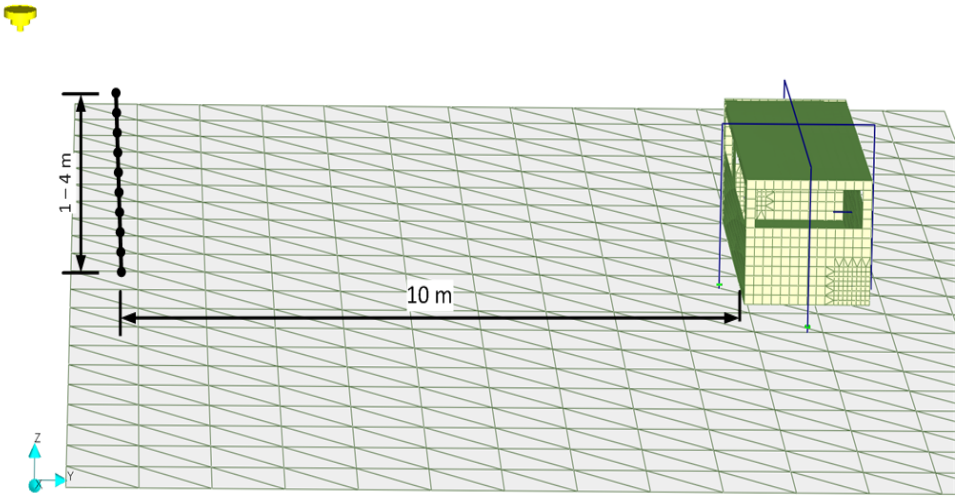

FIGURE 6.19: SVTC EM Model E-Field Points Used

From the data recorded it is possible to produce a polar diagram of the E-field radiation pattern, in the azimuth plane, for each frequency. As detailed in earlier sections all polar plot data was normalised to a maximum value of 0 dB.

6.2.1.5 SVTC Physical Model Measurements

As the model being used was a $\frac{1}{3}$ scale of the simulation model, measurements were performed on the model at frequencies between 200 MHz and 1 GHz, in 100 MHz steps (giving a scaled frequency range of 66 MHz to 334 MHz approximately). Due to time limited access within the required measurement facility, the number of frequencies investigated was limited. The model was setup 100 mm above the turntable, supported on low dielectric constant insulating foam, inside the semi anechoic chamber at 'HORIBA MIRA'. Initial measurements were performed with the model rotated through 360^0 in 10^0 increments (the increment angle was chosen in order to minimise measurement time). The receive antenna was positioned 3 m away from the model at a height of 1.8 m above the facility floor. Ideally measurements would have been performed with the antenna 10 m from the model, however, due to to the size of the semi-anechoic chamber used 3 m was the maximum achievable distance. E-field data, both horizontal and vertical polarisation of the receive antenna, was recorded using source positions 1 to 5, as detailed in Figure 6.6. Note that the measurements detailed in Figure 6.6 were scaled by a factor of $\frac{1}{3}$ to account for the model not being full size, as detailed earlier. From the E-field

data recorded, normalised polar plots were produced. Figures 6.22 to 6.25 below shows typical example plots.

A single receive antenna height was used for this phase of the research, as the measurements were performed to investigate the proof of concept. This would lead to EB results that offered a direct comparison to those obtained using the CISPR 12 method where a single antenna height is also used.

The voltage across the terminations of Test Wire 1 and Test Wire 2 was then measured at each frequency with the source in positions 1 to 5. The Test Wire measurements were also performed with the SVTC model inside the semi anechoic chamber at MIRA. The termination on each Test Wire was connected to an EMC measurement receiver outside the chamber via a low loss screened RF cable.

6.2.2 Results

6.2.2.1 EM Model Simulated Error Bias Results

Once the simulations had been performed the results were analysed. The maximum value, over a spherical scan, of the horizontal and vertical component of the electric field were compared to the value that was recorded at the E_{LHS} and E_{RHS} positions relative to the vehicle model, as defined in Table 4.3. A typical CISPR 12 measurement would be performed using an antenna height of 3 m above the ground.

The E-field recoded at the E_{LHS} and E_{RHS} positions was compared to the maximum E-field recorded over all of the planar scans performed, E_{max}, for the model, from this data a EB between E_{max} and the field recorded at the CISPR 12 equivalent positions was calculated.

In contrast to the results discussed in Sections 4.2 and 4.3 the EB data presented in this Section is calculated using the E-field amplitude recorded from height scanning of the receive antenna and azimuth scanning of the EUT. The height scanning of the receive antenna was achieved by the use of the the field probe positions detailed in Figure 6.19.

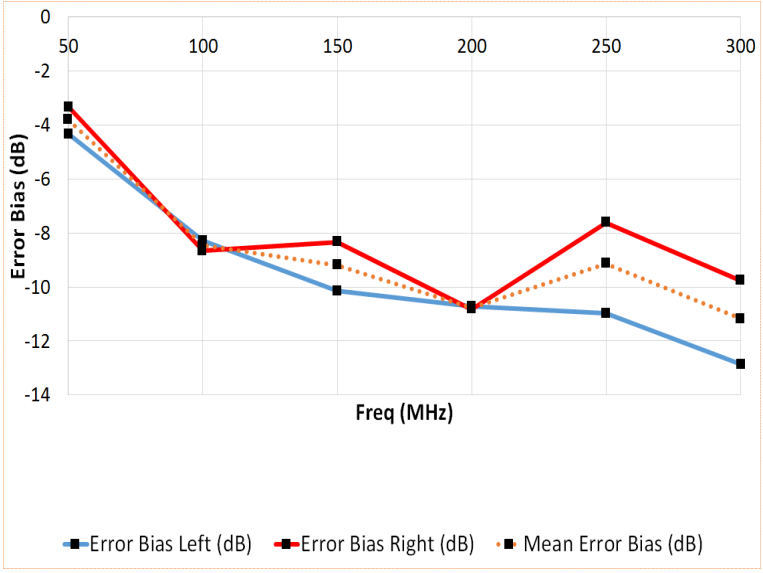

FIGURE 6.20: SVTC Model CISPR 12 Method Mean Error Bias for All Source Positions

The data in Figure 6.20 shows the mean of the linear average for the EB recorded for all 5 source positions for the SVTC model.

It can be seen that between 100 MHz and 300 MHz a mean EB of between 9 dB and 11 dB was recorded. As was highlighted in Section 4.4 this frequency range is where a large percentage of the total emissions from a typical vehicle occur. In the vehicle data examined in Figure 4.87 it can be seen that between 50 MHz and 300 MHz, the mean of the emissions amplitude is approximately 20 dB above the measurement system noise floor, above 600 MHz the mean of the amplitude is approximately 6 dB.

Figure 6.21 below shows the the range of EB values recorded for all 5 source positions compared to E_{max}, A maximum value of approximately 27 dB was recorded across all five source positions simulated. The coloured symbols in the diagram show the EB for the E_{LHS} and E_{RHS} equivalent measurement positions, for each of the six frequencies investigated.

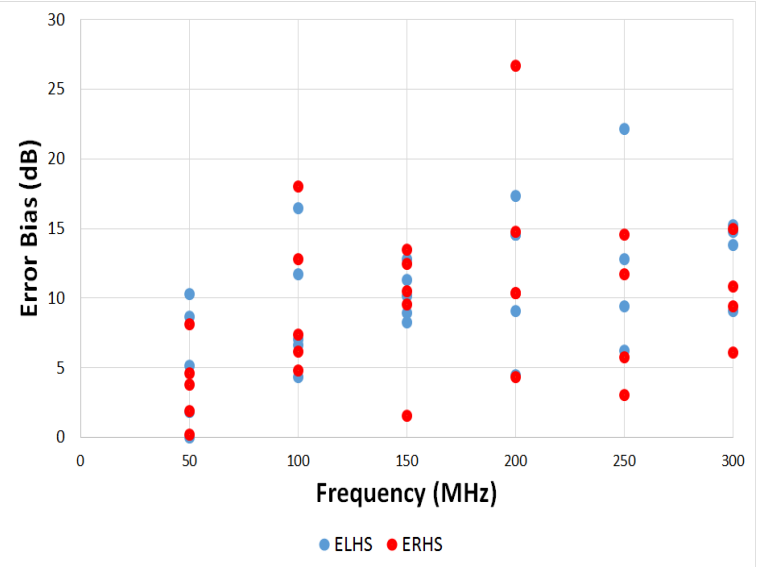

FIGURE 6.21: Error Bias for All Sources (50 -300 MHz)

6.2.2.2 Physical Model 'Error Bias' Results

Example plots of the measured electric field for source position 1 are shown in Figures 6.22 to 6.25. Note that the polar plot data is for the absolute frequency the data was recorded at, as the mode being tested was $\frac{1}{3}$ normal size, the frequencies equate to a scaled frequency of 3 times the value.

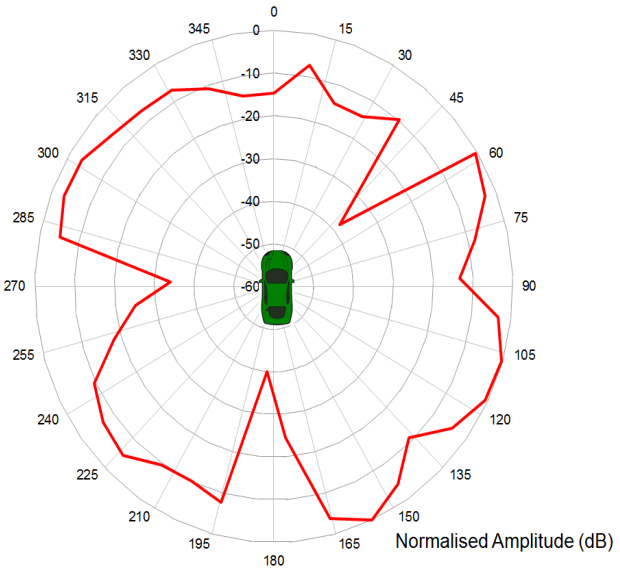

FIGURE 6.22: Polar Diagram of Measured E-Field Emissions from Source 1 at 300 MHz (100 MHz Scaled), Horizontal Polarisation

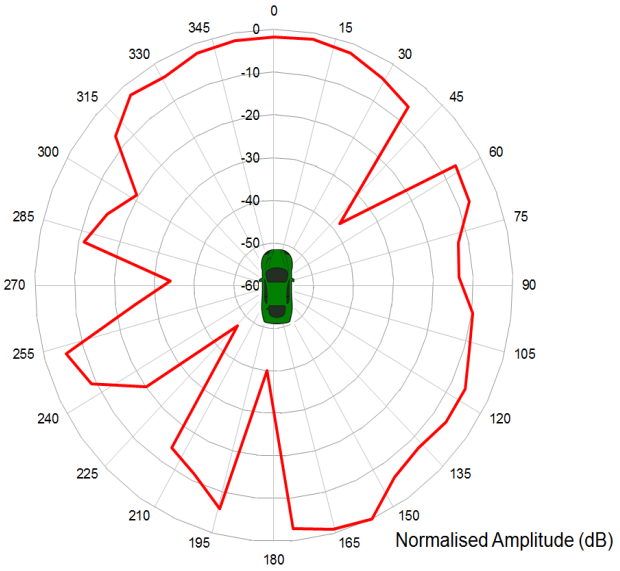

FIGURE 6.23: Polar Diagram of Measured E-Field Emissions from Source 1 at 300 MHz (100 MHz Scaled), Vertical Polarisation

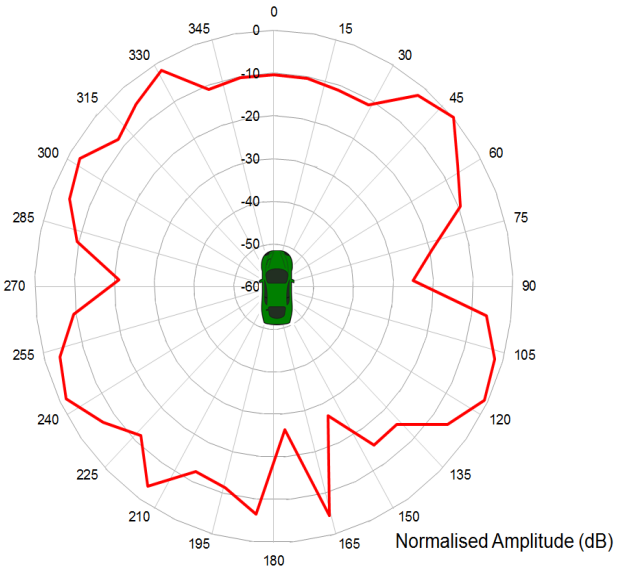

FIGURE 6.24: Polar Diagram of Measured E-Field Emissions from Source 1 at 450 MHz (150 MHz Scaled), Horizontal Polarisation

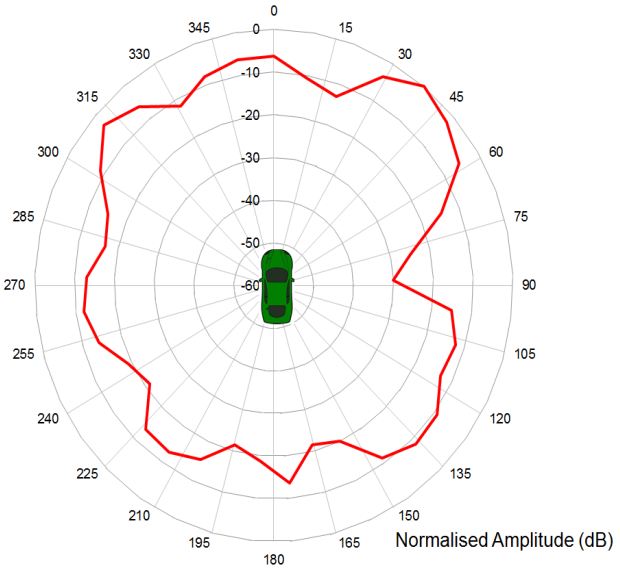

FIGURE 6.25: Polar Diagram of Measured E-Field Emissions from Source 1 at 450 MHz (150 MHz Scaled), Vertical Polarisation

Due to the azimuth increment angle used, the polar patterns may be considered as under-sampled, however, what is still evident are the deep nulls in the polar patterns recorded.

The polar patterns show that even at the relatively low scaled frequencies shown, the patterns display a directive nature. The 100 MHz vertically polarised plot shows a number of deep nulls, a particularly deep one is evident at 270^0, one of the CISPR 12 measurement points. This null accounted for an EB of over 30dB for this particular configuration. When the plots in Figures 6.22 to 6.25 are examined it can be seen that the maximum amplitude of emissions was not recorded at the CISPR 12 positions in any of the examples shown. Even utilising the under-sampled nature of the patterns, a considerable level of EB was recorded.

6.2.2.3 Derivation of the K-Factor

As described in Section 5.1.7.2 the Test Wire relies upon a 'calibration' factor to convert the voltage amplitude measured across the termination of the Test Wire to an equivalent E-field value. In addition to acquiring the maximum amplitude of the received E-field from each source, using the CISPR 32 method, the voltage across the termination resistor for each of the Test Wires was also recorded for each source. The facility measurement receiver was connected to the Test Wire end with the 280Ω termination resistor and

the voltage across the termination resistor was measured at each frequency of interest. Figure 6.26 shows an example of the measured termination voltage and E-field measured using the traditional CISPR 32 antenna method, recorded for Source position 1 over the 200 MHz to 1000 MHz band.

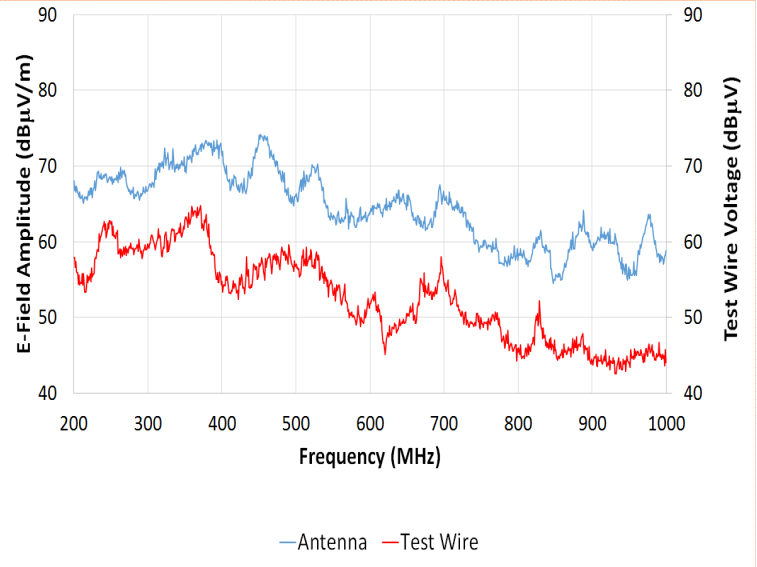

FIGURE 6.26: Test Wire Measured Voltage and Maximum E-Field Measured Against Frequency, Source Position 1, Horizontal Polarisation

The termination voltage and the measured E-field were then used to determine the K-Factor for each measured frequency, as detailed in Equation 5.2. The data recorded resulted in a range of values at each frequency, based upon the source position used in the model, the receive antenna polarisation and the voltage across the Test Wire termination. Figure 7.35 details the spread of the K-factor values recorded for each source position at each of the frequencies investigated.

As can be seen in Figure 6.27 a range of values of K-Factor for each frequency varied from approximately ±10 below 300 MHz to approximately +10 dB to +30 dB between 300 MHz and 1 GHz. The plot shows the mean of the linear EB for each frequency point, designated K-Factor$_m$ and the linear regression line between all the data points shown with a dotted line, designated K-Factor$_l$.

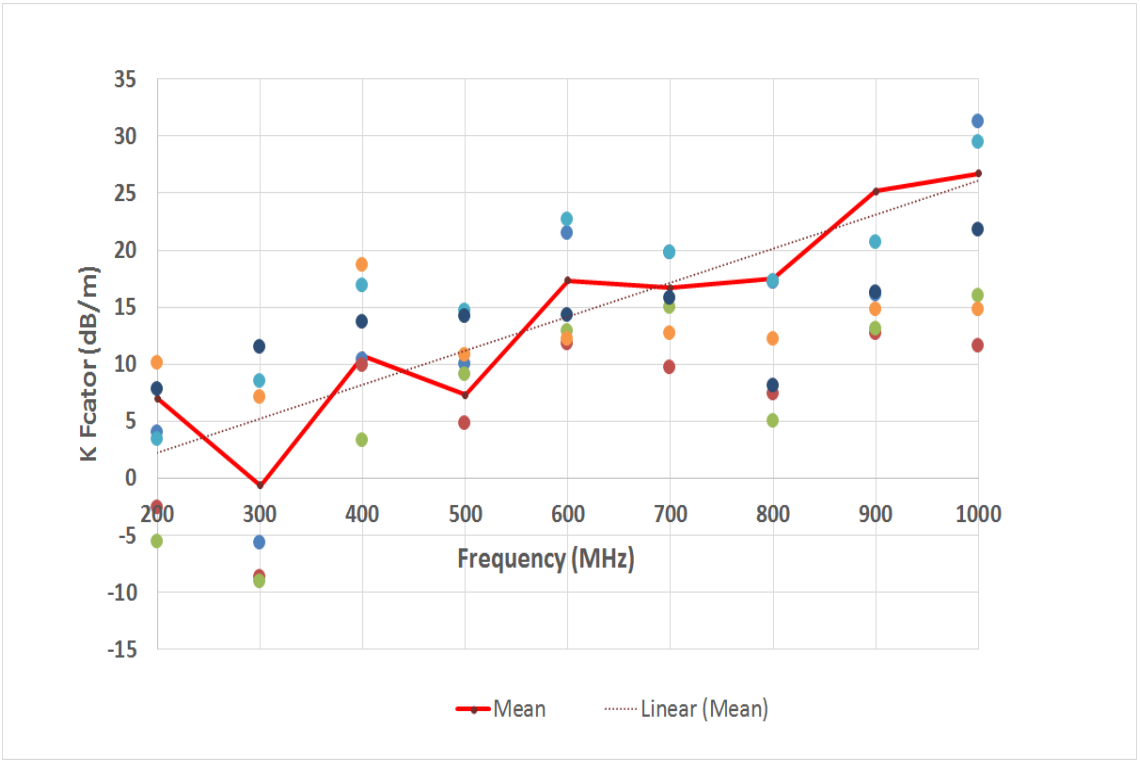

FIGURE 6.27: Spread of Measured K-Factor for Source Positions 2 to 5

The data from source positions 2 to 5 were used to derive the K-Factor. The Test Wire measurements recorded from source position 1 was used as an independent data set. The Error Bias recorded was then compared to that recorded using the CISPR 12 method.

6.2.2.4 Test Wire Measurement Results

Based on the K-Factor values detailed in Figure 6.27 the difference between the Error Bias using the Test Wire method with K-Factor$_m$ was compared with the results using K-Factor$_l$. The data recorded from source position 1 was analysed with both variants of K-Factor applied in turn. As detailed earlier, the Test Wire data from source position 1 was not used in the derivation of the K-Factors. The resulting Error Bias values were then calculated at each frequency. At all frequencies used, the EB recorded using K-Factor$_l$ was either the same as when K-Factor$_m$ was applied or lower. At 300 MHz, 500 MHz and between 800 MHz and 1 GHz the EB using K-Factor$_l$ was between 1.6 dB and 4.8 dB lower than when K-Factor$_m$ was applied. The mean of the linear values of Error Bias was

3.9 dB using K-Factor$_m$ and 2.1 dB using K-Factor$_l$. Figure 6.28 shows the comparison in EB results graphically.

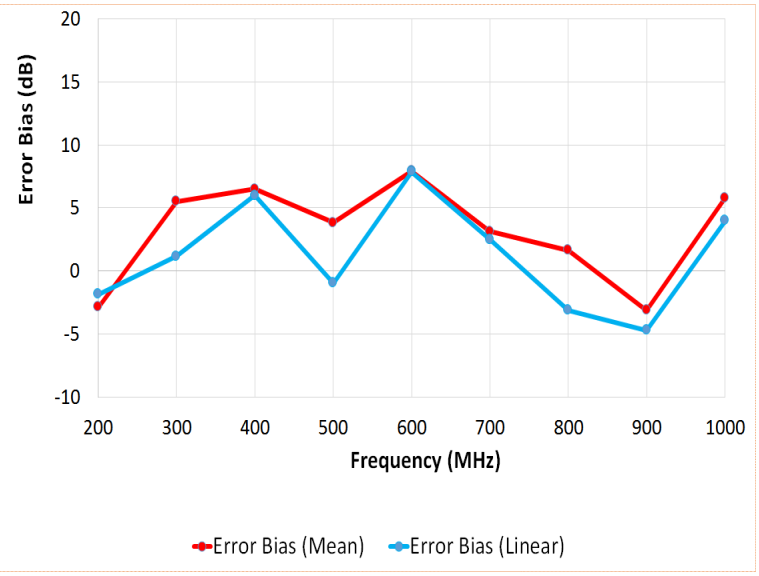

FIGURE 6.28: Comparison of the Error Bias Using K-Factor$_l$ and K-Factor$_m$

The EB recorded from the Test Wire data with K-Factor$_l$ applied was then compared to the CISPR 12 method results.

The graph in Figure 6.29 shows the mean Error Bias recorded using the Test Wire Method is typically lower than that when the CISPR 12 method is employed.

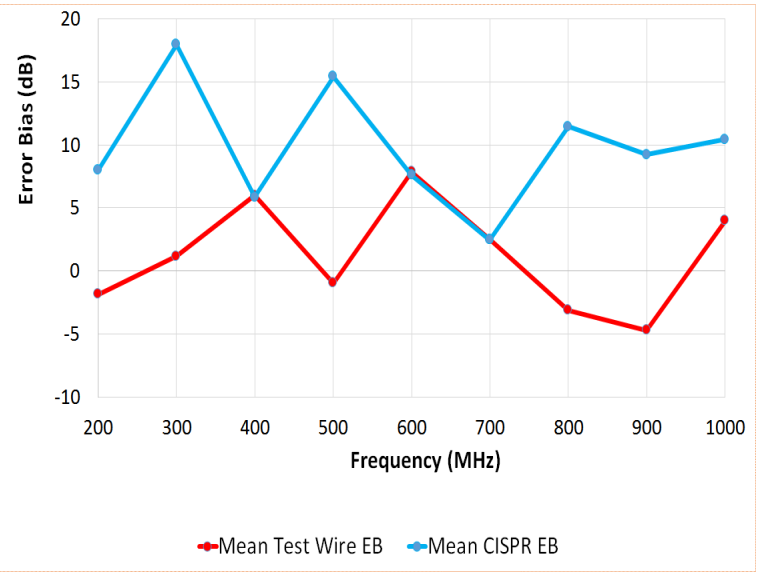

FIGURE 6.29: Comparison of the Average CISPR 12 Method Error Bias with Test Wire Method, Source 1

Across all frequencies and receive antenna polarisations, a mean Error Bias of 11 dB was recorded using the CISPR 12 setup compared to approximately 2 dB using the Test Wire Method. As has been previously noted, a high EB value, approximately 17 dB for this configuration, was again recorded at 300 MHz using the CISPR 12 method, compared to a very low value of 2 dB using the Test Wire method.

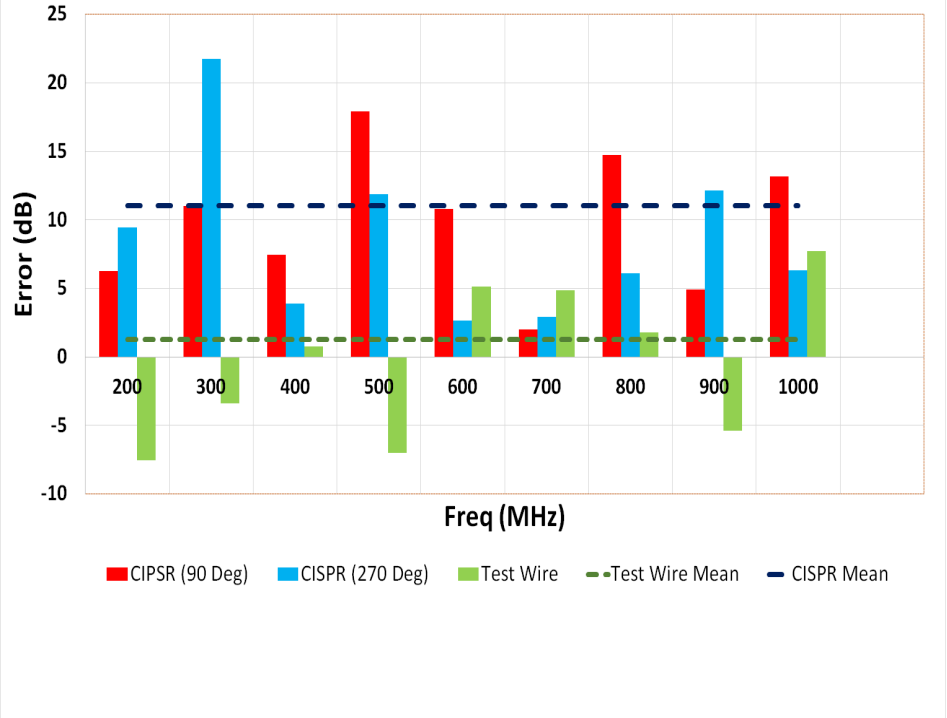

FIGURE 6.30: Comparison of the CISPR 12 Method Error Bias with Test Wire Method, Source 1, Horizontal Polarisation

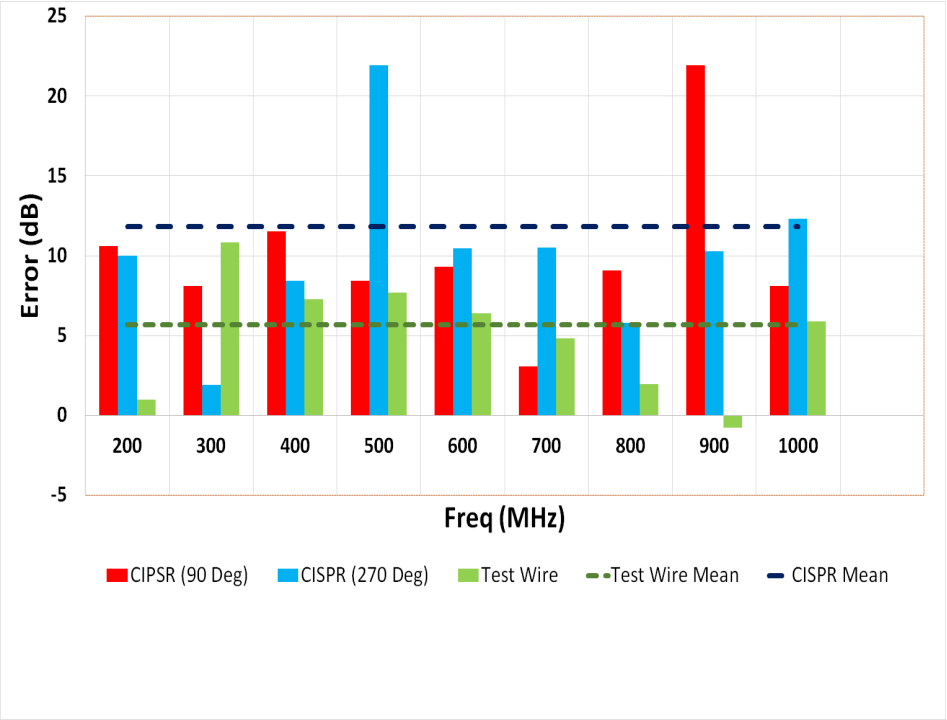

FIGURE 6.31: Comparison of the CISPR 12 Method Error Bias with Test Wire Method, Source 1, Vertical Polarisation

It can be seen from Figures 6.30 and 6.31 that although the Test Wire method does not produce a lower value of EB at every frequency, the overall mean EB across all frequencies investigated is significantly lower. For this particular model configuration, the Test Wire results compared to the CISPR 12 results using a horizontally polarised antenna showed an almost 10 dB lower EB.

6.2.2.5 Original TWM Conclusions

The results reported in this section show that the original version of the TWM can offer a reduction in the EB recorded when measuring the radiated emissions of a test vehicle. The results presented a mean reduction in EB to approximately 2 dB compared to 11 dB using the current CISPR 12 method for performing vehicle level radiated emissions measurements. It should also be noted that the Test Wire positions were not optimised and were based upon ease of construction rather than where the best likelihood of recording the maximum emissions amplitude is. The results presented in Chapter 7 of this thesis, a more optimised position on a representative body shell was investigated.

The results detailed in this chapter were based upon a limited sample of data points being used to record the maximum E-field radiated by the device under test. Only a single antenna height was utilised, which has been shown in earlier sections, will reduce the possibility that the maximum emissions will be recorded. The maximum E-field amplitude recorded was used for producing the EB figure was also used to produce the K-Factor.

The Test Wire method is not, however, without its disadvantages, these can be summarised as:

- The system is 'intrusive' to the test vehicle as a physical ground connection is required to terminate the Test Wire
- The impedance of the Test Wire is not easy to maintain due to the apertures in the vehicle leaving parts of the Test Wire without a ground reference plane underneath.
- The physical construction of the Test Wire would need to be modified for each different vehicle tested .
- Maintaining a constant height above the surface of the vehicle could prove difficult with a 'real' vehicle due to its complex shape

Whilst the Test Wire method has been shown to offer a reduction in EB in the maximum amplitude of E-field recorded compared to using the CISPR 12 method, the disadvantages listed above suggest that further development of the system is required. Chapter 7.1 describes the MicroStrip method that was implemented and details the further reduction in EB achieved using the method.

Chapter 7

MicroStrip Method

7.1 MicroStrip Method

7.1.1 Introduction

One of the main drawbacks with the TWM is maintaining a constant input impedance, due to difficulties with keeping a uniform spacing between the test wire and the device under test as highlighted in Section 6.2.2.5. As previously described in Section 5.1.7.3 possible alternatives to using the original Test Wire method is the Surface Current Sense Wire method suggested by Coenen [79] and the FlexμStrip method as suggested by Cartysse et al [74].

The first variants of the Test Wire method were based around a transmission line formed by a wire above a ground plane. The 'FlexμStrip' system modified the wire over a ground plane to a traditional microstrip configuration of a wide, flat strip above the ground plane.

While both methods offer advantages of a better input impedance match to the measurement system, the Sense Wire method still requires a physical bond to the chassis of the EUT. Quite often, during commercial measurements the vehicle being tested is a customer owned item, and modifying the vehicle to allow the connectors to be grounded to the body shell is not an ideal solution.

As the The 'FlexμStrip' system does not require a physical bond to the device being tested, it has been further developed as the basis of an alternative to the CISPR 12

method. For the purposes of this thesis the author has designated his variant of the 'FlexμStrip' used as a 'MicroStrip'

In this chapter a brief overview of microstrip design parameters and how these affect the performance will be presented. The design used for this research is then described; detailing how the dimensions and materials used were determined. The remaining sections of the chapter will then detail measurements performed to firstly derive the K-Factor and then how this was applied to the MicroStrip measurements in order to determine the EB in the maximum amplitude of the radiated E-field recorded. This EB is then compared to that recorded using the traditional CISPR 12 antenna measurement method. The chapter closes with conclusions on the performance of the MicroStrip method for recording the E-field emissions for vehicles.

7.1.2 Microstrip Theory / History

The microstrip is a planar transmission line and is often used as an interconnect in high speed and RF PCB designs. It is typically created using a wide metallic strip or PCB trace, mounted above a conductive ground plane, separated by a dielectric slab, hence a PCB lends itself to the design very easily.

The origins of the early microstrip can be traced back to work performed by Rumsey and Jamieson in the early 1940's [80]. Their work investigated using a coaxial line with a flat centre conductor instead of the traditional cylindrical version. In a project run by R Barrett, whilst working for the Air Force Cambridge Research Centre [81], a further development was performed whereby the side walls of the coaxial line were removed and the top and bottom walls were extended, forming an early incarnation of the stripline. Around the same time as Barrett was developing his stripline design Grieg and Engleman of the Federal Telecommunications Laboratories of ITT, in 1952 [82], were developing a microstrip design. The main difference between the two designs was where the Barrett design used a flat conductor between two metal slabs, the Grieg and Engleman design featured a line that sat on the surface of the substrate, the bottom face of the substrate was covered in a metallic groundplane. This was the first version of the microstrip as it later became known.

The early stripline designs offered many advantages over traditional coaxial lines, however, one disadvantage was that due to the strip being embedded between the two metallic slabs, making connection to the line was very difficult. As the strip in microstrip line is exposed, connections to it are far easier than with the stripline system. Figures 7.1 and 7.2 show a simplified Stripline and Microstrip layout respectively.

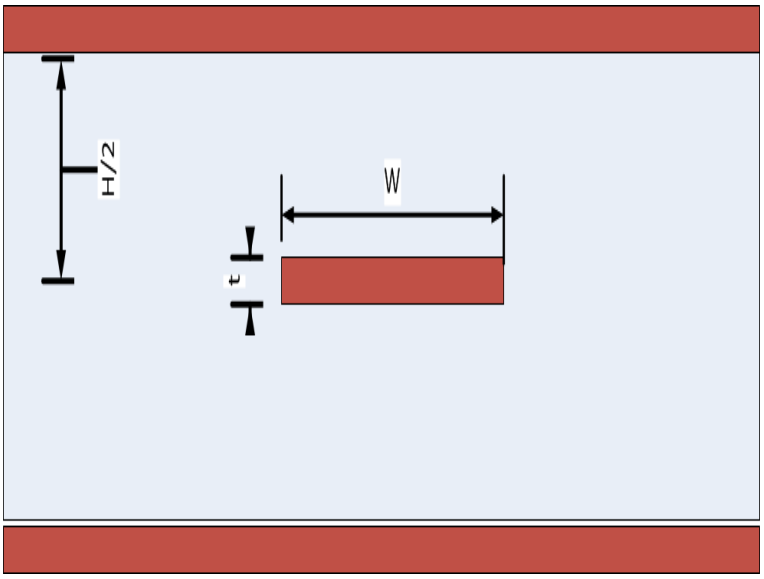

FIGURE 7.1: Basic Stripline Design

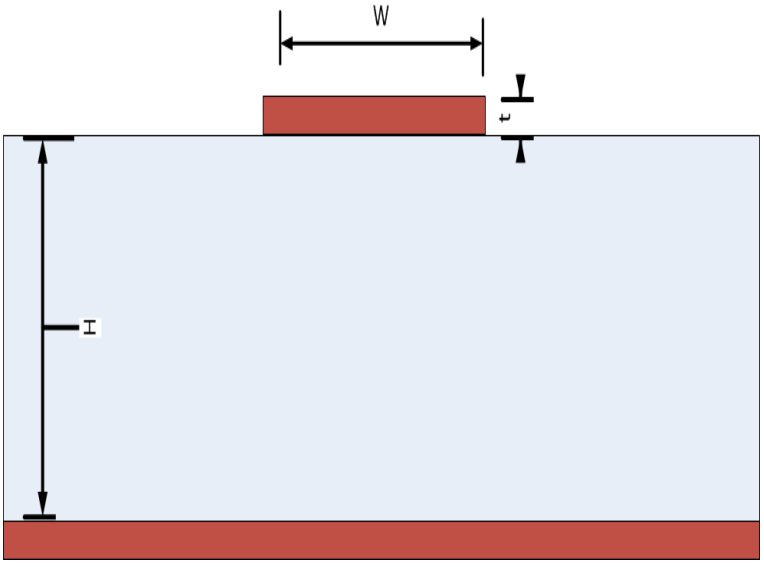

FIGURE 7.2: Basic Microstrip Design

When a stripline is used at radio frequencies the electromagnetic wave carried by the line is enclosed almost entirely within the structure, meaning that very little energy is radiated by the line. Another consequence of the wave being entirely within the structure

of the stripline is the field vectors of the electric and magnetic fields are transverse to the direction of propagation along the line and also are always orthogonal to each other. This Transverse Electromagnetic Mode, TEM mode, as it is known has a property that in an ideal transmission line there is no change in the characteristic impedance with varying frequency.

However, as the strip is open to the air in a microstrip design, the wave carried by the line exists not only within the substrate but also in the surrounding air above the line. If the wave is launched into the microstrip from an ideal coaxial connector, it will begin propagating as a pure TEM wave for that very instant. As the wave begins to travel along the microstrip, the dielectric constant of the substrate will begin to slow the wave in comparison to its speed in the air above. The consequence of this difference in speed will be to 'bend' the field lines towards the longitudinal direction. The microstrip design, thus, is unable to support a true TEM mode of operation beyond its initial launch point. Microstrip lines support a hybrid mode that contains both longitudinal, in the direction of travel of the wave, and transverse components. This hybrid mode has very similar behaviour to a pure TEM mode. As the longitudinal component is small,compared to the transverse component, the supported mode is often referred to as quasi-TEM [83]. At very low frequencies, the quasi-TEM mode can be treated as a pure TEM mode. However, at higher frequencies, a consequence of the quasi-TEM mode is that the characteristic impedance of the line will have a certain amount of frequency dependence. One method of controlling the field being outside of the substrate and closer approximate a TEM mode of transmission is by the use of a material with a high permittivity. Radiation from the microstrip design is far higher than from an equivalent stripline configuration, which as will be shown, is a positive advantage for its use during this research.

7.1.3 Microstrip Design Parameters

An approximation of the characteristic impedance of a stripline can be calculated using the following, assuming that the thickness of the strip is less than $\frac{1}{1000}$ of the height of the structure [84]:

$$Z_0 = \frac{60}{\sqrt{\varepsilon_r}} * ln(\frac{4H}{0.67\pi W(0.8 + \frac{t}{W}}) \tag{7.1}$$

Where H is the substrate height, W is the strip width and t is the strip thickness.

As the microstrip design has part of the strip exposed to the air, the characteristic impedance is not only dependant upon the dielectric constant of the substrate but also that of the air above the strip. The effective dielectric constant, a 'hybrid' or intermediate value between that of the dielectric and air is needed to estimate the impedance of the line. As simple, and relatively accurate estimate of the characteristic impedance for the microstrip, based upon the work carried out by Wheeler [85] is:

$$Z_o = \frac{120\pi}{\sqrt{\varepsilon_{eff}}\left[\frac{W}{H} + 1.393 + \frac{2}{3}ln\left(\frac{W}{H} + 1.444\right)\right]} \tag{7.2}$$

where ε_{eff} is the effective dielectric constant of the line.

$$\varepsilon_{eff} = \frac{\varepsilon_r + 1}{2} + \frac{\varepsilon_r - 1}{2}\left(1 + 12(\frac{H}{W})\right)^{\frac{-1}{2}} \tag{7.3}$$

This is true for values of ε_{eff} when:

$$\left(\frac{W}{H}\right) \geq 1 \tag{7.4}$$

Radiation from the microstrip has been shown to increase as the height of the strip above the ground plane increases [86]. The width of the strip will also affect the amount radiated, a wide strip, with respect to the overall microstrip width, will have lower radiation losses than a thin strip, as more or the field will be enclosed within the substrate [87]. Microstrip with low dielectric constant substrates (< 5) are more likely to radiate, or couple fields, due to lower concentration of the energy in the substrate region. Using the above formulae, the effect of the dielectric constant value of the substrate on the characteristic impedance was investigated. As highlighted in 7.2 the ratio of the strip width to its height above the ground plane will also affect the characteristic impedance of the line. The impedance was calculated for different ratios of width against height and for different values of ϵ_r. The results are presented in Figure 7.3

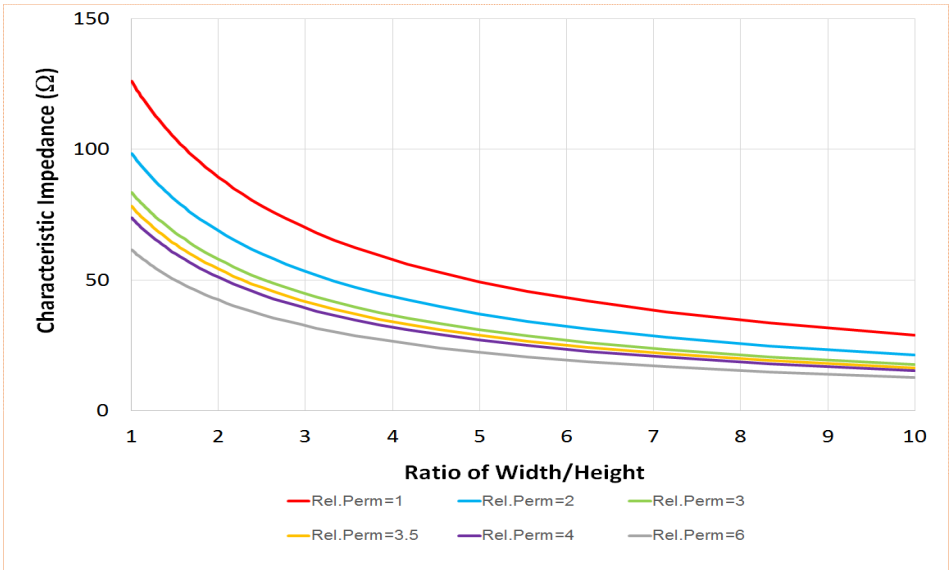

FIGURE 7.3: Characteristic Impedance for Strip Line For Different Values of ϵ_r

7.1.4 Microstrip Design Used

The MicroStrip used for the purposes of this research, was based upon the 'FlexμStrip' [74] referenced in Section 5.1.7.3.

Based on the characteristics detailed in Section 7.1.3 the parameters that affect the characteristic impedance and E-field coupling into the strip were investigated.

The MicroStrip to be used for this research was devised around the parameters and guidelines highlighted in Table 7.1. These parameters were then utilised during the MicroStrip design process:

TABLE 7.1: MicroStrip Parameters.

Design Component	**Parameter**	**Reason for Value Chosen**
Substrate	Low Permittivity	Increase radiation losses[1]; ϵ_r values < 5 will have higher losses that high permittivity substrates.
Substrate	Material	Material needs to be easily machined and cut and readily available to purchase
Strip	Width	A narrow strip will have higher radiation losses than a wider strip
Strip	Height	Height should not be $< \frac{\lambda}{40}$, if height is lower microstrip radiation losses are reduced [88]
Strip	Height above Ground Reference Plane	Determined in relation to width to ensure 50Ω impedance
Strip	Height above Ground Reference Plane	Height above the ground reference plane will affect the radiation losses, larger separation will give higher losses

Note[1]: in Table 7.1 where 'radiation losses' are detailed, applying the Reciprocity Theorem [89], it has been shown [90] that the proprieties of a receive antenna may be deduced from antenna transmission characteristics and vice versa. In the same way that currents flowing on a transmission line will result in EM fields being radiated, an external EM field will also induce currents to flow on a nearby transmission line. Many papers have been published detailing the response of transmission lines excited by an external EM field. Tylor, Satterwhite and Harrison produced the seminal paper on the subject [91], published in 1965, which has been expanded upon by many other authors in subsequent years [92], [9], [93], [94], [95]. The reciprocity theorem has been directly investigated with relation to transmission lines [96] and shown that the traditional coupling models suggested by Taylor et al., Agrawal and Rachidi can be applied equally well to the radiation and coupling problems for transmission lines. For the purposes of this research, the field coupling into the strip is of interest rather than its ability to radiate a field. The

radiation losses detailed in Table 7.1 will, therefore be relevant from a coupling point of view, to the MicroStrip when it is being used to measure E-fields being radiated from the vehicle.

Suitable materials for the substrate were investigated to determine a substance that would satisfy the low permittivity requirements detailed along with being easily machined and strong enough to withstand being used as part of a test device.

The traces detailed in Figure 7.3 show that a characteristic impedance of nominally 50Ω for the MicroStrip can be obtained by using a width to height ratio of between 1 and 5 for the strip, along with a relative permittivity value of between 1.5 and 5 for the substrate.

Polycarbonate sheet was found to offer a relative permittivity of approximately between 2.8 and 3.4, could be purchased in a range of thicknesses from < 0.2 mm to > 10 mm and at a reasonable cost. All of these factors meet the requirements highlighted in Table 7.1.

Both the height of the strip above the ground reference plane and the width to height ratio of the strip have an affect on the characteristic impedance, as defined in the Wheeler Equations 7.2. Using a nominal 10 mm wide strip, the impedance was calculated as a function of height above the ground plane for a range of heights between 2 mm and 7 mm. Figure 7.4 shows the range of impedances for the strip above a polycarbonate substrate. A 10 mm width was used for the strip as a nominal value, as it is a readily available width in copper sheet.

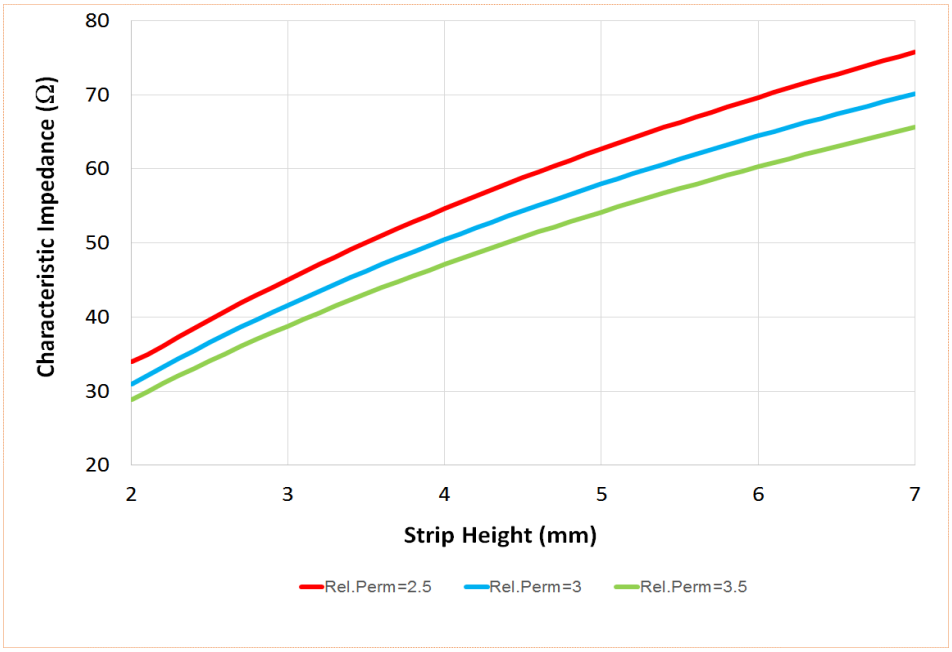

FIGURE 7.4: Strip Height Against Characteristic Impedance

Based upon the results shown in Figure 7.4 a strip height of 4 mm was determined for the MicroStrip design as this produced an impedance of between 47Ω and 54Ω over the possible range of relative permittivity values for polycarbonate.

Using the 10 mm wide strip and 4 mm substrate thickness, as detailed above, the characteristic impedance was then calculated using range of values of relative permittivity quoted for polycarbonate, as detailed in Figure 7.5.

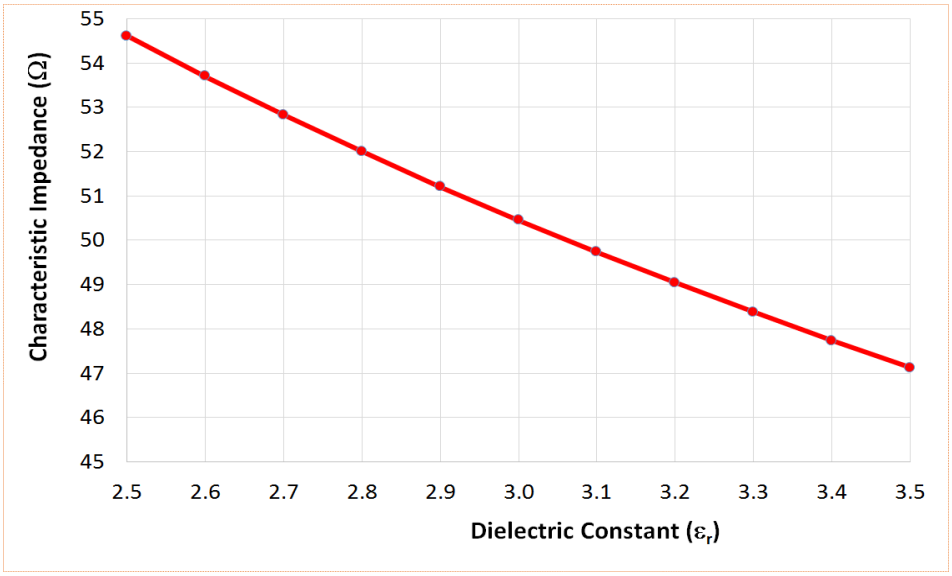

FIGURE 7.5: Characteristic Impedance for Strip Line with Polycarbonate Substrate

As can be seen, the impedance varies between approximately 52Ω and 47Ω for the range of ϵ_r values quoted.

Using the results shown in Figures 7.4 and 7.5, as validated using Equation 7.2, a nominal characteristic impedance of 50Ω was determined and a MicroStrip was built using the following: a 300 mm long, 10 mm x 0.7 mm copper strip positioned on top of a 4 mm sheets of Polycarbonate, 50 mm wide, 300 mm long, this whole arrangement was then placed onto a copper sheet 50 mm x 300 mm x 0.7 mm. The strip was terminated to two N connectors; one for connection to the measurement receiver, the second was terminated with a 50Ω load. The constructional details of the MicroStrip are shown in Figure 7.6. The two N connectors were enclosed in a small metallic box in order to ensure that only field coupled directly into the strip and not the connectors was recorded. The two screening boxes are not shown in Figure 7.6 in order to show the detail of the 50Ω load and the N Connectors. The length of the MicroStrip was specified at 300 mm in order that it remain electrically small at all frequencies under consideration. Studies performed by Coenen [79] and Tektas et al. [73] suggest that longer wires, as used in the Test Wire Method, yielded unpredictable results.

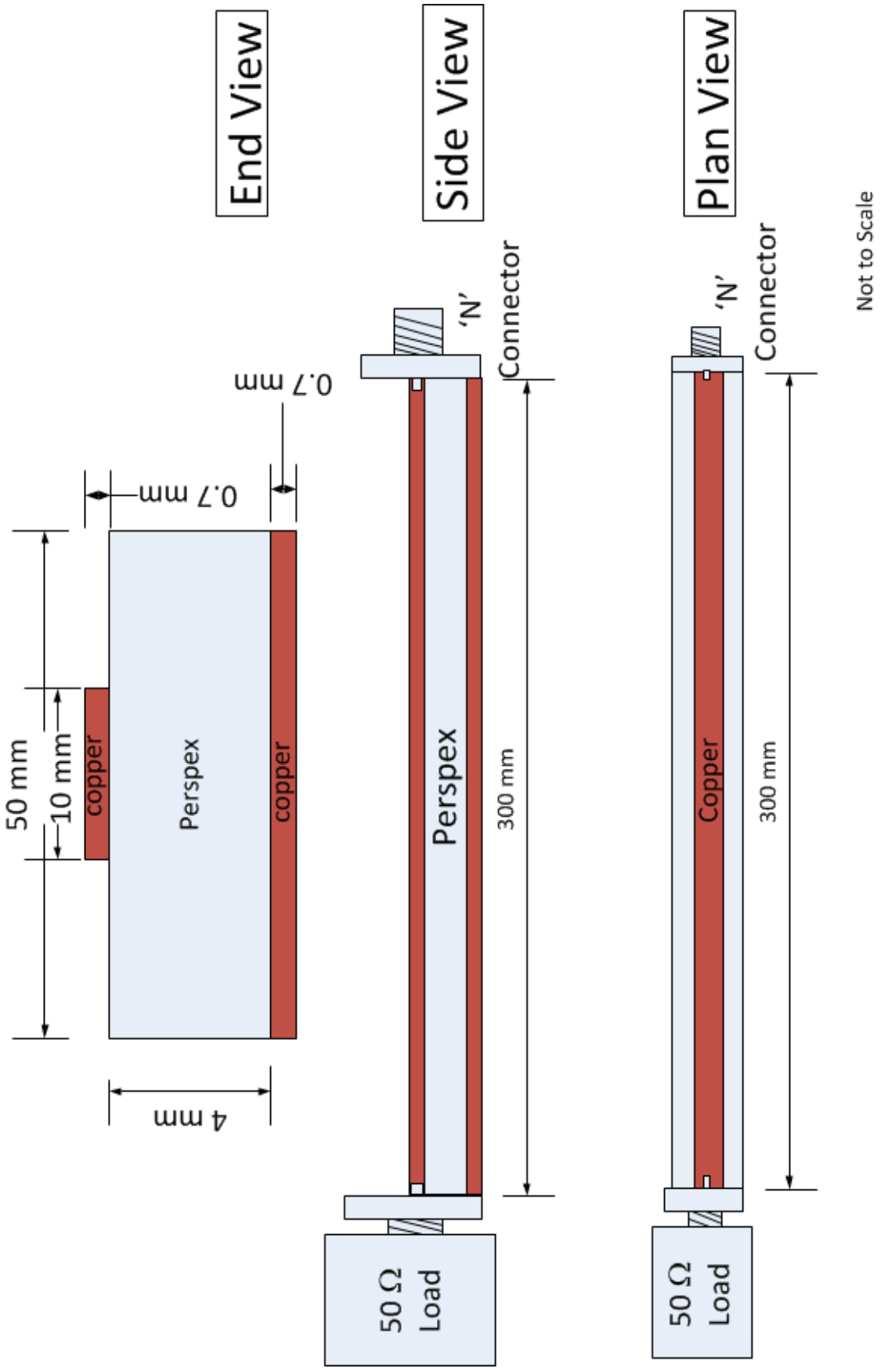

FIGURE 7.6: MicroStrip Construction Diagram

Before the MicroStrip was used to perform any emissions measurements the characteristic impedance was verified, to confirm that a 50Ω termination impedance calculated would be presented to the measurement receiver. Prior to building the physical MicroStrip an EM model was developed within CST Studio Suite [97]by the Horizon Scanning team at HORIBA MIRA. Simulations were then performed in order to determine the reflection coefficients (S_{11}) and the impedance of the MicroStrip. Figure 7.7 shows the EM model used to perform the impedance investigations. The model was terminated with a 50Ω load at one end, the opposite end was used as the measurement point. The plot in Figure 7.8 shows a nominal 50Ω impedance across the frequency range of 50 MHz to 1 GHz. Very minor dips in the impedance at approximately 600 MHz and 900 MHz were observed where the impedance was shown to fall to a minimum of 49Ω.

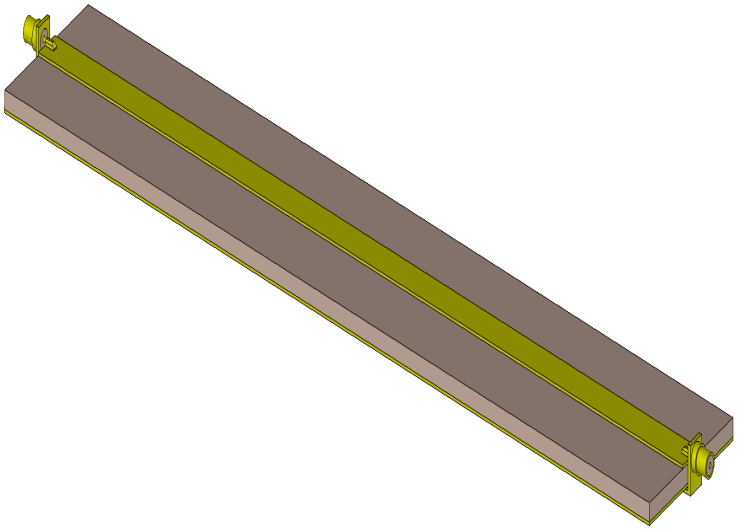

FIGURE 7.7: MicroStrip Simulation Model

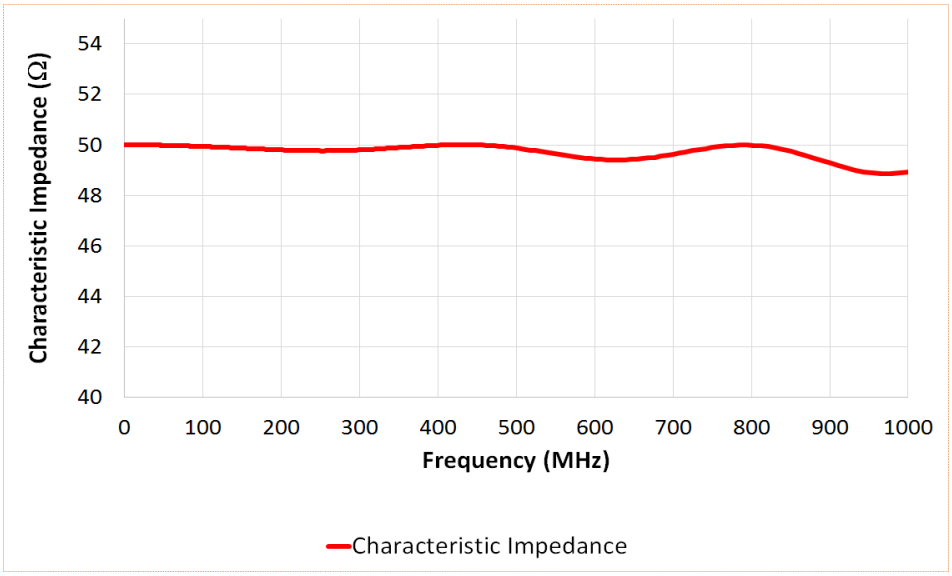

FIGURE 7.8: MicroStrip Impedance (Simulated)

A physical MicroStrip was then built as described in the opening paragraph of this section. The S-Parameters were measured using a vector network analyser to confirm the simulation results were also achieved. The physical model was measured from 50 MHz to 1 GHz in 2.25 MHz steps. The network analyser recorded the magnitude and phase of the reflection coefficient, (S_{11}), at each frequency. From this data the real and imaginary component of the characteristic impedance was calculated using Equations 7.5 and 7.6 [76]

$$Z_{inReal} = Z_0 \frac{1 - S_{11mag}^2}{1 + S_{11mag}^2} - \frac{2S_{11mag}cos(S_{11ph})}{1 + S_{11mag}^2 - 2(S_{11mag}cos(S_{11ph}))} \tag{7.5}$$

$$Z_{inImag} = \frac{(2S_{11mag}sin(S_{11ph} * 50))}{(1 + S_{11}^2) - (2S_{11mag}cos(S_{11ph]}))} \tag{7.6}$$

Where Z_{inReal} and Z_{inImag} are the real and imaginary components of the characteristic impedance of the MicroStrip respectively, S_{11mag} and S_{11ph} are the magnitude and phase of the measured S_{11} value.

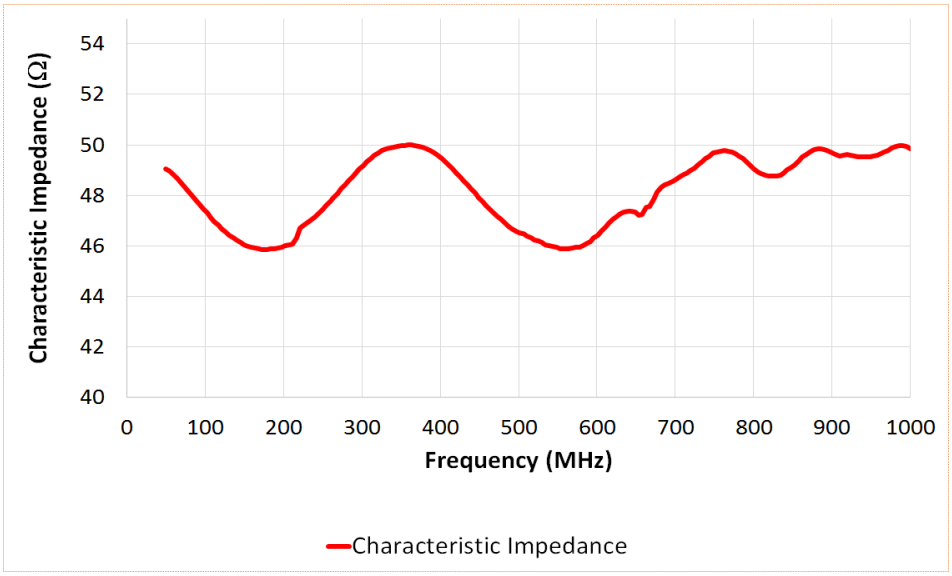

FIGURE 7.9: Measured MicroStrip Impedance (Real Values)

A nominal 50Ω impedance was achieved across the majority of the frequency range, with slight dips in the impedance noted at 200 MHz and 550 MHz, as detailed in Figure 7.9.

As expected the impedance measured for the physical model was not as closely matched to 50Ω) as the numerical model results. This difference can be attributed to mismatches introduced due to connectors and cables required to physically connect the MicroStrip to the network analyser, measurement uncertainty within the network analyser, and cables. The impedance was, however, a much closer match to the calculated value than those obtained when the measurements were performed on the original Test Wire model.

7.1.5 Surface Currents

7.1.5.1 Introduction

During the initial investigations described in Section 6.2 the Test Wires were located along the mid-line of the the length and width of the model. These positions were used to simplify the construction of the model. In the reviewed literature there was no information regarding specific positions where the test wires should be positioned. It was suggested, however, that multiple locations should be used and the diagrams presented showed them along the centre of the length and width and diagonally from corner to corner of the device under test.

Before further development of the TWM into the MicroStrip method was implemented, the location for the MicroStrip to be positioned was investigated as it was unclear from both the literature review or the results presented in Section 6.2 if the positions used offered the best results.

As the MicroStrip method uses a small sensor rather than a long wire over the entire model, as used in the Test Wire Method, the configurations detailed in Section 5.11 were deemed not suitable. In order to determine if there were in fact better positions for the location of the wires, areas of high surface currents on the model were investigated using both simulations and measurements on a full scale vehicle, with the aim of using potential 'Hot Spots' as locations for the MicroStrip.

7.1.5.2 Investigation of Vehicle Surface Current Distribution

The investigations performed in this section were performed on the VBS model and the VBS2 model as detailed in Section 3.1.4.2, in order to offer a closer match to the vehicles that the system was intended to be used for than the SVTC model.

The surface currents of the VBS and VBS2 models were simulated over the frequency range of 100 MHz to 500 MHz. The models were excited with a 300 mm long radiator positioned at different locations inside the vehicle. The radiators were located at the positions detailed in Figure 7.10 for VBS and in Figures 7.11 and 7.12 for VBS2.

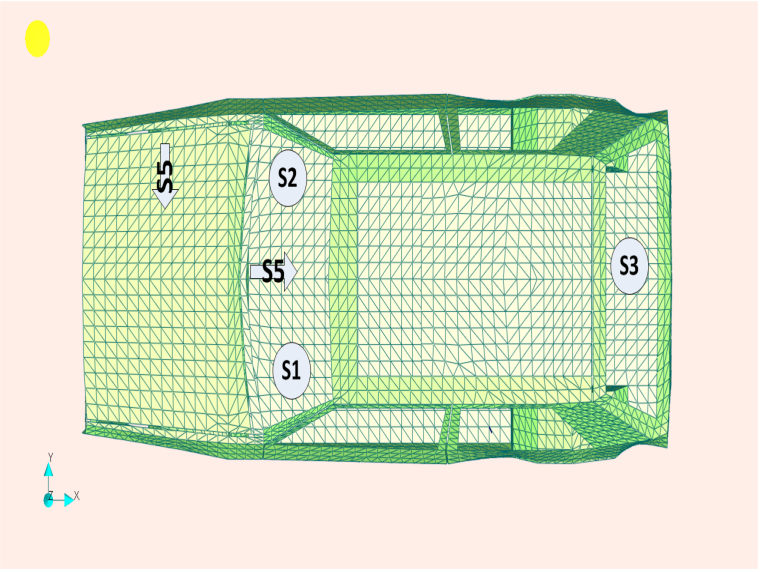

FIGURE 7.10: VBS Source Positions (Plan View)

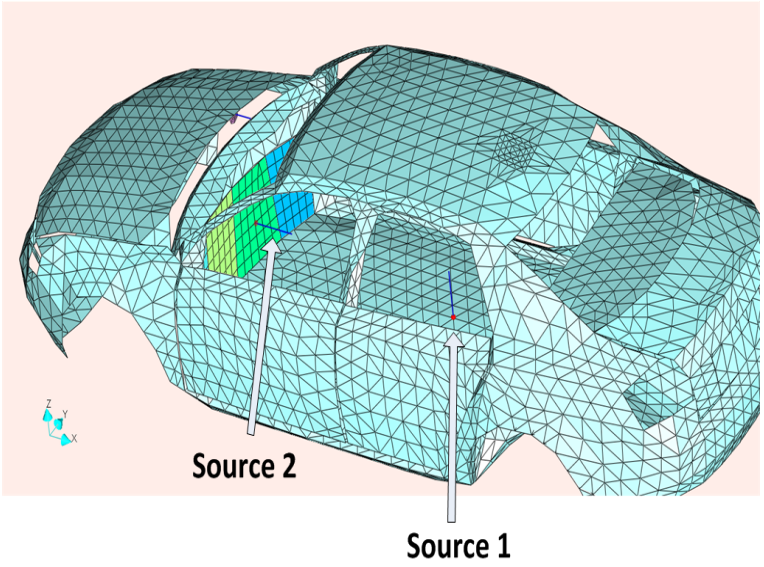

FIGURE 7.11: VBS2 Source Positions - Source 1 and 2

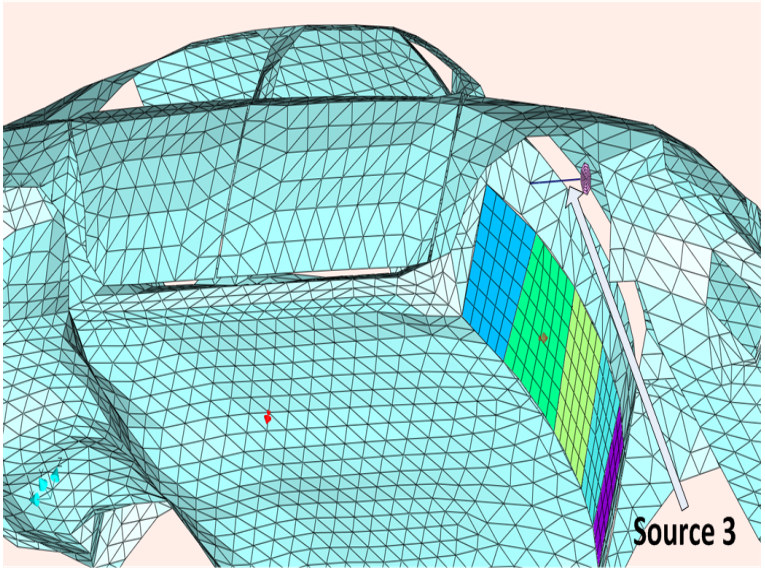

FIGURE 7.12: VBS2 Source Positions - Source 3

At each frequency a 'surface map' plot of current density was produced for each source position, example plots are shown in Figures 7.13 to 7.16. The aim of these plots was to determine common areas of high surface current density and rapid spatial rate change of the current, as these are likely to be areas of higher field radiation. The results from both numerical models were compared to determine if common areas were recorded, these high points were then investigated as being possible areas for the MicroStrip to be placed.

As one might expect there were a number of points on both vehicle body shells where the surface current density was high and circulating currents were evident, most notably

around the seams between the main body shell and the doors, as detailed in Figures 7.13 to 7.14, and along the seam between the bonnet and the vehicle bodyshell, as detailed in Figure 7.16.

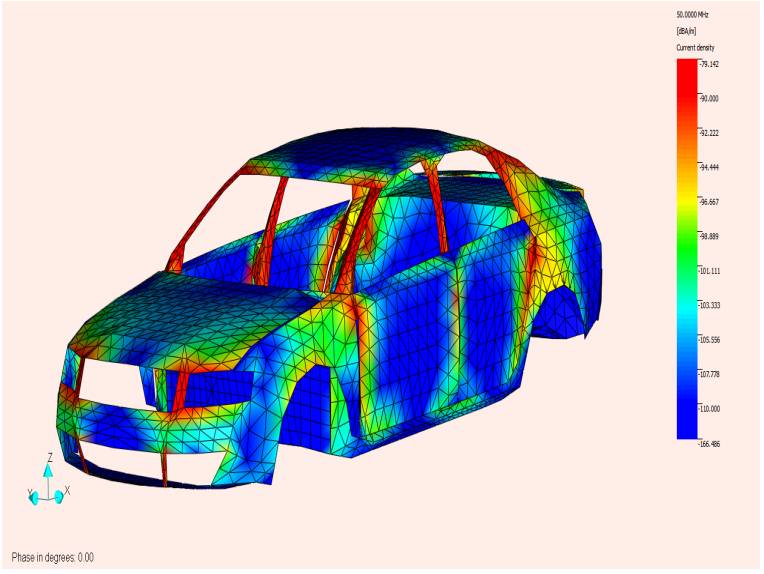

FIGURE 7.13: VBS2 at 50 MHz, Single Source in Position 1

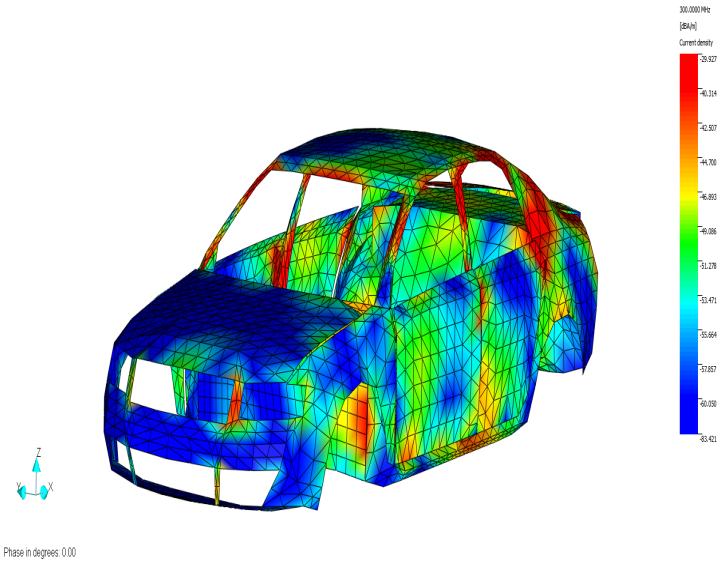

FIGURE 7.14: VBS2 at 300 MHz, Single Source in Position 1

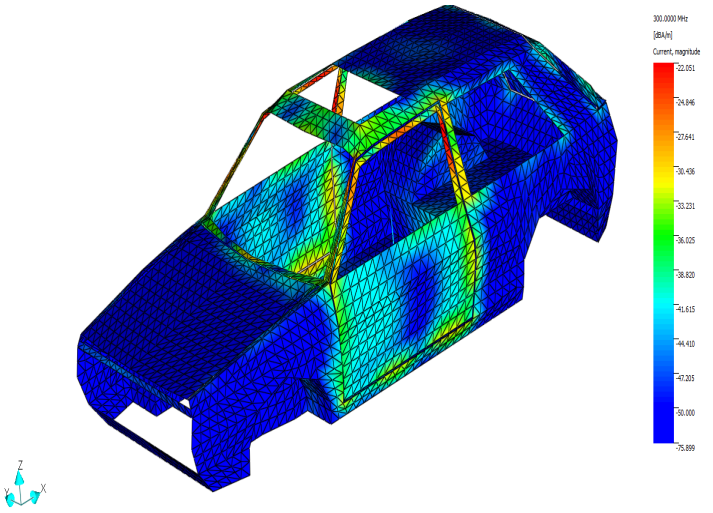

FIGURE 7.15: VBS at 300 MHz, Single Source in Position 1

When a source was added inside the engine bay the seams around the bonnet became the major 'hotspots' as seen in Figure 7.16.

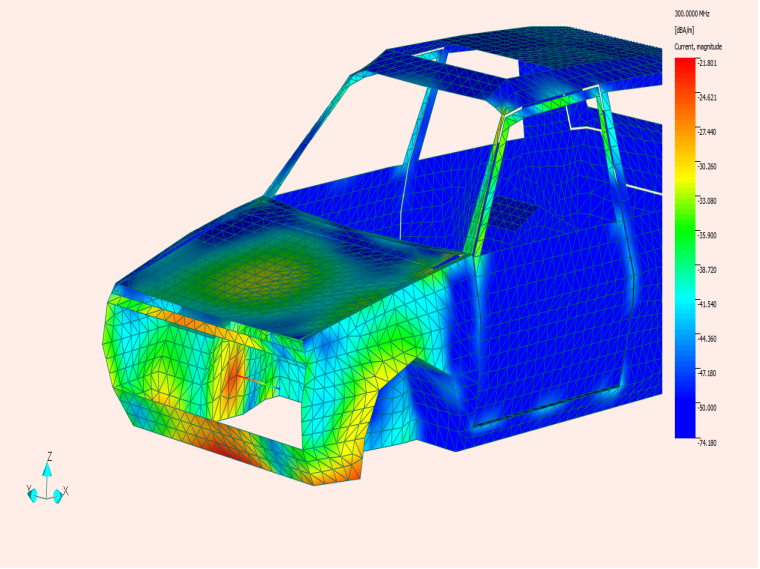

FIGURE 7.16: VBS at 300 MHz, Single Source in Position 5

Locations of the seams around the bonnet can be seen in Figure 7.17.

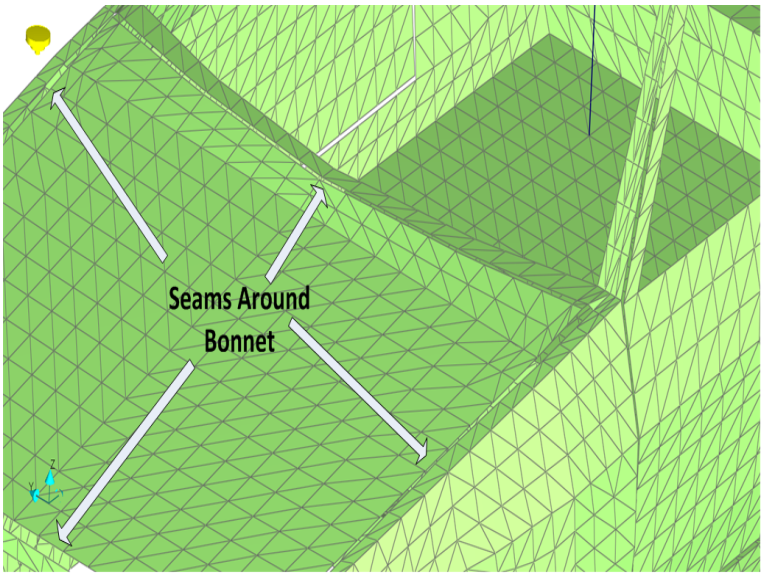

FIGURE 7.17: VBS Model, Detailing Seams Around Bonnet

A noticeable feature of the surface current map noted on both the VBS and VBS2 models was the 'B' pillars of the vehicle showed high levels of surface current, particularly at the lower frequencies of between 50 MHz and 100 MHz.

As the frequency increased the pillars still showed higher levels of surface current than much of the rest of the body shell, but by a smaller margin. At 300 MHz the surface currents were noticeably higher than over the majority of the rest of the body shell, though as can be seen in Figure 7.15, the difference was much reduced compared to the 50 MHz results.

The areas where high levels of surface current were observed required further refinement of the mesh element size as described in Section 3.1.4.2. A mesh of approximately 0.03 m x 0.03 m was used around the window pillars and bonnet seams on both models.

The location of the test points where the surface current level was noted can be seen in Figure 7.18. The amplitude of the measured current was recorded at each frequency for each test point and collated into a data set for analysis once the measurements on a physical vehicle had been performed.

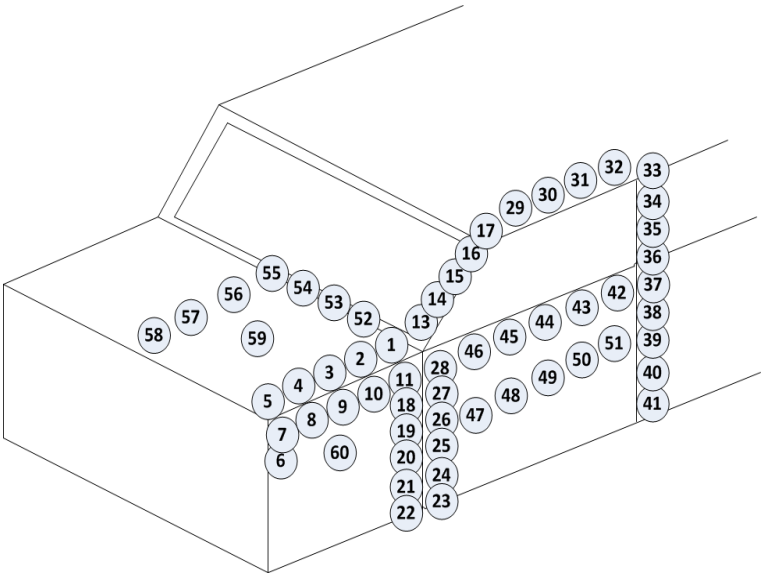

FIGURE 7.18: Surface Current Test Positions

7.1.5.3 Surface Current Investigation Measurements

Based upon the areas of high surface current determined from the simulation results, measurements were then performed on a full scale production vehicle in an attempt to validate the simulation results findings. Due to simulation model availability, the vehicle type used for the measurements was not the same as used in the simulations, a saloon car was used for the simulations, whereas a 4 x 4 type vehicle was used for the measurements. However, as the purpose of this investigation was to determine if the 'hot spots' recorded on the simulation model were replicated on the physical vehicle and whether they occurred at similar positions across different vehicle types, absolute values were not compared, just relative high and low levels. A wide band noise source, York EMC CNE 3, was placed at similar locations inside the vehicle as those used during the simulations to induce the required currents into the body shell. The noise source was located on the centre of the drivers and passenger seats and middle of the dashboard.

Figure 7.19 shows an example of the noise source inside of the vehicle. The amplitude of the surface current recorded with the noise source in the boot of the vehicle was found to be very low in comparison to the positions inside the passenger compartment. Due to the low amplitude being so close to the measurement system noise floor they were not included in the analysis.

FIGURE 7.19: Noise Source Inside Vehicle, Source Position 1

Surface current measurements were performed between 100 MHz and 300 MHz at each of the selected test points using a Fischer Custom Communications Skin Current Probe (Model F-92) connected to an EMC measurement receiver. The vehicle was located inside the xEV facility at HORIBA MIRA whilst the measurements were performed. The xEV facility is a large metal walled building with a conductive ground plane on the floor, there is no RF absorbent materials on any of the walls or ceiling of the facility. The measurement equipment was separated from the vehicle by approximately 8 m, this distance was limited by the length of RF cables used between the current probe and the receiver. The cable used to connect the current probe to the receiver and pre-amplifier had a large ferrite clamp positioned at each end and in the middle to try and minimise ambient signals being coupled onto the cable and corrupting the signals being measured at the test point on the vehicle. The frequency range investigated was limited in its upper and lower bounds by the specification of the available measurement current probe.

FIGURE 7.20: Surface Current Measurement Setup

FIGURE 7.21: Surface Current Probe, Test Position 33

Surface current measurements were performed at each of the test points detailed in Figure 7.18. As the simulation model used was of a different vehicle type to that used for the measurements, the test point positions had to be 'translated' into a matching point on the measurement vehicle. This was achieved by dividing the vehicle, top of the door frame, top edge of wing, rear seam of bonnet etc. and then the number of test points used on the simulation model were positioned at an equal spacing along the length of each section of the vehicle as detailed in Figure 7.22.

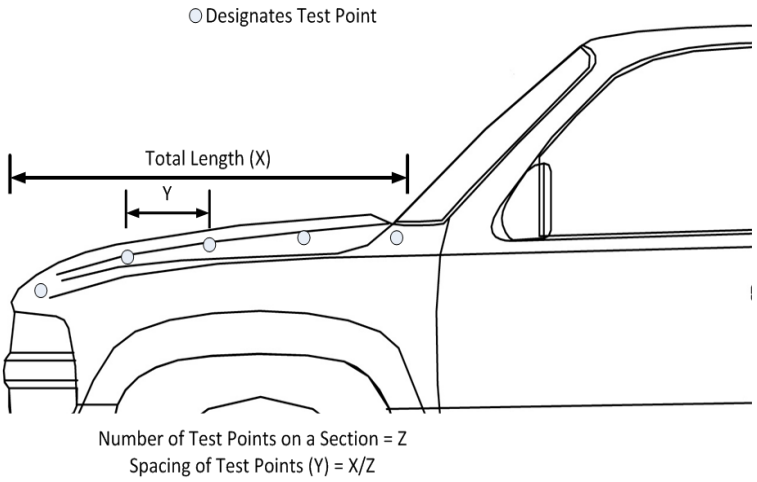

FIGURE 7.22: Surface Current Measurement Point Conversion

Additional current points to those investigated during the simulations of the drivers side of the vehicle were also measured and the surface current recorded. For clarity on the diagram, only the test points on the passenger side of the vehicle are shown and labelled. A total of 120 test positions were used to perform surface current measurements, 60 on the passenger side of the vehicle and a further 60 on the driver side.

Figure 7.23 shows the setup used to perform the surface current measurements. Note: for purposes of the photograph the measurement receiver is shown by the side of the vehicle, during the test the receiver was moved as far away as the RF cables would allow.

FIGURE 7.23: Surface Current Probe Measurement Equipment Setup

7.1.6 Surface Current Investigations Results

The surface currents recorded from the simulations performed on the VBS model were initially visually compared with the measurement results to determine if there were any common areas of high surface current in the two sets of data. In order to allow the data to be analysed further, the amplitude of the measured current recorded at each test point was normalised to a maximum value of one to aid comparison of the measurement and simulated data. The normalised data for the simulated and measured results were then presented on the same axis in Figures 7.25 to 7.32. The scatter plot presented shows the data for the passenger side of the vehicle only.

FIGURE 7.24: Surface Current Amplitude Recorded at 50 MHz Compared of to Amplitude Recorded at 200 MHz

The measured surface current amplitude below 100 MHz was found to be very low when compared to the higher frequency results. The amplitude was found to be too low to allow for the 'hot spots' to be distinguished. This was thought to be due to the sensitivity of the current probe at the lower frequencies. Figure 7.24 highlights the difference in the amplitude between the 50 MHz results and those recorded at 200 MHz.

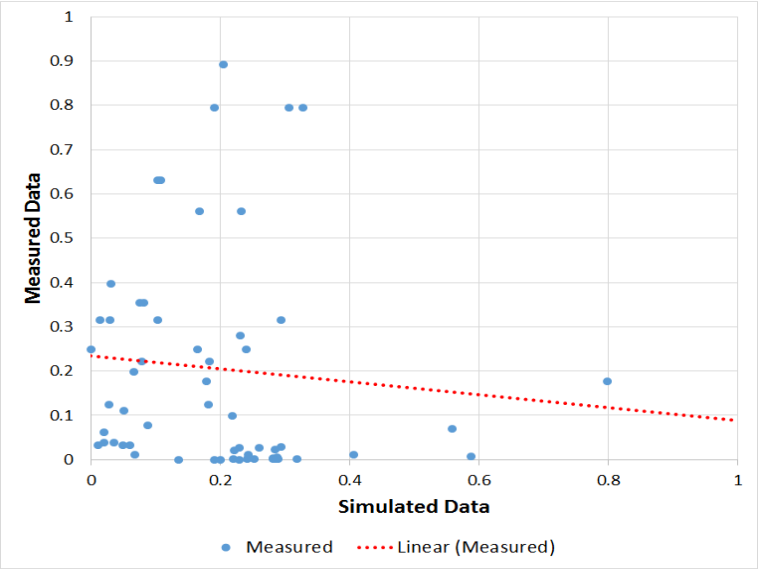

FIGURE 7.25: Scatter Plot of Simulated Surface Current to Measured Data (150 MHz)

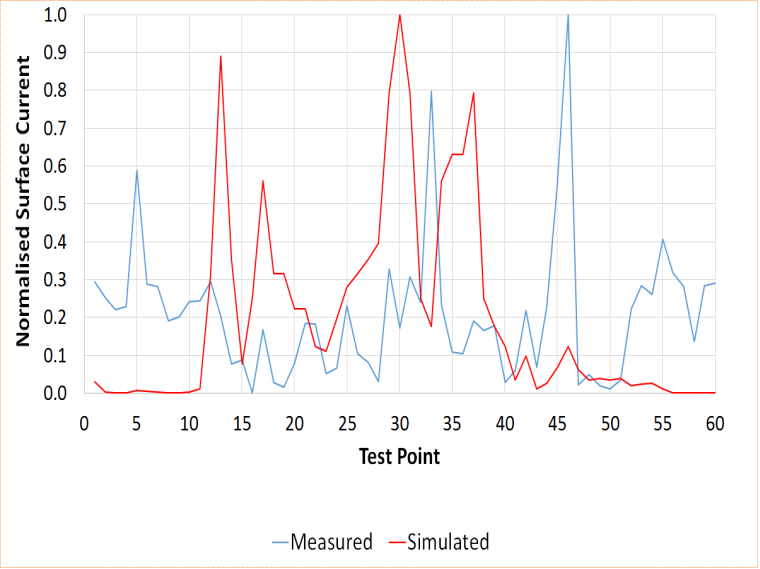

FIGURE 7.26: Plot of Simulated Surface Current to Measured Data (150 MHz)

The 150 MHz data sets showed a poor correlation, with the measured data failing to highlight particular hotspots. The amplitude of the measured surface current at 150 MHz was compared to the amplitude at 200 MHz, a frequency where a good level of agreement between the measured and simulated data was recorded. The amplitude recorded at 150 MHz was found to be very similar to that at 200 MHz. A mean surface current amplitude of -95 dBμA was recorded at 150 MHz and -102 dBμA at 200 MHz. It is thought that a problem occurred with the measurements at 150 MHz, but as the data

was processed post-test the error was not picked up until after the tests were finished and the current probe had been returned to the hire company.

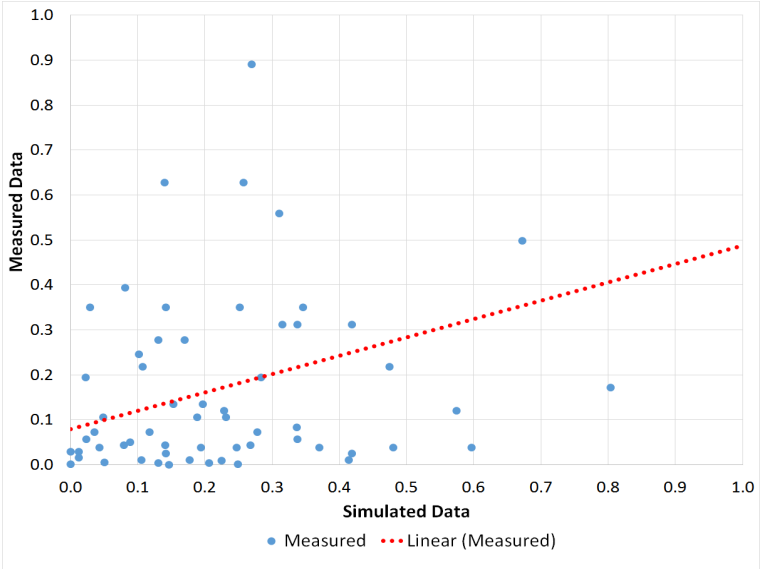

FIGURE 7.27: Scatter Plot of Simulated Surface Current to Measured Data (200 MHz)

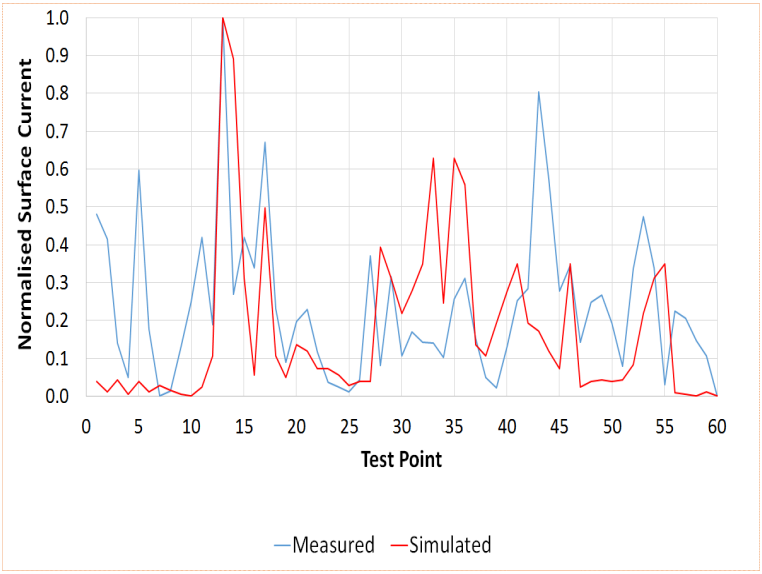

FIGURE 7.28: Plot of Simulated Surface Current to Measured Data (200 MHz)

It can be seen that in the major hot spot areas, test points 13 to 17, there is a good level of similarity between the measured and simulated data. The measurements showed a slightly lower amplitude for test points 29 - 32, with the hotspot not being as evident as in the simulations. A major hot spot was measured at positions 5, 43 and 44 at 200 MHz.

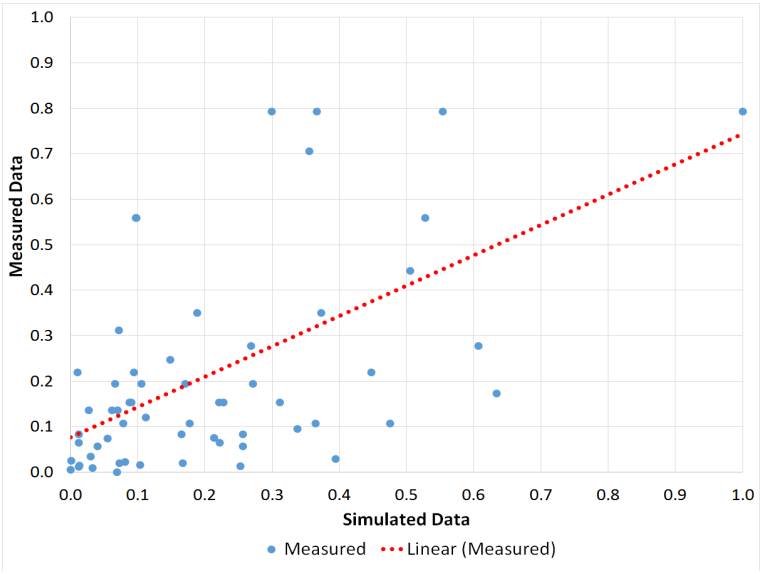

FIGURE 7.29: Scatter Plot of Simulated Surface Current to Measured Data (250 MHz)

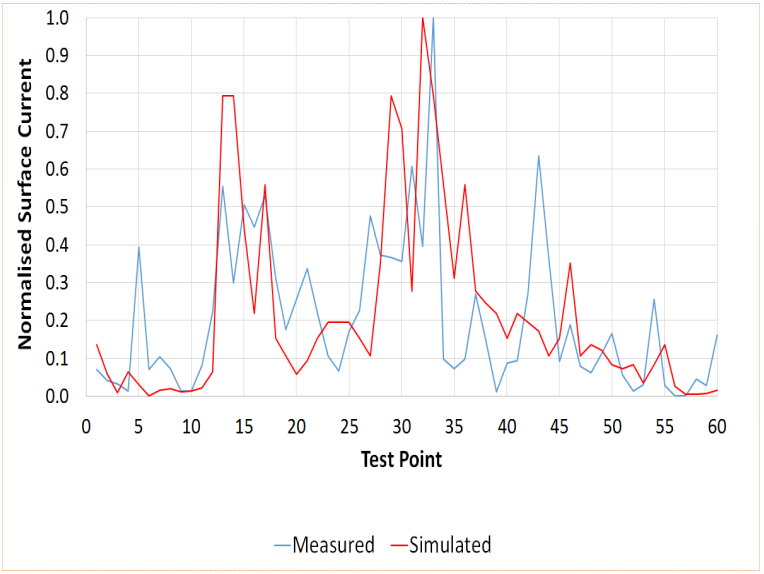

FIGURE 7.30: Plot of Simulated Surface Current to Measured Data (250 MHz)

The results at 250 MHz showed a good level of similarity with the major hot spot areas of points 13 to 17 and 25 to 35 being evident in both the measured and simulated results. The measured results recorded a high level of surface current around position 43 that was not evident in the simulated data.

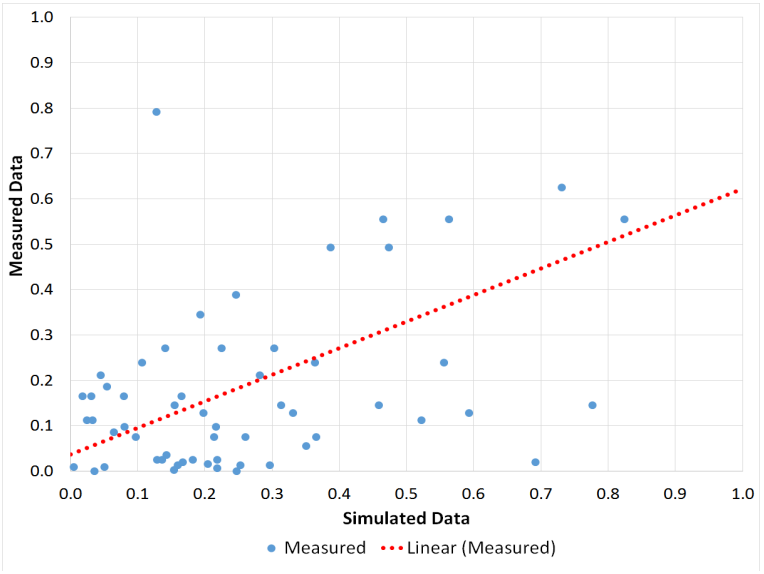

FIGURE 7.31: Scatter Plot of Simulated Surface Current to Measured Data (300 MHz)

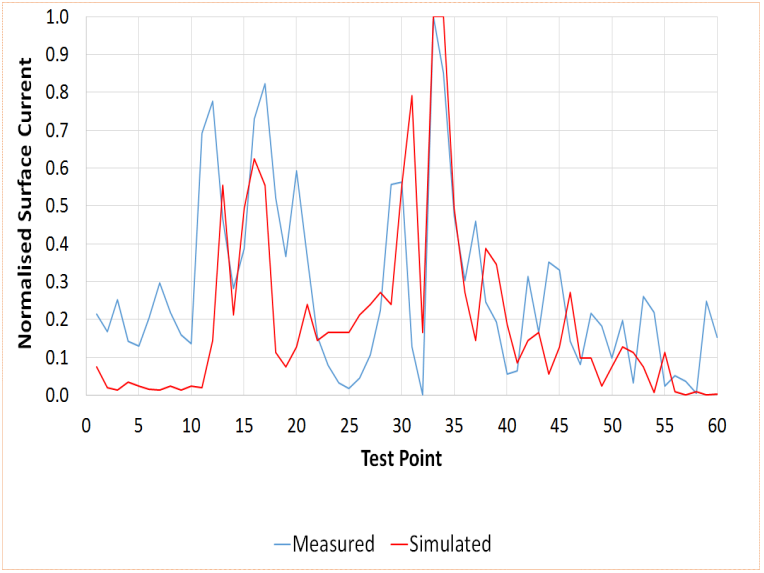

FIGURE 7.32: Plot of Simulated Surface Current to Measured Data (300 MHz)

At 300 MHz, all the major hot spot areas recorded in the simulation data were again evident in the measured results. No additional hotspots were recorded in the measured data that were not seen in the simulations.

When the data sets were analysed a ρ value of 0.4 was obtained at 200 MHz with 0.6 being recorded at 250 MHz and 300 MHz. The main areas of high surface current amplitude were recorded in both the simulation model and the 'real vehicle' measurements, despite the fact that the simulation model was of a different vehicle type to that used for the measurement. These similarities were observed at frequencies above 150 MHz, with

the lower frequency results showing a poorer overall agreement, ρ value of < 0.1 being recorded at 150 MHz. The poor correlation results at lower frequency were thought to be due to possible coupling of the radiated signal into the measurement system used and lower sensitivity of the measurement probe. As the surface current probe was only available for a short period of time as it was a hired unit, further investigations into the poorer low frequency results were not possible.

When the measured and simulated results were compared, it was noted that the areas of particularly high surface current were the main windscreen pillars, along the top of the door seams when the noise source was inside the passenger compartment and across the front of the bonnet when the source was mounted in the engine bay. The engine bay source position could not be checked when the measurements were performed as there was insufficient room inside the engine bay to locate the noise source, whereas the VBS model had an empty engine bay with room to model the monopole antenna.

7.1.7 MicroStrip Calibration for Vehicle Measurements

Based upon the results of the surface current investigations, above 150 MHz, locations for the MicroStrip measurements were selected. The ranges of locations selected for the initial investigations were (1 - 3),(13 - 17) and (29 - 33). These positions covered the major hot spots highlighted in the surface current investigations.

An example setup photograph can be seen in Figure 7.33, showing the MicroStrip on the vehicle.

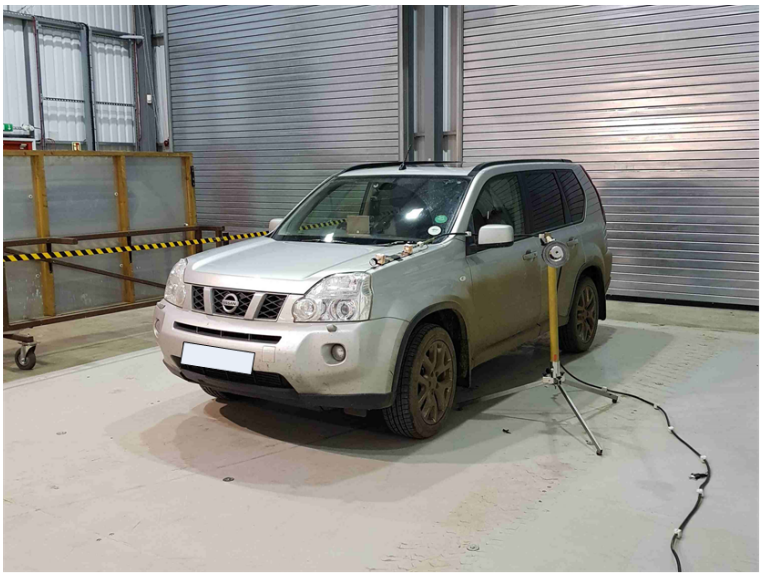

FIGURE 7.33: MicroStrip Measurement Setup, Position 3

The location of the test points used can be seen in Figure 7.34.

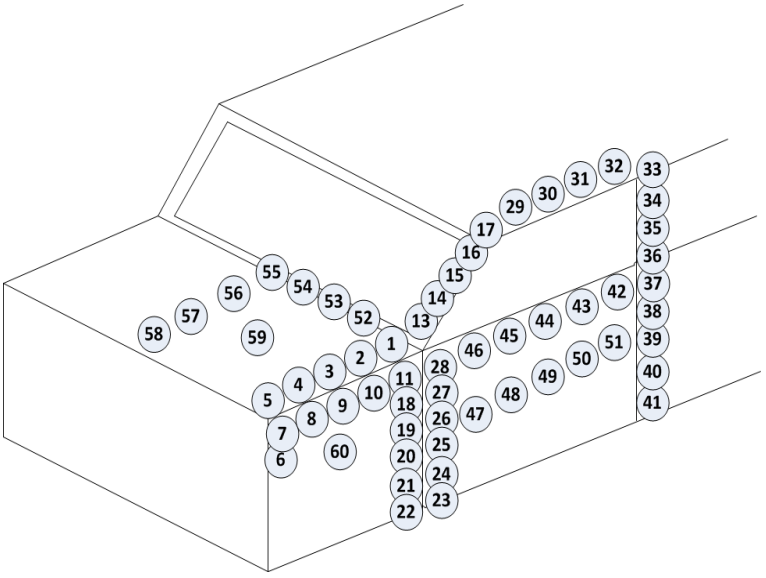

FIGURE 7.34: Surface Current Test Positions

Measurements were performed with a wide band noise source, a York CNE 3, at 4 different positions inside a Nissan X-Trail: on the passenger seat, drivers seat, in the middle of the boot and on the centre of the dashboard. The measurements were again performed in the HORIBA MIRA xEv Facility. The MicroStrip was connected to an EMC receiver and external pre-amp using a 10 m low loss coaxial cable, the cable had three large ferrite clamps around it to reduce field being coupled onto the cable itself. The receiver was

moved as far away from the vehicle as possible; again to reduce any direct coupling on to the wiring. The measured voltage across the terminals of the MicroStrip was recorded over a frequency range of 50 MHz to 500 MHz for each noise source position. The source positions used were the same as those used during the surface current investigations detailed in Section 7.1.5. The centre of the MicroStrip was positioned at each test point, initially, parallel to the length of the vehicle. The MicroStrip was then rotated through 90^o and a second measurement was taken in this position to try and maximise the amplitude recorded. The maximum value of the two was taken as the MicroStrip Voltage for each measurement point.

Once the MicroStrip measurements had been performed, a CISPR 12 type radiated emissions measurement of the test vehicle was performed; using the same vehicle and noise source positions. The emissions measurements were performed at HORIBA MIRA OATS facility. The electric field was recorded while the vehicle was rotated through 360^0 in 5^0 increments. The increment angle was chosen in order to ensure the measurements were completed within the time sensitive period, as the measurement facility was only available for a limited period of time due to HORIBA MIRA's commercial testing commitments.

The receive antenna was located 3 m from the test vehicle and scanned in height between 1 m and 3 m above ground level, in 0.5 m increments. A 3 m test distance was used due to the emissions from the noise generator being 'swamped' by the ambient signal at the more commonly used measurement distance of 10 m as was highlighted in Section 4.2.5.2. Due to the azimuth increment angle used the polar patterns are probably under-sampled. Whilst this method does not give the maximum E-field amplitude that might be obtained from a full hemispherical scan it will give an approximation of the 'absolute' maximum emissions from the vehicle.

7.1.8 Deriving the K Factcor

Once both the CISPR type antenna emissions and MicroStrip measurements had been performed, the voltage at the termination of the MicroStrip and the recorded E-field were then used to determine the K-Factor for each measured frequency and source position (as detailed in Equation 5.2).

The range of K-Factor values was obtained at each frequency, based upon the source position in the vehicle, the receive antenna polarisation and the voltage across the Test Wire termination, this is shown graphically in Figure 7.35.

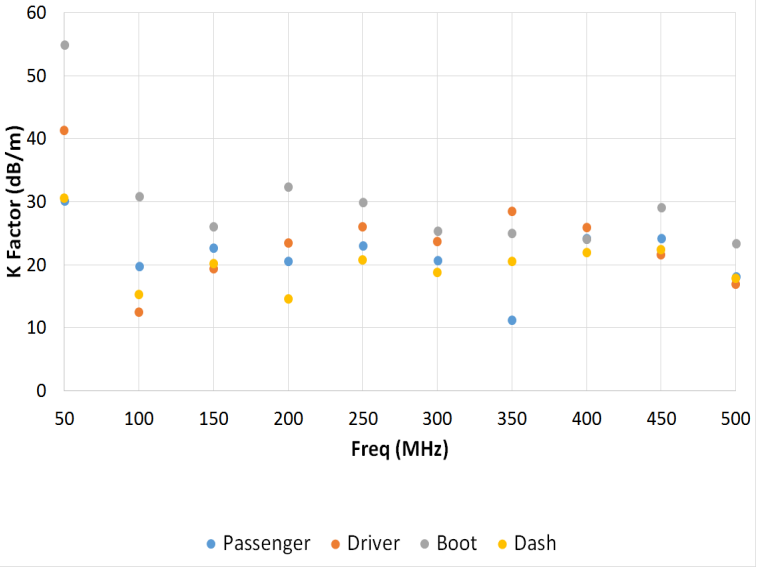

FIGURE 7.35: Measured K-Factor for Source Positions 1 to 4

Across all the recorded data the average of the K-Factor was found to vary in value by between 19 dB/m and 26 dB/m, with the exception of the value calculated at 50 MHz, where 45 dB/m was recorded. At each frequency, the mean of the linear value of the K-Factor calculated at each source position was used to define a K-Factor to be used in Equation 5.2. Between 100 MHz and 500 MHz the K-Factor was found to vary between approximately 19 dB/m and 26 dB/m. The mean of the linear values was then used as the final K-Factor over this frequency range, this value was calculated at 24 dB/m, as shown in Figure 7.36

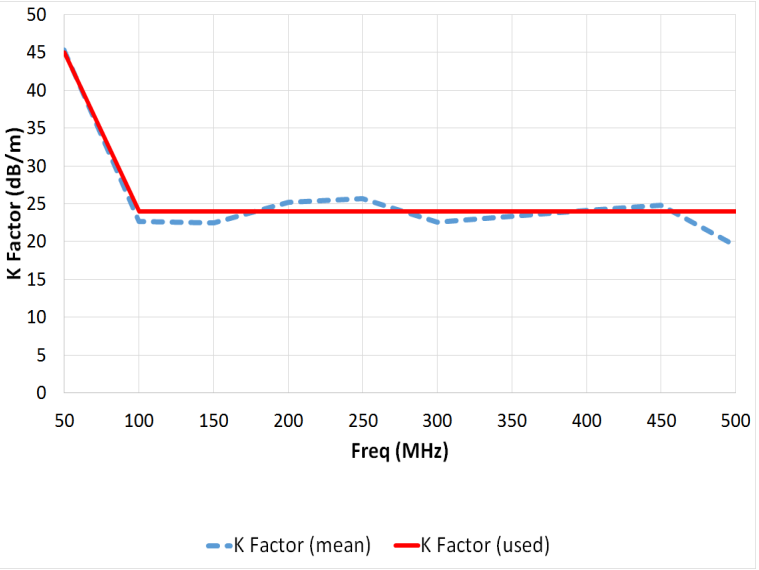

FIGURE 7.36: Final K-Factor

The spread of values calculated for the MicroStrip K-Factor is much lower than the equivalent values derived when using the Test Wire Method. An increasing value with frequency was noted for the Test Wire Method, whereas the MicroStrip has an almost constant mean vale above 100 MHz. The Test Wire method K-Factor was derived from a much smaller data set, only considering two Test Wires, compared to over 100 test points that were used for the MicroStrip measurements.

7.1.9 MicroStrip Measurement Setup

For the purposes of this research it was still necessary to perform both radiated emissions and MicroStrip measurements. The radiated emissions results were used to determine the maximum amplitude of E-field for the vehicle being measured, which in turn was then used to calculate the EB that would have been recorded during a CISPR 12 measurement. Without the radiated emissions results it would not be possible to quantify any difference in EB between the Test Wire method and the CISPR 12 method of measuring the maximum E-field. Future vehicle tests would only require MicroStrip measurements to be performed.

Three different vehicle types were chosen on which to perform MicroStrip measurements, they were a town car (Nissan Micra), a medium size family hatchback (Ford Focus)

and a medium sized panel van (Fiat Berlingo). From the results of the MicroStrip measurements an EB was calculated and compared to the CISPR 12 EB.

Using the same methods as described earlier in Section 7.1.7 the E-field was measured for each of the the three vehicles. Again a York CNE 3 was used as a noise source within the vehicles, the CNE was placed in the middle of the passenger seat. The electric field was recorded while the vehicle was rotated through 360^0, the receive antenna was scanned between 1 m and 3 m above the facility ground plane. Once the data had been recorded for all three vehicles the CISPR 12 error was calculated for each frequency investigated, again limited to 50 MHz to 500 MHz in 10 MHz steps.

The next step was to perform MicroStrip method measurements to record the emissions with the noise source in the same positions within the vehicles. Measurements were again performed in the HORIBA MIRA xEv Facility using the methods described in Section 7.1.7. The voltage across the termination of the MicroStrip was recorded whilst it was located at test positions 15 - 17 and 30 - 32. The test points used were selected by analysing the surface current maps obtained during the investigations detailed in Section 7.1.5, the positions where the highest amplitude of surface current was seen were selected as the test points to be used.

As the tests were to be performed on multiple vehicle types the test positions were derived in accordance with the details shown in Figures 7.37 to 7.38. For each range of positions, 13 - 17 and 29 - 33, three locations in each were used. Using the positions highlighted it was possible to use similar locations on vehicles of differing sizes.

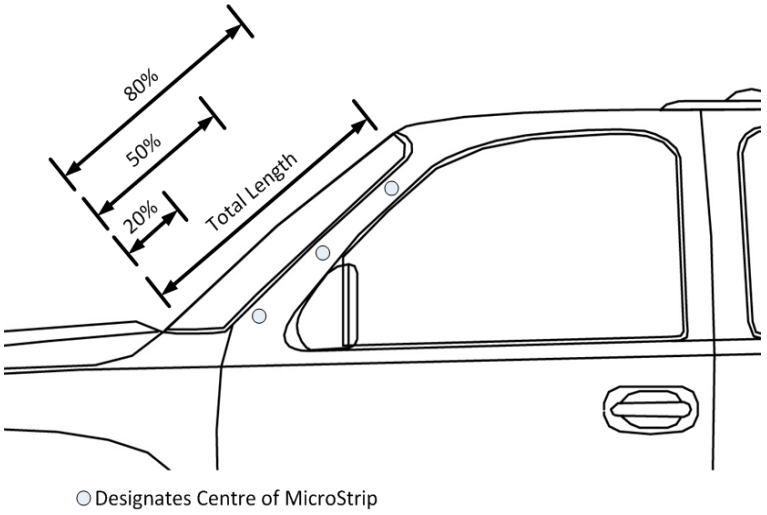

FIGURE 7.37: MicroStrip Measurement Positioning on Different Vehicles, A Pillar

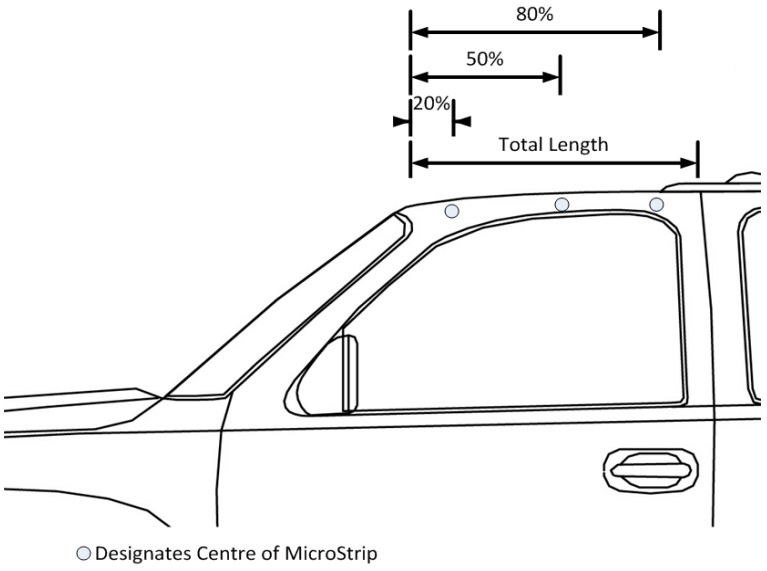

FIGURE 7.38: MicroStrip Measurement Positioning on Different Vehicles, Top of Door

Figure 7.39 shows an example of the measured MicroStrip termination voltage and measured E-field recorded for Source position 1 in the Ford Focus over the 30 MHz to 500 MHz band.

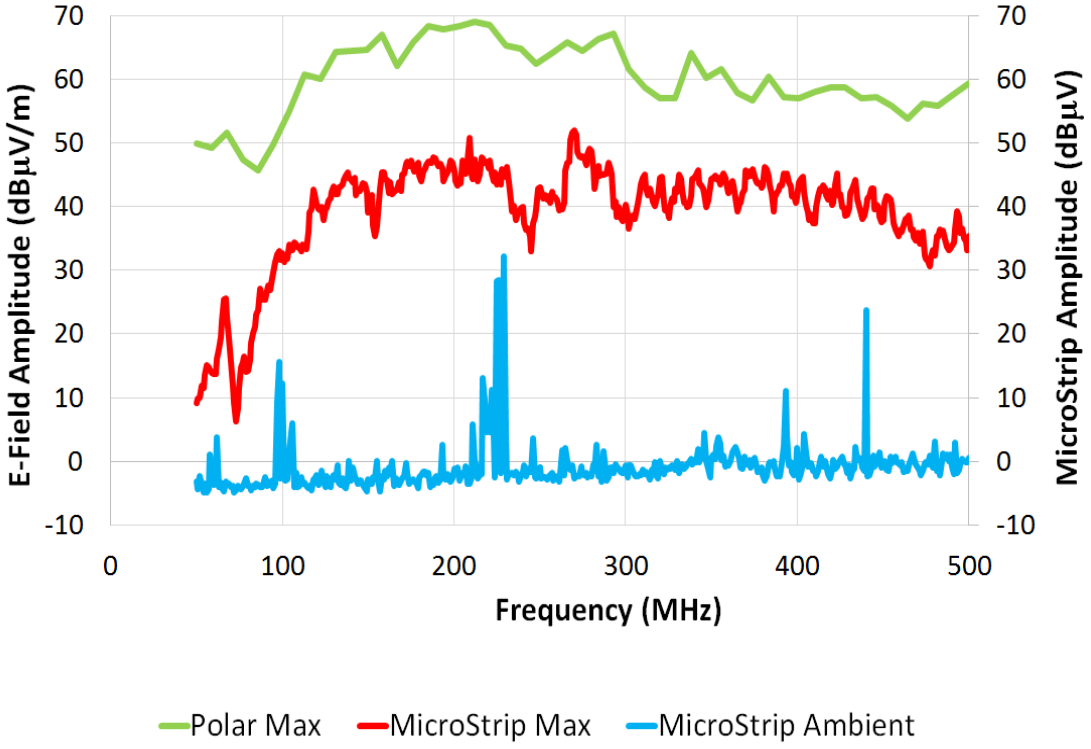

FIGURE 7.39: Test Wire Measured Voltage and Maximum E-Field Measured Against Frequency, Source Position 1, Horizontal Polarisation

A noticeable drop off in measured amplitude can be seen in the data below approximately 100 MHz. A margin of greater than 10 dB is achieved between the ambient noise and the EUT signal, however, this is much lower, by around 40 dB, than the difference noted at frequencies above 150 MHz. This fall off in sensitivity is possibly the reason for the much higher K-Factor values being recorded at 50 MHz, as detailed in Figure 7.36.

Once the MicroStrip measurements had been performed and the data collected, the K-Factor calculated in Section 7.1.7 was then applied to the data for each test point and frequency respectively. The K-Factor 'calibrated' amplitude data was then used to determine the difference in Error Bias between the MicroStrip method and the traditional CISPR 12 method.

7.2 MicroStrip Measurement Results

Once all the data had been analysed graphs of the mean CISPR EB and corresponding MicroStrip EB were produced for each of the three vehicles tested. On each graph the

minimum CISPR 12 EB recorded at the E_{LHS} and E_{RHS} positions were plot along with the MicroStrip EB for each frequency investigated. Each graph also details the E_{max} amplitude for each measurement frequency.

The graph depicted in Figure 7.40 shows the minimum CISPR 12 EB recorded for each vehicle along with the mean of the linear EB for all three vehicles at each frequency. The minimum EB was derived from the lowest value of EB recorded at the E_{LHS} and E_{RHS} positions of each vehicle at each frequency. A mean EB of approximately 13 dB was recorded across all frequencies and vehicles. In line with the results detailed in Section 4.3.3.2 significant errors were recorded using the CISPR 12 method, up to a maximum of almost 45 dB in some cases.

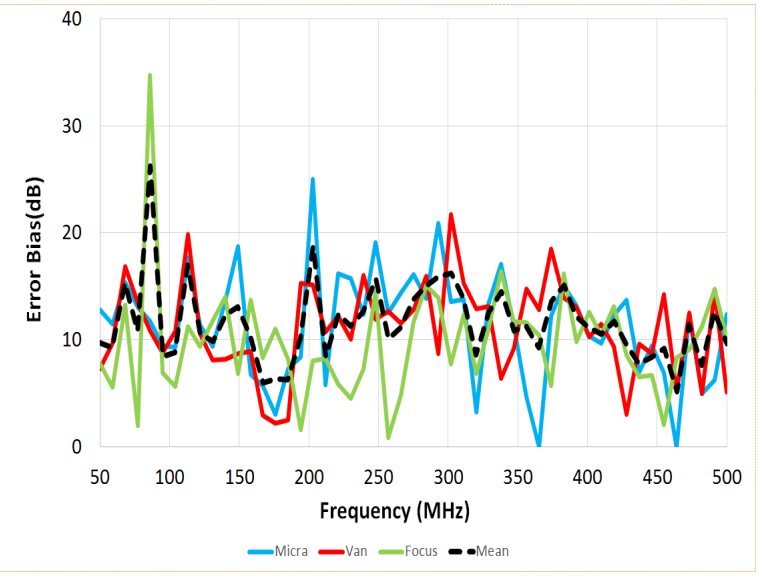

FIGURE 7.40: CISPR 12 Error Bias Recorded for Three Test Vehicles

The graphs shown in Figures 7.41, 7.44 and 7.47 detail the measured maximum E-field amplitude recorded at the E_{LHS} and E_{RHS} positions, designated E_{CISPR}, the maximum E-field amplitude over all antenna heights and azimuth positions for each frequency, designated E_{max}, and the K-Factor calibrated MicroStrip field level, designated E_{strip}. For each vehicle measured a scatter plot of the normalised values of E_{max} and E_{strip} are presented along with a ρ value for each scatter plot. The scatter plots are shown in Figures 7.42, 7.45 and 7.48 Finally the EB recorded using the MicroStrip method for each vehicle is shown in Figures 7.43, 7.46 and 7.43.

7.2.1 Nissan Micra Results

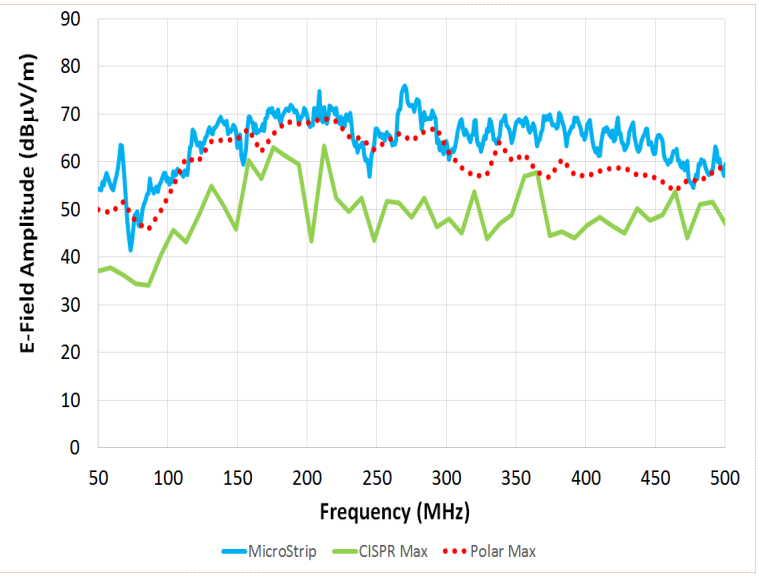

FIGURE 7.41: Maximum E-Field,E_{max}, Maximum CISPR 12 Amplitude, E_{CISPR} and Maximum MicroStrip Amplitude, Nissan Micra

In Figure 7.41 it can be seen that E_{strip} very closely matches E_{max}, values of within less than ± 5 dB of E_{max} are recorded between 100 MHz and 250 MHz. Between 300 MHz and 500 MHz there is a mean difference of approximately 5 dB between E_{strip} and E_{max}.

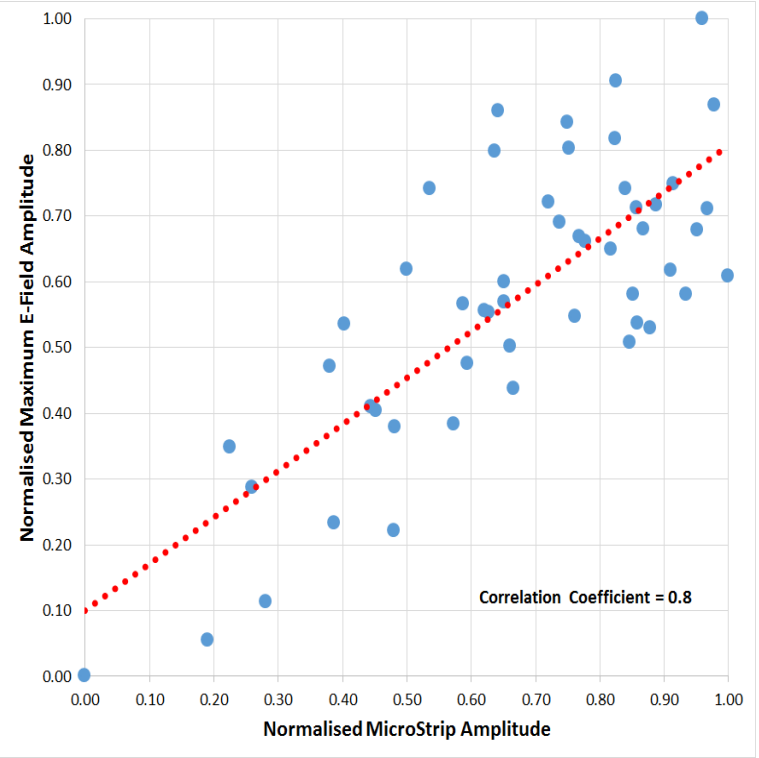

FIGURE 7.42: Scatter Plot of MicroStrip Amplitude Against Maximum E-Field Amplitude, Nissan Micra

The MicroStrip amplitude after calibration with the K-Factor was normalised and then plot against the normalised E_{max} value as depicted in scatter plot Figure 7.42. When the data was analysed a ρ value of 0.8 was calculated.

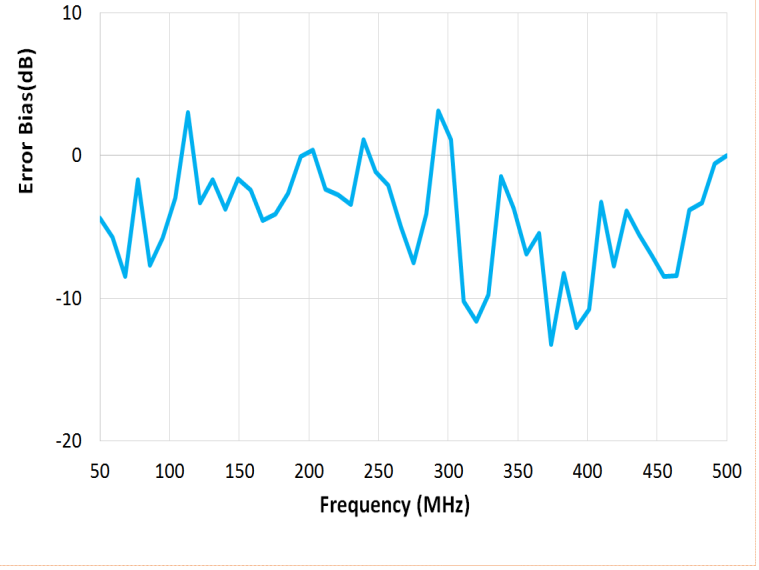

FIGURE 7.43: MicroStrip Error Bias, Nissan Micra

When the EB was calculated for all frequencies between 50 MHz and 500 MHz a maximum of 13 dB and a minimum EB of approximately 0 dB were recorded, a mean of the linear EB of 3.7 dB was noted. The EB for the E_{LHS} and E_{RHS} positions, in contrast was a mean value of 12.8 dB and a minimum of 0 dB and a maximum of approximately 30 dB

7.2.2 Fiat Van Results

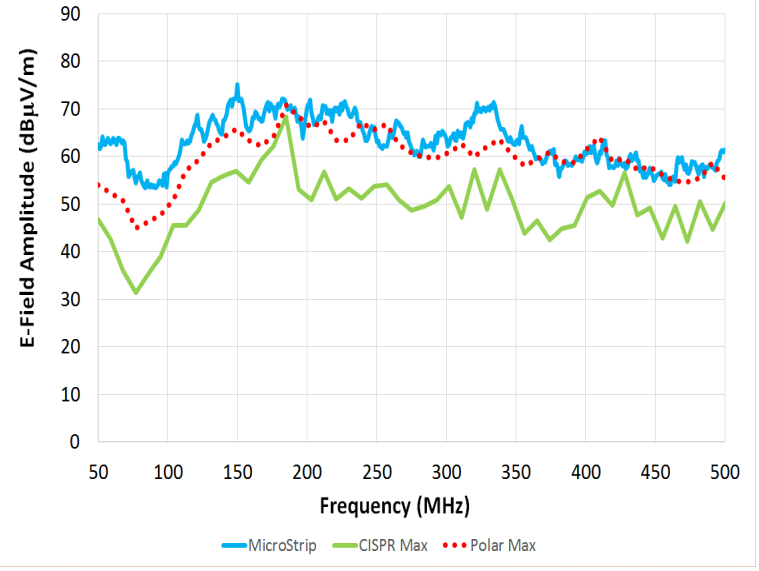

FIGURE 7.44: Maximum E-Field Amplitude, Fiat Van

The results for the Fiat Van measurements showed a very good level of correlation with the E_{max} value between 100 MHz and 500 MHz, with the exception of an difference of approximately 8 dB between 320 MHz and 340 MHz. Below 100 MHz the profile of the E_{max} data and E_{max} is very similar, but with an offset of 10 dB over the range of 50 MHz to 100 MHz. A mean value of the linear EB of 2.5 dB was recorded over the frequency range of 50 MHz to 500 MHz.

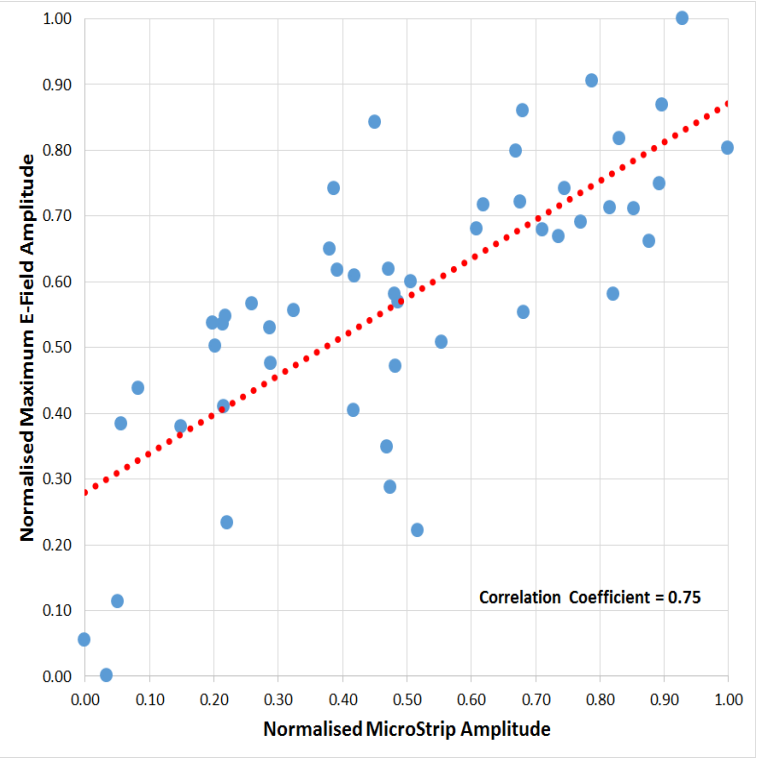

FIGURE 7.45: Scatter Plot of MicroStrip Amplitude Against Maximum E-Field Amplitude, Fiat Van

When the normalised E_{max} data against the normalised E_{max} value was analysed on a scatter plot, as shown in Figure 7.45, a ρ value of 0.75 was calculated.

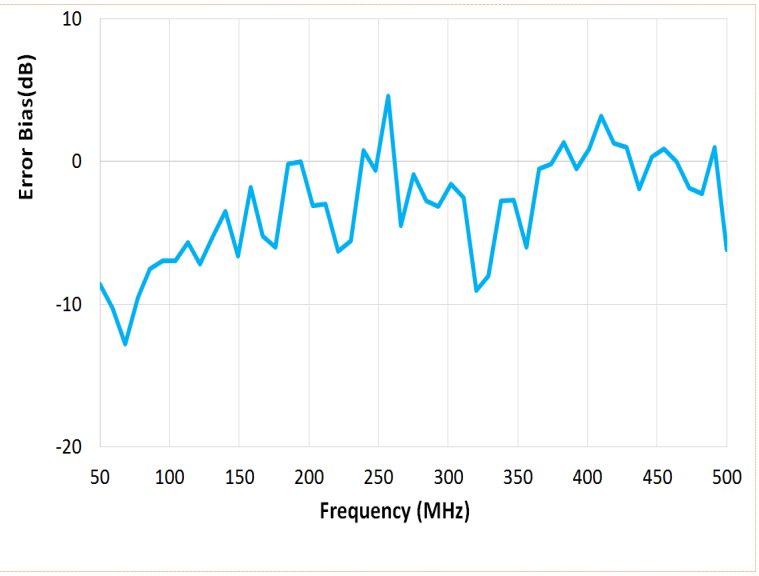

FIGURE 7.46: MicroStrip Error Bias, Fiat Van

On examining the EB results for the MicroStrip in Figure 7.46 a minimum EB of 0 dB

and a maximum of 12.8 dB was noted. This compares to a maximum of almost 22 dB and a minimum of 2.3 dB for the CISPR 12 method.

7.2.3 Ford Focus Results

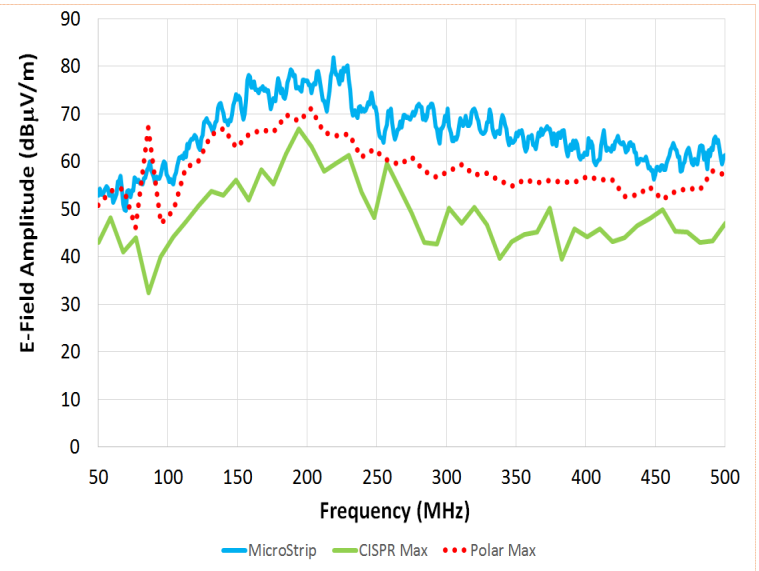

FIGURE 7.47: Maximum E-Field Amplitude, Ford Focus

The E_{max} results for the Ford Focus showed a higher overall amplitude, by a mean value of 5.8 dB over the range of 50 MHz to 500 MHz, compared to the results noted for the other two vehicles measured.

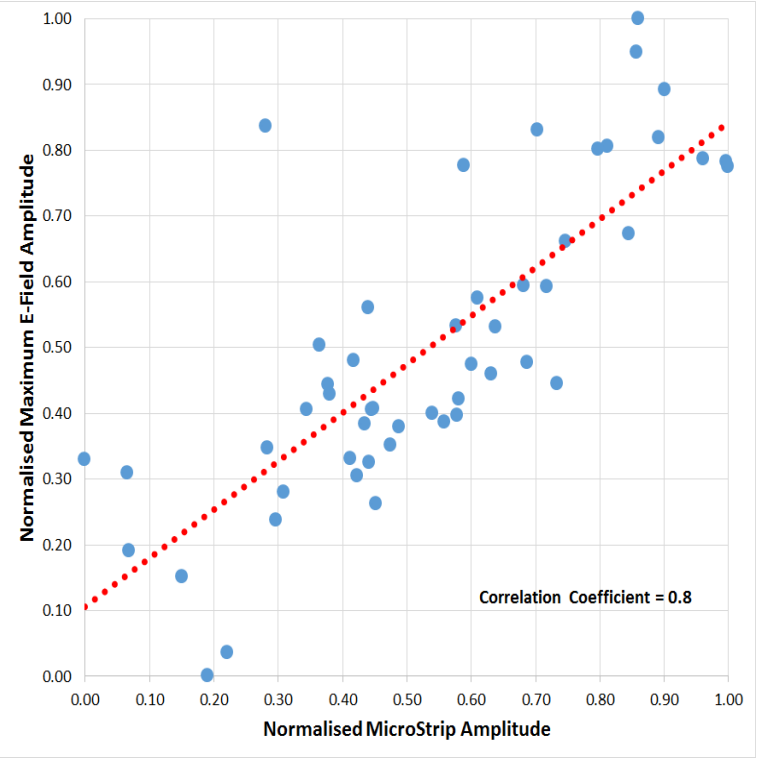

FIGURE 7.48: Scatter Plot of MicroStrip Amplitude Against Maximum E-Field Amplitude, Ford Focus

A ρ value of 0.8 was calculated for the Ford Focus. While the profile of the E_{max} results followed the E_{max} data, there was an overall shift in amplitude between the two sets of values.

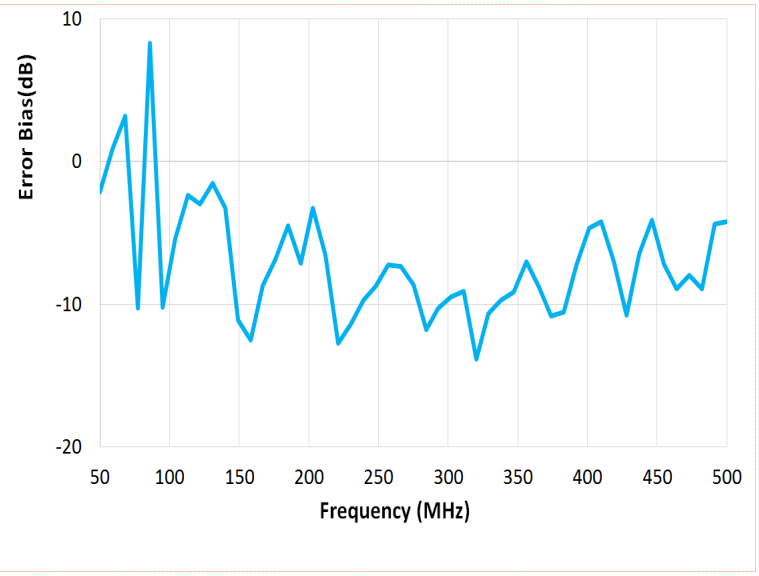

FIGURE 7.49: MicroStrip Error Bias, Ford Focus

Although the overall EB for the MicroStrip method was higher for the Ford Focus that the two vehicles detailed earlier in this section of the thesis, a mean EB of 5.8 dB was calculated. The MicroStrip results were still lower than the mean value of 12.5 dB recorded using the CISPR 12 method.

For all three vehicles a mean CISPR EB of approximately 13 dB was recorded, whilst for the MicroStrip method a mean of <4 dB was recorded.

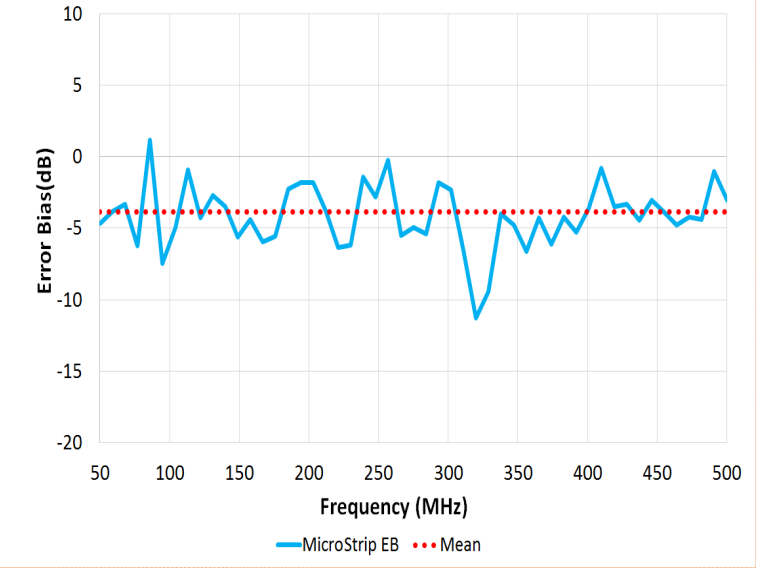

FIGURE 7.50: MicroStrip Error Bias, All Vehicles

Figure 7.51 shows the difference between the MicroStrip EB and E_{max} for each vehicle at a selected number of frequencies. The frequencies displayed are between 50 MHz and 500 MHz in 50 MHz increments. The reduced number of frequencies is shown to allow for an easy comparison of the EB recorded using the MicroStrip method and the overall maximum amplitude of the E-field using antenna height and azimuth maximisation. In the graph positive EB values denote that the MicroStrip has a lower value than the CISPR 12 method at that frequency, whereas a negative value signifies a frequency where the MicroStrip recorded a higher value of EB. As is evident, the majority of the results are within the positive half of the plot. Across all vehicles and frequencies, a total of 30 data sets, the Microstrip returned a lower EB in 75% of cases. By analysing the results presented in this section, it can be seen that the MicroStrip method, on the whole, over estimates the amplitude of the E-field when the K-Factor correction has been applied, whereas the CISPR 12 method will under-estimate the maximum amplitude. However,

the margin by which the MicroStrip method over-estimates the amplitude is significantly lower than the under-estimation recorded using the CISPR 12 method.

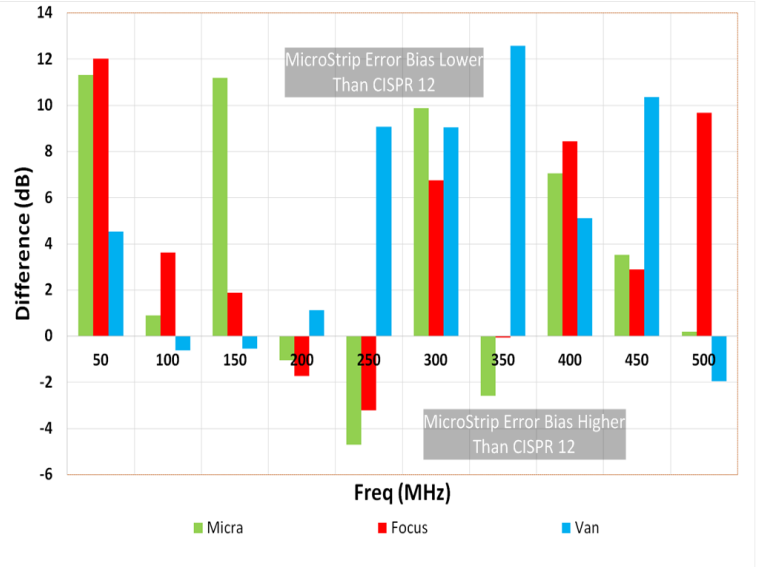

FIGURE 7.51: Error Bias Comparison Using MicroStrip Method for All Vehicles

The results show that for the three vehicles tested the MicroStrip method produced a lower Error Bias than the CISPR 12 method at the majority of frequencies measured when the results from each individual vehicle is considered. When mean EB using the two methods is compared across all three vehicles, it can be seen in Figure7.52 that the MicroStrip method returns a significantly lower EB value at all frequencies.

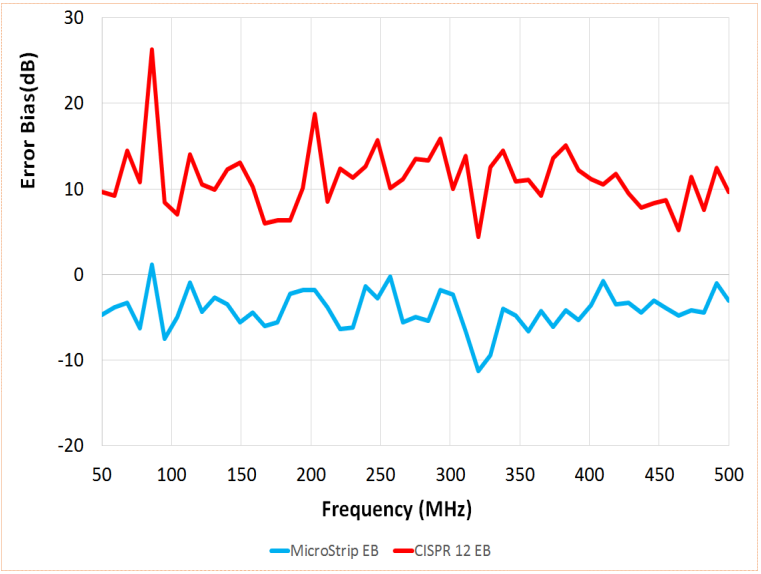

FIGURE 7.52: Error Bias Comparison of MicroStrip Method to CISPR 12 for All Vehicles

7.3 MicroStrip Conclusions

The results in Section 7.2 show that by using the MicroStrip method an improvement in the EB recorded when measuring the radiated emissions of a range of test vehicles can be achieved over the frequency range investigated. The results presented a mean EB of approximately 4 dB using the Microstrip method compared to approximately 13 dB when performing a standard CISPR 12 type radiated emissions measurement.

The MicroStrip method has overcome some of the problems raised with the Test Wire method highlighted in Section 6.2.2.5.

The MicroStrip method is non-intrusive to the test vehicle, no physical connections to the chassis of the vehicle are required. This is of particular relevance if the MicroStrip method were to be used in a commercial test environment. Quite often the vehicle being tested is a customer owned item, so any measurement system that required a physical bond to the chassis of the vehicle would be far from ideal. As the MicroStrip method is fully self contained, with the exception of the RF cable to connect the strip to the measurements receiver, no physical bonds to the vehicle are required.

A characteristic impedance that more closely matches the measurement system input impedance is achieved. As the MicroStrip has a ground reference plane under its entire length, a more stable impedance value can be achieved, compared to the Test Wire Method. As the MicroStrip can be made with a nominal 50Ω characteristic impedance, it can be directly connected to the measurement receiver without the need for any matching networks.

The same MicroStrip was used on all vehicle sizes and types tested, modifications to the size of the strip were not needed to enable it to be used.

Due to its construction, the MicroStrip does not have the same issues as the Test Wire Method of maintaining a constant height above the EUT. As the MicroStrip has it own ground reference plane and the strip is a fixed distance above it, due to the dielectric substrate, hence it is always the correct height above the ground reference plane to maintain the required impedance match.

The physical size of the MicroStrip allows it to be quickly positioned on the vehicle to be tested, this ensures minimal setup time is required; though care is needed to determine

the locations where it will be positioned prior to test. In order to reduce coupling onto the RF cables connecting the MicroStrip to the measurement receiver, it is recommended that ferrite clamps are fitted to the cables and that the cables are routed away perpendicular to the body of the vehicle in order to minimise coupling onto the cable.

The MicroStrip method has been used to test a range of vehicles in a large warehouse type structure and seemed to be tolerant of high levels of ambient background RF noise. The CISPR 12 type measurements performed during the course of this research were not, however, as tolerant of the high ambient signal levels observed. It was found that at the frequencies detailed in Table 4.1, in particular, that the emissions radiated from the vehicle were 'swamped' by the ambient signals and measurements were not possible at those frequencies. The measurements performed during this research were performed using a wide band noise source, to excite the vehicle, rather than using the actual vehicle emissions. The noise source has a relatively high output amplitude, leading to the radiated signal being higher in amplitude than the ambient noise by between 30 dB and 40 dB at the frequencies measured.

However, due to the design of the MicroStrip used for this research, there is one issue that could be improved upon. As the MicroStrip is a rigid construction, conforming to the shape of the EUT is not possible. The test points used during this investigation were mostly flat in profile enabling the MicroStrip to sit against the surface, however, a more flexible unit would allow for a better fit to the exact shape of the vehicle being tested. If time had allowed, a more flexible MicroStrip would have been designed and built and the Error Bias results compared with the rigid variant. It is thought that the EB could be improved upon further through the use of a conformal strip.

The MicroStrip Method has been shown to offer reduction in the errors in recording the maximum amplitude of radiated emissions from a vehicle when compared to using the CISPR 12 method. The amplitude of the K-Factor calibrated E-field recorded during this research was almost exclusively higher than the maximum measured using the traditional antenna method. The CISPR 12 method, in contrast, will always record an amplitude that is lower than the maximum obtained by rotating the vehicle and scanning the receive antenna in height during the test. However, a mean EB of approximately 4 dB using the Microstrip method has been recorded compared to approximately 13 dB when performing a standard CISPR 12 type radiated emissions measurement

Chapter 8

Conclusions and Further Work

8.1 Conclusions

Having worked within an automotive research organisation for many years, predominantly within the EMC department of a commercial test house, I have developed a keen interest in the methods employed during automotive radiated emissions measurements. In particular why the methods employed differ from those used for almost all other product types and the impact this may have not only upon electronic devices in the near vicinity, but also on drivers, passengers and road users. Fundamentally this research has identified that the level of measurements performed to record the radiated emissions of a typical piece of home electronics, a TV or DVD player for example, is far more rigorous than that used on a car, van or lorry. The potential safety implications due to the use of this narrower field of testing should not be overlooked.

As has been highlighted through the preceding chapters of this thesis, little research has been published to investigate either: the effect that the limited scope of the test methods defined in CISPR 12 has on the maximum amplitude of the measured emissions, or possible alternative methods that could be employed to address this problem.

The scope of the research presented in this thesis was detailed as:

- Measurement and simulation of the radiated emissions from a range of devices, both electrically small and large devices using both the CISPR 12 and CISPR 22 method with the aim of quantifying the error in between the two methods.

- Define the upper and lower frequency of emissions from a range of commercially available vehicles
- Perform a study into possible alternative techniques to the CISPR 12 method that could potentially reduce the errors recorded in the maximum emissions amplitude
- Development of the Test Wire Method for automotive emissions measurements
- Production of the MicroStrip Method for measuring vehicle level radiated emissions

Through the course of this research the objectives detailed above were met and the following contributions to the state of the art of automotive radiated emissions measurements have been made:

1. The analysis of the error in the maximum amplitude of the electric field, recorded during a CISPR 12 radiated emissions test, as a consequence of performing measurements at a limited number of azimuth angles around the vehicle, and using a single receive antenna height. This analysis enabled the following:
    - Consequences of not using EUT azimuth scanning during a CISPR 12 measurement, error introduction for both electrically small and large EUTs was determined and additionally quantified.
    - Consequences of not using antenna height scanning during a CISPR 12 measurement, error introduction for both electrically small and large EUTs was determined and additionally quantified.
2. A novel, new method for measuring the radiated emissions from a vehicle, that reduces the errors in the maximum amplitude of the electric field recorded by over 10 dB, compared with those recorded during a CISPR 12 full vehicle radiated emissions test. The background and development of the MicroStrip method is detailed in Section 7.1, measurement results from the validation of the MicroStrip Method are detailed in Section 7.2 of this thesis.

The receive antenna height scanning measurements confirmed, as expected, that the maximum emissions amplitude is not recorded with the antenna at a single height above the ground. Comparisons were made between the maximum amplitude recorded when

the antenna was scanned between 1 m and 4 m above the ground and using a single height of 3 m as prescribed in the CISPR 12 method. For the electrically small EUT a mean EB of 4.4 dB was recorded for the horizontally polarised antenna position and 8.1 dB for the vertically polarised antenna. Comparing these results to those recorded when measuring the electrically large EUT showed similar levels for both. The electrically large EUT recorded EB figures of approximately 4 dB and 6 dB for the horizontal and vertical polarisations respectively.

The azimuth scan measurements were performed on a range of commercially available vehicles of differing type and size. Radiated emissions measurements were performed at an OATS facility with a noise source located at various positions within each vehicle. The vehicles were rotated through an azimuth angle of 360^o using an increment angle of 5^o. Whilst this angle could be considered too coarse and the resulting emissions plots potentially under-sampled, the results still show a mean EB of 16 dB was recorded across the four vehicles tested. Maximum EB values up to 30 dB were recorded at some frequencies.

Both the height scan and azimuth scan investigations were performed using a limited number of frequencies, due to the time taken processing and then analysing the data. However, the limited data set allowed the EB to be quantified, confirming that the current CISPR 12 method for performing radiated emissions measurements has the potential to considerably underestimate the amplitude of the emissions radiated by a range of vehicle types.

The further function of this thesis was the development of an alternative test method to the CISPR 12 approach with the aim of the new method reducing the level of Error Bias described in the previous paragraph. Research was conducted into a number of possible alternatives to the CISPR 12 method, they were:

- Spherical Scan Around the EUT
- Reverberation Chamber
- Test Wire Method

Of the three methods investigated, both the spherical scan and reverberation chamber were discounted on the grounds of the time that is required to perform the tests.

The 'Test Wire' Method was used initially as a 'proof of concept' idea. The original TWM was used to perform radiated emissions measurements on large industrial machines that were not able to be moved to a measurement facility to be tested. The TWM was tried on a small $\frac{1}{3}$ scale model of a very simplified vehicle body shell with measurements being performed using just two Test Wire positions around the model. Based upon the initial tests, the EB was reduced from approximately 11 dB using the CISPR 12 method to 2 dB using the TWM. Although the tests were performed over a limited scaled frequency range of approximately 50 MHz to 300 MHz, the method returned a reduced EB and proved worthy of further development. The Test Wire had a few issues that would potentially cause a problem if it were ever to be used on a commercial basis. The main issues were that the system required a physical bond to the chassis of the EUT. While for a industrial machine this may not be a problem, very often when vehicles are tested commercially they have already been sold to the final customer, meaning that making modifications to the vehicle to allow a bonding point may not be acceptable to them. The Test Wire does not have a 50Ω input impedance meaning that a matching network was required in order to not have impedance mismatches when connecting the Test Wire to the measurement receiver. It was also found that due to the geometry of the EUT being tested, maintaining a stable impedance with frequency was not easy to achieve.

With the noted disadvantages of the Test Wire System in mind, the method was further developed to address the problems whilst still maintaining the improvement in EB over the CISPR 12 method. The final design used for this research was designated the MicroStrip Method. The MicroStrip method differed to the TWM by having a self contained ground reference plane, and as such, did not require a physical bond to the vehicle being tested. The MicroStrip was also designed to have a characteristic impedance of 50Ω and as it did not rely on its spacing above the body of the EUT, it did not have the same problem with the geometry of the vehicle affecting the impedance. MicroStrip measurements were performed on a range of different types of vehicles, from a small town car to a large 4x4 vehicle. A mean EB using the MicroStrip method of 4 dB was recorded compared to the CISPR 12 mean error of 13 dB across all of the vehicles tested. The main advantages the MicroStrip method has over the CISPR 12 method is that it does not require an expensive measurement facility, the tests performed as part of this research were carried out in a large 'hangar' type building, the metallic building did not require any absorbent material on the walls and ceiling as is the case with a semi-anechoic

chamber; or should it require a metal ground plane beneath the vehicle.

The MicroStrip method has currently been tested on a small range of vehicle types and the results produced have given confidence that it could be used as an alternative to the current CISPR 12 method. A 10 dB reduction in the Error Bias, compared to that recorded using the CISPR 12 method, has been achieved.

In summary this research has delivered the following achievements with relation to vehicle level radiated emissions measurements:

- The Error Bias when performing CISPR 12 Type radiated emissions tests has been quantified.
- Upper and lower frequency range of emissions radiated by a variety of vehicle types was quantified.
- An investigation into alternative test methods to CISPR 12 has been conducted, the relative advantages and disadvantages of three alternative methods were discussed.
- The Test Wire Method was researched and used as 'proof of concept' as an alternative method to CISPR 12 for measuring the radiated emissions of vehicles.
- The Test Wire Method was further developed into the MicroStrip Method; a self contained, novel alternative to the CISPR 12 method.
- Calculation of a 'K-Factor' that can be used to calibrate MicroStrip measurements to a far field equivalent E-field value.
- A reduction in the Error Bias was achieved using the MicroStrip Method compared to the CISPR 12 method without any significant increase in the time taken to perform the tests.

8.1.1 Overall Conclusion

The CISPR 12 method of performing vehicle level radiated emissions measurements is used as a regulatory Standard by many countries. The procedures described within it define how the tests should be performed and the measurement equipment setup required in order to perform those tests. While the text of the Standard provides the information

required to ensure that the tests are performed in the same manner, ensuring consistency between different test houses, the method its self has been shown to have a low likelihood of recording the maximum amplitude of the emissions.

Alternative test methodologies are available that could address the issue of not recording the maximum amplitude of the emissions radiated by the vehicle under test. However, some of the alternative methods described in Chapter 5 of this thesis would be far too time consuming for them to be used on a commercial test basis. For an alternative method to be a viable option it would need to offer a reduction in the errors inherent in the CISPR 12 method without additional time being required to complete the tests.

The MicroStrip method was developed through this research, as an alternative approach to performing vehicle level radiated emissions using the procedures detailed in CISPR 12. Through a program of measurements and simulations the new method was used to record the amplitude of the emissions from a range of vehicle types over the frequency range of 50 MHz to 500 MHz. A reduction in the EB was achieved over the entire frequency range, with a mean reduction of almost 10 dB noted compared to performing measurements on the same vehicles using the CISPR 12 method. The MicroStrip method is no more arduous or time onerous than the CISPR 12 procedures, with the added benefit that they can be performed without the need for an extensive test site.

In summary the objectives laid out at the beginning of this thesis have been met and a program of suggested work to further develop the new test method has been determined and is detailed below.

8.2 Further Work

The measurements and simulations presented in this thesis have produced some very useful insight into the CISPR 12 method of performing radiated emissions tests and identified some major flaws in the methodology. The research performed allowed the effect of the flaws identified on recording the maximum emissions amplitude to be quantified. An alternative method to performing the emissions measurements with a traditional antenna at an OATS or in a semi-anechoic chamber has been suggested along with results to validate its performance. The results detailed in the preceding chapter highlighted the improvement in the EB recorded using the MicroStrip method compared

to the CISPR 12 method and, as such, has shown that the new proposed method has the potential to become a viable alternative to the current test procedure.

The results contained within this thesis are based upon measurements and simulations performed over a frequency range of 50 MHz to 500 MHz. Due in the main to availability of test lab time to perform the required measurements, higher and lower frequencies have not yet been researched. In the following section, possible future developments to the MicroStrip method are discussed that would address this, along with a number of other parameters that would allow for the scope of the MicroStrip method to be extended.

A summary of the main areas of further development are:

- The upper frequency range investigated was 500 MHz.
- The K-Factor was derived from one vehicle
- The MicroStrip construction was not conformal to the profile of the vehicle being tested
- The emissions measurements were performed using a 'noise source' at various positions within the vehicle and not the actual vehicle emissions
- The vehicle was excited by a noise source in a single position at a time, real vehicle emissions will be from a more diverse area.
- The MicroStrip method has only been validated on a range of cars and a van, CISPR 12 also covers boats and internal combustion engines
- The MicroStrip method has only, so far, been used to perform emissions measurements, not immunity

8.2.1 Frequency Range and K-Factor

Due to the time required to collect, process and analyse the data the frequency range over which the measurements were performed was limited to 50 MHz to 500 MHz. The use of the MicroStrip method at frequencies below 50 MHz and above 500 MHz needs to be investigated further to determine if the method can produce the same reduction in Error Bias as evidenced in this thesis. Over the frequency range investigated so

far, a limited number of individual frequencies has been analysed, in order to further validate the EB reductions quote earlier, measurements would need to be repeated at a much smaller frequency increment. An increment corresponding with those detailed in CISPR 12 would be more appropriate if the MicroStrip method were to be used as an alternative.

The K-Factor value calculated at 50 MHz was much higher than for frequencies between 100 MHz and 500 MHz. Data from a wider range of vehicles would allow for a larger data set to be used to determine a new K-Factor and ascertain whether the high value recorded was dependent on the vehicle type. It could be suggested that the K-Factor used in this thesis was derived from too limited a data set to provide a 'universal' correction factor that could be used to calibrate the MicroStrip measurements from any vehicle. Further investigations on a more diverse range of vehicles covered by CISPR 12 would allow for further validation of the MicroStrip method. As the scope of devices covered by CISPR 12 is wide ranging, research into the use of the MicroStrip system on devices such as lawn mowers and agricultural equipment is planned.

8.2.2 MicroStrip Design

As noted in Section 7.1.4 the MicroStrip used in this thesis was constructed of 0.7 mm thick copper sheet and a 4 mm polycarbonate substrate. These materials produced a MicroStrip that was rigid and unable to conform to the exact profile of the vehicle body work. An updated design using thinner and more flexible materials, whilst still maintaining a 50Ω input impedance is envisaged, this design would allow the MicroStrip to follow the exact shape of the vehicle being tested. This new design would need a full program of measurements performing in order to produce a new K-Factor and then further MicroStrip measurements on a range of vehicles to quantify the EB recorded.

8.2.3 Vehicle Emissions and Ambient Signal Levels

The tests performed to date are based upon a single noise source; a York Comparison Noise Emitter, CNE 3, being used to excite the vehicle body shell. Whilst the CNE was useful, and practical, for the initial proof of concept for the MicroStrip method, it is not representative of the RF signature that would be generated by a vehicle being excited

by its own sources of noise. When the engine of a vehicle is running and the electrical system is active, RF noise will be generated from numerous sources located at multiple positions around the vehicle simultaneously again this was not simulated by the CNE being in a single position during this research. As the emissions generated by the vehicle engine and electrical system is typically of a lower amplitude than the output of the CNE, further tests would need to be performed in a large semi-anechoic chamber in order to screen out ambient signals that could swamp out the vehicle emissions. The emissions signature, in terms of frequency range, used to perform the research detailed in this thesis is based on a petrol or diesel Internal Combustion Engine, ICE. The advancements in electric and hybrid vehicles in recent years has increased massively and the ICE can no longer be though of as the only propulsion method to power a vehicle. The emissions signature of an electric vehicle would need to be analysed to determine if the frequency range considered so far would be usable.

8.2.4 Using the MicroStrip Method on Boats and Internal Combustion Engines

The K-Factor detailed in Section 7.1.8 was derived from data recorded from a typical family car. As previously noted, CISPR 12 covers a multitude of other vehicle types and engines, including motor bikes, boats and a wide range of equipment such as lawn mowers and chainsaws. It is thought that the K-Factor derived in this thesis may only be suitable for cars and small vans. Further work to develop either a 'universal' K-Factor or a range of vehicle and engine type factors would make the MicroStrip method a more complete alternative to the CISPR 12 method. Due to the large variation in size and shape of items covered by CISPR 12 a survey could be performed in order to determine which types of item could potentially use a common K-Factor.

8.2.5 Using the MicroStrip Method to Perform Radiated Immunity Tests

To date, the MicroStrip method has only been used to perform radiated emissions measurements. As discussed in Section 7.1.3, through the principle of reciprocity, if an antenna operates efficiently to receive signal, it will also operate to transmit signals. Hence the same principles used during the emissions measurements could be applied and

the MicroStrip method could be modified to perform an immunity type test. Further investigations would be required to determine the optimum positions for the MicroStrip to be located during the test. If similar performance to those obtained during the emissions tests could be recorded, it is feasible that through the use of the MicroStrip method, immunity tests could be performed without the need for vehicle rotation and antenna height scanning. Using a device with a known susceptibility problem, initial investigations could be performed using a traditional antenna free field method, this would allow thresholds in E-field amplitude to be taken, at which the susceptibility issue could be invoked into the EUT. This threshold would need to be determined from a comprehensive scan around the device, a hemispherical scan around the EUT of the transmit antenna, for example, to determine the lowest level threshold. Once this level had been determined, RF current could be injected into the MicroStrip, whilst it was located at a range of positions over the surface of the EUT, and the amplitude of the injected signal increased until the event occurred. By performing this test at multiple MicroStrip positions, both the minimum required injected current amplitude and optimum MicroStrip test position could be found. In line with how the MicroStrip emissions investigations were performed, the immunity tests would need to be validated on a number of different vehicle sizes and types. This would confirm if an optimum MicroStrip test position could be found, that was usable on all vehicle types, and also allow a calibration factor to convert the MicroStrip injected RF current to an equivalent free field amplitude to be determined.

8.2.6 Further Work - Summary

The MicroStrip method has been shown to offer an improvement in the Error Bias recorded when compared to CISPR 12, through further development it is thought that these improvements could be further enhanced. The upper frequency range is the first planned extension to the system. By extending the upper frequency to 1 GHz, the full range required by CISPR 12 could be covered with the MicroStrip method. To cope with future developments, such as in-vehicle communication networks, drive by wire technologies and advanced entertainment and radar systems, frequencies in excess of 1 GHz will then also need to be considered.

The MicroStrip method will be used as a platform for further research into its use for vehicle level emissions tests and how its application can be broadened to encompass the ever evolving automotive vehicle market.

Abbreviations

ALSE	**A**nechoic **L**ined **S**hielded **E**nclosure
AM	**A**mplitude **M**odulation
ANSI	**A**merican **N**ational **S**tandards **I**nstitute
ASA	**A**merican **S**tandards **A**ssociation
BEM	**B**oundary **E**lement **M**ethod
CAD	**C**omputer **A**ided **D**esign
CATIA	**C**omputer **A**ided **T**hree Dimensional **I**nteractive **A**pplication
CECIMO	**C**omité **E**uropéen de **C**oopération des **I**ndustries de la **M**achine-**O**util
CEM	**C**omputational **E**lectro**M**agnetic
CENELEC	**C**omité **E**uropéen de **N**ormalisation ´**E**lectrotechnique
CISPR	**C**omité **I**nternational **S**pécial des **P**erturbations **R**adioélectriques
CNE	**C**omparison **N**oise **E**mitter
EB	**E**rror **B**ias
EM	**E**lectro**M**agnetic
EMC	**E**lectro**M**agnetic **C**ompatibility
EMI	**E**lectro**M**agnetic **I**nterference
ERAH	**E**ffective **R**eceive **A**ntenna **H**eight
EU	**E**uropean **U**nion
EUT	**E**quipment **U**nder **T**est
FAR	**F**ully **A**nechoic **R**oom
FCC	**F**ederal **C**ommunication **C**ommission
GTO	**G**eneric **T**est **O**bject
ICE	**I**nternal **C**ombustion **E**ngine
IEC	**I**nternational **E**lectrotechnical **C**ommission
IEV	**I**nternational **E**lectrotechnical **V**ocabulary

IT	**I**nformation **T**echnology
ITE	**I**nformation **T**echnology **E**quipment
MIRA	**M**otor **I**ndustry **R**esearch **A**ssociation
MoM	**M**ethod of **M**oments
MSM	**M**icro**S**trip **M**ethod
OATS	**O**pen **A**rea **T**est **S**ite
OTS	**O**utdoor **T**est **S**ite
PC	**P**ersonal **C**omputer
PEC	**P**erfect **E**lectrical **C**onductor
PEEC	**P**artial **E**lement **E**quivivalent **C**ircuit
PRF	**P**ulse **R**epetition **F**requency
RC	**R**everberation **C**hamber
RF	**R**adio **F**requency
RFI	**R**adio **F**requency **I**nterference
SCSW	**S**urface **C**urrent **S**ense **W**ire
SVTC	**S**imple **V**ehicle **T**est **C**ase
TCF	**T**echnical **C**onstruction **F**ile
TEM	**T**ransverse **E**lectro**M**agnetic
TLM	**T**ransmission **L**ine **M**ethod
TWM	**T**est **W**ire **M**ethod
UN	**U**nited **N**ations
UNECE	**U**nited **N**ations **E**conomic **C**omission for **E**urope
US	**U**nited **S**tates

Physical Constants

Speed of Light	c	=	$2.997\ 924\ 58 \times 10^8$ $\mathrm{ms}^{-\mathrm{S}}$ (exact)
Speed of Light	c	=	3×10^8 $\mathrm{ms}^{-\mathrm{S}}$ (approximate)

Symbols

ϵ_r	Relative Permittivity
ϵ_{eff}	Effective Relative Permittivity
η_1	Refractive Index of Air
η_2	Refractive Index of Ground
θ	Brewster Angle
λ	Wavelength
ρ	Pearson Correlation Coefficient
ϕ	Tilt Angle
ω	angular frequency
Γ	Coefficient of Reflectivity
Ω	Impedance
A_f	Antenna Factor
a	Radius of Sphere Enclosing EUT
d'	Receive to Transmit Antenna Distance - Direct Path
d"	Receive to Transmit Antenna Distance - Reflected Path
d_0	Receive to Transmit Antenna Separation Distance
EB	Error Bias
$\overrightarrow{E}_d$	Direct Vector E-Field
$\overrightarrow{E}_r$	Reflected Vector E-Field
$\hat{E}_r$	Unit Vector of Reflected E-Field
$\hat{E}_i$	Unit Vector of Incident E-Field
E_{max}	Maximum Emissions - Spherical Scan
E_{min}	Minimum Emissions - Spherical Scan
E_{CISPR}	Maximum Emissions - CISPR 12 Method
E_{meas}	Emissions - Measured at Single Antenna Height

E_{LHS}	E-Field recorded at Left Hand Side of Vehicle
E_{RHS}	E-Field recorded at Right Hand Side of Vehicle
f	Frequency
h_r	Receive Antenna Height
h_t	Transmit Antenna Height
K	'K' Factor
R	Real Part of S_{11} Measurement
X	Imaginary Part of S_{11} Measurement
Z_0	Characteristic Impedance

Bibliography

[1] CISPR, *Vehicles, Boats, and Internal Combustion Engines, Radio Disturbance Characteristics-Limits and Methods of Measurement for the Protection of Off-Board Receivers*, CISPR Std. 12, Rev. Edition 6, 2007.

[2] P. Wilson, D. Hill, and C. Holloway, "On Determining the Maximum Emissions From Electrically Large Sources," *Electromagnetic Compatibility, IEEE Transactions on*, vol. 44, no. 1, pp. 79 –86, Feb. 2002.

[3] P. Wilson, "Emission and Immunity Testing: Test Object Electrical Size and its Implication," in *Electromagnetic Compatibility, 2004. EMC 2004. 2004 InternationalSymposium on*, vol. 2, aug. 2004, pp. 349 – 352 vol.2.

[4] M. Paterson and J. F. Dawson, "An Investigation into the Errors in the CISPR 12 Full Vehicle Radiated Emissions Measurements Due to Vehicle Directivity," in *Electromagnetic Compatibility (EMC EUROPE), 2013 International Symposium on*, 2013, pp. 310–315.

[5] CISPR, *International Special Committee on Radio Interference: Information Technology Equipment Radio Disturbance Characteristics Limits and Methods of Measurement*, CISPR Std. 22, 2005.

[6] Official Journal of the European Communities, *Automotive EMC Directive*, Official Journal of the European Communities Std. 95/54/EC, October 2014.

[7] CISPR, *Vehicles, Boats, and Internal Combustion Engines, Radio Disturbance Characteristics-Limits and Methods of Measurement for the Protection of On-Board Receivers*, CISPR Std. 25, Rev. Edition 3, 2008.

[8] The German Government, "Telegraph Law of the German Empire," German Law, Apr. 1892.

[9] C. Paul, *Introduction to Electromagnetic Compatibility*, 2nd ed. John Wiley and Sons, 2006.

[10] American Standards Association, *Army-Navy Specification JAN-I-225*, Sectional Committee C63, Radio-Electrical Coordination Std. Jan-I-225, 1945.

[11] A. R. Foundation, "Conference on Radio Interference Reduction." Army Research Foundation, 1954.

[12] The European Union, *EMC Directive 89/336/EEC*, European Union Std. 89/336/EEC, May 1989.

[13] Official Journal of the European Communities, *Automotive EMC Directive*, Official Journal of the European Communities Std. 95/54/EC, October 2014.

[14] The European Union, *Medical Devices Directive 93/42EEC*, European Union Std. 93/42/EEC, 1993.

[15] ——, *Marine Equipment Directive 2014/90/EU*, European Union Std. 2014/90/EU, Jul. 2014.

[16] ——, *Agricultural or Forestry Tractors Directive 2009/64/EU*, European Union Std. 2009/64/EU, Jul. 2009.

[17] European Commission, *Uniform Provisions Concerning the Approval of: Vehicles with Regards to Electromagnetic Compatibility*, European Commission Std. 10, Rev. 05, October 2014.

[18] The European Union, *Radio Equipment Directive 2014/53/EU*, European Union Std. 2014/53/EU, 2014.

[19] European Commission, *on Radio Suppression and Electromagnetic Compatibility*, European Commission Std. 72/245/EEC, Jun. 1972.

[20] ——, *Directive 95/54/EC*, European Commission Std. 95/54/EC, Rev. L 266, November 1995.

[21] The European Union, *Automotive EMC Directive*, European Union Std. 2004/104/EC, Oct. 2004.

[22] CISPR, *Specification for Radio Disturbance and Immunity Measuring Apparatus and Methods - Part 1-4: Radio Disturbance and Immunity Measuring Apparatus - Antennas and Test Sites for Radiated Disturbance Measurements*, CISPR Std. 16-4-2, Rev. Amd2, Jan. 2017.

[23] T. Williams, *EMC for Product Designers*. BH Newnes, 1996.

[24] A. Ruddle, "Investigation of Automotive Emission Measurement Frequencies, Test Methods and Operating Modes." Laboratory for Electromagnetic Fields and Microwave Electronics, 2005.

[25] T. Williams. (1994, February) Measurement Techniques and Test Methods Developments, Costs and Options. ERA. [Online]. Available: http://www.elmac.co.uk/meast_t.htm

[26] British Standards Institute, *Information Technology Equipment. Radio Disturbance Characteristics. Limits and Methods of Measurement*, British Standard Std. EN55 032, Rev. 2015, Jul. 2015.

[27] M. H. Weik, *Inverse Square Law.* Boston, MA: Springer US, 2001, pp. 834–834. [Online]. Available: https://doi.org/10.1007/1-4020-0613-6_9566

[28] H. Garn, E. Zink, and R. Kremser, "Problems with Radiated Emission Testing at 3 m Distance According to CISPR 11 and CISPR 22," in *Electromagnetic Compatibility, 1993. Symposium Record., 1993 IEEE International Symposium on*, Aug. 1993, pp. 216 –221.

[29] D. Hoolihan, "Radiated Emission Measurements at 1/2/5/10/30 Meters," *Interfernece Technology*, pp. 24–31, 2010. [Online]. Available: http://www.nxtbook.com/nxtbooks/item/emcdirectory-design_2010/index.php?startid=22#/26

[30] International Electrotechnical Committee. (2018) International electrotechnical vocubulary. International Electrotechnical Committee. [Online]. Available: http://www.electropedia.org/

[31] CISPR, *Electromagnetic Compatibility of Multimedia Equipment - Emission Requirements*, CISPR Std. 32, Rev. Edition 1, 2015.

[32] ——, *Information Technology Radio Disturbance Characteristics- Limits and Methods of Measurement*, CISPR Std. 22, Rev. 6, 2008.

[33] G. Moore, "Cramming More Components Onto Integrated Circuits," *Electronics Magazine*, no. S 0019-9219(98)00753-1, pp. 114–117, 1965.

[34] A. Ruddle, "Validation of automotve electromagnetic models," Ph.D. dissertation, Loughborough University, Sep. 2002.

[35] GEMCAR, "Guidelines for electromagneic compatibility modelling for automotive requirements," Tech. Rep. GRD1-1999-10453, April 2003.

[36] C. Geuzaine and J. Remacle, "GMSH: a three-dimensional finite element mesh generator with built-in pre- and post-processing facilities," *International Journal for Numerical Methods in Engineering*, vol. 79, no. 11, pp. 1309–1331, 2009.

[37] IEEE, *Draft Standard for Validation of Computational Electromagnetics Computer Modeling and Simulations*, IEEE Standards Activities Department Std. IEEEP1597.1, Rev. Draft, June 2008.

[38] T. Rylander, P. Ingelstrom, and A. Bondeson, *Computational Electromagnetics, Texts in Applied Mathematics 51.* Springer Science+Business Media New York, 2012, ch. Chapter 2 Convergence, pp. 11–18.

[39] H. Bruns and C. Schuster. (2011, August) Concept II Electromagnetic Simulation Software. Technische Universtat Hamburg-Harburg. [Online]. Available: http://www.tet.tu-harburg.de/concept/index.en.html

[40] A. Ruddle, "Computed Impact of Optional Vehicle Features Sunroof and Windscreen Heaters) on Automotive EMC Characteristics." Zurich: 15th International Zurich EMC Symposium, February 2003.

[41] ——, "The EU Framework V Project "GEMCAR": Practical Aspects of the Development of Whole Vehicle Electromagnetic Models." Zurich: International Zurich EMC Symposium, February 2003.

[42] Y. Kelong and G. Yougang, "Research for the Radiated Emission Test," in *Environmental Electromagnetics, 2003. CEEM 2003. Proceedings. Asia-Pacific Conference on*, November 2003, pp. 613 – 616.

[43] A. Kriz, "Calculation of Antenna Pattern Influence on Radiated Emission Measurement Uncertainty," International Symposium on Electromagnetic Compatibility. IEEE, August 2008, pp. 1–7.

[44] CISPR, *Specification for radio disturbance and immunity measuring apparatus and methods - Part 1-4: Radio disturbance and immunity measuring apparatus - Antennas and test sites for radiated disturbance measurements*, CISPR Std. 16-1-4:2010 + Amd 2:2017, 2010.

[45] H. Coolican, *Research Methods in Statistics in Psychology*, 7th ed. Routledge, Nov. 2018.

[46] S. Batterman and H. Garbe. (Undated) Subjects of Discussion in Radiated Emission Measurements Above 1 GHz. [Online]. Available: http://www.adv-radio-sci.net/6/299/2008/ars-6-299-2008.pdf

[47] G. Freyer and M. Backstrom, "Some Implications of a Single Aspect Angle Electromagnetic Compatibility Test," in *Digital Avionics Systems Conference, 2000. Proceedings. DASC. The 19th*, vol. 1, 2000.

[48] P. Landgren, "Some Directivity Properties of Test Objects in the Microwave Region," in *Electromagnetic Compatibility, 2001. EMC. 2001 IEEE International Symposium on*, vol. 2, 2001, pp. 887–891 vol.2.

[49] CISPR, *Specification for Radio Disturbance and Immunity Measuring Apparatus and Methods*, CISPR Std. 16-2-1, Rev. Edition 1.1, September 2005.

[50] ANSI, *American National Standard for Methods of Measurement of Radio Noise Emission from Low Voltage Electrical Equipment in the Range 9 kHz to 40 GHz*, ANSI Std. C63.4, 2001.

[51] M. L. L. Low, "Hidden antennas for automobiles," Ph.D. dissertation, University of Kent, September 2005.

[52] M. Cerretelli and G. Gentili, "Accuracy in Modelling Conformal Window Glass Automotive Antennas by EM Numerical Solvers," European Microwave Conference. European Microwave Conference, 2009, pp. 1472–1475.

[53] C. Balanis, *Antenna Theory Analysis and Design*, 2nd ed., S. Elliot, Ed. J Wiley and Sons, 1997.

[54] S. Battermann and H. Garbe, "Influencing Factors and Possible Improvements for Emission Measurements Above 1 GHz," in *Electromagnetic Compatibility - EMC Europe, 2008 International Symposium on*, sept. 2008, pp. 1 –5.

[55] H. Mendes, "A New Approach to Electromagnetic Field Strength Measurements in a Shielded Enclosure." Los Angeles, California, USA: Wescon Tecnical Papers, August 1968.

[56] Siepel, *Mode Stirred Reverberation Chambers, Reference Guide*, version 1 ed., Siepel, France, 2010.

[57] R. Heinrich and U. Karsten. (2018) Reverberation Chambers Design and Application for EMC. http://www.teseq.de/com/en/service support/technical papers/03 RCdesign application EMC.pdf.

[58] R. Wen, "Using Reverberation Chamber for Vehicle Radiated Emission Measurement," in *2015 Asia-Pacific Symposium on Electromagnetic Compatibility (APEMC)*, May 2015, pp. 75–77.

[59] IEC, *Electromagnetic compatibility (EMC) - Part 4-21: Testing and measurement techniques - Reverberation chamber test methods*, IEC Std. 61 000-4-21, 2011.

[60] Madsen, Hallbjorner, and Orlenius, "Models for the Number of Independent Samples in Reverberation Chamber Measurements with Mechanical, Frequency, and Combined Stirring," *IEEE Antennas and Wireless Propagation Letters*, vol. 3, pp. 48–51, 2004.

[61] C. Lemoine, P. Besnier, and M. Drissi, "Estimating the Effective Sample Size to Select Independent Measurements in a Reverberation Chamber," *IEEE Transactions on Electromagnetic Compatibility*, vol. 50, no. 2, pp. 227–236, May 2008.

[62] A. Sorrentino, P. Kildal, U. Carlberg, and E. Pucci, "Accuracy in Reverberation Chamber for Wireless Testing: Simple Formulas for the Number of Independent Samples," in *2009 3rd European Conference on Antennas and Propagation*, March 2009, pp. 2673–2677.

[63] X. Chen, "Experimental Investigation of the Number of Independent Samples and the Measurement Uncertainty in a Reverberation Chamber," *IEEE Transactions on Electromagnetic Compatibility*, vol. 55, no. 5, pp. 816–824, Oct 2013.

[64] TEMCA2 Project, "Alternative EMC Test Method for Large Machines," V Framework Programme of EU, Tech. Rep. Contract CT-2002-00865, 2002.

[65] The European Union, *EMC Directive*, European Union Std. 2014/30/EU, 2014.

[66] British Standards Institute, *Electromagnetic Compatibility (EMC). Product Family Standard for Machine Tools. Emission*, British Standard Std. EN50 370-1, 2005.

[67] ——, *Electromagnetic compatibility (EMC). Product family standard for machine tools. Immunity*, British Standard Std. EN50 370-2, 2003.

[68] TEMCA, "Alternative EMC Testing Methods for Large Machines," TEMCA2, Tech. Rep., 2006.

[69] J. Catrysse, F. Vanhee, J. Knockaert, I. Hendrickx, and V. Beauvois, "In Situ Testing of Large Machines: Alternative Method for Radiated Emission Measurement," in *Electromagnetic Compatibility, 2008. EMC 2008. IEEE International Symposium on*, Aug 2008, pp. 1–6.

[70] F. Schroder, H.-K. Gonschorek, and H.-G. Krauthauser, "Emission Testing of Large Equipment - Test Wire Method - 2nd Approach," in *Electromagnetic Compatibility - EMC Europe, 2008 International Symposium on*, Sept 2008, pp. 1–5.

[71] J. P. Parmantier, "The Test Wiring Method," no. 551, Oct. 1998.

[72] M. Coenen, T. Maas, Y. Hu, and A. van Roermund, "In-Situ EMC Testing Using Surface Current Sense Wires," in *Electromagnetic Compatibility (APEMC), 2010 Asia-Pacific Symposium on*, April 2010, pp. 586–589.

[73] B. Tektas, O. Sen, S. Cakir, and M. Cetintas, "Improvements in Alternative Radiated Emission Test Methods With Surface Wire," in *2016 International Symposium on Electromagnetic Compatibility - EMC EUROPE*, Sep. 2016, pp. 799–804.

[74] J. Catrysse, F. Vanhee, and D. Pissoort, "Flexμstrip: A New Measuring Probe for the Characterisation of Large Machines In Situ," International Conference on EMC. EMC Europe, Sep. 2010.

[75] Analog Devices, "Microstrip and Stripline Design," Analog Devices, Application Note Rev 0, Jan. 2009.

[76] Maxim. (2003) Tutorial 2866. [Online]. Available: https://www.maximintegrated.com/en/app-notes/index.mvp/id/2866

[77] D. Pissoort, F. Vanhee, B. Boesman, and J. Catrysse, "Mode-Based Semi-Analytical Model to Characterize the Coupling from Large Machines to Test Wires," in *10th International Symposium on Electromagnetic Compatibility*, Sept 2011, pp. 488–493.

[78] K. H. Goschorek and F. Schlagenhaufer, "An Alternative Test Method for In-Situ Radiation Measurements." EMC Europe, 2006.

[79] M. Coenen, T. Maas, Y. Hu, and A. van Roermund, "In-Situ EMC Testing Using Surface Current Sense Wires," in *Electromagnetic Compatibility (APEMC), 2010 Asia-Pacific Symposium on*, April 2010, pp. 586–589.

[80] R. M. Barrett, "Microwave Printed Circuits - The Early Years," *IEEE Transactions on Microwave Theory and Techniques*, vol. 32, no. 9, pp. 983–990, September 1984.

[81] ——, "Microwave Printed Circuits," *Radio and TV News*, vol. 46, p. 16, Sep. 1951.

[82] IRE, Ed., *Microstrip - A New Transmission Technique for the Kilomegacycle Range*. IRE, 1952.

[83] S. Vaitheeswaran Iyer, "Study of Some Microstrip Resonators with Reference to Microstrip Antennas," Ph.D. dissertation, University of Poona, 1993.

[84] S. B. Cohn, "Characteristic Impedance of the Shielded-Strip Transmission Line," *Transactions of the IRE Professional Group on Microwave Theory and Techniques*, vol. 2, no. 2, pp. 52–57, July 1954.

[85] H. A. Wheeler, "Transmission-line properties of a strip on a dielectric sheet on a plane," *IEEE Transactions on Microwave Theory and Techniques*, vol. 25, no. 8, pp. 631–647, Aug 1977.

[86] D. D. Grieg and H. F. Engelmann, "Microstrip-A New Transmission Technique for the Kilomegacycle Range," *Proceedings of the IRE*, vol. 40, no. 12, pp. 1644–1650, Dec 1952.

[87] H. A. Wheeler, "Transmission-Line Properties of a Strip on a Dielectric Sheet on a Plane," *IEEE Transactions on Microwave Theory and Techniques*, vol. 25, no. 8, pp. 631–647, Aug 1977.

[88] P. J. Bevelacqua. (2019) Microstrip Patch Antennas. Accessed 8 January 2019. [Online]. Available: http://www.antenna-theory.com/antennas/patches/antenna.php

[89] J. R. Carson, "A Generalization of the Reciprocal Theorem," *The Bell System Technical Journal*, vol. 3, no. 3, pp. 393–399, July 1924.

[90] M. S. Neiman, "The Principle of Reciprocity in Antenna Theory," *Proceedings of the IRE*, vol. 31, no. 12, pp. 666–671, Dec 1943.

[91] C. Taylor, R. Satterwhite, and C. Harrison, "The Response of a Terminated Two-Wire Transmission Line Excited by a Nonuniform Electromagnetic Field," *IEEE Transactions on Antennas and Propagation*, vol. 13, no. 6, pp. 987–989, November 1965.

[92] A. A. Smith, "A More Convenient Form of the Equations for the Response of a Transmission Line Excited by Nonuniform Fields," *IEEE Transactions on Electromagnetic Compatibility*, vol. EMC-15, no. 3, pp. 151–152, Aug 1973.

[93] A. Agrawal, H. Price, and S. Gurbaxani, "Transient Response of Multiconductor Transmission Lines Excited by a Nonuniform Electromagnetic Field," in *1980 Antennas and Propagation Society International Symposium*, vol. 18, June 1980, pp. 432–435.

[94] F. Rachidi, "Formulation of the Field-to-Transmission Line Coupling Equations in Terms of Magnetic Excitation Field," *IEEE Transactions on Electromagnetic Compatibility*, vol. 35, no. 3, pp. 404–407, Aug 1993.

[95] Y. Kami and R. Sato, "Circuit-Concept Approach to Externally Excited Transmission Lines," *IEEE Transactions on Electromagnetic Compatibility*, vol. EMC-27, no. 4, pp. 177–183, Nov 1985.

[96] M. Stumpf and G. Antonini, "Electromagnetic Field Coupling to a Transmission Line - A Reciprocity-Based Approach," *IEEE Transactions on Electromagnetic Compatibility*, pp. 1–9, 2018.

[97] Computer Simulation Technology. (2018) CST studio suite. [Online]. Available: http://www.cst.com/Content/Products/CST-S2/Overview.aspx